Blooming Surfactants: Small Molecule Segregation from PVA Films

Rebecca Fong
Department of Chemistry
Durham University
2019

A thesis presented for the degree of Doctor of Philosophy

"A cover is nice but the cover is not a book"

Mary Poppins

Abstract

The segregation of small molecules in polymers is hugely relevant for a wide range of industrial systems. This thesis focuses on the segregation of surfactants in poly(vinyl alcohol) films, which are models for the films used to encapsulate detergent in unit-dose applications. The aim is to isolate and understand factors responsible for segregation observed in a range of model systems, that can ultimately be used to predict and control this behaviour.

A diverse range of surfactant segregation behaviours has been identified. The anionic surfactant, SDS, segregates extensively from PVA, with plasticisation by glycerol enhancing the surface excess, and enabling the formation of thermodynamically stable, stacked structures on the film surface. However, the behaviour of zwitterionic amine oxide surfactants in PVA has been shown to reflect their behaviour in water, forming a single monolayer on the surface.

By considering the interactions of these film components in solution using surface tensiometry and by determining their phase behaviour, the roles of surface energy and compatibility in segregation have been assessed. A significant synergistic effect was observed in model film systems comprising two surfactants, and these observations could also largely be explained by surface energy and compatibility arguments.

Assessing the effect of temperature on the distribution of film components has revealed some further migration, or surfactant restructuring after spin-coating. The properties of the polymer matrix is particularly important for this, particularly as the incorporation of plasticisers has been shown to have a significant impact on the distribution of surfactant in films. This has been addressed by exploring the effect of plasticisation and resin degree of hydrolysis on the free volume properties, which are likely to be linked to additive mobility.

Contents

Statement of Copyright

Dedication

To Mum, Dad and James

Acknowledgements

"Piglet noticed that even though he had a Very Small Heart, it could hold a rather large amount of gratitude."

A. A. Milne

First, my utmost thanks go to my supervisor, Dr Richard Thompson. I couldn't have asked for a better, more supportive supervisor. Thanks also to Dr Florence Courchay, my industrial supervisor at P&G, for useful direction in the project. Thank you to Prof. Peter Mallon at Stellenbosch University for guidance in the PALS experiments.

Thanks must go to all of the instrument scientists for their invaluable help in collecting neutron reflectivity and SANS data: Dr Nina-Juliane Steinke, Dr Jos Cooper, Dr Rob Dalgliesh, Dr Max Skoda, and Dr Becky Welbourn at ISIS, and Dr Philipp Gutfreund at ILL. Thanks also to Doug Carswell at Durham for the DSC and TGA measurements, and Alex Robertson for running some of the DMA. Thanks to Matt, Colin, Ophélie, Elise, Carl, Sifiso and Oliver for their help on beamtimes.

Thanks to my SOFI CDT cohort, a thoroughly good bunch, for of the helpful discussions as well as a huge amount of fun.

I would like to thank all of the Thompson group members, past and present, for their helpful thoughts and advice, and entertaining tea and lunch breaks. Particular thanks have to go to all those who dealt with many rants and grumbles while I was writing up. #thompsongroupontour

Finally, for their unending support, patience and help though the tricky moments, and sorting me out when I got in a pickle, I will be forever grateful to Mum and Dad and James.

List of Publications

- Briddick, A.; Fong, R.J.; Sabbatié, E. F. D; Li, P.; Skoda, M.W.A.; Courchay, F.; Thompson, R.L. "Blooming of Smectic Surfactant/Plasticizer Layers on Spin-Cast Poly(vinyl alcohol) Films." *Langmuir*, 34, 1410-1418, 2018.

- Fong, R.J.; Robertson, A.; Mallon, P.E.; Thompson, R.L. "The Impact of Plasticizer and Degree of Hydrolysis on Free Volume of Poly(vinyl alcohol) Films." *Poylmers*, 10, 1036, 2018.

List of Symbols and Abbreviations

β	Interaction parameter (Chapter 8)
β	Peak full width half maximum (Chapter 9)
γ	Surface tension
Γ	Surface excess in solution
θ	Scattering angle
λ	Wavelength
μ	Chemical potential
ρ	Scattering length density
σ	Scattering cross section
τ_1	p-Ps lifetime
τ_2	Free positron lifetime
τ_3	o-Ps lifetime
$\phi(z)$	Additive volume fraction
ϕ_b	Additive bulk volume fraction

AFM	Atomic force microscopy
AO	Amine oxide
b_i	Atomic scattering length contributions
c	Concentration
$C_{12}E_5$	Pentaethylene glycol monododecyl ether
CAC	Critical aggregation concentration
cm-	Contrast-matched
CMC	Critical micelle concentration
CTAB	Cetyl trimethyl ammonium bromide
d_1	Thickness of surface layer
d-	Deuterated
D	Density (Chapter 7)
D	Diffusion coefficient (Chapter 2)

DDAO	*N,N*-dimethyldodecylamine *N*-oxide
DH	Degree of hydrolysis
DMA	Dynamic mechanical analysis
DP	Degree of polymerisation
DTAO	*N,N*-dimethyltetradecylamine *N*-oxide
f	Fraction of segregated additive
f_1, f_2	Activity coefficients
ΔG_{mix}	Free energy of mixing
F	Free energy
Gly	Glycerol
ΔH_{mix}	Enthalpy of mixing
ΔH_{vap}	Enthalpy of vaporisation
h-	Hydrogenated
HLB	Hydrophilic-lipophilic balance
I	Intensity
I_3	Relative intensity of *o*-Ps annihilation
IBA	Ion beam analysis
k	Boltzmann constant
LCST	Lower critical solution temperature
M	Molar mass
M_n	Number-average molecular weight
M_w	Weight-average molecular weight
n	Refractive index
N_A	Avogadro constant
NR	Neutron reflectivity
p	Pressure
o-Ps	Ortho-positronium
p-Ps	Para-positronium
PALS	Positron annihilation lifetime spectroscopy
PEO	Poly(ethylene oxide)
PG	Propylene glycol
PVA	Poly(vinyl alcohol)
PVAc	Poly(vinyl acetate)
PVP	Poly(vinylpyrrolidone)
Q	Momentum transfer vector
R	Molar gas constant
R	Free volume cavity radius (Chapter 9)
$R(Q)$	Reflectivity

R_a	Average roughness
$R_{\max}$	Maximum roughness
R_q	Root mean square roughness
RBS	Rutherford backscattering
S	Entropy
ΔS_{mix}	Entropy of mixing
SANS	Small angle neutron scattering
SDS	Sodium dodecyl sulfate
SLD	Scattering length density
T_{g}	Glass transition temperature
t_{crys}	Crystallite size
TGA	Thermal gravimetric analysis
U	Internal energy
UCST	Upper critical solution temperature
V	Volume
v_m	Molar volume
z^*	Surface excess
XRD	X-Ray diffraction

Chapter 1

Overview

The segregation and migration of small molecules in multi-component soft matter systems is of huge commercial importance in a wide range of systems, including tackifiers in adhesives and plasticisers in packaging. One area where this is particularly relevant is in the possible migration and segregation of components in films used for unit-dose laundry detergents. The encapsulation of detergents in PVA films is an area of increasing importance for P&G as there is growing popularity in this form of detergent. The construction is a PVA-based pouch, often compartmentalised to prevent components from mixing prior to the dissolution of the pouch in water. The successful utility of this technology, and the ability to extend the range of components that may be encapsulated in this way, depends on achieving an appropriate balance between mechanical strength, lifetime and solubility of the PVA film.

Films used to construct these unit-dose detergent pouches are $\approx$70 µm thick, and contain a wide range of additives including, but not limited to, plasticisers. One challenge to be addressed relates to the distribution of these components in the PVA films. A better understanding of the segregation of film additives would enable this behaviour to be both controlled and exploited. If it can be predicted, the process by which the additive migrates to the surface will be effective in design development and additive prescription. This is particularly important to consider when creating the seals in the pouches, which are formed by wetting the PVA, partially dissolving the film. When two films are placed together, the polymer chains will interdiffuse allowing a seal to be formed. Segregation of film additives could detrimentally affect the sealing ability of the films, which could ultimately lead to product failure during transport.

This work aims to understand the segregation behaviour of additives in PVA by characterising their distribution in a number of model systems, in order to provide results that can ultimately be linked with data from theory and simulation

to predict and control segregation.

Throughout this thesis, a range of surfactants are used as model additives in the PVA film. Although the unit-dose pouches contain surfactants as detergent components, it should be noted that in this thesis the surfactants studied do not represent encapsulated detergent. In Chapter 4 the segregation behaviour of an anionic surfactant, SDS, will be explored as this is a model for anionic surfactants commonly found in laundry detergents.

Furthermore, this work aims to better understand and isolate the factors responsible for migration of different additives. Therefore, in Chapter 5, solution state studies of film components will be used to identify factors involved in surfactant segregation. Building on these findings, in Chapter 6 the segregation behaviour of amine oxide surfactants in PVA films will be presented and considered, alongside their solution behaviour. In this way, insights gained from additive properties in solution, and the relationship to segregation and wetting behaviour from Chapter 5 can be tested.

As well as attempting to obtain a clearer picture of factors responsible for segregation, it is of interest to begin bridging the gap between the simplest model film systems and the complex films used in industrial formulations. To this end, Chapters 7 and 8 will begin to explore how these insights may translate to industrial systems. In Chapter 7 the effect of heating spin-cast films is explored. In Chapter 8 the presence of multiple segregating species on additive segregation will be considered in order to add a level of complexity to the model systems, by considering the interactions between components.

A different approach to understanding the segregation and migration of small molecules in PVA films will be taken in Chapter 9, where positron annihilation lifetime spectroscopy will be used to understand the effect of matrix properties, including additive incorporation and degree of hydrolysis, on the microscopic free volume properties of the polymer.

Finally, the results from each of these chapters will be summarised in Chapter 10 to provide an overview of the impact of additives and storage conditions on their behaviour in PVA films, and suggestions for the direction of future work directions will be presented.

Chapter 2

Introduction

2.1 Poly(Vinyl Alcohol)

Poly(vinyl alcohol) (PVA) is a synthetic, water-soluble, semi-crystalline polymer. It is transparent, has good mechanical properties and excellent capability to form films.[1] One of its main applications is in food packaging, which makes use of its barrier properties to oxygen and carbon dioxide.[2] Its water solubility, high hydrophilicity and good biocompatibility have also led to a wide range of biomedical applications, with PVA having been shown to be suitable for tissue mimicking, cell culturing and vascular implanting.[3–6] PVA is valued for its non-toxicity and biodegradability, which contribute to its low overall environmental impact. These properties, together with its resistance to organic solvents, have led to its increased use in the laundry industry, particularly as a film for packaging unit-dose detergents.

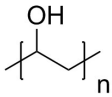

Figure 2.1: Structure of poly(vinyl alcohol).

The structure of PVA is shown in Fig. 2.1. The monomer, vinyl alcohol, does not exist in a stable form, instead rearranging into its tautomer, acetaldehyde. PVA is therefore prepared from the hydrolysis of poly(vinyl acetate) (PVAc) via saponification. The characteristics of the PVA consequently depend on its degree of hydrolysis (DH), which dictates the percentage of hydroxyl groups present on the backbone. This is particularly significant for the water solubility of the polymer, with solubility lower with decreasing DH. A lower DH (and higher proportion of residual acetate groups) also leads to a lower degree of hydrogen bonding, reducing stereoregularity and decreasing the degree of crystallinity.[7,8]

It is important to note that hydrolysis via saponification tends to lead to a blocky character because the presence of a few -OH groups on the polymer catalyses the hydrolysis reaction at adjacent sites in preference to random positions on the backbone. This blockiness is important in determining the properties of the polymer, as well as the density of acetate groups.[9]

The properties of the polymer, including its water solubility, are also dependent on the degree of polymerisation (DP), with lower molecular weight chains exhibiting greater water solubility. The increase in tensile strength with molecular weight means that PVA must be tailored to the application by altering these parameters.

2.1.1 Properties of PVA

PVA undergoes extensive hydrogen bonding between the hydroxyl groups of the repeat units. This high capability for hydrogen bonding means that PVA is somewhat crystalline at ambient temperatures. Despite being atactic, which would normally lead to highly amorphous structures, the very small size of the hydroxyl side groups permits the dense packing of polymer chains into crystalline regions. PVA resins with a high DH exhibit greater crystallinity than resins with lower DH as the residual acetate groups lower the stereoregularity of the polymer chains, disrupting both intra- and intermolecular hydrogen bonding.

As a semi-crystalline polymer, PVA has a glass transition temperature (T_g), which is the temperature above which there is sufficient free volume for significant polymer chain motion in the amorphous regions, and the material transitions from a glassy to rubbery state. This is distinct from the melting point, which is the temperature at which the crystalline regions of the polymer flow. The glass transition temperature is dependent on the degree of hydrolysis of the polymer, and has been reported to be 85 °C for PVA with a DH of 87-89 % and 58 °C for almost fully hydrolysed PVA.[10] However, the glass transition of PVA is difficult to measure calorimetrically.

2.1.2 Plasticisation

Additives are often required to give favourable properties to PVA. In particular, the addition of a plasticiser can be required to overcome its brittleness and improve processability and flexibility for many industrial applications, including unit-dose detergents. Plasticisers are involatile, low molecular weight molecules that, when blended with polymers, can modify the polymer matrix, increasing the free volume and chain mobility of the polymer by increasing the intermolecular

spacing between the chains. As a result of the decrease in strength of intermolecular forces, the density of the polymer decreases, improving the extensibility and flexibility of the material, and lowering the glass transition temperature.[11]

The theory of free volume was initially developed by Flory and Fox[12] to explain the plasticising effect of chain ends, observed as a reduction in the glass transition temperature of polymers upon decreasing molecular weight. The Flory-Fox equation links the number average molecular weight, M_n, to the glass transition temperature,

$$T_{\mathrm{g}} = T_{\mathrm{g}\infty} - \frac{K}{M_n} \tag{2.1}$$

where $T_{\mathrm{g}\infty}$ is the glass transition temperature at a theoretical limit of infinite molecular weight and K is an empirical parameter linked to the free volume. This was explained in terms of the greater free volume of chain ends: decreasing the molecular weight leads to an increase in concentration of chain ends, and thus total free volume, lowering the glass transition temperature.

The most frequently studied plasticisers are polyols, and mono-, di- and oligosaccharides.[13] The effects of composition, shape, polarity and chain length and number of functional groups on the plasticising ability of additives have been extensively investigated.[14–17] In general, additives with a small molecular size, high polarity and a greater number of polar groups tend to have a greater plasticising effect on a polymer. A greater distance between the polar groups in the additive also tends to correspond to a greater plasticising effect. However, the plasticiser selection for a given polymer system is based on the compatibility of the plasticiser with the host polymer, the amount necessary to achieve plasticisation, and the desired physical properties of the film.[13]

A variety of environmentally-benign plasticisers have been incorporated into PVA, including glycerol,[11] sorbitol[18] and propylene glycol[19] in order to improve the extensibility and flexibility of the polymer, whilst maintaining the desirable mechanical properties. Glycerol is one of the most widely used plasticisers, with its incorporation having been shown to decrease the hardness and elastic modulus of PVA films. Glycerol has been shown to increase the free volume of poly(vinyl alcohol), occupying the regions between polymer chains and disrupting the hydrogen bonding between them. The resultant decrease in T_{g} demonstrates the plasticising behaviour of this molecule.[20] When plasticised with glycerol, the melting point of PVA also decreases by a value proportional to the glycerol content.[11]

2.1.3 Solution State Properties of PVA

Throughout this project, the properties of PVA in solution are important, as they are likely to be relevant to the formation of spin-cast films. PVA can self-associate in solution into "pseudo-micelles". When DH is close to 100 %, this occurs as a result of the formation of intermolecular paracrystalline domains and/or by hydrogen bonding. Wang et al.[21] reported that the size of these colloidal particles is in the range of 6-23 nm. Polymers with a lower degree of hydrolysis (and therefore with lower crystallinity and a lesser ability to hydrogen bond) have also been shown to self-associate. Typically this occurs in PVA with a DH of 70-80 mol% as a result of hydrophobic interactions between vinyl acetate sequences. However, in contrast to the observation of Wang et al.,[21] Atanase and Riess[22] and Budhlall et al.[23] found that PVA chains with a DH between 80 and 90 % did not self-associate.

Thermoresponsive properties of PVA

Solutions of water-soluble polymers can show thermoresponsive properties. There are two types of behaviour that can be observed: the lower critical solution temperature (LCST), where above a certain temperature the system will demix and the polymer will precipitate, and the upper critical solution temperature (UCST) where the polymer and water will mix only above a specific temperature. The LCST is also referred to as lower critical demixing, and is the consequence of a balance of effects between the solvent and the hydrophilic and hydrophobic regions of the polymer molecule, with the hydrophobic effect (an entropic structuring effect) becoming more dominant at higher temperatures. Elevation of temperature reduces the hydration of these materials, thereby making the desolvated molecules aggregate and precipitate.

The thermoresponsive behaviour of PVA was first reported by Nord et al.[24,25] who reported that PVAs with a DH of 80-85 % are soluble in cold water but separate out of solution upon heating, exhibiting a LCST. There have been a number of subsequent studies, including that of Shiomi et al.[26] where it was reported that some fractionated, butanoylated PVA resins displayed both LCST and UCST thermal transitions. For example, a resin with a degree of degree of butanoylation of 7.4 mol% exhibited a LCST of 25.1 °C and an UCST of 135 °C.

The effects of a number of factors on the thermoresponsive behaviour of PVA have been studied. Furusawa et al.[27] reported that the LCST decreased with degree of hydrolysis but increased with degree of polymerisation. This property can be used to fractionate the polymer according to the critical temperature of phase separation. Crowther et al.[28] also studied the effect of molecular weight and

sequence of acetate functionality on the thermoresponsive behaviour, suggesting that random regions of hydroxyl/acetate groups contribute less to the driving force for demixing compared to blockier regions. Congdon et al.[9] demonstrated that the thermoresponsive properties of PVA are highly tunable by selective alkanoylation; increasing the hydrophobicity (acetyl < propanoyl < butanoyl) of side groups, or decreasing the density of these side groups along the chain lowers the LCST.

Surface Properties of PVA Solutions

The surface properties of PVA are important to consider in the frame of this project, as its surface activity is likely to influence the adsorption of other additives in solution-cast films. These properties of PVA solutions have been extensively studied, primarily using surface tensiometry.[29,30] At low concentrations PVA decreases the surface tension of water. The extent to which surface tension is reduced is dependent on molecular weight and stereochemistry. Surface tension has also been shown to decrease with acetate content.[29,31]

Moll et al.[32] investigated the surface structure of PVA solutions in water using heterodyne-detected vibrational sum-frequency generation (HD-VSFG) spectroscopy to probe the air-solution interface in the presence of 0.0625-6 wt.% PVA. At low concentrations (<1 %) of two different grades of PVA: one with a M_w of 10 000 g mol^{-1} and DH of 80 %, and one with a M_w of 125 000 g mol^{-1} and DH of 98 %, they identified that the interfacial water molecules prefer to orient themselves with their hydrogen-bonded -OH groups pointing away from the bulk. They attributed this preferred orientation of the water molecules to the ongoing hydrolysis of residual acetate groups, which leads to the production of negatively charged acetate ions with a high surface activity, despite the different DH of the two polymers. When the polymer concentration in solution is high (≥1 %), the lower molecular weight PVA completely covers the surface of the solution. However, the surface is not completely covered by the higher molecular weight PVA, which was still found to contain a relatively high density of interfacial water molecules. This was proposed to be a result of the formation of aggregated pores at the interface. It is difficult to ascribe the results uniquely to either the degree of polymerisation or degree of hydrolysis, due to both parameters being varied simultaneously. Nevertheless, this observation is consistent with the previous finding by Rošic[33] that in solutions of high molecular weight PVA, although surface tension initially decreases with concentration, beyond a certain concentration, surface tension rises, with its value at PVA concentration >10 % similar to that of pure water.

2.2 Surfactants

In this thesis, the segregation of surfactant additives in PVA is predominantly explored. These are amphiphilic molecules, consisting of a hydrophobic tail group and a hydrophilic head group. Their name, derived from "surface-active agent", indicates a key property: the ability to adsorb onto interfaces, reducing the surface tension compared to that of pure water. The amphiphilicity of surfactants enables their use as detergents as the hydrophobic tail associates with oily substances, such as grease, which reduces their adhesion to the surface and means they can more be easily removed by mechanical action, and solubilised by water due to the hydrophilicity of the head group.[34]

Surfactants can be broadly classified as either anionic, cationic, non-ionic or zwitterionic, based on the nature of the headgroup. In this thesis, at least one example of each category of surfactant is studied. The behaviour of each specific surfactant will be covered more extensively in the relevant chapters.

Surfactants can be characterised by the hydrophilic-lipophilic balance (HLB), which is the degree to which the surfactant is water-loving or oil-loving. The calculation of HLB values for non-ionic surfactants was initially described by Griffin,[35,36] and is given by Equation 2.2

$$\mathrm{HLB} = 20 \cdot \frac{M_h}{M} \tag{2.2}$$

where M_h is the molecular weight of the hydrophilic section of the molecule and M is the molecular weight of the entire molecule. The higher the HLB of the surfactant, the greater the hydrophilicity of the surfactant. A value of 0 therefore corresponds to a completely hydrophobic molecule, and a value of 20 corresponds to a completely hydrophilic molecule. This value can be used to indicate applications in which a surfactant is likely to be particularly effective. For example, an effective detergent requires a surfactant with a high HLB.

This approach to characterise surfactants is limited, however, as it cannot be used to characterise ionic surfactants, and does not work for different chemistries (e.g. hydrocarbon vs. fluorocarbon tails). Davies[37] therefore suggested an alternative method to determine HLB, whereby a value is calculated based on the chemical groups in the molecule, allowing the hydrophilicity of different groups to be accounted for. This is done by assigning group numbers to various structural elements, and combining them using Equation 2.3

$$\mathrm{HLB} = \sum_i H_i + nL + 7 \tag{2.3}$$

where H_i is the group number of the ith hydrophilic chemical group in the molecule, L is the group number of the lipophilic groups in the molecule (for -CH_2 and -CH_3 $L = -0.475$), and n is the number of lipophilic groups is the molecule. Some example group numbers for hydrophilic groups are given in Table 2.1.[37]

Table 2.1: Hydrophilic group numbers (taken from reference 37).

Hydrophilic group	**H_i**[37]
-$SO_4^-Na^+$	38.7
N(tertiary amine)	9.4
-OH(free)	1.9
-O-	1.3

Based on Equation 2.3, the HLB of some example surfactants used in this thesis are reported in Table 2.2, as calculated using the Griffin and Davies methods (Equations 2.2 and 2.3 respectively). Due to the limited number of reported group numbers, the Davies method cannot be used calculate the HLB for the cationic or zwitterionic surfactants studied in this thesis.

Table 2.2: HLB values for surfactants featured in this thesis.

Surfactant	**HLB (Griffin)**	**HLB (Davies)**
SDS	8.3	40
DDAO	5.2	-
DTAO	4.7	-
CTAB	7.7	-
$C_{12}E_5$	11.7	4.9

2.2.1 Surfactant Surface Adsorption and Self-Assembly

Surface adsorption is one of the defining features of surfactants, which results in the surface tension reduction of a solution. Surface tension (γ) is a result of the imbalance of intermolecular forces at the air-liquid interface, due to there being fewer molecules on the air side, and is given by the work (w) required to create an area, ΔA, of surface (Equation 2.4). It is also equivalent to the force per unit length required, and is thus expressed in mN m^{-1}.

$$w = \gamma \Delta A \tag{2.4}$$

Another fundamental property of surfactants is their tendency to aggregate in solution. One of the main types of associated units are micelles, which consist

of a core of hydrophobic chains, shielded from contact with water by hydrophilic head groups. The dominant driving force for micellisation is the entropy gained when the hydrophobic portion of the molecule is removed from the aqueous environment. These are known as hydrophobic interactions, and are driven by the repulsion between the non-polar tail and the surrounding water. The hydrogen bonding between the water molecules excludes other solutes, giving the non-polar tails a low solubility and a preference to aggregate with other non-polar molecules.[38,39]

Micelles can be spherical, but may also be extended into ellipsoids or rods, depending on the size of the head group relative to the tail group. A number of other aggregates can form in solution, including lyotropic liquid crystalline phases, such as the lamellar, hexagonal and cubic phases. In particular, the lamellar lyotropic liquid crystal phase is often formed in detergent solutions.[34] All of these phases are birefringent and so polarising optical microscopy can be used to identify the phase type.

The onset of surfactant micellisation usually occurs at a well-defined concentration. This is known as the critical micelle concentration (CMC). Each surfactant has a characteristic CMC at a given temperature and electrolyte concentration. Non-ionic surfactants (such as ethoxylated surfactants) tend to have lower CMCs than the corresponding ionic surfactant of the same chain length, but increasing the length of the hydrophilic group increases the CMC. The CMC decreases with increasing hydrophobic chain length. The valency of the counter-ion is also important for ionic surfactants; increasing the valency can drastically reduce the CMC. The addition of co-solutes, both electrolytes and non-electrolytes can also significantly impact the CMC.[34]

The CMC can be identified from the concentration dependence of the surface tension of surfactant solutions. Upon increasing the concentration (c) of the pure amphiphile, there is a rapid decrease in surface tension from the surface tension of pure water. At the CMC, however, the surface tension levels off and becomes almost independent of concentration. This is because when $c >$ CMC the activity of the surfactant in solution is almost independent of the concentration.

Surface tension measurements are very sensitive to impurities present in the surfactant, such as alcohols, which can lead to a pronounced minimum when γ is plotted against c. This is because the alcohols are also surface active, and bring about a greater reduction in surface tension than the surfactant alone. At higher concentrations, however, the surfactant can sequester the alcohol into the micelle so that surface tension increases to the value of the pure surfactant solution.[34]

The solubility of ionic surfactants can be very temperature-dependent. Mi-

celles only form above a certain temperature, which is known as the Krafft point, where there is a dramatic increase in solubility. Below the CMC, surfactant solubility is limited by the low solubility of the single molecules. Above the CMC, however, increasing the temperature leads to a great increase in surfactant solubility as soluble micelles form.[34]

2.2.1.1 The Gibbs Adsorption Equation

The Gibbs adsorption equation can be used to relate the change in surface tension of a solvent to the concentration of a solute, such as a surfactant, on the surface.

First, the excess of a species, j, at an interface, σ, between two pure phases, α and β, (n_j^σ) is given by

$$n_j^\sigma = n_j - \{n_j^\alpha + n_j^\beta\} \tag{2.5}$$

where n_j^α and n_j^β are the amounts of j in each of the pure phases and n_j is the total amount of j. The surface excess of j, Γ_j, is then defined as the excess per unit area, A,

$$\Gamma_j = \frac{n_j^\sigma}{A}. \tag{2.6}$$

The internal energy, U of the total system is given by

$$U = U^\alpha + U^\beta + U^\sigma \tag{2.7}$$

where

$$U^\alpha = TS^\alpha - pV^\alpha + \sum_j \mu_j n_j^\alpha \quad \text{and} \quad U^\beta = TS^\beta - pV^\beta + \sum_j \mu_j n_j^\beta \tag{2.8}$$

and S is the entropy, T is temperature, p is pressure, V is volume and μ is the chemical potential. The equation for the internal energy of the interfacial region is then given by Equation 2.9.

$$U^\sigma = TS^\sigma - pV^\sigma + \Sigma_j \mu_j n_j^\sigma \tag{2.9}$$

For any infinitesimal change, differentiation of Equation 2.9 gives

$$\mathrm{d}\,U^\sigma = T\,\mathrm{d}\,S^\sigma + S^\sigma\,\mathrm{d}\,T + \gamma\,\mathrm{d}\,A + A\,\mathrm{d}\,\gamma + \sum_j \mu_j\,\mathrm{d}\,n_j^\sigma + \sum_j n_j^\sigma\,\mathrm{d}\,\mu_j. \tag{2.10}$$

The differential internal energy at the interfacial region is

$$\mathrm{d}\,U^{\sigma} = T\,\mathrm{d}\,S^{\sigma} + \gamma\,\mathrm{d}\,A + \sum_{j} \mu\,\mathrm{d}\,n_{j}^{\sigma}. \tag{2.11}$$

Then, subtracting Equation 2.11 from Equation 2.10 yields the Gibbs adsorption equation (Equation 2.12), which at constant temperature becomes Equation 2.13.

$$S^{\sigma}\,\mathrm{d}\,T + A\,\mathrm{d}\,\gamma + \sum_{j} n_{j}^{\sigma}\,\mathrm{d}\,\mu_{j} = 0 \tag{2.12}$$

$$\mathrm{d}\,\gamma = -\sum_{j}^{\sigma} \mathrm{d}\,\mu_{j} \tag{2.13}$$

In the case of a surfactant (s) adsorbed to the surface of a solvent (l), this reduces to

$$\mathrm{d}\,\gamma = -\Gamma_{\mathrm{l}}^{\sigma}\,\mathrm{d}\,\mu_{\mathrm{l}} - \Gamma_{\mathrm{s}}^{\sigma}\,\mathrm{d}\,\mu_{\mathrm{s}} \tag{2.14}$$

and if the position of the surface is chosen that $\Gamma_{\mathrm{l}}^{\sigma} = 0$, this is simplified to

$$\mathrm{d}\,\gamma = -\Gamma_{s}^{\sigma}\,\mathrm{d}\,\mu_{\mathrm{s}}. \tag{2.15}$$

In the limit of an ideally dilute solution the chemical potential of the surfactant is

$$\mathrm{d}\,\mu_{s} = RT\,\mathrm{dln}\,c \tag{2.16}$$

where c is the concentration of the surfactant. The surface excess is therefore

$$\Gamma_{\mathrm{s}} = -\frac{1}{RT}\left(\frac{\partial\gamma}{\partial \ln c}\right)_{T}. \tag{2.17}$$

In the case of an ionic 1:1 surfactant, both surfactant and counterion adsorb at the interface.[34] Therefore Equation 2.17 should be modified by a factor of 2 to give Equation 2.18.

$$\Gamma_{\mathrm{s}} = -\frac{1}{2RT}\left(\frac{\partial\gamma}{\partial \ln c}\right)_{T} \tag{2.18}$$

2.2.2 Polymer-Surfactant Interactions

Understanding the nature of the interactions of PVA with different types of surfactants (anionic, cationic, non-ionic) in solution would be beneficial in rationalising the segregation behaviour of each system. As Quijada-Garrido et al.[40] demonstrated that morphological factors including the degree of hydrogen bonding dictate the diffusion behaviour of small molecules in polymer films, an

awareness of interactions in the film is vital. The importance of the polymer-surfactant interactions on the properties of polymer films has also been illustrated by Edler et al.,[41,42] who demonstrated the spontaneous formation of films at the air-water interface from solutions of surfactants and neutral polymers including poly(ethyleneimine) (PEI) and polyacrylamide. The self-assembled films are an unusual class of aggregate, found to contain an ordered micelle phase encapsulated in a polymer gel matrix.

The importance of the intermolecular interactions and, in particular, the degree of surfactant self-association in the film was also highlighted by Wakabayashi et al.[43,44] who showed that differences in the diffusion behaviour of erucamide and behenamide in a polypropylene film could be attributed to the self-association of behenamide. An understanding of the degree of surfactant association in the bulk polymer could therefore be helpful in predicting behaviour in the spin-cast films.

As the films studied throughout this thesis are prepared from aqueous solution, the interactions between components in water are particularly relevant. Polymer-surfactant interactions in solution have been extensively studied and reviewed, by virtue of their extensive range of applications including detergents and personal care products.[45–48]

Interactions between polymers and surfactants give rise of the formation of association structures, modifying both the bulk solution and interfacial properties. The surfactant and polymer generally associate cooperatively and the behaviour of surfactant/polymer mixtures can be very different from the individual polymer or surfactant solutions.[49] An extensive range of techniques has been used to investigate the aggregation and interactions in solution, including surface tensiometry, conductivity, viscometry, laser light scattering, neutron scattering, NMR, size exclusion chromatography and fluorescence.

The driving force for the polymer-surfactant interaction is often the reduction of the area of contact between hydrocarbon tails and water. The interactions are therefore controlled by a balance between hydrophobic and electrostatic effects. Polymer-surfactant mixtures can be classified as strongly or weakly interacting; weakly interacting mixtures usually comprise a neutral polymer and an ionic surfactant, with strongly interacting mixtures usually comprising a polyelectrolyte and a surfactant of the opposite charge. Weakly interacting systems will be primarily considered here.

The association between ionic micelles and polymers usually stabilises the micelles, leading to a reduced value for the CMC. The concentration above which the surfactant forms a complex with the polymer is known as the critical aggregation

concentration (CAC). The CAC is usually lower than the CMC, and the strength of the interaction between polymers and surfactants can be semi-quantitatively characterised by the CAC/CMC ratio.[45,50]

Surface tensiometry is the main tool for the study of the air/solution interface. The surface tension behaviour of weakly interacting polymer-surfactant systems (containing an uncharged polymer) was investigated by Jones[51] and Lange,[52,53] who studied systems containing sodium dodecyl sulfate (SDS) and either polyethylene oxide (PEO) or poly(vinylpyrrolidone) (PVP). In the presence of polymer, there are two identifiable transition points, conventionally referred to as T_1 and T_2. This behaviour can be accounted for by variations taking place in the bulk phase. The first break point (T_1) is the CAC. The second (T_2) is the point at which the bulk polymer is saturated with surfactant micelles, although this point is generally less well defined.[47] This is illustrated in Fig. 2.2. It has been demonstrated that T_1 is only weakly dependent on the concentration of polymer, whereas T_2 is directly proportional to the concentration of polymer.[49]

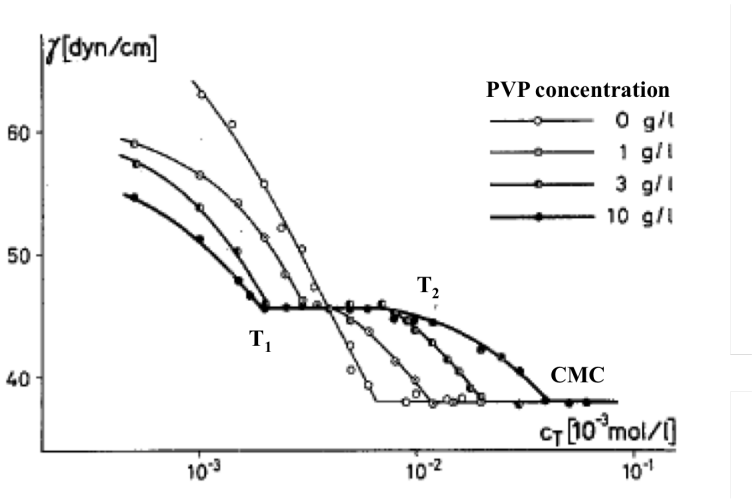

Figure 2.2: Effect of PVP concentration on the surface tension of aqueous SDS solutions, indicating T_1 and T_2. Reproduced with permission from reference 52.

As T_1 is normally lower than the CMC of surfactant in the absence of polymer, this shows that aggregation with the polymer is more favourable than normal micellisation. At concentrations above T_2, there is a further lowering of the surface tension due to the presence of free surfactant molecules in solution. After the CMC is reached, however, the surface tension is constant. It should be noted that surface tension data can be difficult to interpret if the polymer is also surface active.

The interaction of a water-soluble polymer with a surfactant in solution can be described using one of three behavioural types. One case is where surfactant mi-

cellisation occurs prior to aggregation with the polymer. This binding approach is preferred for polymers with hydrophobic groups. Another case is where surfactant binding to the polymer occurs below the CMC, with the polymer becoming saturated with surfactant before micellisation. This behaviour was previously described for SDS and PVP. The surfactant molecules aggregate on the polymer in the form of bound micelles, with each polymer chain linking several micelles to form a "pearl necklace" structure. This model was first proposed by Shirahama et al.[50] and is preferred for polymers with hydrophilic groups. Finally, more complex behaviour can also exist between these two extremes.[54]

The interaction of neutral polymers with surfactants can exhibit any of the types of behaviours discussed. The strength of the interaction is strongly dependent on the surfactant chain length and charge, as well as on the presence of salts in the solution. It has been established that there is also a significant influence exerted by the hydrophobicity of the polymer. This has been highlighted by the differences in the binding of cationic surfactants to poly(propylene oxide) (relatively strong) and poly(ethylene oxide) (small to negligible).[55] This is thought to be a result of the stabilisation of the interface between the hydrophobic core of the micelle and water.

Neutron reflectivity (NR) is another technique that has been employed to probe interactions between polymers and surfactants in solution, and identify the structure of adsorbed complexes at the air-water interface. For example, NR and surface tension were used by Penfold et al. to characterise the adsorption of a mixture of the polyelectrolyte polyethylene imine (PEI) and SDS.[56] From this, the authors identified that SDS adsorption was strongly dependent on the degree of branching of the polymer. SDS adsorption was also found to be affected by charge, with the most surfactant adsorption to the polymer observed at high pH when the polymer is essentially uncharged. By using NR to determine the interfacial composition profile of a mixture comprising SDS and poly(2-(dimethylamino) ethyl methacrylate), a weak polyelectrolyte, Moglianetti et al.[57] revealed the complexation of SDS to polymers occupying an extended conformation on the surface, with a stoichiometry that varies with SDS concentration. Furthermore, at high SDS concentration (0.1 and 1 mM at pH 3 and 9 respectively), multilayer structures could be identified on the surface using this technique.

The behaviour of uncharged polymers with anionic and cationic surfactants has been shown to be very different; cationic surfactants generally show very little affinity for neutral water-soluble polymers, whereas anionic surfactants tend to bind very strongly to them. These large differences in interaction strengths have been linked to the size of the hydrated head group of the surfactant, which is

generally bulkier for cationic and non-ionic surfactants. However, most studies have dealt with systems containing anionic surfactants as a result of the stronger interactions generally observed.[50–54,58,59]

Phase Behaviour

Characterising the phase behaviour of polymer-surfactant systems could be useful in providing insight into the effect of different parameters, including surfactant and plasticiser concentration, on the behaviour of additives in PVA films prepared from aqueous solutions. There have been a number of different approaches to determine phase behaviour. Cloud point measurements are one frequently used experimental tool. Some uncharged polymers (and surfactants) exhibit a lower critical solution temperature (LCST), above which phase separation occurs as the hydrophobic effect becomes more dominant. By taking cloud point measurements Liu et al.[60] constructed binodal curves, representing the border between the one phase and the two-phase regions, for systems consisting of aqueous solutions of polyethylene glycol and two nonionic surfactants: polyoxyethylene octyl phenyl ether (Triton X-100) and polyoxyethylene sorbitan monooleate (Tween 80). The authors determined the effect of temperature on the binodal curves, which can be seen in Fig. 2.3, finding that for both the systems, solubility decreases with increasing temperature, with the non-ionic surfactants dramatically reducing the solubility of the polymer. This highlights the sensitivity of the cloud point to interactions in the system, and shows the value of cloud point measurements to identify relative strengths of interactions in polymer-surfactant solutions.

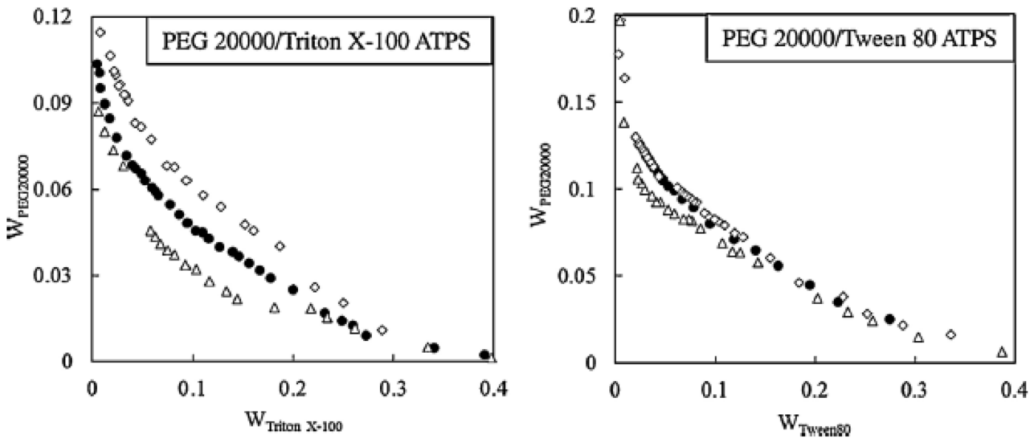

Figure 2.3: Effect of temperature on binodal curves of polymer/surfactant systems. Open diamonds, 273.15 K; filled circles, 293.15 K; open triangles, 313.15 K. Reproduced with permission from reference 60.

Interactions of Surfactants with PVA

Whilst the interactions of surfactants with a wide range of water-soluble polymers have been investigated, with studies focussing heavily on poly(vinyl pyrrolidone) and poly(ethylene oxide), the interactions of surfactants with PVA are of particular relevance to this thesis.

It has been demonstrated that the PVA aggregates present in aqueous solution known as "pseudo-micelles", can be disrupted by anionic surfactants. SDS is the most extensively studied surfactant, and its interactions with PVA of a range of DH have been investigated by a number of authors.[22,50,59,61–65]

The degree of hydrolysis has a significant effect on the intermolecular interactions of PVA in solution and therefore also on its interaction with surfactants. This was first explored by Arai and Horin,[61] who studied the nature of the polymer-SDS complex as a function of the hydrophobic character of the polymer, finding that the degree of SDS adsorption in solution increased with polymer hydrophobicity.

Lewis and Robinson[59] used viscometry to show that partially hydrolysed PVA forms polyelectrolyte complexes with SDS as a result of hydrophobic interactions between the polymer and the surfactant tails. These hydrophobic interactions disrupt the intermolecular interactions between polymer chains, leading to dissociation of the "pseudo-micelles". At very low SDS concentration the surfactant begins bind to the vinyl acetate sequences, causing disaggregation of the polymer assemblies. At surfactant concentrations greater than 5 wt.% and polymer concentrations of 0.1 wt.%, no PVA aggregates were found to remain. Atanase and Reiss[22] also observed that PVA in solution could be disaggregated by SDS, finding that interaction with the surfactants has a strong influence on the LCST of PVAs over a range of DH. The cloud point of each polymer increased with SDS concentration, although a smaller effect was observed for polymers with a greater degree of hydrolysis (80-90 %), where the lower concentration of hydrophobic groups means that the polymer is not in the form of "pseudo-micelles" and therefore not aggregated in the absence of SDS.

Although the interactions between PVA and anionic surfactants have been more extensively studied, Shirahama and Nagao[63] investigated the effect of DH on the interactions between PVA and the cationic surfactant tetradecylpyridinium bromide, finding that increasing the hydrophobicity of the polymer increases its binding tendency in aqueous solution. By determining binding isotherms, they showed that the binding constant does not change significantly with the degree of hydrolysis, whereas the binding saturation increases with acetyl content. This was interpreted in terms of the acetyl groups acting together with the vinyl backbone

to afford hydrophobic regions into which the surfactant is partitioned. From this, they concluded that the increased number of sites causes the binding tendency to increase with hydrophobicity, with the binding affinity remaining constant. The authors calculated that approximately three acetyl groups in the polymer are aggregated to provide a hydrophobic binding site for each surfactant molecule.

The importance of the hydrophobic interactions was also illustrated by Damas et al.,[64] who studied the interaction of PVA (98 % DH) with a number of short chain, non-ionic polyol surfactants using dynamic light scattering, tensiometry and viscometry in order to explore the effect of the polyol structure. In these weakly interacting systems, despite the presence of hydroxyl groups in both the surfactant and polymer, the -CH_2OH groups of the surfactants were found to have an unfavourable contribution to the polymer-surfactant interaction, whereas the -CH_2 groups interact favourably with the polymer.

In order to identify factors that influence the degree of binding, Shirahama et al.[62] studied the binding of four cationic surfactants (tetradecylpyridinium chloride and bromide, dodecyl pyridinium chloride and dodecylammonium chloride) to PVA with a degree of hydrolysis of 90 %. Although only a narrow range of alkyl chains were studied, the group found that the length of the alkyl chain plays only a minor role in the binding of these cationic surfactants. This is interesting given the importance of the hydrophobic interactions in the binding of both nonionic and anionic surfactants,[64] and the significance of the degree of hydrophobicity of the polymer.[61] However, the polar headgroup was found to contribute significantly to the binding affinity.

Tadros[65] used surface tensiometry, viscometry and conductivity to provide evidence of interaction between between PVA and the cationic surfactant, cetyl trimethyl ammonium bromide (CTAB). The mixed solution showed behaviour typical of a polyelectrolyte. As PVA in uncharged, this therefore suggests the formation of a polymer-surfactant "complex" or polymer-nucleated micelle. Upon increasing the polymer concentration, the CMC of CTAB became ill-defined, with the transition disappearing for PVA concentrations greater than 0.1 wt.%. This was attributed to the adsorption of all surfactant molecules onto the polymer chains.

2.3 Molecular Migration and Segregation

There are many examples where additives spontaneously migrate to surfaces. The migration of low molecular weight components to interfaces in polymer films can be part of an unwanted degradation mechanism; in most cases, the loss of

the additive to the surface and further loss by evaporation, leaching or blooming (where the additive precipitates on the surface) can cause failure of the material. This is particularly relevant in the blooming of small molecule additives such as plasticisers and antioxidants in polymers, which is significant for food packaging applications and medical devices.[66–68]

For the purposes of this thesis, it is important to distinguish between migration and segregation. Here, segregation will refer to the separation of components into regions enriched in respective components, where at least one region is at a surface or interface. Migration, on the other, hand will refer specifically to the movement of molecules, and has a kinetic consideration. This may indeed result in segregation, although this is not necessarily the case.

This thesis will focus predominantly on the segregation and migration of surfactant additives in PVA films. Despite the segregation of surfactants to solution-air interfaces having received much attention, the case where the solvent is replaced by a solid polymer is relatively unexplored.

Although the case of migration and segregation in polymer blends, block copolymers or end-functionalised polymers has been extensively studied[69,70] this will not be discussed in depth. The case of the migration of small additive molecules, including surfactants, has been much less extensively studied, and will be covered in the following section.

2.3.1 Surfactant Segregation in Polymers

It is known that certain surfactants incorporated during polymer fabrication localise at the surface, altering the surface structure and properties. These are most commonly surface active block copolymers or well-defined graft copolymers. Whilst these high molecular weight additives are removed less easily from the surface than lower molecular weight surfactants, they have the disadvantage of slow diffusion through the bulk material, which is undesirable when the additive is designed to modify the surface.[71]

Melt blending of surface-segregating additives is one approach used for surface modification, whereby the host polymer is blended with an additive and extruded into a fibre or a film, with the additive allowed to bloom to the surface. This method furnishes the product with desirable surface properties (such as hydrophobicity) using a low total additive concentration, and causing little alteration of the bulk properties. Indeed, Datla et al.[72] modified the surface of polypropylene films by melt-blending with stearyl alcohol ethoxylated additives. In all samples, the concentrations of the additives were found to be significantly higher at the surface

than in the bulk. Similarly, Zhu and Hirt investigated the migration of additives, including polyethylene glycol and hydroxyl-terminated four-arm polyethylene oxide, as a means to increase the hydrophilicity of polypropylene surfaces, finding greater concentrations of all additives in the near-surface region.[73]

Torstensson et al.[71] modified the surface of PMMA and a UV-curable acrylic lacquer using small amounts of polymerisable, monomeric surfactants. By using a low molecular weight surfactant, the additive diffused rapidly through the bulk material to the surface. However, as the monomers are polymerisable, they were subsequently made to react in order to chemically bond to the surface of the polymer in order to prevent additive loss.

2.3.1.1 Surfactant Distribution in Latex Films

One area in which surfactant distribution in polymer films has been extensively studied is latex films. Latexes (or latices) are colloidal dispersions of polymeric particles in water from which polymeric films can be obtained by coalescence of the particles. The resultant structure of the films is therefore different to that of a film produced from polymer in solution as it can retain the memory of the particular structure of the polymer in the latex. One specific class of these materials is pressure sensitive adhesives (PSAs). A PSA is an adhesive capable of bonding to most material surfaces through the application of light pressure. Surfactants are important in these systems as they ensure the colloidal stability of the dispersions during synthesis, enabling the generation of high-solids latices. Surfactants are also known to affect the ordering and deformation of the particles, as well as the interdiffusion of the polymer chains.[74]

The film forming process can be divided into stages. First, water evaporates until the particles come into contact and densely pack together. Second, the polymer particles are deformed as the drying proceeds. Finally, the boundaries between particles disappear as they coalesce, and the polymers comprising adjacent particles interdiffuse.[75]

The final distribution of the surfactants is a topic of interest. These molecules are adsorbed to the surface of the latex particles in solution, and are capable of migrating during film formation, which leads to their inhomogeneous distribution throughout the dry film. The presence and distribution of these surfactants is known to affect the final properties of the latex films; for example, it is believed that their heterogeneous distribution due to migration in a PSA film can result in poor adhesive performance and water resistance.[74] Although, the initial conditions for the film forming process are very different in films prepared from polymer solutions rather than suspensions of colloidal particles, the driving forces

responsible for observed surfactant distribution in latex films are important to consider in this project.

The discussion over the fate of surfactants in latex films began in 1936 when Wagner and Fischer suggested that the polymer and surfactant could form two interpenetrating networks.[76] The distribution of surfactants in these films has since been extensively experimentally investigated using a range of techniques including Rutherford backscattering,[74,77,78] confocal Raman spectroscopy,[79] atomic force microscopy[80] and attenuated total reflectance (ATR) Fourier transform infra-red spectroscopy (FTIR).[81,82] However, as these techniques do not provide information about the size and morphology of surfactant aggregates, a number of higher resolution techniques including small angle X-ray scattering[75,83,84] and small angle neutron scattering[85,86] have been more recently employed to provide representative information about the whole film.

The surfactant distribution is affected by a huge range of factors including the chemical functionality of polymer, nature of the surfactant, substrate and ageing conditions. Depending on the compatibility of the polymer and surfactant, there have been three main possibilities suggested: (1) dissolution of the surfactant in the polymer, (2) phase separation of the surfactant from the polymer and migration of the surfactant to interfaces, and (3) the surfactant remaining at the interfaces between particles.

Much of the work on latex systems in the 1980s and 1990s was devoted to investigating the surfactant at the air and substrate interfaces. In particular Zhao et al.,[81,87] showed that surface enrichment was dependent on the nature of the surfactant/polymer couple and a function of the initial surfactant concentration in the latex. From the study of anionic surfactants, Zhao et al.[88] also first provided a mechanism for the surfactant transport in latexes. They reported that it is the tendency of the surfactant to reduce the interfacial energy that drives it to the two interfaces, with surfactant-polymer incompatibility providing the driving force for long-time migration. Their proposed mechanism involves the water flux carrying the non-adsorbed surfactant to the film-air interface, which results in the more pronounced enrichment of surfactant at this interface.

These arguments have subsequently been employed to explain surfactant segregation in other systems. The role of interfacial energy in surfactant segregation to the film-air and film-substrate interfaces was confirmed by Evanson et al.,[89,90] who demonstrated that greater surface enrichment of surfactants at the substrate interface could be induced when there is a high interfacial energy, providing the impetus for adsorption and thus segregation.

The subject of surfactant-polymer compatibility has also been addressed by

Evanson et al.[89,90] and by Zhao et al.[88] Evanson et al.[90] showed that better compatibility between nonionic surfactants and an ethyl acrylate/methyl methacrylate (EA/MMA) latex resulted in a lower degree of interfacial surfactant segregation. Zhao et al.[88] addressed the role of incompatibility of styrene and the anionic surfactant sodium dioctylsulfosuccinate (SDOSS) on the observed stratifications in films comprising these components, and demonstrated that surfactant segregation could be controlled by adjusting the binding isotherm of the latex surfactant system.[91,92]

Kientz and Holl[82] studied the evolution of the distribution of a wide range of surfactants in poly(2- ethylhexyl methacrylate) latex films. In this case, these systems were incompatible, and thus there was little dissolution of the surfactant into the polymer. They showed that the surfactant distribution was established during the drying period, with the incompatibility of the surfactant and the polymeric medium allowing only a slow evolution of structure in the dry film. This observation was later corroborated by Belaroui et al.[79]

Kientz and Holl[82] listed three factors that can determine surfactant distribution in latexes: the initial surfactant distribution, the surfactant desorption during the drying of the film, and the mobility of the surfactants after desorption. Based on the latter two factors, the authors stressed the importance of polymer-surfactant interactions in understanding surfactant distribution.[82] Although Kientz and Holl argued that, due to its substantially lower surface area, there is little surfactant on the air-water interface compared to the particle-water interface, Tzitzinou et al.[77] proposed an alternative mechanism for their observed enrichment of surfactant at the surface of acrylic latex films, whereby the surfactant at the air-water interface adsorbs onto particles as the drying front moves as water evaporates.

Gundbala et al.[74] proposed a model to predict the distribution of surfactant in latex coatings established during the solvent evaporation stage. They showed that an adsorption isotherm (which determines the amount of surfactant adsorbed onto the particles and the amount of surfactant present in the bulk solvent at equilibrium for a given surfactant concentration) and the diffusion of the surfactant control the surfactant distribution in the final film.

In this model, the authors used a Langmuir expression for the adsorption isotherm to give the concentration of surfactant on the particle surface, $\Gamma = \Gamma_\infty C_S/(A+C_S)$, where Γ_∞ is the maximum surface adsorption onto the particles, A is the concentration at which half the maximum surface adsorption occurs, and C_S is the surfactant concentration in the bulk.

The authors then used transport equations to account for diffusion of the

surfactant. Their model also uses the Peclet number, Pe_s, of the surfactant, defined as $Pe_s = H\dot{E}/D_S$, where H is the film thickness, $\dot{E}$ is the evaporation rate and D_S is the diffusion coefficient of the surfactant. The Peclet number determines the ability of the surfactant on the surface to redistribute itself into the bulk solution. Using these contributions, alongside the particle volume fraction and the close packed volume fraction, the authors were able to determine C_S and Γ for each distance from the substrate.

This model always predicts a surface excess at the top surface, but the magnitudes of the isotherm parameters determine whether the surfactant would be expected to be enriched or depleted at the substrate. This model was found to agree qualitatively with the distribution of the cationic surfactant CTAB, and the nonionic surfactant Triton X-100 in a styrene-butyl acrylate copolymer latex determined by ATR FTIR spectroscopy. This model also adequately predicted the near-surface concentrations of a number of surfactants (sodium dodecyl sulfate (SDS), lithium dodecyl sulfate (LiDS) and sodium triflate (ST)) in poly(styrene-*co*-butyl acrylate) measured using Rutherford Backscattering.[78] However, the near surface concentrations of LiDS and SDS were somewhat lower than that predicted, and the model could not adequately predict the distribution of sodium octyl sulfate. In the latter case, a surfactant concentration close to 0 in the bulk film was observed, whereas a much higher surfactant bulk surfactant concentration was predicted. This discrepancy was suggested to be caused by large accumulation of the surfactant at the film air-interface, and thus depletion of the bulk concentration.

2.3.2 Factors Affecting Segregation and Migration

In order to rationalise the segregation of some additives to the film surface, the driving forces for segregation should be considered in greater depth. The following section will cover surface energy, entropy and compatibility as potential driving forces for segregation and migration.

2.3.2.1 Role of Additive Surface Energy

The differences in surface energy between the polymer matrix and additive will first be considered. The component with the lowest surface energy should be enriched on the surface as this decreases the overall free energy of the system. The greater the difference in surface tension, the greater the reduction in the free energy of the system upon segregation ($\Delta F \sim \Delta\gamma$). The selective migration of one component to the surface is usually driven by this reduction in the surface

energy, F, of the system at interface[70] and is apparent from the Gibbs equation in Section 2.2.1.1.

This concept has explained the selective enrichment of one component of a block copolymer in a number of systems, and the surface enrichment of deuterated polymer in a blend with hydrogenated polymer (deuterated analogues have a slightly lower surface energy).[93] Surface energy gradients have indeed been used to functionalise polymer surfaces by the migration of a copolymer additive within the matrix.[94] The surface energy induced segregation of copolymer additives, as well as the enrichment of end groups or one block of a block copolymer, has been extensively reported, characterised and utilised. For example, incorporating surface active perfluoroalkyl groups to polymers has been extensively used as a surface modification strategy.[69,95–98] Lee and Archer[94] reported that the large difference in the surface tension of components was responsible for the segregation of polystyrene-*b*-poly(dimethylsiloxane) additives in polystyrene hosts. However, this chemical dissimilarity is not, in fact, necessary for surface energy driven segregation, as the surface tension of a homopolymer follows a simple scaling relationship with molecular weight,

$$\gamma = \gamma_\infty - k_0/(M_n)^\alpha$$

where γ_∞ is the surface tension in the limit of infinite molecular weight, k_0 is a constant that can be positive, negative or zero, and α reflects the interaction strength between the end groups of the polymer chain and the surface; for repulsive interactions $\alpha \approx 1$ and for attractive interactions $\alpha \approx 0.5$. This means that for a polymer where k_0 is positive, surface tension should increase with increasing molecular weight.

Although migration in polymer blends will not be considered in detail, the migration of other additives has been used as an approach to functionalise polymer surfaces. For example, by functionalising fullerene (C_{60}), with perfluoroalkyl groups, Chen and McCarthy[99] induced surface activity of the additive in a polystyrene matrix.

The role of interfacial tension on additive migration has also been treated theoretically. It is clear that the case of the migration of small molecules to interfaces has been much less extensively considered than the migration of minor-component polymers in blends,[100,101] which are of less relevance to the work contained in this thesis. However, the migration of plasticisers is one area that has attracted particular attention. This is largely due to the implications of leaching packaging additives, and the resulting detrimental effects on the mechanical properties of the polymer. The weak interactions between the plasticiser and host matrix gives

these molecules a tendency to migrate, and surface and interfacial tension can be used to interpret these migration phenomena.

Zanjanijam et al.[102] studied the migration of plasticiser in a polymer matrix during processing. In this case, localisation of the plasticiser to the interface of two polymers in a phase-separated blend, rather than the polymer-air interface was considered. The authors calculated the interfacial tension values of each components in a plasticised blend of poly(vinyl butyral) (PVB) and polypropylene (PP) using the Parachor method (Equation 2.19),[103] which is used to estimate surface tensions using a sum of atomic and group contributions, P_s, and the molar volume per structural unit, V. By determining the polar (γ_p) and dispersive (γ_d) contributions to the surface tension, they were able to subsequently calculate the interfacial tension between the components (Equation 2.20). The authors rationalised the localisation of the plasticiser and the interface between the two polymers by the resultant decrease in interfacial tension between PP and PVB.

$$\gamma = \left(\frac{P_s}{V}\right)^4 \tag{2.19}$$

$$\gamma_{12} = \gamma_1 + \gamma_2 - 2\sqrt{\gamma_1^d \gamma_2^d} - 2\sqrt{\gamma_1^p \gamma_2^p} \tag{2.20}$$

The Harkins equation uses the surface tensions of a liquid and a substrate, and their interfacial tension, to define a spreading coefficient, which provides a measure of the ability of one liquid to spontaneously spread across another, and indicates the possibility of one phase being located at the interface.[104] A modified Harkins equation (Equation 2.21), in which surface tensions are substituted with interfacial tensions, has been used to determine the spreading coefficient for a plasticiser encapsulating one component (in this case PVB) in a mixture of two dissimilar polymers, $\lambda_{\mathrm{plast/PVB}}$, thereby assessing the tendency of a plasticiser to migrate to the interface and separate the phases of two polymers.

$$\lambda_{\mathrm{plast/PVB}} = \gamma_{\mathrm{PP\text{-}PVB}} - \gamma_{\mathrm{PP\text{-}plast}} - \gamma_{\mathrm{PVB\text{-}plast}} \tag{2.21}$$

As Zanjanijam et al. determined that $\lambda_{\mathrm{plast/PVB}}>0$, this indicates that spreading and encapsulation of PVB by plasticiser is favourable, and results in a reduction in free energy. This can therefore, in part, explain the migration of plasticiser to the interface of the polymer blend. This provides some thermodynamic reasoning for the observed changes in glass transition of the PVB and PP phases, which are indicative of plasticiser migration.

Harkins' spreading theory was also used by Taguet et al.[105] to predict the surface energy-driven formation of a thin layer of plasticiser, localised at the interface

between two blended polymers. In this case, the authors observed the migration of plasticiser to the interface in polyethylene/thermoplastic starch blends.

Rezaei Kolahchi et al.[70] considered the differences in interfacial tension and spreading coefficients of poly(ethylene terephthalate) containing a range of blended polymers to predict surface morphology and wetting behaviour of minor components. However, despite this example of interfacial energy differences driving the development of complex droplet morphology, which can be predicted using spreading coefficients, the case of surface energy differences driving migration of an additive to the top surface layer of films, (as opposed to an interface between two polymers[106–109]), is less extensively reported.

2.3.2.2 Role of Entropy in Additive Segregation

The configurational entropy per segment of polymer chains near rigid surfaces is substantially lower than in the bulk. As a result, the highest molecular weight component experiences an entropic penalty for residing at the surface. In a monodisperse, homopolymer system, it has been suggested that this should result in a greater concentration of chain ends at the surface.[110] In a polydisperse system, the surface region would be expected to be enriched in the lower molecular weight components.[111]

The segregation of additives to the surface therefore depends on a balance between the reduction in surface energy and gain in translational entropy. In the absence of a discernible surface energy difference, molecular size becomes an important factor, with the lowest molecular weight component being enriched on the surface.[112] This was demonstrated by Harihan, Kumar et al.,[113–115] who showed that when the difference in surface energy is small, molecular weight can become significant in polystyrene blends.

Lee and Archer[112] investigated additive segregation when the difference in free energy in the system was small, in a system consisting of polystyrene-*b*-poly(methyl methacrylate) block copolymer additives in polystyrene host, and explored the effect of the host and additive molecular weights. They reported a surface enrichment of the methyl methacrylate groups at the surface when the molecular weight of the polystyrene host was substantially higher than that of the additive. When a high molecular weight additive copolymer was used, however, the surface was actually depleted of methyl methacrylate groups. The absence of surface segregation in materials when the matrix molecular weight is comparable to, or lower than, that of the copolymer additive supports a mechanism based on the differences in polymer configurational entropy between the bulk and the interface.

Tanaka et al.[116] observed the surface enrichment of low molecular weight PMMA in high molecular weight polystyrene films. In this case, the PMMA additive has a higher surface tension than the polystyrene host. The authors explained these observations in enthalpic and entropic terms. First, as the polymers were synthesised using living anionic polymerisation, one chain end is composed of the *sec*-butyl initiator fragment. The surface tension of this end group is substantially lower than that of vinyl polymers, which results in the preferential adsorption of chain ends to the surface. Therefore, with decreasing molecular weight of the low molecular weight additive, and thus increasing density of chain end groups, this effect becomes more significant. Second, the conformational entropic penalty of the polymer chain on the surface decreases with decreasing molecular weight. As a result, when these effects outweigh the difference in surface tension of the main chain parts of the two species, there is enrichment of the higher surface tension component at the film surface.

2.3.2.3 Role of Polymer-Additive Compatibility in Segregation

Flory Huggins Theory

Flory Huggins theory is a useful tool for assessing compatibility of multi-component systems. In this model, Flory and Huggins addressed the statistical thermodynamics of polymer mixing in solution to predict the free energy of mixing (ΔG^{mix}) of polymer solutions.[117,118] This theory uses a lattice model, composed of square cells of volume v_0. This volume approximately corresponds to the volume of a solvent molecule and a segment of the polymer chain. Each site in the lattice is then singly occupied either by a polymer segment or solvent molecule, so that its segments occupy a continuous sequence of cells.

An expression for the enthalpy term of the free energy of mixing, ΔH^{mix}, can be obtained by considering the intermolecular interactions in the system. This is restricted to first neighbour interactions, and considers three types of contact: solvent-solvent, solvent-segment and segment-segment interactions (g_{11}, g_{12} and g_{22} respectively). From these, the enthalpic part of the Gibbs free energy change for the formation of one solvent-segment contact, Δg_{12}, is given by

$$\Delta g_{12} = g_{12} - \frac{1}{2}(g_{11} + g_{22}) \tag{2.22}$$

Then, by determining the number of solvent-segment contacts in the solution, and defining the volume fractions of the solvent and polymer (ϕ_1 and ϕ_2 respectively) using Equations 2.23 and 2.24, where N_1 is the number of solvent molecules

and N_2 is the number of polymer molecules with degree of polymerisation x,

$$\phi_1 = \frac{N_1}{N_1 + xN_2} \tag{2.23}$$

$$\phi_2 = \frac{xN_2}{N_1 + xN_2} \tag{2.24}$$

the enthalpy of mixing can be written as

$$\Delta H^{\text{mix}} = (z-2)N_1\phi_2\Delta g_{12}. \tag{2.25}$$

where z is the number of nearest neighbours of a cell.As Δg_{12} and the lattice parameter are not easily accessible, they can be replaced by a single parameter, the Flory Huggins polymer-solvent interaction parameter, χ. The enthalpy of mixing can therefore be more simply expressed as

$$\Delta H^{\text{mix}} = kTN_1\phi_2\chi \tag{2.26}$$

The Flory Huggins interaction parameter, defined by Equation 2.27, is a temperature-dependent dimensionless parameter, which can yield insight into the compatibility of a system.

$$\chi = (z-2)\frac{\Delta g_{12}}{kT} \tag{2.27}$$

As the Gibbs free energy of mixing can be defined as

$$\Delta G^{\text{mix}} = \Delta H^{\text{mix}} - T\Delta H^{\text{mix}}, \tag{2.28}$$

and the entropy of mixing, ΔS^{mix} can be expressed as

$$\Delta S^{\text{mix}} = -R[n_1 \ln\phi_1 + n_2 \ln\phi_2] \tag{2.29}$$

combining expressions for the entropy and enthalpy of mixing yields the Flory-Huggins equation for the Gibbs free energy of mixing (Equation 2.30).

$$\Delta G_m = RT[n_1 \ln\phi_1 + n_2 \ln\phi_2 + n_1\phi_2\chi] \tag{2.30}$$

Application of Flory Huggins theory to polymer blends

Flory Huggins theory was initially developed to consider the interactions of polymer chains in a solvent. However, it has since been applied to polymer blends, where the second polymer is treated like a solvent. For two polymers, A and B,

Equation 2.30 can be modified to give

$$\frac{\Delta G^{\text{mix}}}{kT} = \frac{\phi \ln \phi}{v_A N_A} + \frac{(1-\phi)\ln(1-\phi)}{v_B N_B} + \frac{\chi\phi(1-\phi)}{v_0} \tag{2.31}$$

where N_A and N_B are the degrees of polymerisation and v_A and v_B are the volume of monomer units of the two polymers. As v_0 is defined as the volume of each site in the lattice, in this case it is usually given by the geometric mean of v_A and v_B.

If χ is assumed to depend only on temperature, volume fraction-temperature phase diagrams can be constructed, which allow determination of the spinodal, binodal, critical point, and upper and lower critical solution temperatures.[119] The spinodal defines the boundary between stability and instability of a single phase mixture with respect to a two phase mixture. At the spinodal, Equation 2.32 holds.

$$\left(\frac{\partial^2 \Delta G\text{mix}}{\partial \phi^2}\right)_{T,p} = 0 \tag{2.32}$$

The binodal refers to the boundary between the stable and metastable compositions, and defines the equilibrium composition of the two phase mixture. It can be determined by equating the chemical potential of the individual components of the two coexisting phases. The point at which the binodal and spinodal curves meet is the critical point.[120] From this value, the critical interaction parameter, χ_c, can be determined, below which any homogeneous composition of the system is stable.

The Flory Huggins parameter is the simplest numerical criterion of compatibility. It has been used to predict polymer-plasticiser compatibility; a good plasticiser has a low χ value and it has been shown that if the interaction parameter exceeds a critical value then phase separation will occur.[121]

Flory Huggins theory is limited in that assumes incompressibility, also treating all interactions as isotropic and thus cannot account for species where interactions are directional. It is therefore inappropriate for dealing with the interactions between charged surfactants and polymers. However, although Flory-Huggins theory is not applicable to systems which are strongly interacting or have directional bonds, a number of modifications have been used, for example the inclusion of a separate term to account for electrostatic interactions, or the inclusion of the electrostatic interactions into the interaction parameters.

For example, Liu et al.[60] determined the phase diagrams of aqueous two-phase systems comprised of water, polethylene glycol and one of the surfactants Triton X-100 or Tween 80. The authors correlated the liquid-liquid equilibrium data using Flory Huggins theory, with 3 interaction parameters, referred to as λ_1, λ_2

and λ_3, where 1, 2, and 3 represent the polymer, nonionic surfactant and solvent respectively. The temperature dependence of the interaction parameters was discussed regarding the surfactant both as single molecules and micellar aggregates. A better fitting effect was observed when the surfactant was considered in micelles and the very low standard deviation (<0.1 %) showed the good descriptive quality and applicability of the Flory Huggins model.

Foroutan et al.[122] used a modified Flory Huggins theory to calculate the phase behaviour of quaternary systems comprising poly-*N*-vinylcaprolactam (PVCL) and polyethylene glycol (PEG) and four salts in water. By including two electrostatic terms (the Debye Hückel and the Pitzer Debye-Hückel-equations), they found good agreement to experimental data.

Solubility Parameters

Solubility parameters (δ) can also be used to evaluate compatibility in mixtures. The Hildebrand parameter is defined in terms of the cohesive energy density, $c_E = -U/V$, where U is the molar internal energy and V is molar volume:

$$\delta = c_E^{0.5} = (-U/V)^{0.5} \tag{2.33}$$

It is also related to the enthalpy of vaporisation by

$$\delta = \left(\frac{\Delta H_{\text{vap}} - RT}{V}\right)^{0.5} \tag{2.34}$$

Hildebrand and Scott[123] showed that molecules with similar c_E will mix readily as there is minimal cohesive exchange energy needed for this interaction. The Hildebrand-Scatchard equation describes the heat of mixing, ΔH_m, of regular solutions of two components based on their solubility parameters (δ_1 and δ_2), where V_m is the volume of the mixture.

$$\frac{\Delta H_m}{V_m} = (\delta_1 - \delta_2)^2 \phi_1 \phi_2 \tag{2.35}$$

For the two components to be miscible $(\delta_1 - \delta_2)^2$ must be small. This approach relies on a number of assumptions, however, such as the interaction forces acting between the centre of the molecules. As a result, this solubility parameter does not describe the enthalpy change of mixing in polar systems well, and notably cannot account for a negative enthalpy of mixing.

Hansen's total solubility parameter (δ_t) splits the Hildebrand solubility parameter into the dispersive component (δ_d), the polar component (δ_p) and the hydrogen bonding component (δ_h) (Equation 2.36). This approach can better

predict the miscibility of polar components, since it can distinguish between materials of differing polarity but similar overall cohesive energy density.[124]

$$\delta_t^2 = \delta_d^2 + \delta_p^2 + \delta_h^2 \tag{2.36}$$

2.3.3 Small Molecule Migration

Whereas thermodynamic parameters such as solubility can predict if segregation will occur, the kinetics of migration are concerned with additive diffusion in the matrix. The distribution and segregation of surfactants during film preparation will be the primary consideration in the frame of this project. However, in order to predict and control the migration of additives, it is essential that the timescales and mechanisms associated with migration and the potential formation of surface structures are understood. It is therefore important to consider the diffusion process of the small molecules in the polymer matrix.

2.3.3.1 Fickian and non-Fickian Diffusion

The diffusion process can be classified based on the relative rates of diffusion and polymer relaxation. Fickian (Case I) diffusion is characterised by a linear dependence of diffusion over time, obeying Fick's first law (Equation 2.37)

$$J = -D\left(\frac{\partial c}{\partial x}\right) \tag{2.37}$$

where J is the diffusion flux in the x direction, c is the concentration of the diffusing species, D is the diffusion coefficient and x is distance. Fick's second law describes how the concentration of the diffusing species changes with time, and is given in 1 dimension by Equation 2.38.

$$\frac{\partial c}{\partial t} = -D\left(\frac{\partial^2 c}{\partial x^2}\right) \tag{2.38}$$

Case II diffusion usually involves a front propagating at a constant velocity, and therefore total sorption is linear with time. Whereas Fickian diffusion rates are proportional to $t^{1/2}$, Case II sorption is observed to be linear with t.[125] Case II diffusion has a diffusion coefficient with a strong concentration dependence, which is not true for Case I diffusion. Other diffusion behaviours also exist, which have a dependence on t^n with n between 0.5 and 1.

2.3.3.2 Measuring Small Molecule Diffusion in Polymers

The diffusion of small molecules in polymers and their migration to surfaces has been studied in a wide range of systems. Much of the work undertaken in this area is in the context of the migration of additives from packaging into food, due to the potential adverse effects on food quality and on human health.[126] Nevertheless, the time-dependent additive concentration profiles of some other polymer/small molecule systems, including a range of polymer-plasticiser systems have also been characterised. An overview of these will be given in the following section.

Small molecule penetration into glassy polymers typically exhibits Case II diffusion, with a sharp diffusion front moving through the polymer at constant velocity. The diffusion of a molecule in a polymer is mainly determined by three factors: the free volume of the polymer, the molecular size of the diffusing species, and the interaction between the diffusing species and the polymer matrix.[127] The penetration of small molecules into polymers has received much interest over recent years, and there have been a number of approaches used to monitor the diffusion of small molecules in polymer films, including the study of the absorption and release of additives in films.

One approach to investigate the kinetics of additive migration out of a film has been analysing the additive concentration after extracting the remaining diffusing species. This method was employed by Haider and Karlsson[128] to monitor the diffusion coefficient of antioxidants from polyolefin films. Hsu et al.[129] used FTIR microspectroscopy to map the concentration profile of a UV stabiliser in polypropylene plaques after placing the powdered stabiliser in contact with the neat plaque, and obtained diffusion coefficients from the concentration profiles. Sanke and Hirt[130] also used FTIR microspectroscopy to track the profiles of erucamide (1,3-*cis*-docosenamide) slip agents diffusing out of thick ($\sim$50 µm) films of linear low-density polyethylene (LLDPE) and a polyolefin plastomer (PO). They identified a greater accumulation of the additive at the surface of the polyolefin plastomer compared to the linear low-density polyethylene, alongside a greater rate of additive migration from the PO, highlighting the dependency of the polymer matrix on the rate of additive partitioning.

Neutron reflectivity has also been used to study small molecule diffusion at polymer interfaces. This technique allows accurate determination of the interfacial profile between interdiffusing species and the width of the interface. An "anneal-quench" procedure can be used, where a sample is heated for a given time, before it is rapidly quenched and a reflectivity profile is collected, from which the distribution of the additive can be determined. This approach has proven to be successful in monitoring the diffusion of amorphous polymers when the glass

transition temperature is above room temperature. An example of the use of this approach is in the work by Geoghegan et al.[93] who measured the kinetics of the growth of surface enriched layers of deuterated polystyrene in a blend with fully hydrogenated polystyrene. However, this approach has also been extended to the diffusion of small molecules in polymer matrices. For example, Smith et al.[131] measured the diffusion, surface enhancement and evaporation of a plasticising additive from polymer films using neutron reflectivity and an "anneal-quench" procedure.

The "anneal-quench" method cannot easily be used, however, if the polymer of interest has a glass transition below room temperature, or if the ingress of small molecules is to be studied. An alternative approach to enable real-time measurement was therefore demonstrated by Bucknall et al.[125] Although a measurement time of 1-2 hours is usually required for the collection of a reflectivity profile over the full available (Q) range, by measuring at a single angle, a reflectivity profile over a limited Q range can be collected within a few minutes. One approach to real-time NR involves preparing a bilayer of two polymers of which interdiffusion is to be measured on the substrate, and then using a heated sample stage to anneal the sample, quickly aligning the sample before collecting the reflectivity profile. However, this approach is not possible if diffusion occurs below the T_g of the polymer. In order to study the ingress of smaller molecules into polymer films, Bucknall et al.[125] therefore used a special reflectivity cell that allowed the penetrant to come into contact with the polymer film on a remotely controlled stage, after the sample had been aligned in the neutron beam. This method allows data collection to begin the moment than contact between the polymer and penetrant is made, which is particularly important for rapidly changing systems.

This method was first used to obtain interdiffusion coefficients for hydrogenated and deuterated polystyrene, but subsequently enabled the diffusion of plasticisers (oligo methyl methacrylate and polyethylene glycol oligomers) in deuterated poly(methyl methacrylate) to be studied. By determining the composition of the layers in the sample from the obtained reflectivity profiles, the velocity of the diffusion front could be calculated, which could subsequently be used to evaluate diffusion coefficients of the plasticisers.[125] This approach was also used to study the penetrant behaviour of phthalate ester plasticisers of different molecular weights in thin PMMA films. Bucknall et al.[127] showed that the plasticisers diisononyl phthalate (DINP, 418.6 g mol^{-1}) and dioctyl phthalate (DO, 390.5 g mol^{-1}) penetrate the polymer and swell the film. This swelling was found to occur in three phases: first, during an "induction phase" lasting a few minutes, the thickness of the dPMMA layer was constant, although an increase in

interfacial width between the polymer and plasticiser layers was observed. This was associated with the establishment of a gel layer between the dPMMA and the plasticiser. Following this induction phase, a rapid increase in dPMMA layer thickness in both plasticiser systems with a linear time dependence was observed. This stage was therefore associated with the ingress of the plasticisers into the polymer at a certain velocity, indicative of a Case II diffusion process. By determining this velocity, a lower rate of ingress into the polymer film was identified for the larger, less mobile DINP. Finally, a second, much slower, phase of growth was observed. This phase of growth could also be described by a linear time dependence. The authors attributed this phase to a balancing of the osmotic pressure, causing a "suction of plasticiser" into the polymer and a misfit-induced pressure.

2.3.3.3 Migration Mechanisms

A number of approaches have been taken in order to develop a better mechanistic understanding of the displacement of small molecules in polymer matrices. An area of particular relevance is the work undertaken on the surface segregation of long-chain fatty acid slip agents in polyolefins. In particular, there has been a substantial body of work into the behaviour of slip additives such as erucamide. Although the studies into the diffusion of small molecules in polymer films have been prevalent,[132] these longer chain molecules (C22 for erucamide) are relevant when considering the migration of additives such as surfactant molecules in polymer films, and thus will be reviewed in the following section.

Quijada-Garrido et al.[133,134] determined the diffusion coefficient of erucamide in an isotactic polypropylene (iPP) film. By studying the desorption rate of the additive, they determined that at low erucamide concentrations (4.6 and 8 %) the kinetic curves show good agreement with Fickian law. However, at higher additive loading (24 and 44 % erucamide), diffusion of erucamide to the film surface occurs by a non-Fickian mechanism. This was accounted for by the incompatibility of erucamide with iPP, and the microstructure of the films, which consist of polypropylene spherulites (with amorphous regions between the lamellae) and globules of excess erucamide. The results could therefore be explained by assuming two transport processes. The authors proposed a model comprising a linear superposition of two simultaneous Fickian diffusion processes: the diffusion of the additives in the amorphous regions of the spherulites, and the release of the additive from the globules into the spherulites. This highlights the importance of the morphology of the films in additive diffusion. From the temperature dependence of the diffusion coefficients, the authors identified that this two-Fickian

diffusion model follows an Arrhenius type relationship, (Equation 2.39), where E_d is the activation energy and D_0 is the pre-exponential factor, and were able to estimate activation energies. Furthermore, they could to use the diffusion data to estimate the solubility of erucamide in iPP as a function of temperature, by extrapolating the diffusion data to a penetration depth equal to zero.

$$D = D_0 \exp\left(\frac{-E_d}{RT}\right) \tag{2.39}$$

Quijada-Garrido et al.[40] also investigated the diffusion of erucamide in nylon 12, finding that the observed concentration profiles showed good agreement with Fickian law at all concentrations, contrasting the diffusion of the additive in iPP. This again demonstrates the importance of morphological factors, including inter- and intramolecular hydrogen bonding, in diffusion behaviour. This also highlights the necessity of understanding the location of the additive molecules in semicrystalline systems in order to predict behaviour.

In another study, Taraszka and Weiss[135] observed similar behaviour for the diffusion of *N*,*N*-dioctadecylaniline in a low-density polyethylene film, identifying two simultaneous Fickian processes that could be fitted to a dual pathway model. This was interpreted as being due to the presence of a series of barriers associated with the movement of a molecule as it migrates among many host sites. The authors suggested that the faster component is attributable to the diffusion of molecules within the amorphous domains of the polymer, with the slower component attributable to diffusion within the interfacial regions between the amorphous regions and microcrystallites. This contrasts the diffusion behaviour of the much smaller *N*,*N*-dimethylaniline, which could be fit to a series expansion form of Fick's second law with a single diffusion coefficient, and showed much faster diffusion, demonstrating that this molecule experiences a different rate-limiting step.

Wakabayashi et al.[43] developed a model that adequately described the blooming of erucamide and behenamide (another anti-slip agent) to the surface of isotactic polypropylene films, highlighting the importance of both additive solubility in the host polymer and the diffusion coefficients in this process. In their model, the additive dissolves in an amorphous region until saturation solubility is reached. The additional additive migrates to the film surface at a speed according to the diffusion process, in accordance with the findings of Quijada-Garrido et al.[133,134] This model was modified to account for the different contributions of the amorphous and crystalline regions of the polymer by considering that a portion of the excess additive beyond the saturation solubility was restricted within the crystalline regions (consisting of spherulites), with the remaining excess additive

localised in the amorphous regions. The extent of restriction within crystalline regions was assumed to increase according to the initial amount of additive. By assessing the temperature dependence of the diffusion of these two additives, the authors identified that the diffusion coefficients follow the Arrhenius rule (Equation 2.39).

Wakabayashi et al.[44] showed that the values of activation energy and pre-exponential factor are larger for behenamide than for erucamide. They postulated that the differences in the diffusion behaviour of the two additives are the result of the self-association of behenamide, which gives the diffusing species a larger size. As a result, behenamide becomes more easily restricted within the crystalline regions in the spherulites, where diffusion is slower. The difference in the diffusion coefficients of additives in this two-step transport between the amorphous and crystalline regions in an ethylene copolymerised polypropylene film was later corroborated using molecular dynamics simulations, which demonstrated the significance of self-association by hydrogen bonding.[136] This proposed two-step diffusion model could also adequately explain the blooming process of UV stabiliser additives, such as 2-(2H-benzotriazol-2-yl)-4-(1,1,3,3,-tetramethylbutyl)phenol and 2-(2H-benzotriazol-2-yl)-4-methylphenol.[44] This highlights the importance of considering additive self-assembly when attempting to understand additive migration in a matrix.

Effect of additive structure on migration

No general diffusion model can predict the broad range of diffusion coefficients of organic solutes in solid polymers. However, various efforts have been undertaken to correlate additive structure with diffusion behaviour in polymer films, in order to better understand the diffusion.

From the analysis of diffusion coefficients of several categories of molecules in polyolefins, Vitrac et al.[137] highlighted the strong dependence on additive molecular weight, M. D was found to be related to M by $D \propto M^{-\alpha}$, with values for α typically greater than 2.

Fang et al.[66,138] investigated the diffusion of aromatic solutes in aliphatic polymers above the T_g in order to provide a polymer-independent description of the dependence of the diffusion coefficient on molecular weight. Using a number of homologous series of bulky aromatic solutes in different polymers, they introduced several scaling relationships based on $D \propto M^{-\alpha(T-T_g)}$, showing that aromatic solutes have a parallel behaviour to linear aliphatic solutes, but with a temperature shift $(T - T_g)$. Diphenylalkanes, where a flexible unit is present between the two phenyl rings, were associated with a much larger temperature

shift. These dramatic effects of the solute chemical structure were found to be independent of the aliphatic polymer.

Reynier et al.[139] correlated the diffusion coefficients of a broad set of molecules, with molecular weights ranging from 100 to 800 g mol^{-1}, to parameters describing their size, shape and flexibility, enabling their classification according to their modes of displacement. One such diffusion mode is a crawling mode which relies on the large number of degrees of freedom of long alkyl chains. Other, more rigid, molecules diffuse by jumps, from one free volume site to another. This mode is common for molecules such as heterocycles. Intermediate diffusion behaviours were also observed, which can be described by jump displacements facilitated by the easy relaxation of other parts of the molecule. By introducing the concept of weighted fractionated volume, which corresponds to the sum of the different partial volumes from groups in the molecule, in order to evaluate the influence of the flexibility, it is possible to classify molecules according to the modes of displacement.

Wang et al.[126] used molecular dynamics simulations to investigate the diffusion behaviour of additives in polypropylene. They reported that the diffusion of the additive is attributed to a number of factors including the interaction energy between the diffusant and the polymer; a strong interaction between the polymer and the diffusant decreases the diffusion coefficient. Diffusion is also affected by free volume, molecular weight, molecular size and shape, as well as the mobility of the polymer chains. Larger molecules, particularly those with rigid parts, need large free volume holes to diffuse (correlating well with the earlier work of Reynier et al.),[139] which results in a lowering of their diffusion coefficients. Greater flexibility of the polymer chains provides more opportunities for diffusion through transport channels. These findings demonstrate the importance of additive structure on their mobility, and thus migration, in a polymer matrix. In addition, the relevance of free volume in additive diffusion indicates the value in measuring the free volume properties of model systems in order to better understand, and ultimately predict, migration behaviour.

2.3.3.4 Additive Loss

An additional consideration when studying the surface segregation of small molecules is additive loss from films. This may be particularly significant for the low molecular weight plasticiser molecules.

Loss of plasticiser is one of the main degradation mechanisms of plasticised polymer products, and will decrease the flexibility, toughness and extensibility of the material. It can also lead to the contamination of the surrounding environ-

ments, which is a problem for many industries such as food packaging, medical materials or toys.[140] Although plasticisers can be lost into neighbouring polymers or liquids (such as biological fluids or food),[67] only evaporation into the air is of relevance to this project, and thus will be primarily considered here.

Calvert and Billingham[141] developed a theoretical model to describe the loss of additives from a polymer in terms of three variables: evaporation rate, diffusion coefficient and additive solubility. If the additive concentration is above its saturation solubility in the polymer, the additive can bloom on the surface. If the additive concentration is below its saturation solubility, however, blooming cannot occur and rate of additive loss is determined by volatilisation and diffusion.

Considering the case where an additive is below its saturation solubility in the polymer, the migration of plasticiser from polymers to a gas phase is a two step process, involving the diffusion from the bulk polymer to the surface, and the subsequent evaporation to the gas phase. The initial diffusion process can be described by Fick's second law (Equation 2.38). The diffusion coefficient of the plasticiser generally increases with plasticiser concentration, as a result of its greater mobility in the polymer as free volume increases. The concentration (C) dependence of D can be described by an exponential function (Equation 2.40),

$$D(C) = D_{C0}e^{\alpha C} \tag{2.40}$$

where D_{C0} is the zero-concentration diffusion coefficient and α relates to the plasticisation efficiency of the plasticiser. Alternatively, the concentration dependent evaporation can be expressed in terms of the free volume (f) of the polymer upon plasticiser incorporation (Equation 2.41), where A and B are constants.[142]

$$D = Ae^{-B/f} \tag{2.41}$$

The overall rate of plasticiser loss is determined by the slower process, and thus the process is either diffusion- or evaporation-controlled. In the diffusion-controlled case, evaporation is faster than the diffusion of the plasticiser to the surface. In the evaporation-controlled case, evaporation is slower than the rate of diffusion to the surface, which can lead to the formation of a thin film of plasticiser on the surface.[142]

The rate of evaporation (ν_0) of the plasticiser from a strip of width l over which gas flows at velocity u can be calculated by applying the mass transfer theory of evaporation from a stationary liquid into a stirred gas, given by Equation 2.42,[143]

$$\nu_0 = 0.33\left(\frac{u^{\frac{1}{2}}}{l^{\frac{1}{2}}}\right) S_g D_g^{\frac{2}{3}} \left(\frac{\rho}{\mu}\right)^{\frac{1}{6}} \tag{2.42}$$

where S_g is the concentration of the plasticiser in the gas phase, D_g is the diffusion coefficient in the gas phase, and ρ and μ are the density and viscosity of the gas phase respectively. As rate of evaporation is zero when gas flow is zero, this does not allow for loss of volatilised components when it has to diffuse through still air. Nevertheless, using this approach, Bellobono et al.[143] have found good agreement with experimentally determined values of ν_0.

The dominating mode of diffusion depends on a number of factors including temperature and the characteristics of the polymer and plasticiser. Factors affecting small molecule diffusion in polymers have been previously discussed, and are equally important in diffusion-limited plasticiser loss. However, in an evaporation-limited case, plasticiser loss is not affected by interactions between the polymer and plasticiser, and is thus mainly affected by temperature and the properties of the plasticiser, including its molecular shape and vapour pressure, as well the gas surrounding the polymer (flow rate and volume).[142]

Smith et al.[144] studied the diffusion, evaporation and surface enrichment of a plasticising additive in a thin film of a segmented polyester-polyurethane thermoplastic polymer. By determining the volume fraction profiles of the plasticiser using neutron reflectivity, they found that the diffusion of the plasticiser is sufficiently rapid that the concentration can adjust itself throughout the film over timescales much shorter than that of the rate of mass loss due to evaporation. In this case, plasticiser loss was therefore determined to be evaporation-limited. It should be noted, however, that neutron reflectivity is not very sensitive to gradual variations in concentration. A flat concentration profile of a volatile additive is therefore indicative of an evaporation-limited loss process, and could therefore be useful in assessing additive loss in the model systems considered in this thesis.

By identifying the migration mode for different polymer-plasticiser systems, Wei et al.[142] determined that evaporation is generally rate-limiting for plasticiser loss at low temperatures, with diffusion rate-limiting at higher temperatures. They were able to identify a transition temperature at which there is a change in the rate limiting process. For example, this occurs between 110 and 120 °C for a PVC-di(2-ethylhexyl)phthalate (DEHP) system, and between 90 and 120 °C for a nitrile butadiene rubber-DEHP system.

The Hertz equation (Equation 2.43) relates the rate of evaporation (ν_0) to the partial pressure of the plasticiser, p, temperature, T, plasticiser molecular

weight, M, and the rate constant plasticiser transfer from the material, k.[145]

$$\nu_0 = \frac{p}{\sqrt{2MkT}} \tag{2.43}$$

As the partial pressure is largely affected by the volatility of the plasticiser, molecules with a high enthalpy of vaporisation (and therefore high boiling point) should have a slow rate of evaporation. However, despite having a boiling point of 290 °C,[146] evaporation of glycerol from thin PVA films has previously been identified.[147] Loss of a range of additive molecules, including surfactants as well as plasticisers, could therefore be significant throughout this work. Whereas much of this thesis considers the distribution of surfactants established during spin-coating, additive loss will become increasingly important in the context of heating and ageing polymer films containing low molecular weight additives.

2.4 Summary

In this thesis, the overarching objective is to explore the segregation of a range of additives in spin-cast PVA films in order to understand the factors responsible for this behaviour. By building on current understanding of factors affecting additive distribution in polymers, as well as the interactions between polymers and surfactants in solution, that have been presented in this chapter, the aim is to provide insights into model films that can ultimately translate to predictive models and industrial systems.

Chapter 3

Methods

3.1 Materials

The following PVA resins were purchased from Sigma Aldrich and used as received.

Table 3.1: Details of PVA resins

Material Reference	Product	M_w/ kg mol^{-1}	DH /%
PVA-70-88	P8136	30-70	87-90
PVA-23-98	348406	13-23	98
PVA-23-88	363170	13-23	87-89
PVA-50-98	363138	31-50	98-99
PVA-50-88	363073	31-50	87-89
PVA-125-98	563900	130	99
PVA-125-88	81365	130	88

The surfactants sodium dodecyl sulfate (SDS), *N*,*N*-dimethyldodecylamine *N*-oxide (DDAO), *N*,*N*-dimethyltetradecylamine *N*-oxide (DTAO), pentaethylene glycol monododecyl ether ($C_{12}E_5$), and cetyltrimethylammonium bromide (CTAB), and plasticisers glycerol and propylene glycol were purchased from Sigma Aldrich and used as received.

Deuterated analogues of SDS, $C_{12}E_5$, DDAO and DTAO were synthesised at Rutherford Appleton Laboratories. All 25 hydrogen atoms of the alkyl chain in SDS were labelled. All hydrogen atoms in the long alkyl chains of the amine oxide surfactants (25 and 29 hydrogen atoms for DDAO and DTAO respectively) were labelled, but hydrogen atoms on the methyl groups were not labelled. Only hydrogen atoms on the hydrocarbon chain of $C_{12}E_5$ were labelled (d_{25}), with the hydrogen atoms present in the ethylene glycol repeat units unlabelled. Deuterated analogues of glycerol (99 % isotopic enrichment) and propylene glycol (98

% isotope enrichment) were purchased from CK isotopes. Only the non-labile carbon-bonded hydrogen atoms in the plasticiser molecules were labelled in order to prevent isotope exchange between labile -OH and -OD groups on the plasticiser, polymer and solvent.

3.2 Film Preparation

The majority of the work comprising this thesis is performed using thin, spin cast films of poly(vinyl alcohol) and additives. For most neutron reflection and AFM measurements, films were spin cast from aqueous solutions with a total solute concentration of 4 wt.%.

To prepare these films, PVA was dissolved in deionised water by heating to 75 °C with stirring to create 4 wt.% solutions. Similar aqueous solutions of other components (surfactants and plasticisers) were also prepared at 4 wt.%. Solutions containing the desired proportion of the polymer with surfactant and/or plasticiser with a total solute concentration of 4 wt.% were prepared by mixing the relevant solutions. These solutions were spin-cast into films of 40-100 nm, varying with surfactant and glycerol content, by using a rotational speed of 3500 rpm during the drying stage. For neutron reflectivity measurements, solutions were spin-cast onto 55 mm diameter, 5 mm thick silicon blocks that had been first cleaned using permanganic acid, and subsequently acetone, to remove traces of hydrophobic impurities and ensure film consistency. For AFM measurements, solutions were spin-cast onto 0.75 mm thick silicon wafers (approximately 15 × 15 mm). For ion beam measurements, thicker films (150 nm) were prepared by spin-casting from solution, with total solute concentrations of 6 wt.% onto the same type of wafers as for AFM experiments but typically with a slightly larger area.

3.3 Neutron Scattering

Neutron scattering can be a powerful technique for the study of soft matter systems. The neutron is a subatomic particle, that also behaves as a wave, with its wavelength, λ, given by the de Broglie relationship,

$$\lambda = h/mv \tag{3.1}$$

where h is Planck's constant and m and v are the mass and velocity of the neutron respectively.

Neutrons can either be scattered through interactions with the nucleus or through the interactions of unpaired electrons with the magnetic moment of the neutron. However, only nuclear scattering with be used in this work.

The momentum transfer vector, Q, is defined as the difference in the momentum of the incident wave ($\mathbf{k}_i$) and the final wave ($\mathbf{k}_f$), described by Equations 3.2 and 3.3, and illustrated in Fig. 3.1. In this thesis, only elastic neutron scattering will be considered, where no energy changes occur during the collision.

$$|\mathbf{k}_i| = |\mathbf{k}_f| = \frac{2\pi}{\lambda} \tag{3.2}$$

$$Q = |\mathbf{k}_i - \mathbf{k}_f| = \frac{4\pi}{\lambda} \sin\theta \tag{3.3}$$

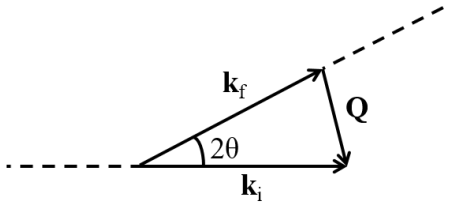

Figure 3.1: Schematic of elastic neutron scattering.

Substituting Equation 3.3 into Bragg's Law, Equation 3.4, yields Equation 3.5, which expresses the relationship between the size of objects under study and the momentum transfer vector.[148]

$$n\lambda = 2d \sin\theta \tag{3.4}$$

$$Q = \frac{2\pi}{d} \tag{3.5}$$

The strength of the interaction between the neutron and the nuclei is governed by the scattering length of the nucleus, b. The amplitude of the wave squared determines the probability of finding the neutron at that point in space and b^2 represents the probability of the neutron being scattered somewhere in space, per nucleus, per incident neutron, per solid angle. As solid angle is expressed in steradians and there are 4π steradians in a sphere, the probability of a neutron being scattered is $4\pi b^2$. This quantity is termed the scattering cross section, σ, which is a measure of the scattering power of a material and is isotope dependent. It should be noted that some nuclei, such as hydrogen, possess a negative value for b, which still gives rise to a positive value of σ. The difference in scattering lengths of different isotopes is the origin of contrast in this technique. In particular, there is huge difference in scattering length of hydrogen and deuterium, which have both

different magnitudes and different signs. This highlights one main advantage of neutron scattering: selective deuteration of parts of the sample can be used to manipulate the contrast.[149,150] In order to consider the probabilities of neutrons being scattered into a solid angle element, $d\Omega$, the differential cross section, $\frac{d\sigma}{d\Omega}$ can be defined.

The total scattering cross section is a sum of two components: the coherent and incoherent cross sections,

$$\sigma_{\mathrm{s}} = \sigma_{\mathrm{coh}} + \sigma_{\mathrm{incoh}}. \tag{3.6}$$

The incoherent term accounts for the correlation between the position of the same nucleus at different times, and the coherent cross section involves correlation between the position of different nuclei. Structural information on samples is contained in the coherent component, but the incoherent component contributes only to noise.[150]

3.3.1 Small Angle Neutron Scattering

Small angle neutron scattering (SANS) can be used to obtain structural information about a system, including the size, polydispersity and interactions within a wide range of disordered materials. SANS is capable of probing lengthscales from approximately 1-100 nm, depending on the neutron wavelength and instrument geometry.[150]

Lengthscales are explored in reciprocal space by detecting the number of scattered neutrons as a function of the scattering vector, Q. As Q is related to the wavelength and scattering angle (2θ) by

$$Q = \frac{4\pi \sin(\theta)}{\lambda} \tag{3.7}$$

and Q is related to distance by Equation 3.5, the use of very small incident angles allows the larger structures of polymers and surfactants to be probed.

When probing large-scale structures (such as polymer and surfactant assemblies), the lengthscales in question are much greater than atomic dimensions. It is therefore helpful to define the scattering length density of the material. The scattering length density, ρ, is calculated according to Equation 3.8 from the scattering length contributions b_i of each atom in a unit cell of volume, v_m. M and D represent the molar mass and the density of the material respectively.

$$\rho = \frac{\Sigma_{i=1}^{n} b_i}{v_m} \quad \text{where} \quad v_m = \frac{M}{D} \tag{3.8}$$

SANS measures intensity, often called $I(Q)$, which is formally defined as the absolute differential scattering across section, $\frac{d\Sigma}{d\Omega}$. $I(Q)$ has units of reciprocal centimetres and represents the probability of a neutron of wavelength λ being scattered, per unit solid angle, at that Q.[150]

Experimental Procedure and Fitting

SANS measurements were carried out on solution cast films, approximately 70 µm thick. The Larmor instrument at ISIS was used with a incident beam, yielding a fixed momentum transfer range of approximately $0.003 < Q < 0.7$ Å^{-1}. Scattering was recorded as 2D detector images, and was seen to be uniform in all directions for each sample. The 2D images were then radially-averaged to give the differential scattering cross-section, after reduction to correct for detector efficiency and background scattering from the substrate. Data modelling was conducted using the software Sasview.[151] A broad peak mode was used to fit the data. This will be discussed more extensively in Chapter 6, but an example set of data and its fit is shown in Fig. 3.2.

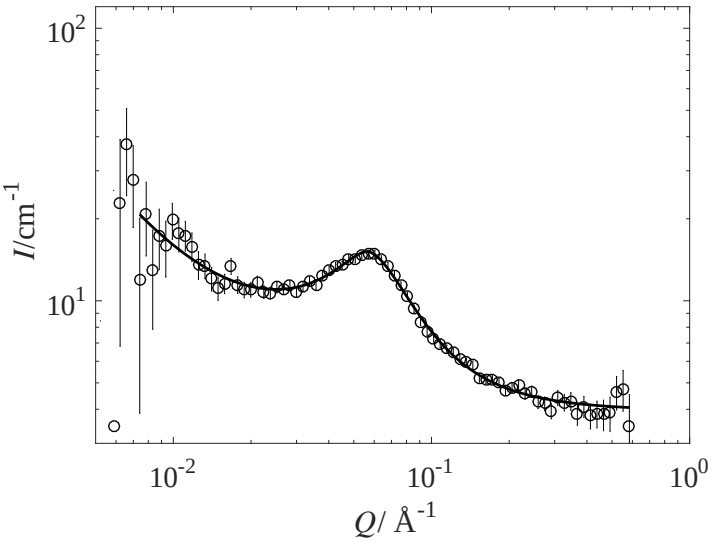

Figure 3.2: SANS data and broad peak model fit for PVA containing 5 wt.% DDAO.

3.3.2 Neutron Reflectivity

In contrast to SANS, a bulk technique, neutron reflectivity (NR) is a surface-sensitive depth profiling technique. Neutrons are capable of reflection and refraction when passing between media. NR usually involves measuring the specular reflection, (where the angle of incidence is equal to the angle of reflection), as a function of the wavevector perpendicular to the surface, when a highly collimated

beam of neutrons is directed onto an extremely flat surface. This is illustrated in Fig. 3.3. Reflectivity is determined by the refractive index profile perpendicular to the interface. As refractive index is related to the scattering length density, reflectivity measurements provide information about the composition profile perpendicular to the surface. It is a powerful technique for probing both surface structures and buried interfaces on the nanometre scale.[150,152]

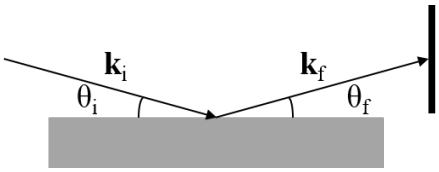

Figure 3.3: Schematic of specular neutron reflectivity.

As Golderger and Seitz[153] showed that neutrons follow the same laws as electromagnetic radiation with the electric vector perpendicular to the plane of incidence, formalisms from classical optics can be used. As in classical optics, the refractive index, n, is defined as

$$n = \frac{k_2}{k_1}, \tag{3.9}$$

where k_2 and k_1 are the wavevectors inside and outside the medium respectively. Although it is possible to measure reflection at non-specular angles to obtain information on the in-plane sample structure, here only specular reflection will be considered. It should therefore be noted that the only change in wavevector is perpendicular to the interface (in the z-direction).

For most materials, a good approximation for n is given by

$$n \approx 1 - \frac{\lambda^2 \rho}{2\pi}, \tag{3.10}$$

where ρ is defined as the scattering length density of the medium and λ is the neutron wavelength. As usually $n < 1$, total external reflection occurs from most materials (N.B. this contrasts with the behaviour of light, where $n > 1$, and thus the opposite change in wavelength occurs, resulting in *internal* reflection).

The critical angle, θ_c, below which total reflection occurs is given by Snell's law,

$$\cos\theta_c = \frac{n_2}{n_1}. \tag{3.11}$$

There is a simple relationship between the critical angle, neutron wavelength and the scattering length density of the matrerial,

$$\theta_c = \lambda\sqrt{\frac{\rho}{\pi}}, \tag{3.12}$$

and the critical value for the wave transfer vector, Q_c, is given by

$$Q_c = \sqrt{16\pi\rho}. \tag{3.13}$$

Neutron radiation is partly reflected and partly transmitted at each interface. Again, using classical optics, the reflectivity, R, from a single interface is given by Fresnel's law, where $R = 1$ for $\theta < \theta_c$ and R is given by Equation 3.14 for $\theta > \theta_c$. This is illustrated in Fig. 3.4.

$$R = \left|\frac{n_1 \sin\theta_1 - n_2 \sin\theta_2}{n_1 \sin\theta_1 + n_2 \sin\theta_2}\right|^2. \tag{3.14}$$

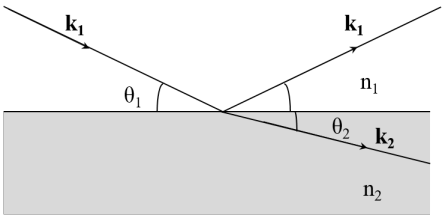

Figure 3.4: Schematic of specular neutron reflectivity from a single interface.

With the Born approximation, which assumes that a neutron is only scattered once while passing through the sample, and weak multiple reflection processes can be ignored, an expression for the reflectivity can then be obtained as

$$R(Q) = \frac{16\pi^2}{Q^4}\left|\int \rho(z)\, \mathrm{e}^{izQ}\, dz\right|^2, \tag{3.15}$$

and from a single interface, this reduces to a simple expression with a Q^{-4} power law (Fig. 3.5),

$$R(Q) = \frac{16\pi^2}{Q^4}\Delta\rho^2. \tag{3.16}$$

From a single thin film at an interface (illustrated in Fig. 3.6), reflectivity becomes

$$R(Q) = \left|\frac{r_{01} + r_{12}e^{i\beta}}{1 + r_{01}r_{12}e^{i\beta}}\right|^2, \tag{3.17}$$

where r_{ij} is the Fresnel coefficient at the ij interface, defined as

$$r_{ij} = \frac{(p_i - p_j)}{(p_i + p_j)} \quad \text{with} \quad p_i = n_i \sin\theta \tag{3.18}$$

and β_i is the optical path length of the film,[152]

$$\beta_i = \frac{2\pi}{\lambda} n_i d_i \sin\theta_i. \tag{3.19}$$

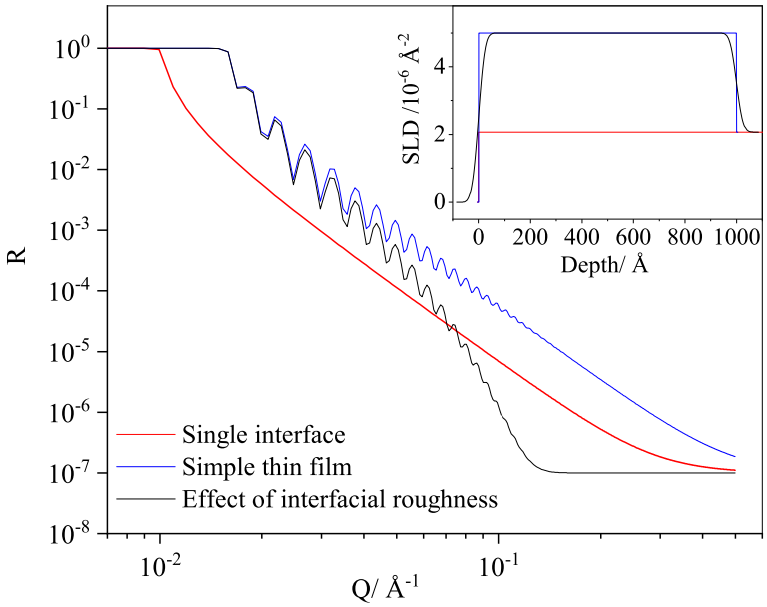

Figure 3.5: Theoretical reflectivity from a bare silicon-air interface (red), from a perfectly smooth 1000 Å film with SLD of 5×10^{-6} Å^{-2} (blue) and the same film with 20 Å interfacial roughness (black). Corresponding SLD profiles are shown in the inset.

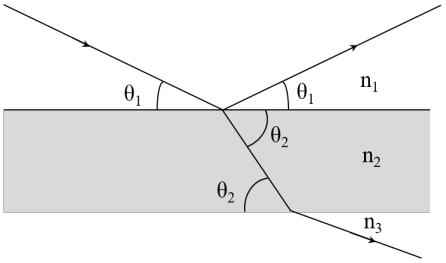

Figure 3.6: Schematic of specular neutron reflectivity from a thin film.

Fig. 3.5 shows reflectivity from a simple thin film, resulting in the presence of Kiessig fringes due to the constructive and destructive interference of the waves reflected from the two interfaces. The spacing of the Kiessig fringes is given by

$$\Delta Q = \frac{2\pi}{d}. \tag{3.20}$$

Although this approach to to calculate the exact reflectivity can be extended to three or four layers, calculating reflectivity from a system with many layers requires a general technique, such as the approach described by Born and Wolfe;[154]

applying the conditions that wave functions and their gradients are continuous at each interface gives a characteristic matrix for each layer,

$$\mathbf{M}_j = \begin{bmatrix} \cos\beta_j & -(i/p_j)\sin\beta_j \\ -ip\sin\beta_j & \cos\beta_j \end{bmatrix} \tag{3.21}$$

where p_j and β_j were previously defined by Equations 3.18 and 3.19 respectively. The resultant reflectivity can then be calculated from the product of the characteristic matrices for each layer, $\mathbf{M}_R = [\mathbf{M}_1][\mathbf{M}_2]...[\mathbf{M}_n]$,

$$R = \left| \frac{(M_{11} + M_{12}p_s)p_a - (M_{21} + M_{22})p_s}{(M_{11} + M_{12}p_s)p_a + (M_{21} + M_{22})p_s} \right|. \tag{3.22}$$

These calculations are only valid for smooth interfaces. However, in real samples there is likely to be interfacial roughness, or a diffuse interface which will modify the specular reflectivity by a Nevot-Croce factor

$$R = R_0 \exp(-q_o q_1 \sigma^2), \tag{3.23}$$

where σ is the root mean square roughness and $q_i = 2k\sin\theta$ ($k = 2\pi/\lambda$). Fig. 3.5 shows that upon inclusion of roughness the reflectivity decays more rapidly than Q^{-4}.

The matrix method described above is incapable of accounting for surface roughness, and therefore an alternative formulation is required. One such method is that of Abeles,[155,156] which applies a Gaussian roughness to the Fresnel coefficients of each interface (Equation 3.24) and then defines the characteristic matrix for each layer as in Equation 3.25.

$$r_{ij} = \left(\frac{p_i - p_j}{p_i + p_j}\right) \exp[-0.5(q_i q_j \sigma^2)], \tag{3.24}$$

$$\mathbf{C}_M = \begin{bmatrix} e^{i\beta_{m-1}} & r_m e^{i\beta_{m-1}} \\ r_m e^{-i\beta_{m-1}} & e^{-i\beta_{m-1}}. \end{bmatrix} \tag{3.25}$$

For N layers, the resultant matrix, $\mathbf{M}_N = [\mathbf{M}_1][\mathbf{M}_2]...[\mathbf{M}_{M+1}]$, then yields the reflectivity

$$R = M_{21}M_{21}^*/M_{11}M_{11}^*. \tag{3.26}$$

Experimental Procedure

Specular neutron reflectivity measurements were taken using the INTER, OFFSPEC and CRISP reflectometers at ISIS.

Deuterium labelling of additives was used to provide contrast via the difference

in scattering length density (SLD) of the components. A complete reflectivity profile, from critical edge to background, was collected using three incident angles (generally 0.25°, 0.6° and 1.5°) in order to obtain a momentum transfer range of $0.008 < Q/\text{Å}^{-1} < 0.47$. This required an acquisition time of between 1 and 2 h per sample (depending on the reflectometer).

For all data collected on the reflectometers at ISIS, the reflectivity at $Q > 0.25$ Å^{-1} is dominated by the sample-dependent background, arising primarily from incoherent scattering. For these measurements, a constant background, determined from reflectivity in the limit of high Q is assumed.

Fitting

The MOTOFIT package[157] was used to fit the reflectivity data to scattering length density profiles, with a least-squares approach to minimize the deviation of the fit. The reflectivity is calculated using the Abeles matrix method for stratified interfaces.[155] The scattering length density profiles, $\rho(z)$, were optimised using a genetic algorithm in which the layer thicknesses, scattering length densities, and roughnesses are varied to minimize χ^2 between the measured and calculated reflectivities. The obtained profiles typically include 3 layers, corresponding to a surface excess, bulk film, and substrate, with each layer characterised by a scattering length density, a thickness and a Gaussian roughness value. SLD-depth profiles could be converted into volume fraction, $\phi(z)$, profiles in order to calculate the surface excess, z^*, total additive volume fraction in the films, ϕ_{tot}, and fraction of segregated surfactant, f. This is described more thoroughly in Chapter 4. Reported errors in these values are obtained by adding the fitting errors on the relevant parameters in quadrature.

An example set of data and the fit, alongside the corresponding SLD profile is shown in Fig. 3.7. This fit consists of three layers, corresponding to a thin surface excess layer (depth < 2 nm), the bulk film (2 < depth < 82 nm), and the silicon oxide substrate layer (> 82 nm).

3.4 Image Analysis

In order to scale the SANS data to account for the varying thickness of films and quantify $I(Q)$ in units of cm^{-1}, image analysis was used to accurately determine the area of the irregularly shaped films so that thickness could be calculated from their mass and density. This is a more reliable approach than using callipers, which would be likely to damage the relatively soft film and yield low values for sample thickness. Images were captured using a diffuse light source and

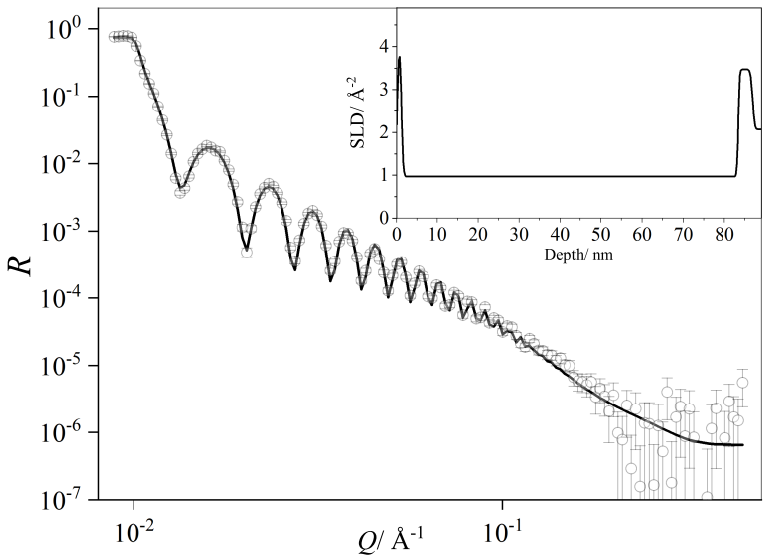

Figure 3.7: Example set of NR data and fit, corresponding to a hydrogenated polymer film with thin surface excess (cast onto a silicon substrate).

image analysis was subsequently performed using ImageJ.[158] The stages of image processing are shown in Fig. 3.8. First, channels of the initial image (3.8a) were split, and only the red channel (3.8b) was used. To remove background, maximum, minimum and Gaussian blur filters were applied to a duplicate image which was subtracted from the original red-channel image. Threshold levels were adjusted to produce 3.8c, and particle analysis was used to determine the film area. The final image 3.8d shows an overlay onto the original red channel image to confirm it captures the film region accurately. In order to determine the area, a ruler was included in the original image as a scale bar. The film area in pixels could then be converted to mm^2.

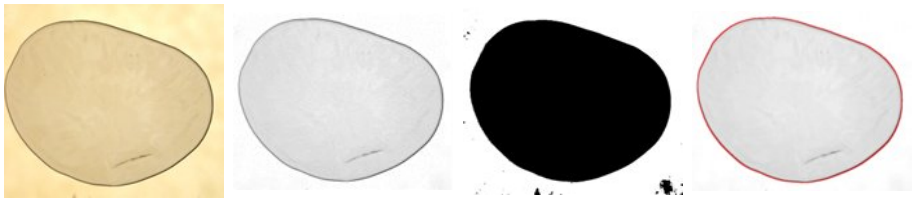

(a) 1 **(b)** 2 **(c)** 3 **(d)** 4

Figure 3.8: Image analysis steps used to determine film thickness in order to scale the SANS data.

3.5 X-Ray Diffraction

X-ray scattering can also be used to obtain structural information on samples. In contrast to neutrons, X-rays are scattered by the electrons in a material. As a

result, scattering cross section scales with atomic number. As for neutron scattering, from Bragg's law (Equation 3.4) structural size is inversely proportional to scattering vector.

Samples were prepared by casting aqueous solutions containing PVA (and additives) into PDMS moulds (20 mm disks) at 40 °C, and subsequently drying under vacuum for 24 h.

X-ray diffraction was used to determine the degree of crystallinity and crystallite size of PVA samples. Crystallinities of PVA-30-88 and PVA-50-98 samples were examined using a Bruker D8 diffractometer operating with a 1D detector in reflection mode using Cu Kα radiation. Diffracted intensity is plotted as a function of 2θ, with a range of $5° \leq 2\theta \leq 90°$. Data was obtained by Gary Oswald, Department of Chemistry, Durham University.

3.6 Ion Beam Analysis

Ion beam analysis is a family of real-space techniques that use medium energy (MeV) ions to quantify depth distributions in materials and obtain concentration profiles. A range of techniques have been used to study polymer surfaces and interfaces.[159,160] These techniques include elastic recoil detection analysis, nuclear reaction analysis and Rutherford backscattering (RBS), although only the latter technique will be used in this thesis.

When an incident ion strikes an atom with a higher atomic number on the sample surface the incident atom can undergo an elastic collision and be backscattered. RBS uses this principle, measuring the energy of the backscattered particles. It can be used for elemental determination and to depth profile heavier elements in the sample. It is necessary for the target atom to have a higher mass than the incident ion (usually $^4He^+$ for polymeric samples). As it is an elastic collision, the conservation of momentum and energy can be used to derive the relationship between the geometry and the energy of the incoming and scattered particles. The energy of the backscattered projectile of mass M_p after backscattering from the target atom of mass M_t is determined by the kinematic factor, K, which relates the energies of the incoming (E_p) and scattered (E_d) particles.

$$K = \frac{E_p}{E_d} = \left(\frac{\sqrt{(M_t^2 - M_p^2 \sin^2\theta)} + M_p \cos\theta}{M_p + M_t} \right)^2 \tag{3.27}$$

This is the origin of the mass sensitivity; each element scattered from the surface produces a backscattered ion with a characteristic E_d, with K determining the amount of energy transferred to the target atom. The majority of collisions

do not occur with atoms on the sample surface, and the beam penetrates into the film. The ion interacts with electrons in the sample, losing energy with each collision. The amount of energy lost is very well defined and is related to the distance travelled by the projectile before it undergoes a nuclear scattering event.

This technique can be used to obtain information on the composition of materials containing elements heavier than carbon, but is not suitable for studying the concentration distributions of lighter elements. This restricts its applicability to the investigation of polymer films. As the samples used in this study are thin polymer/surfactant films spin-cast onto silicon substrates, backscattering will be dominated by the silicon. However, the sodium and sulfur present in SDS should be detectable.

RBS was carried out using a National Electrostatics Corporation 5SDH Pelletron Accelerator with RC43 endstation. In order to prevent loss of the low molecular weight components, the films were cooled using liquid nitrogen immediately after spinning, and their temperature maintained below -50 °C by cooling the sample chamber. RBS experiments were carried out using a 1.5 MeV $^4He^+$ ion beam incident on the sample surface using a range of angles from 60 to 80° to the sample normal. The energy of backscattered $^4He^+$ ions was determined using a Canberra passivated implanted planar silicon (PIPS) detector with a nominal energy resolution of 17 keV at 170° to the incident beam in a Cornell geometry. Ion beam analysis data was analysed using the Surrey University DataFurnace software.[161] In order to convert the depth scale of the obtained concentration-depth profiles from atoms per cm^2 to nm, the densities of the film components are needed. Values of 1.19, 1.26 and 1.01 g cm^{-3} were used for PVA, glycerol and deuterated SDS respectively.

3.7 Atomic Force Microscopy

Atomic force microscopy (AFM) was used to measure lateral $(x - y)$ variation in the surface properties of polymer/surfactant films on the nanometre to micron scale. This technique uses the deflection of a cantilever to obtain information about a sample surface. A piezo-ceramic element capable of expanding or contracting when a voltage gradient is applied moves the position of the sample relative to the cantilever. Its deflection, as a result of changes in interactions between the cantilever and the sample, is amplified by the position of a laser reflected onto a photodiode.

A force-distance curve is generated at each pixel, describing the force exerted

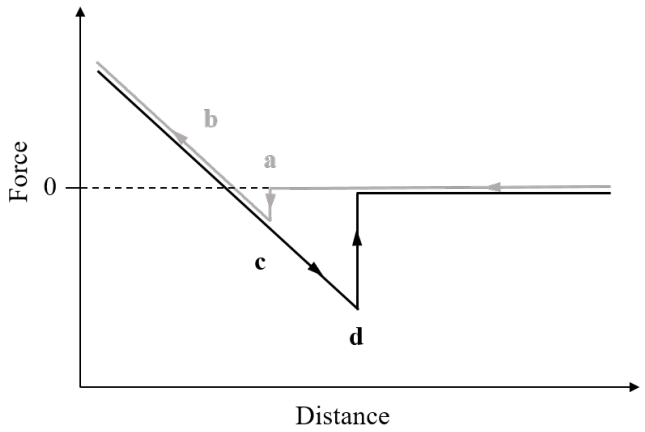

Figure 3.9: Force distance curve showing the adhesion force between the sample and cantilever as the sample approaches the tip (grey) and as it is subsequently retracted (black).

on the probe. A sketch of a representative force-distance curve is shown in Fig. 3.9. As the probe approaches the surface, attractive van der Waals forces exceed the normal spring contact and the tip snaps into contact with the sample (**a** in Fig. 3.9). As the distance between the probe and the sample decreases further, the repulsive force increases (**b**). When the probe is subsequently withdrawn, and distance increases, the tip remains in contact until strength of the Van der Waals forces decrease such that the spring constant of the probe overcomes the attractive interactions (**c**). At this point the cantilever snaps back to the undeflected position (**d**).[162]

AFM can be used in either contact mode or tapping mode. In contact mode, the tip is in physical contact with the surface, and scans the surface either with a specific height or under a constant force. This suffers problems with sample damage due to adhesive and frictional forces. In tapping mode, when the cantilever is oscillated, these problems are circumvented.

A Bruker MM8 Multimode AFM was used to characterise lateral variations in the film surface properties. Films were spin cast onto silicon wafers (as described in Section 3.2) which were cut to a size of 10 × 10 mm, and applied to a stainless steel disk using double-sided tape, which was held by a magnet inside the AFM sample housing. Analysis was made with a least 256 line resolution in Peakforce quantitative nanoscale mechanical characterisation (QNM) mode at 2 kHz in the vertical direction with a Bruker ScanAsyst-Air silicon tip on nitride layer probe, with a force constant of 0.4 Nm^{-1}. QNM is a variation of tapping mode in which the sample is oscillated and the probe deflection is measured.

A number of parameters can be extracted in order to quantitatively assess the surface topography of films. In this thesis, roughness will be primarily consid-

ered. Prior to making taking roughness measurements, it is necessary to apply a "Flatten" function to transform the image in order to remove distortion resulting from any tilt and bow in the image.

Statistical values are calculated according to the heights of each pixel in the image. A number of parameters can be obtained as statistical measurements of roughness. In this thesis, average roughness R_a, root mean square roughness R_q, and maximum roughness, $R_{\max}$, will be considered. R_a is the arithmetic average of the surface height deviations from the mean plane, as defined by Equation 3.28, where N is the number of points, and Z represents the height values.

$$R_a = \frac{1}{N}\sum_{j=1}^{N}|Z_j| \tag{3.28}$$

The root mean square roughness, R_q, represents the standard deviation of the distribution of height values, calculated using Equation 3.29. This parameter is greater than R_a, and is more sensitive to the larger deviations from the mean plane.

$$R_q = \sqrt{\frac{\sum_{j=1}^{N}(Z_j)^2}{N}} \tag{3.29}$$

Finally, $R_{\max}$ represents the maximum vertical distance between the highest and lowest height values.

3.8 Surface Tensiometry

There are a wide range of experimental methods used to determine the surface tension, γ, of liquids, including the drop weight method and the Wilhelmy plate method.[163] In this thesis, the du Noüy ring method was used. This involves the submersion of a platinum ring in the liquid of interest and measuring the force required to detach it from the liquid surface (Figure 3.10). This force, F, is then related to the surface tension of the liquid,

$$F = w_{\text{ring}} + 2\pi(R-a)\gamma\cos\theta + 2\pi(R+a)\gamma\cos\theta, \tag{3.30}$$

where w_{ring} is the weight of the ring, R is the radius of the ring and the thickness of the ring is $2a$, so that $(R-a)$ and $(R+a)$ are equal to the radii of the inner and outer ring of liquid film respectively. The high surface free energy of the platinum means that it is completely wetted by the solution. As $a << R$, this

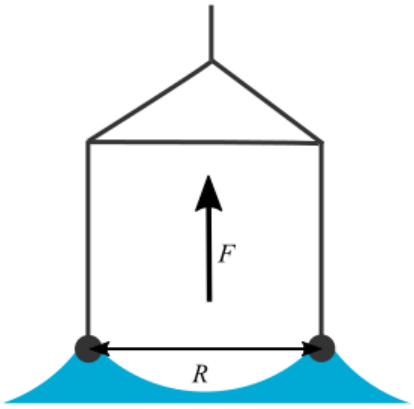

Figure 3.10: Schematic of the du Noüy ring method for surface tensiometry.

equation can be simplified to Equation 3.31, where f is a correction factor to account for the weight of the meniscus,[163]

$$F = w_{\text{ring}} + 4\pi R f \gamma. \tag{3.31}$$

The surface tension of dilute aqueous solutions of PVA, glycerol and surfactants were measured using a Krüss K10 tensiometer, equipped with a du Noüy ring. This force tensiometer automatically calculates and displays the surface tension value corresponding to the force needed to pull the liquid up. To obtain accurate results, it is vital that the ring is very clean. The platinum ring was therefore cleaned prior to measurements by holding it in a flame for ≈10 s. Solutions were prepared using ultrahigh purity water obtained from a Sartorius Arium R Comfort water purification system. Surface tension measurements were subsequently performed at 20 °C. Repeat measurements were performed to check reproducibility and the accuracy of the measurements was taken to 0.1 mN m^{-1}.

3.9 Determination of Phase Diagrams

Solutions containing defined ratios of PVA and surfactant, in which the initial total solute concentration was typically 10 wt.%, were prepared. These solutions were applied to a glass slide which was thermostatted to 40 °C. The mass of solution was regularly monitored and the point at which the solution became cloudy was determined by visual inspection. As the total PVA and additive content of the solution applied to the slides does not change throughout the drying process, the average composition of the films could be determined from the mass of solution at each point. These compositions were used to construct ternary phase diagrams. An example phase diagram is included in Fig. 3.11,

where the red arrow indicates the change in composition upon drying a film containing PVA and DDAO in a 9:1 ratio.

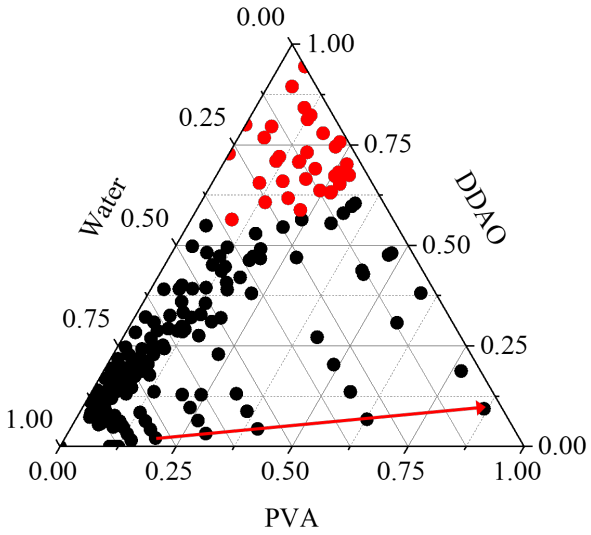

Figure 3.11: Example ternary phase diagram of the PVA/DDAO/water system, with the red arrow indicating the compositional trajectory of a drying film containing 90% PVA and 10% DDAO. Black data points represent the one-phase region, and red data points represent the phase separated region, as indicated by the clouding of the sample.

3.10 Differential Scanning Calorimetry

Differential scanning calorimetry (DSC) can be used to identify thermal transitions in materials including melting points (T_m) and glass transition temperatures (T_g). Although the glass transition of PVA is often not calorimetrically detectable, in this thesis, DSC has been used to identify melting points of samples.

Approximately 10 mg of solution cast film was weighed into DSC pans, which was heated alongside an empty pan at a constant rate. During this heating, the difference between heat flow to the sample-containing pan and the empty pan was measured. Measurements were performed using a Perkin Elmer DSC 8000. Samples were generally heated from 25 to 250 °C at a rate of 10 °C min^{-1} and then subsequently cooled at the same rate. DSC measurements were carried out by Douglas Carswell at the thermal analysis service, Department of Chemistry, Durham University.

3.11 Dynamic Mechanical Analysis

Dynamic mechanical analysis was performed in order to identify the glass transition temperatures of samples. In this technique, a sinusoidal strain is applied to the material, and the resulting stress is measured, allowing the complex modulus to be determined. This consists of the storage modulus (G') and the loss modulus (G"), which represent the viscous and elastic behaviour of the material respectively.

Samples for DMA were prepared by solution casting aqueous solutions of polymer (and additives) containing 10 wt.% total solute, into PDMS moulds (35 × 10 mm rectangles).

DMA was carried out with a temperature ramp from -40 to 100 °C at 3 °C min^{-1}, and subsequent cooling at the same rate, using a TA Instruments DMA Q800 with nitrogen cooling. Samples were oscillated at a frequency of 1 Hz in an 8 mm 3-point bend geometry. The amplitude of the oscillation was set at 2 % strain. The glass transition temperature was inferred from the maximum of the peak in tan δ, where δ is the phase angle, calculated as $\tan\delta = \frac{G''}{G'}$. An average value of the tan delta values determined upon heating and cooling the film was used. Some DMA measurements were carried out by Alex Robertson.

3.12 Thermal Gravimetric Analysis

Thermogravimetric analysis (TGA) is a method of thermal analysis that monitors the mass of a sample over time as the temperature is changed. It can be used to assess the thermal stability and volatility of components, and detect any water desorption upon heating.

TGA was performed on a Perkin-Elmer Pyris 1 TGA under a flow of compressed air. In Chapter 6, samples were heated at a rate of 1 °C min^{-1} to 80 °C, and also at a rate of 10 °C min^{-1} to 400 °C to explore additive volatility. In Chapter 9 samples were heated at a rate of 10 °C min^{-1} to 200 °C in order to determine the water content of the solution cast resins. TGA measurements were carried out by Douglas Carswell at the thermal analysis service, Department of Chemistry, Durham University.

3.13 Positron Annihilation Lifetime Spectroscopy

Positron annihilation lifetime spectroscopy is a valuable technique in probing the free volume properties of polymers.

A positron is the antiparticle of the electron. In normal matter, positrons have very short lifetimes, annihilating with electrons to form gamma rays. There are three modes of positron decay. The fastest decay mode involves the formation of a bound state of a positron with an electron, where the particles have antiparallel quantum spin states. The bound state of a positron and an electron is known as positronium, and the positronium species in which the electron and positron have antiparallel spins is a singlet state, termed *para*-positronium (*p*-Ps). This species has a characteristic lifetime (the mean lifetime associated with the exponential decay to two 0.511 MeV gamma rays), denoted τ_1, of 0.12 ns.[164,165]

Second, positrons can annihilate via direct impact with an electron. This has a longer characteristic lifetime, τ_2, of 0.3-0.5 ns, due to its lower probability of occurrence[164,165]

Third, a positron can form a bound state with an electron where the quantum spin states of the two particles are parallel. This triplet state is termed *ortho*-positronium, *o*-Ps, and has a characteristic lifetime in a vacuum of 142 ns, substantially longer than the mean lifetime of the *p*-Ps. In contrast to *p*-Ps, the decay of *o*-Ps involves the generation of three 0.511 MeV gamma rays. In materials such as polymers, this lifetime is significantly reduced due to the interaction of the positronium with other electrons. Thermally equilibrated positrons that are bound to electrons in the form of *o*-Ps become trapped in voids until the positron is annihilated. The void is assumed to be spherical, with *o*-Ps occupying the centre of the hole and the walls comprising electrons from neighbouring molecules. Importantly, the positron is not annihilated by the electron to which it is bound, but is "picked-off" by an electron in its neighbouring environment. As a result, the lifetime of *o*-Ps is directly related to the size of the voids. This forms the basis of PALS measurements.[165]

Experimentally, ^{22}Na is usually used as a positron source, which decays to ^{22}Ne, emitting a gamma ray of 1.28 MeV. When the positronium annihilates gamma rays of 0.511 MeV are generated. Therefore in order to obtain a lifetime decay curve, two gamma ray detectors are needed in order to detect these two energies, connected to a clock that can resolve events occurring nanoseconds apart. As positrons are emitted from the ^{22}Na source much less frequently ($\approx$ once every 1.5 ms) there is little chance of overlap of annihilation events. When the gamma ray of 1.28 MeV is detected it starts the clock, which stops upon detection of the 0.511 MeV gamma ray. The experimental set-up used in Chapter 9 is shown in Fig. 3.12.

In this study, PALS experiments were carried out in the Department of Polymer Science at Stellenbosch University, South Africa. Samples were solution cast

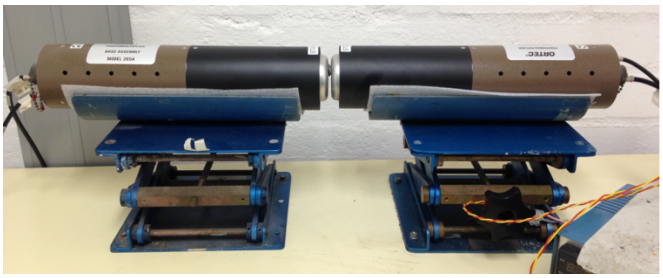

Figure 3.12: PALS experimental setup.

from solutions containing 10 wt.% solute into aluminium dishes at 40 °C. Some samples were then dried under vacuum for 24 h (depending on the study). PALS measurements were carried out using a fast-fast coincidence circuit. A 1 µCi ^{22}Na positron source (in the form of NaCl) was sealed in 6 µm aluminium foil, sandwiched between two identical stacks of film (each 1-2 mm). This thickness of film is required to ensure that there is little chance of the positron annihilating outside of the sample. The sandwich was sealed in aluminium foil and placed between the two detectors to acquire a lifetime spectrum. Each spectrum was collected to 1 million counts from annihilation events. The time resolution was monitored (to 250 ps) using a ^{60}Co source. Temperature control was achieved by attaching the sample sandwich to a temperature-controlled plate placed between the two detectors. Unless otherwise specified, PALS measurements were conducted at 20 °C.

The positron decay spectra are made up of a series of lifetimes attributable to the different positron annihilation mechanisms. The lifetime data was resolved into three finite components, τ_1, τ_2 and τ_3, corresponding to each of the annihilation mechanisms, using the PATFIT program.[166]

As previously described, τ_3 is correlated to the mean hole size, and was used to obtain the medium free volume cavity radius using an empirical equation,[167]

$$\tau_3^{-1} = 2\left[1 - \frac{R}{R_0} + \frac{1}{2\pi}\sin\left(\frac{2\pi.R}{R_0}\right)\right]. \tag{3.32}$$

Here, R is the radius of the hole and $R_0 = R + \Delta R$ where ΔR is the width of the electron layer at the internal surface of the potential well, determined to be 1.656 Å.[167] In the absence of positron or positronium chemical effects, the probability of *o*-Ps formation is proportional to the number of regions of low electron density (where *o*-Ps localisation is possible). The relative intensity of the *o*-Ps annihilation lifetime (I_3) is a percentage of the positrons annihilating by the pickoff mechanism, and is therefore related to the free volume fraction. As a result, the *o*-Ps intensity can be used to assess the influence of different factors

on the fractional free volume change using

$$f_v = CI_3V_f, \tag{3.33}$$

where f_v is the free volume fraction, and V_f is the volume of voids assumed to be spherical cavities of radius R, determined using Equation (3.32). C is a constant which reflects the probability of o-Ps formation and is independent of free volume, estimated to be 0.0018.[167]

Chapter 4

Segregation of SDS in PVA Films

Some of the work comprising this chapter has been published as: Briddick, A.; Fong, R.J.; Sabattié, E. F. D.; Li, P.; Skoda, M. W. A.; Courchay, F.; Thompson, R.L. "Blooming of Smectic Surfactant/Plasticizer Layers on Spin-Cast Poly(vinyl alcohol) Films." *Langmuir*, 34, 1410, 2018.

4.1 Chapter Introduction

This chapter focusses on the distribution of a single surfactant additive, sodium dodecyl sulfate (SDS), in PVA films. By extending the previous characterisation of additive segregation of a cationic and non-ionic surfactant in PVA films,[168] and continuing to explore the behaviour of different additives, the aim is to better understand the factors affecting the surfactant distribution in PVA, including the role of a model plasticiser.

SDS is an anionic surfactant, with the structure shown in Fig. 4.1. SDS is commonly used as an emulsifying cleaning agent in household cleaning products including laundry detergents, spray cleaners, and dishwasher detergents.[169] The interactions of this surfactant with proteins and polymer gels are of huge importance in biology; for example SDS polyacrylamide gel electrophoresis (PAGE) is used as a means to separate proteins according to their size.[170] This surfactant has previously been demonstrated to be capable of modifying the properties of polymer films, affecting the tensile strength, elongation at break and water vapour barrier properties of soy protein isolate films plasticised with glycerol.[171] The wide range of studies using SDS as a model surfactant, particularly in the study of polymer-surfactant interactions,[48,50–52,172,173] make this a useful surfactant to use in a model film system to explore surfactant behaviour in PVA.

In this chapter, neutron reflectivity is used as the primary tool to determine the vertical depth distribution of SDS, and thus quantify its segregation, both in

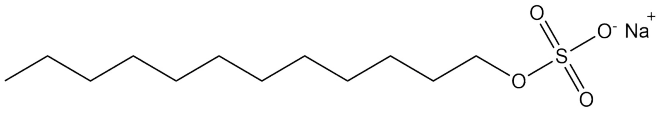

Figure 4.1: Structure of sodium dodecyl sulfate.

binary films (where SDS is the only additive) and in films plasticised by glycerol. This chapter also describes the use of atomic force microscopy to explore the lateral distribution of surfactant and investigate any possible correlation to the observed depth profiles. Finally, neutron reflectivity is used to assess the effect of film thickness on SDS distribution in plasticised films in order to better understand the role of plasticiser in SDS segregation, and begin to bridge the gap between the simplest nanometre scale films previously studied,[147,174] and complex industrial films. Here, Rutherford backscattering is used as a complementary technique to identify the SDS distribution in thick films.

4.2 Results

4.2.1 Surfactant Distribution in PVA Films

4.2.1.1 Binary Films

Neutron reflectivity was used to determine the distribution of surfactant in PVA films. Model films consisting only of PVA and SDS were initially studied, with the deuterium labelling of the surfactant enabling high-precision depth profiles to be measured, as discussed in Chapter 3.

Hydrogenated materials (SDS, glycerol, PVA) were obtained from Sigma Aldrich (Chapter 3), d_{25} SDS (hereafter referred to as "dSDS") was supplied by Rutherford Appleton Laboratories, and d_5 glycerol (hereafter referred to as "d-glycerol") was obtained from CK isotopes. For this study a partially hydrolysed (87-90 % DH) PVA resin with a molecular weight range of 30-70 kg mol^{-1} was used in order to represent the polymer in the industrial films.

$\sim$50 nm thick films, containing 5 and 10 wt.% dSDS were spin-cast, and SLD versus depth profiles were obtained by fitting the obtained reflectivity data, which could be simply converted into an additive depth profile. The observed SLD is made up of contributions from the two film components, and is assumed to vary linearly with composition between the SLDs of pure PVA and pure dSDS (Equation 4.1) (any non-linearity from a non-zero volume of mixing is likely to be negligible). The volume fraction profile of dSDS, $\phi_{\mathrm{dSDS}}(z)$, can therefore be determined from Equation 4.2, where ρ is the measured SLD, and ρ_{dSDS} and

ρ_{PVA} are the SLDs of pure dSDS and pure PVA respectively. The SLDs of all film components used in this chapter are listed in Table 4.1.

$$\rho(z) = \phi_{\mathrm{dSDS}}(z)\rho_{\mathrm{dSDS}} + \rho_{\mathrm{PVA}}(1 - \phi_{\mathrm{dSDS}}(z)) \tag{4.1}$$

$$\phi_{\mathrm{dSDS}}(z) = \frac{\rho - \rho_{\mathrm{PVA}}}{\rho_{d-SDS} - \rho_{\mathrm{PVA}}} \tag{4.2}$$

Table 4.1: Film component SLDs.

Component	**SLD/ 10^{-6}Å^{-2}**
h-PVA (88% DH) (Sigma Aldrich)	0.75
hSDS (Sigma Aldrich)	0.34
d_{25} SDS (Rutherford Appleton Laboratories)	6.77
h-glycerol (Sigma Aldrich)	0.61
d_5-glycerol (CK Isotopes)	4.91

As shown in Fig. 4.2, the obtained reflectivity data does not correspond to a homogeneous film, indicated by the curvature superimposed onto the Kiessig fringes, so it cannot be fitted to a simple 2-layer model. The data was therefore initially fitted using a three-layer model, with the layers corresponding to a silicon oxide layer on the substrate, the bulk film and a surface excess layer. This was found to be the simplest model capable of adequately capturing the features in the reflectivity data.

From these depth profiles it is apparent that SDS shows significant surface segregation. However, the concentration-depth profiles determined from these 3-layer fits show that the films spin cast from solutions containing 5 wt.% and 10 wt.% dSDS, also contain surfactant in the bulk film, with the values for ϕ_{dSDS} in the bulk film being 0.028 and 0.026 respectively (Table 4.2), corresponding to concentrations of 2.6 and 2.4 wt.% dSDS.

Although an adequate fit can be obtained when the reflectivity data for these two films is fitted using an SLD of the bulk film layer corresponding to pure PVA (and thus reflecting complete segregation of the surfactant), the model captures the fringes at lower Q much better if the SLD is allowed to increase to values significantly greater than that of pure PVA. These fits are illustrated in Fig. 4.3.

Determining the total volume fraction of surfactant, $\phi_{\mathrm{SDS,tot}}$, by integrating under the volume fraction-depth profile can provide a good indicator of how well the model represents the film, as it should replicate the fraction of surfactant in the solutions used for spin-coating. In the depth profile shown in Fig. 4.2, $\phi_{\mathrm{SDS,tot}} = 0.055 \pm 0.010$ (corresponding to 0.05 ± 0.01 wt.%) in the film spun

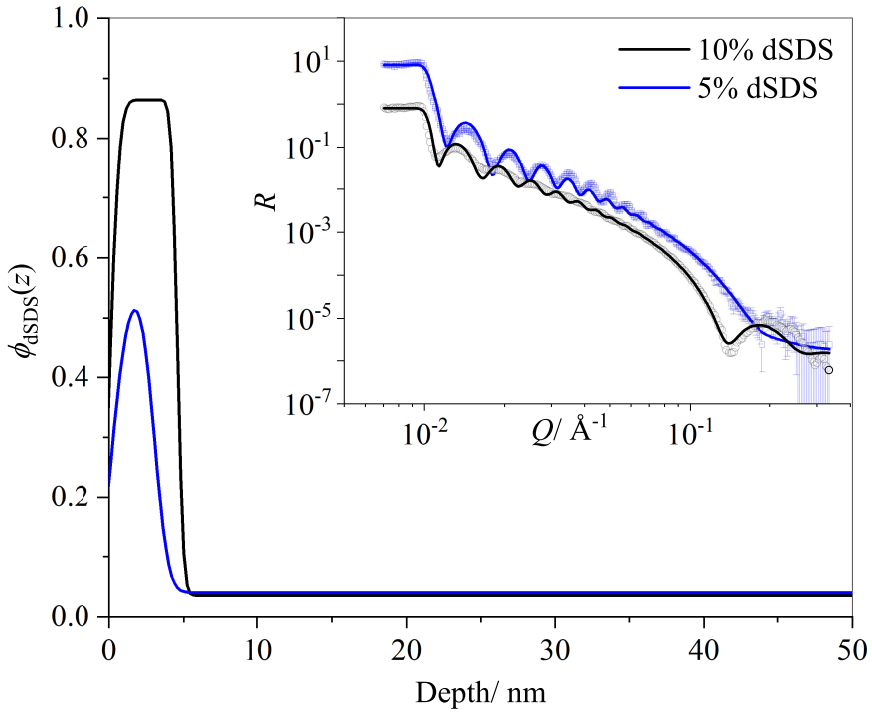

Figure 4.2: Depth profiles of dSDS in PVA films with surfactant loadings of 5 wt.% and 10 wt.%. Neutron reflectivity data and fits according to the three layer model are shown in the inset, with data for 5 wt.% dSDS offset for clarity.

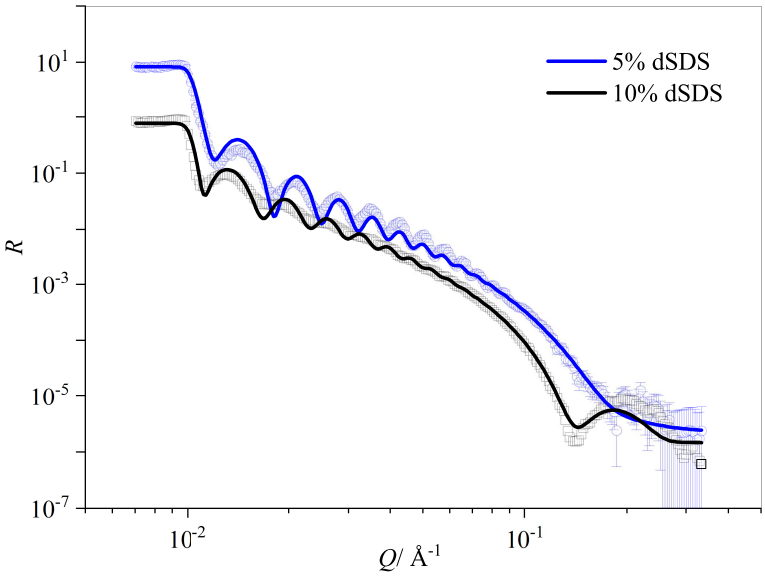

Figure 4.3: NR data and fits obtained when the SLD of the bulk film layer was fixed at the SLD for pure PVA.

from the solution containing 5 wt.% dSDS (of the total solute content), and $\phi_{\mathrm{SDS,tot}} = 0.072 \pm 0.010$ (corresponding to 0.07 ± 0.01 wt.%) in the film spun from the solution containing 10 wt.% dSDS. However, from the volume fraction-depth profile shown in Fig. 4.3, $\phi_{\mathrm{SDS,tot}} = 0.016 \pm 0.003$ for the film containing 5 wt.%

dSDS with $\phi_{\mathrm{SDS,tot}} = 0.034 \pm 0.005$ for the film containing 10 wt.% dSDS. The values obtained from Fig. 4.2 replicates the solution much better, and thus should better represent the structure of the film, signifying that complete surfactant segregation, where all SDS is excluded from the bulk PVA film, does not occur.

Upon increasing the surfactant loading from 5 % to 10 %, the thickness of the segregated layer remains approximately constant, but the SDS volume fraction in this layer increases from 0.51 ± 0.02 to 0.87 ± 0.01 (49 ± 2 to 86 ± 1 wt.%), with very little change in the bulk dSDS concentration. This is therefore consistent with a model for additive migration developed by Wakabayashi et al.,[43] which involves the dissolution of additive into the amorphous regions of polymer until saturation solubility is reached, and the diffusion of additional additive to the film surface.

The surface excess, z^*, defined by Equation 4.3, where ϕ_b is the bulk additive concentration and $\phi(z)$ is the volume fraction profile in the surface region, can be used to quantify additive segregation. The surface excess represents the amount of material segregated from the bulk in excess of what the concentration would be if the bulk concentration persisted all the way to the interface, and it is the equivalent thickness of a pure layer of segregated additive. The fraction, f, of total additive volume fraction ($\phi_{\mathrm{dSDS(tot)}}$) segregated to the surface can also be calculated (Equation 4.4) and compared. These values are included in Table 4.2. Comparison of f values has the advantage of accounting for the variation in total surfactant content in the film, as well as film thickness, thereby scaling for the total amount of surfactant present.

$$z^* = \int_0^\infty \phi(z) - \phi_b \, \mathrm{d}z \tag{4.3}$$

$$f = \frac{z^*}{\phi_{\mathrm{dSDS(tot)}}} \tag{4.4}$$

Integrating under the entire depth profile, from the air to substrate interfaces, provides a value for $\phi_{\mathrm{dSDS(tot)}}$, which can be converted to weight percentage (w), in order to compare with the concentration of surfactant in the solutions used to spin-cast the films, which should be similar. These values are reported in Table 4.3. Although many of the values for the total additive weight percentage in the film are consistent with the concentration of SDS in the solutions used for spin-casting, there are some exceptions where there is a significant discrepancy (for example the binary film containing 10 wt.% dSDS). Although this could in part be due to the ratio of solutes not remaining constant throughout the spin-casting, it would be expected that this effect would be be systematic. This discrepancy is

therefore likely to be a result of the uncertainty in fitting the SLD of the bulk layer; slight variations in this parameter have little effect on the reflectivity, and so the uncertainties reported in this concentration (Table 4.3) may be underestimated. Another factor that should be considered is the presence of atmospheric water absorbed into the spin-cast film. With a low SLD of -0.56 $\times 10^{-6}$Å^{-2}, this is likely to cause a small, but largely systematic, shift in the SLD of the bulk film, and thus lead to slightly lower than true values for the bulk dSDS concentration. This may account for the discrepancy between volume fractions from solutions and those apparent from the neutron reflectivity measurements.

Table 4.2: Surface excess of dSDS and fraction of segregated surfactant in spin-cast PVA films.

[dSDS]/wt.%	z^*/nm		f		$\phi_{\text{dSDS(bulk)}}$/ 10^{-2}	
	Binary	Plast.	Binary	Plast.	Binary	Plast.
2	-	0.2±0.1	-	0.5±0.2	-	0.42 ± 0.01
5	1.3±0.1	2.4±0.4	0.25±0.04	0.5±0.2	2.8 ± 0.1	1.6 ± 0.1
10	3.4±0.1	5.5±0.1	0.3±0.1	0.9±0.1	2.6 ± 0.2	2.5 ± 0.1

Table 4.3: Concentration of dSDS in the solutions used for spin casting, and total surfactant volume fraction and weight percentage in the film as determined from NR.

	$[\text{dSDS}]_{\text{sol}}$/wt.%	$\phi_{\text{dSDS(tot)}}/10^{-2}$	$w_{\text{dSDS(film)}}$/wt.%
Binary	5.0 ± 0.5	5.7 ± 0.1	5.3 ± 0.1
	10.0 ± 0.5	6.9 ± 0.2	6.4 ± 0.2
Plast.	2.0 ± 0.5	0.8 ± 0.2	0.7 ± 0.2
	5.0 ± 0.5	5.9 ± 0.4	5.4 ± 0.4
	10.0 ± 0.5	8.4 ± 0.5	7.8 ± 0.5

4.2.1.2 Plasticised Films

PVA generally requires plasticisation to achieve the required mechanical properties for industrial applications (such as its use as hydrogels for biomedical applications, as well as for the encapsulating film in unit dose detergents).[11] The impact of plasticiser inclusion on the segregation behaviour in this model system was therefore assessed. Glycerol was incorporated as a model plasticiser, with a loading fixed at 20 wt.%. In this plasticised system, conversion of the SLD profiles to volume fraction profiles of the deuterated species is complicated by the presence of three components, but can be estimated by assuming that the ratio of the two hydrogenated components remains constant throughout the film. Although this may not necessarily be the case (as discussed further in Section 4.2.2), the similar SLD of h-PVA and h-glycerol (0.75 $\times 10^{-6}$ Å^{-2} and 0.61

$\times 10^{-6}$ Å^{-2} respectively) means that an inhomogeneous distribution of plasticiser will have little effect on the calculated volume fraction profile of the deuterated species, which has a much higher SLD. The obtained depth profiles of dSDS in the plasticised films are shown in Fig. 4.5, with fitted parameters summarised in Tables 4.2 and 4.3.

As for the binary films, the plasticised films containing 2 and 5 wt.% dSDS could be fitted well using a three-layer model, corresponding to a surface layer significantly enriched in surfactant, a bulk film layer, and the SiO_x substrate layer. However, this model could not satisfactorily fit the reflectivity data obtained from the film containing 10 wt.% SDS. To illustrate, the best 3 layer model fit and profile is included in Fig. 4.4. An improved fit could be obtained by including an additional layer in the surface excess. The depth profile therefore corresponds to a surface layer of almost pure surfactant and a second layer comprising PVA substantially enriched in surfactant.

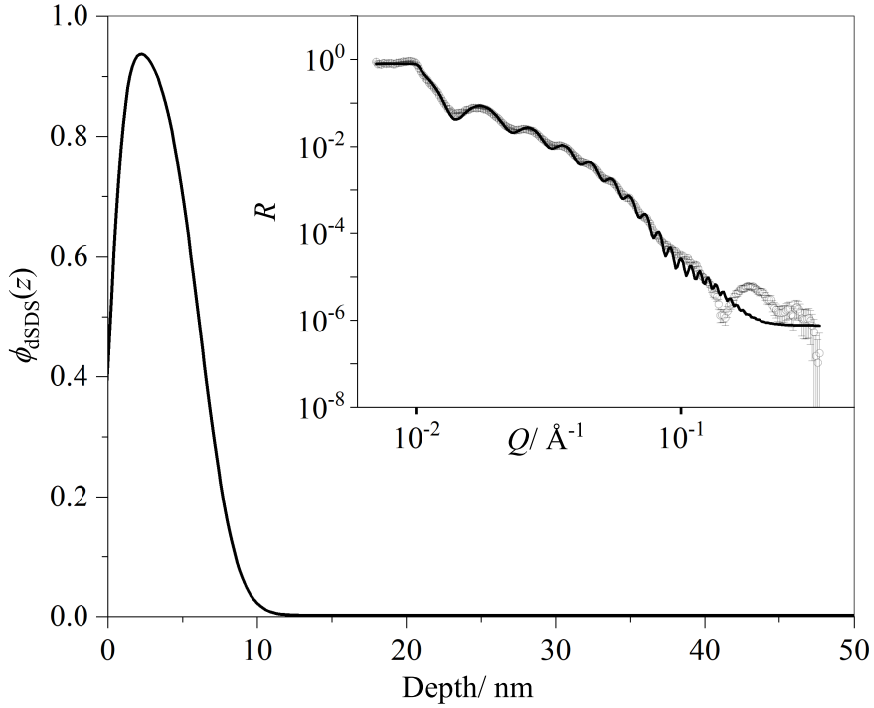

Figure 4.4: Depth profiles of dSDS in PVA films plasticised with 20 wt.% glycerol fitted using a 3-layer model. Neutron reflectivity data and fit are shown in the inset.

Glycerol has been previously demonstrated to have excellent compatibility with PVA, exhibiting no segregation from the PVA matrix in the absence of any other additive.[168] However, from these profiles it can be seen that there is a significant enhancement of surfactant segregation in the presence of glycerol; comparison with the distribution of dSDS in binary films (Fig. 4.2) reveals that the incorporation of plasticiser results in a significant increase in both the thickness

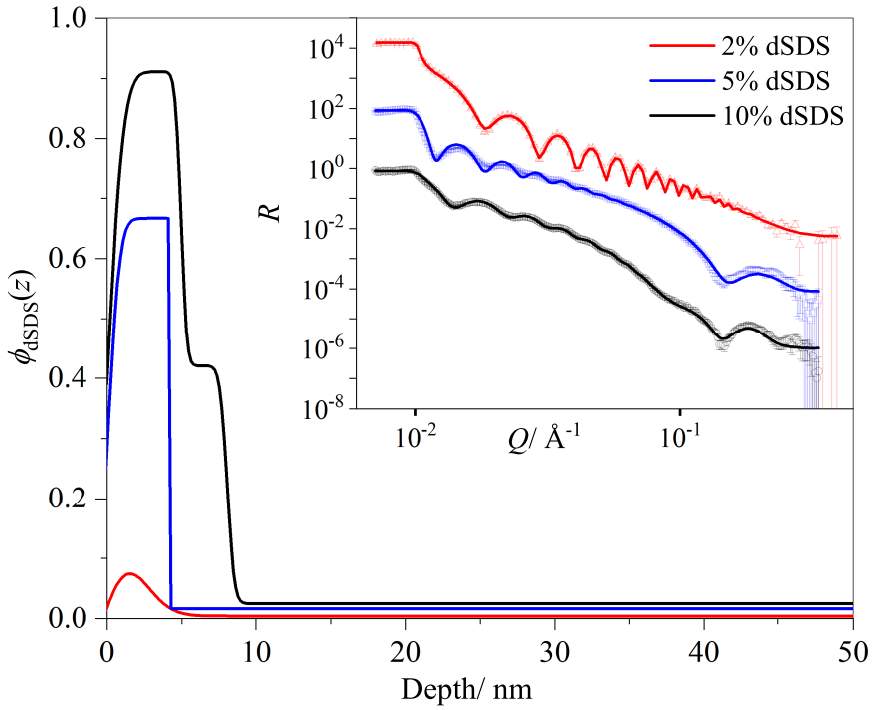

Figure 4.5: Depth profiles of dSDS in PVA films plasticised with 20 wt.% glycerol. Neutron reflectivity data and fits are shown in the inset, with data for films containing 2 wt.% and 5 wt.% dSDS offset for clarity.

of the segregated layer and concentration of dSDS in this layer. As for the binary films, calculation of the surface excess and the fraction of segregated surfactant, f, enables the increasing surfactant segregation in the presence of glycerol to be quantified. These values are reported in Table 4.2, with the total additive volume fractions and weight percentages presented in Table 4.3. From this, it can be seen that the plasticised films exhibit a surface excess even at a surfactant loading as low as 2 wt.%, with z^* increasing with dSDS concentration, as observed for the non-plasticised system. As a result, the volume fraction of surfactant in the sub-surface film is lower in the plasticised films than in the binary films, dropping from 0.028 to 0.016 in the films spun from solutions containing 5 wt.% dSDS, and dropping from 0.036 to 0.025 in the films spun from solutions containing 10 wt.% dSDS. The increase in f upon plasticisation confirms that the enhancement of the surface excess by glycerol is not simply a result of variation in film thickness (and therefore total amount of surfactant molecules present in the film), or slight variations in the total surfactant concentration.

4.2.2 Effect of Film Thickness on Segregation

The effect of film thickness on the distribution of film components was investigated in the PVA/SDS/glycerol system. One motivation for this investigation is

to bridge the gap between the model thin films previously studied and the commercial films used in unit dose detergents. Exploring the effect of film thickness could also help obtain a greater understanding of the reasons for the significant enhancement in the surface excess upon plasticiser incorporation which would help enable the prediction of segregation.

In addition, from Figures 4.2 and 4.5, it can be seen that z^* may be limited by the amount of surfactant available at low dSDS concentrations. At equilibrium, the thickness of the wetting layer formed in a two-phase mixture would be expected to correlate with the total film thickness (and thus total amount of surfactant available that is in excess of the bulk solubility). A more thorough investigation into the effect of film thickness should therefore deliver insights into whether equilibrium in these spin-cast plasticised films is achieved.

Reflectivity data were collected on plasticised films of different total thickness, which was controlled by spin casting films from aqueous solutions of different total solute concentration but with the same ratio of film components. Aqueous solutions with total solute concentrations from 4 wt.% to 12 wt.% were used, which produced films of thicknesses from 50 nm to approximately 1500 nm. The surfactant loading in the film was varied from 2-10 wt.%, with the plasticiser concentration fixed at 20 wt.%. For this part of the study, two contrasts were used: deuterated surfactant with hydrogenated PVA and glycerol and deuterated glycerol with hydrogenated PVA and surfactant. This enables the isolation of the concentration profiles of both SDS and glycerol, allowing the impact of the surfactant on the plasticiser distribution to be determined.

4.2.2.1 Films Containing 2 wt.% SDS

Films with 2 wt.% SDS were initially studied. This surfactant loading is most industrially relevant as doses of additive present in films are typically very low. Figure 4.6 shows the reflectivity data and fits for films containing 2 wt.% dSDS and 20 wt.% glycerol which were spin cast from solutions of 4, 6 and 8 wt.% total solute concentration. For each of these films, the total sample thickness was low enough that the Kiessig fringes (which are present due to the constructive and destructive interference of neutrons reflected from the film surface and substrate) could be resolved in order to accurately determine the total film thickness.

The three samples could all be fitted using a model consisting of a single surfactant-rich segregated layer and a layer corresponding to the bulk film. As the total film thickness increases from 50 nm to 210 nm, there is very little change in the thickness of the surface excess layer, although the concentration of dSDS in this layer increases. With this very low surfactant loading, for each

film thickness, ϕ_{dSDS} in the surface layer is significantly less than 1, and thus it is apparent that there is no full coverage of the surface by a wetting layer of dSDS, with the surface layer consisting of hydrogenated material significantly enriched in surfactant. The obtained depth profiles indicate that the size of the surface excess increases with film thickness, and therefore depends on the total amount of available surfactant, rather than only on the surfactant concentration relative to PVA concentration. However, it is clear that while the SDS volume fraction increases with film thickness (and thus amount of available surfactant), the thickness of this surface layer remains approximately constant. This suggests that in the thinner films, the lack of full coverage of the surface layer is a result of the limited amount of surfactant present in the system. Calculation of z^* and f allows quantification of this effect. Table 4.4 shows that although the surface excess increases significantly with film thickness, the fraction of segregated surfactant appears to be constant for all film thicknesses measured, within the uncertainty of this value. As described in Chapter 3, the reported errors are determined by adding the uncertainties in each of the relevant fitted parameters in quadrature. For both z^* and f this includes the error associated with the volume fraction of surfactant in the bulk film, which is generally captured by the fit with a large relative error.

Table 4.4: Surface excess of deuterated SDS and fraction of segregated surfactant in films spin-cast from solutions containing 2 wt.% dSDS and 20 wt.% h-glycerol.

Film Thickness/ nm	z^*/ nm	f
50	0.2±0.1	0.8±0.1
150	0.6±0.2	1.0±0.3
210	1.5±0.2	0.6±0.1

It is possible to further establish the nature of the surface excess by considering the reflectivity data and obtained depth profiles from films containing d-glycerol and hSDS in order to characterise the distribution of glycerol. SLD-concentration profiles of films containing 2 wt.% hSDS and 20 wt.% d-glycerol of varying film thickness (spun from solutions of different total solute concentration) are shown in Fig. 4.7.

As discussed previously, in order to convert the SLD profiles into volume fraction profiles, it must be assumed that the ratio of the two hydrogenated components remains constant throughout the entire film. From Fig. 4.7, this is clearly not the case. As hSDS has a significantly lower SLD than PVA (Table 4.1), the extensive SDS segregation observed means that calculation of the additive concentration from the SLD profile using the same approach as for the other contrast,

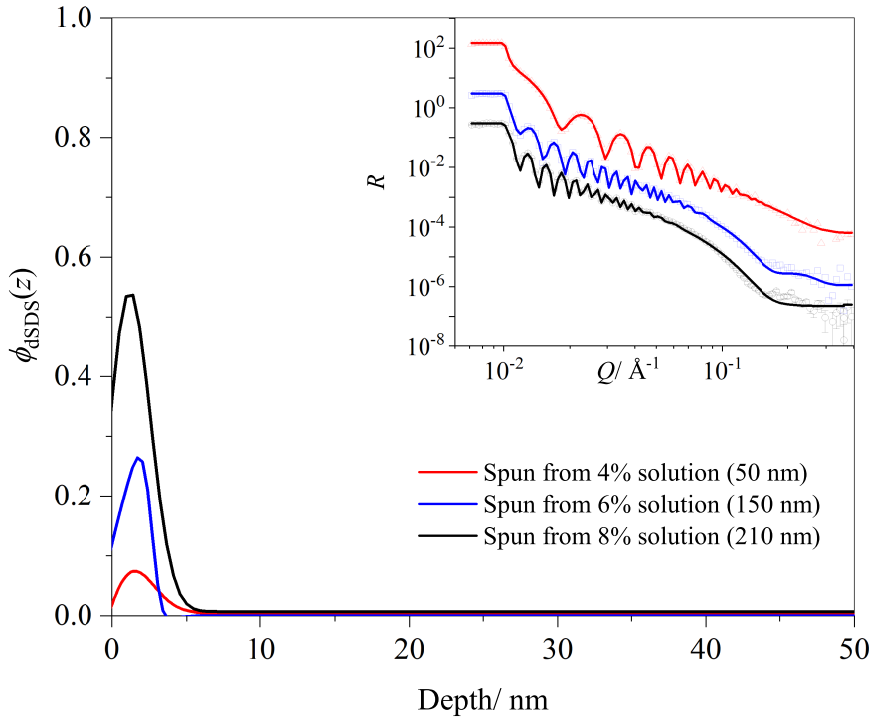

Figure 4.6: Volume fraction depth profiles of dSDS in plasticised PVA films of varying total film thickness. Neutron reflectivity data and fits are shown in the inset, with data for the thickest films offset for clarity.

assuming the ratio of the two hydrogenated species remains constant throughout entire film, would tend to result in the underestimation of the concentration of d-glycerol in the surface layer. Unlike the other contrast, the greater difference in the SLDs of the two hydrogenated components and the strong segregation of SDS means that an average SLD of the two hydrogenated components cannot be assumed throughout the thickness of the film. If the surface of the film was rich in surfactant, the SLD of the first layer would be lower than the weighted average of the two hydrogenated components, and would result in a calculated unphysical negative concentration of d-glycerol. The distribution of glycerol in the films will therefore be assessed directly from the SLD profile. Although collecting data using two contrasts is helpful to fully characterise the distribution of film components, the depth profiles from the films of the two contrasts spin-cast from each concentration of solution cannot generally be superimposed due to slight variations in surfactant loading and film thickness.

The two thinnest films could be successfully fitted using a three-layer model similarly to the other contrast, consisting of a thin layer of polymer apparently enriched in deuterated additive, a layer corresponding to the bulk film where additive is evenly distributed, and the substrate layer. For both films, it can be seen that the concentration of glycerol throughout the bulk remains approximately

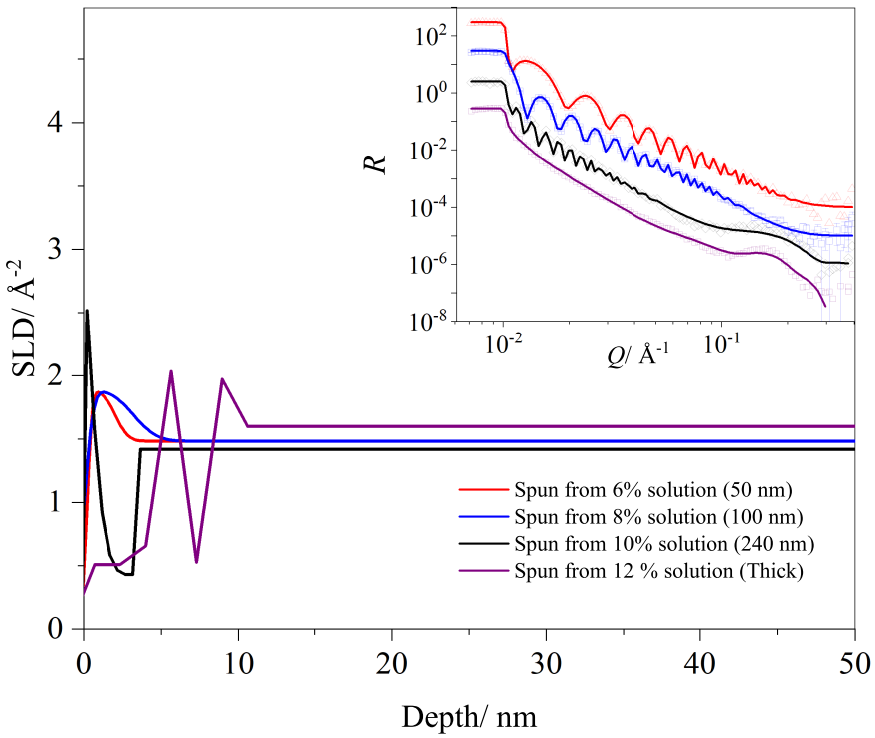

Figure 4.7: SLD-depth profiles of PVA films containing 20 wt.% d-glycerol and 2 wt.% hSDS, with varying total film thickness. Neutron reflectivity data and fits are shown in the inset, with data for the thickest films offset for clarity.

constant, reflecting the very small amount of glycerol that actually segregates. However, a slight enrichment of glycerol on the surface is apparent over the same lengthscale as that of the segregated dSDS observed using the dSDS/h-glycerol contrast, which was not previously observed for binary d-glycerol/PVA films.[168] This suggests the co-adsorption of the two additives on the surface. Upon increasing the film thickness from 50 nm to 100 nm, there is only a very modest increase in the amount of segregated glycerol, as determined by the area under the first "peak", where the SLD of this layer is unchanged, but a slight increase in thickness is observed.

The reflectivity data for the two thicker films contains features at high Q ($> 0.1\,\text{Å}^{-1}$), that can not be adequately captured using a three-layer model. It has previously been shown that when SDS concentration is high (20 wt.%), nanostructuring of the surface excess can occur in thin films, where surfactant bilayers stack on the surface, separated by interstitial glycerol layers.[174] Although not observed in the limited range of film thicknesses studied to determine the depth profiles of dSDS, these features at high Q in the reflectivity obtained for thick films containing d-glycerol and hSDS, suggest that this structured surface excess could occur in films containing low concentrations of surfactant, when the thickness is such that a large amount of the additive is present. These films were

therefore fitted with a model with a higher level of complexity, allowing for a degree of structuring to the surface excess.

The 240 nm thick film could be adequately fitted by incorporating an additional layer of lower SLD below the glycerol-enriched layer. The best fit corresponds to a thin, well-defined layer of high SLD on the surface, and a thicker layer of low SLD (0.35×10^{-6} Å^{-2}) corresponding well to a layer of pure SDS. The layer of glycerol on the film surface is much thinner than for the two films of lower total thickness, and the higher SLD shows there is a higher concentration of glycerol in this layer, compared to in the 50 and 100 nm thick films. The length-scale corresponds well to a surface monolayer of the plasticiser, suggesting that in the thicker film, when there is a greater total amount of surfactant present that is capable of segregating, the additives can begin to form more ordered structures even with a very low surfactant concentration relative to PVA.

The thickest film, spun from solution containing 12 wt.% total solute, must be fitted with a further degree of structure. Although the total thickness cannot be determined as the Kiessig fringes cannot be resolved, it is estimated to be approximately 1.5 µm by scratching a representative film and using AFM to measure the difference in height between the substrate and the film. This value is also consistent with the mass of the film ($\sim$ 0.004g on a 55 mm silicon block). It is clear that the surface region of this film is substantially thicker than that of the 50, 100 and 240 nm films, demonstrating that the size of the surface excess is dependent on the total amount of additive present, rather than solely on its concentration relative to PVA. This could not have been inferred from the limited range of film thicknesses studied with the other contrast. In this thick film containing d-glycerol, below a surface layer of low SLD, there are two thin layers of high SLD separated by another layer of low SLD. The structure fitted to the data therefore corresponds to two layers of almost pure SDS separated by interstitial glycerol layers, as has been previously observed.[174] Although the layers in the SLD profile are not well-defined, this is to be expected for a number of reasons. First, perfectly separated glycerol and surfactant layers are unlikely to be present throughout the entirety of the film surface, and thus the presence of defects is likely. The formation of this structure requires the majority of surfactant molecules to assemble into layers over a very short timescales and as the surfactant concentration is low, the presence of polymer chains trapped within the surface excess are likely to disrupt the structure. Second, an average SLD for each component was used, with the assumption that it does not vary across the molecule. In reality, the variation in SLD from the head group to the tail of dSDS will cause an apparent roughening of the profile and thus loss of definition

of the layers.

Again, in the two thicker films, the SLD remains constant throughout the bulk film, with a value corresponding to $\sim$ 80 % PVA and $\sim$ 20 wt.% d-glycerol, showing the low extent of glycerol segregation.

As it was determined from the other contrast that only a very low concentration of dSDS is present in the bulk film ($\phi_{b\,(\mathrm{dSDS})}$ was determined to be $4.2 \times 10^{-3}, 1.7 \times 10^{-4}$ and 7.0×10^{-3} for the 50 nm, 150 nm and 210 nm films respectively), the concentration of SDS in the bulk film will have little effect on the SLD of the bulk layer. This means that the bulk film can therefore be approximated to have the SLD of PVA. Taking the additional assumption that the surface layer comprises solely of SDS and d-glycerol, the d-glycerol surface excess, z^*, can then be calculated in order to quantify its segregation (Table 4.5). It should be noted that while this assumption is likely to be valid for the two thickest films, the dSDS depth profiles in Fig. 4.6 show a relatively low volume fraction of dSDS in the surface layer of the thinnest film. This suggests that polymer is likely to be present in this layer, which would result in the values presented in Table 4.5 being an overestimate of z^*. To illustrate, if the composition of the hydrogenous components in this layer was 10 % PVA and 90 % SDS (v/v), z^* would become 0.3 nm. From this substantial decrease from $z^* = 0.4$ nm, assuming no polymer on the surface, it is therefore clear that if substantial amounts of polymer are present in this layer, this approach to determine the surface excess of glycerol is unreliable. Indeed, despite there being a peak in the SLD at the surface, should this layer contain substantial amounts of PVA ($> 40\%$), it would actually still correspond to a layer depleted in glycerol.

Table 4.5: Surface excess of deuterated glycerol in films spin-cast from solutions containing 2 wt.% hSDS and 20 wt.% d-glycerol.

Film Thickness/ nm	z^*/ nm
50	0.4±0.1
100	0.6±0.2
240	-0.5±0.2
Thick (>600 nm)	-0.5±0.2

4.2.2.2 Higher Surfactant Loadings

This study was subsequently extended to films containing 5 and 10 wt. % SDS. The concentration-depth profiles of 5 wt.% dSDS in films of different thicknesses are shown in Fig. 4.8.

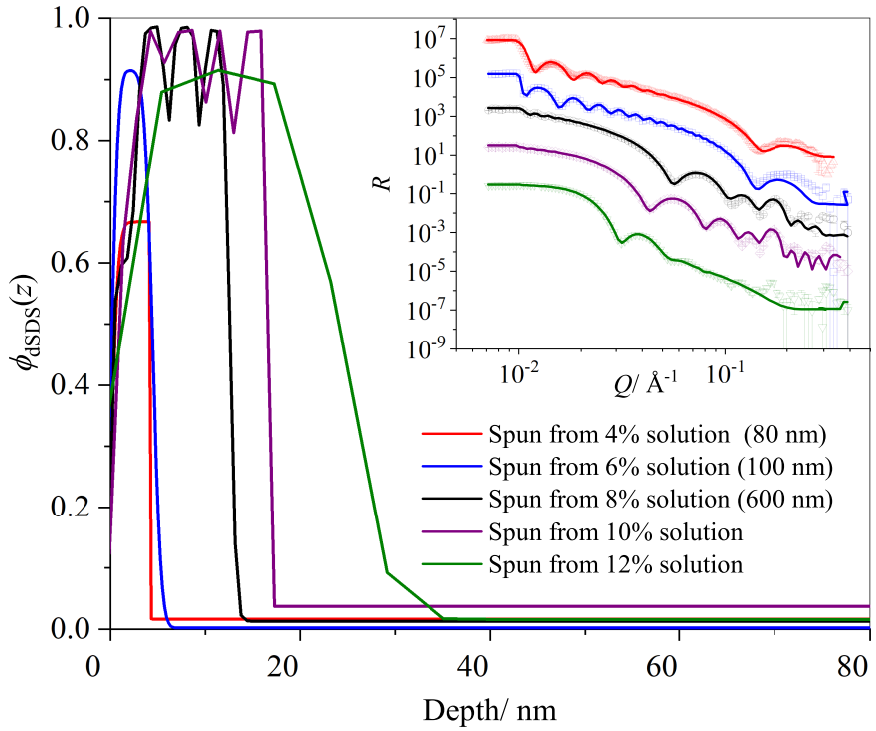

Figure 4.8: Volume fraction-depth profiles of dSDS in plasticised PVA films containing 5 wt.% dSDS of varying total film thickness. Neutron reflectivity data and fits are shown in the inset, with data for the thicker films offset for clarity.

For the two thinnest films, a three layer model (as previously described) can adequately capture all features in the reflectivity data, although the fit to the 100 nm film is imperfect at $Q \approx 0.2$ Å^{-1} for this simple model. The same effect can be seen as for the films containing 2 wt.% dSDS, where increasing the film thickness does not significantly affect the thickness of the surface layer, but increases the volume fraction of SDS in this layer, suggesting that increasing the amount of available surfactant excludes PVA from the surface.

For the thicker films containing 5 wt.% dSDS, a model consisting of a single segregated layer cannot successfully capture the features at high Q (> 0.1 Å^{-1}), notably a weak Bragg peak at $Q \approx 0.15$ Å^{-1}, indicative of repeating structures, which cause interference of scattering. This Bragg peak corresponds to structures on a lengthscale of 4 nm ($= 2\pi/Q_{\text{peak}}$), that are not reproduced by the three-layer model, indicating a depth profile with a greater level of complexity. Here it is helpful to clarify the appearance of Bragg peaks in the reflectivity data, and distinguish them from of fringes, which systematically decrease in size with increasing Q. This is illustrated in Fig. 4.9.

The appearance of this Bragg peak shows the development of multi-layer features begin as SDS loading increases. A profile with a degree of structure to the segregated layer was therefore considered for the thicker films. In order

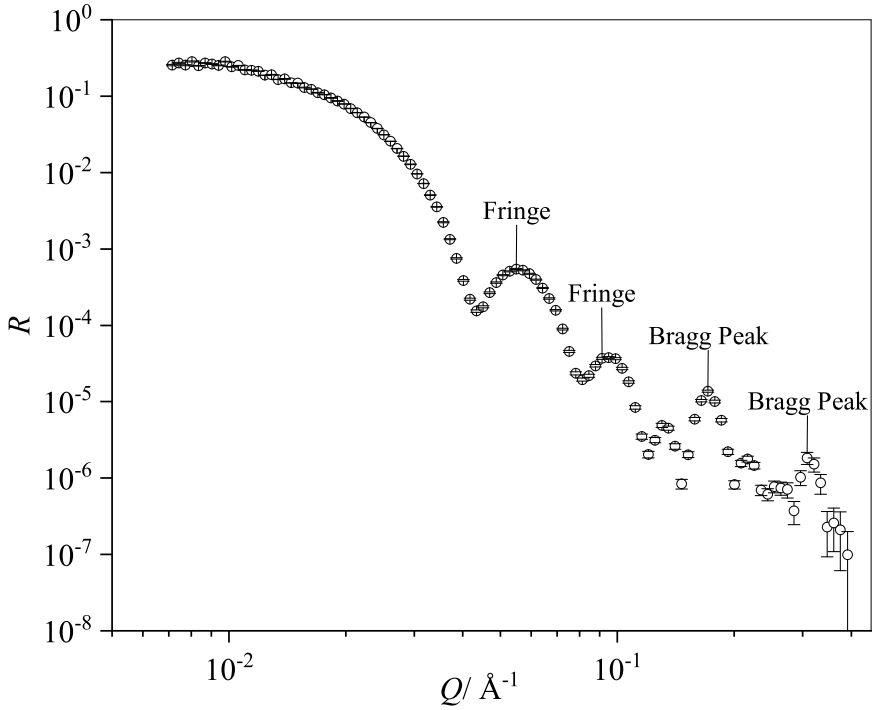

Figure 4.9: NR data obtained from a film spun from and 8 wt.% solution containing 5 wt.% dSDS and 20 wt.% h-glycerol, indicating the presence of both fringes and Bragg peaks.

to avoid over-parameterisation, the simplest multilayer model was used to fit the data, which consists of two repeating layers, where the thickness, SLD and roughness of each of the two layers comprising the multilayer is able to vary during the fitting, but these parameters are constant for each repeat. The number of repeated multilayers was systematically increased until the best fit was obtained. This model allowed a much more precise fit to the data throughout the entire Q range to be obtained. For films containing 5 wt.% dSDS, and spun from 8 wt.% and 10 wt.% solution, it was found that a profile consisting of layers of highly concentrated dSDS (high SLD) separated by layers of hydrogenated material (low SLD) could fit the data precisely throughout the whole Q range. The films spun from 8 wt.% and 10 wt.% solution contain 3 and 4 multilayers respectively, which consist of layers of almost pure dSDS (≈ 30 Å) and layers of hydrogenated material (≈ 3 Å).

As discussed for the lower surfactant loading, the lack of completely defined layers is likely to be a result of the uneven SLD distribution throughout the ordered SDS layers (a degree of roughness arising from variation in SLD along the SDS molecule would be expected even for perfectly aligned surfactant layers), as well as the presence of defects in the highly structured surface excess. It is remarkable that, despite the parameters of the layers comprising the multilayer

being constrained very little, and permitted to vary over wide limits during the fit, very consistent values for thickness and SLD were obtained for the films spun from solution containing 8 and 10 wt.% total solute, with just one extra repeat present for the latter film. Reflectivity data for the thickest film (represented in green in Fig. 4.8) contains fewer features, as they are likely to have been washed out by roughness in the film and defects in a large number of stacked layers, and it is therefore difficult to characterise accurately using the multilayer model. However the reflectivity can be well characterised using the simple 3-layer model used for the thinnest films, with the exception of the small Bragg peak at high Q which cannot be captured by this non-oscillating profile. By assessing the SLD-concentration profiles obtained from each film containing 5 wt.% dSDS, it is immediately clear that the surface excess increases with film thickness.

This same trend is apparent in films containing 10 wt.% dSDS (1:9 ratio of dSDS:PVA). Figure 4.10 shows the approximate distribution of dSDS in films spin-cast from solutions containing 4, 8 and 12 wt.% total solute, each containing 10 wt.% surfactant, where a clear increase in the surface excess with film thickness is again apparent. A Bragg peak can be identified at high Q for the thicker films, but due to the complexity of the imperfect surface structures, and absence of other features, this could not be reliably fitted with the multilayer model. Fitting of the surface was therefore restricted to two layers to prevent over-parametrisation. However, the good fit over the low Q range successfully characterises the overall larger scale feature of the total adsorbate thickness and density, thus enabling quantification of the increase in surface excess with film thickness.

Calculated values for z^* in films containing 5 and 10 wt.% dSDS are included in Table 4.6. Although calculating f would allow clarification of whether the proportion of segregated additive remains constant or increases with film thickness, this is not possible for the thickest films due to large uncertainties in the total film thickness when fringes cannot be resolved, meaning that the total amount of surfactant has a very large associated uncertainty.

Table 4.6: Surface excess of dSDS in films of different thicknesses, spin-cast from solutions containing 5 and 10 wt.% dSDS and 20 wt.% h-glycerol.

Tot. solute conc./ wt.%	5 wt.% dSDS		10 wt.% dSDS	
	Thickness/ nm	z^*	Thickness/ nm	z^*
4	80	2.4 ± 0.4	70	5.5 ± 0.1
6	100	3.8 ± 0.1	-	-
8	600	10.8 ± 0.2	500	11.1 ± 0.2
10	-	15.0 ± 0.2	-	-
12	-	20.2 ± 0.1	-	42.8 ± 0.7

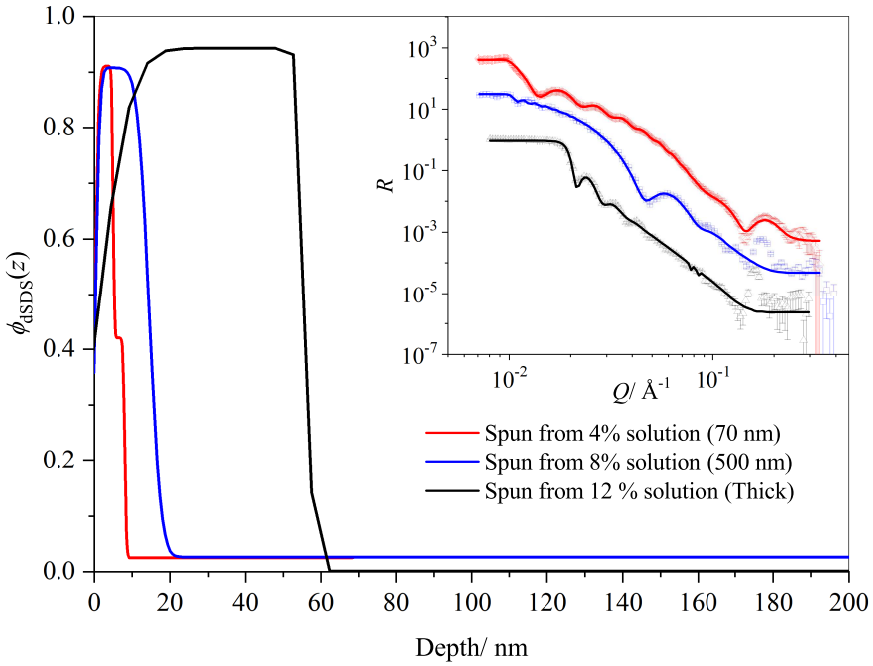

Figure 4.10: Concentration-depth profiles of dSDS in plasticised PVA films of varying total film thickness containing 10 wt.% dSDS. Neutron reflectivity data and fits are shown in the inset, with data for the thickest films offset for clarity.

The distribution of d-glycerol in thick films containing 20 wt.% d-glycerol and 5 and 10 wt.% hSDS are shown in Figures 4.11 and 4.12 respectively. As for the previous contrast, in order to avoid over-parameterisation the structure of the surface excess was fitted with a repeated layer, with the number of repeated layers systematically increased until the best fit was achieved. In this case, the multilayer consists of a thin layer (3 Å) rich in d-glycerol and a thick layer (35 Å) of low SLD, corresponding to surfactant rich regions. Again, it can be seen that very consistent values for the thicknesses of these layers were obtained for each film, despite wide limits (15-50 Å for the surfactant-rich layer and 1-8 Å for the d-glycerol-rich layer) given for these parameters to vary. The SLD values of the surfactant rich layers in the two thinner films containing 5 wt.% hSDS, and in the thinnest film containing 10 wt.% hSDS, correspond to almost pure hydrogenated surfactant, suggesting that the layers of pure components are better defined when there are fewer stacked layers to be arranged during the spin casting. Nevertheless, the excellent fit of the data of thicker films to a repeating layer model shows that the film surface structures are still very well-defined, even when the self-assembly of a large amount of surfactant and plasticiser is necessary. This distribution of d-glycerol in films confirms that it is the plasticiser occupying the regions between surfactant-rich layers in the profile obtained using deuterated surfactant.

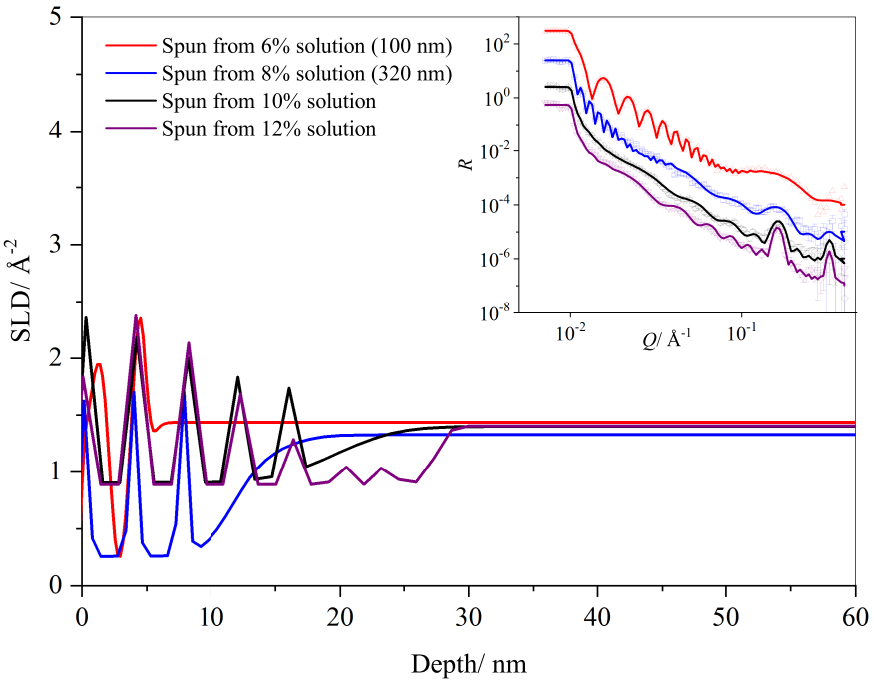

Figure 4.11: SLD-depth profiles of PVA films containing 20 wt.% d-glycerol and 5 wt.% hSDS, with varying total film thickness. Neutron reflectivity data and fits are shown in the inset, with data for the thickest films offset for clarity.

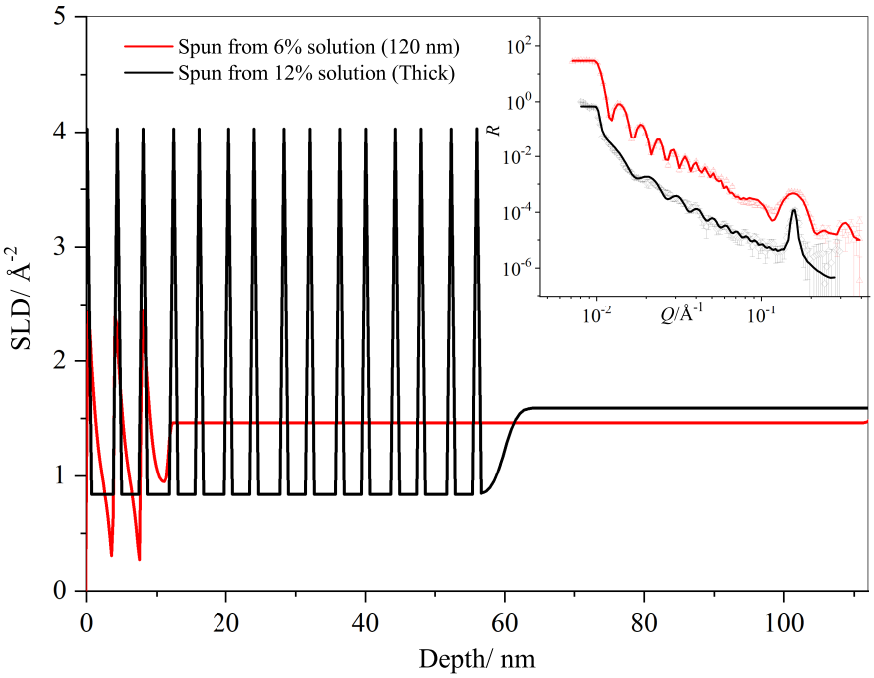

Figure 4.12: SLD-depth profiles of PVA films of varying total film thickness containing 20 wt.% d-glycerol and 10 wt.% hSDS. Neutron reflectivity data and fits are shown in the inset, with data for the thicker film offset for clarity.

An aside: off-specular reflectivity

The 2D detector of the OFFSPEC reflectometer also records the off-specular

reflectivity, which yields information about the in-plane structures. An example off-specular pattern obtained is included in Fig. 4.13, which reveals the presence of a Bragg sheet, coinciding with the Bragg peaks from the specular reflectivity. This suggests that the structure in these films is not entirely perpendicular to the surface, with some lateral variation across the film. The derived vertical profiles, which assume lateral homogeneity, should therefore be treated with a degree of caution.

Some lateral variation across the surface is perhaps to be expected as the deviation of the structure of the lamellar phase from the periodic stacking of amphiphile and solvent molecules in solution has been previously shown by Hendrikx et al.[175] Indeed, Kekicheff et al.[176] have also shown that the flat geometry of the lamellar phase of SDS bilayers is not the lowest free energy conformation, and have identified an array of structural defects of lengthscale 60 Å in the bilayers, as well as the presence of textural defects with dimensions greater than 200 Å.

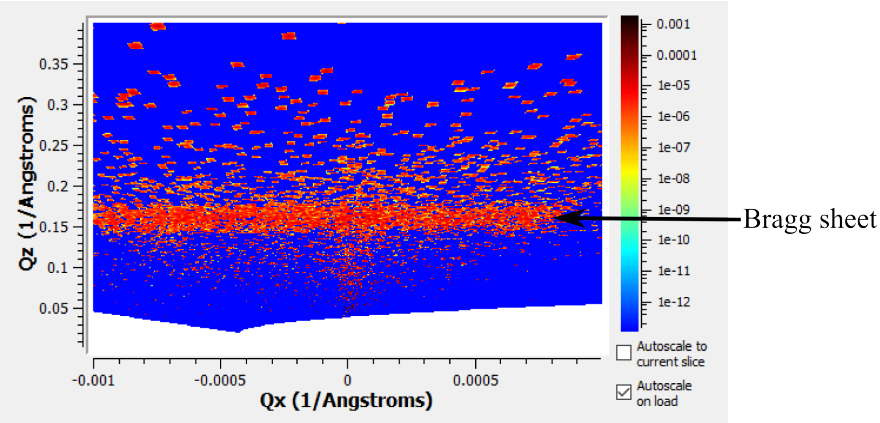

Figure 4.13: Off-specular reflection pattern from a film spin cast from 12 wt.% total solute solution, containing 2 wt.% hSDS and 20 wt.% d-glycerol, illustrating the presence of a Bragg sheet, indicative of structures in the $x - y$ plane.

Another aside: double critical edges

In the thickest films containing high levels of surfactant and deuterated glycerol, double critical edges are apparent upon close inspection of the low Q region of the reflectivity data (for example in the reflectivity data for the thicker film in Fig. 4.12). Critical edges are a result of the total external reflection from an interface, appearing in the data when the refractive index of the phase being entered, n_2, is equal to the product of the refractive index of the incident phase, n_1, and the cosine of the incident reflection angle, θ (Equation 3.11). For all films studied in this thesis, this condition is met when the neutron wave meets the silicon interface, giving a critical edge at $Q \approx 0.01\,\text{Å}^{-1}$, characteristic of a silicon

substrate. The position of the critical edge is related to scattering length density of the material by

$$Q_c = \sqrt{16\pi\Delta\rho}. \tag{4.5}$$

This value of Q therefore gives $\Delta\rho = 1.99 \times 10^{-6}$ Å^{-2}, consistent with the scattering length density of silicon (2.07 $\times 10^{-6}$ Å^{-2}). In thick films containing 20 wt.% d-glycerol, it appears that the condition for a critical edge is also met at the air-film interface.[177] The position of this second critical edge is at $Q \approx 0.008$ Å^{-2}. From Equation 4.5, this gives $\Delta\rho = 1.4 \times 10^{-6}$ Å^{-1}, which is consistent with the SLD of the bulk PVA film containing 20 % d-glycerol (as $\rho_{\text{air}} = 0$).

Normally, the edge at lower Q would not be visible as neutrons would be reflected below any critical edge, and thus reflectivity would be unity until the highest critical edge is reached. However, in this case beam attenuation reduces the scattering between the two critical edges, meaning both are visible. Although this was not accounted for in this analysis, this demonstrates the effect of the film thickness on neutron absorption, which is related to the absorption cross section, σ_a. This is given by Equation 4.6, where b'' is the imaginary component of the scattering length ($b = b' - ib''$) and k is the wavevector of the incident neutron. Unlike the coherent and incoherent scattering cross sections, σ_s, σ_a is wavelength dependent.[149] Although negligible in thin polymer films, the presence of two critical edges shows that absorption starts to become relevant as films become much thicker.

$$\sigma_a = \frac{4\pi}{k} b'' = 2\lambda b'' \tag{4.6}$$

As no widely accessible reflectivity analysis packages are suitable for use in systems with thick layers, the thickest films containing d-glycerol were fitted using the same protocols as the thinner films, with a constant reflectivity for Q values below the silicon critical edge. This approach has successfully captured the surface features of these thick films, but it is worth being aware of the limitations of this method of analysis for these films.

4.2.2.3 Rutherford Backscattering

Rutherford backscattering is an ion beam analysis technique that can provide complementary analysis to neutron reflectivity. Unlike NR, which can be performed under atmospheric conditions, RBS operates under vacuum and so the sample must be vitrified prior to measurement in order to prevent loss of volatile film components. The depth profiles of films containing 10 wt.% SDS and 20

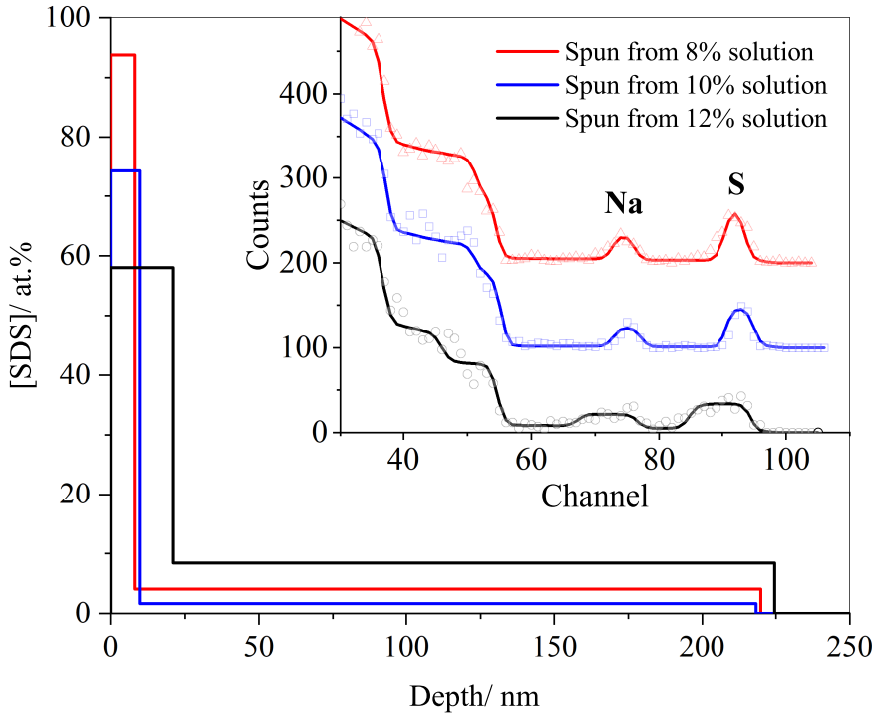

Figure 4.14: Depth profiles of SDS in PVA films of varying thickness, containing 10 wt.% SDS and 20 wt.% glycerol. RBS data and fits are shown in the inset.

wt.% glycerol spun from solutions containing 8, 10 and 12 wt.% total solute are shown in Fig. 4.14.

Although the significantly lower resolution means that surfactant nanostructures identified with NR cannot be resolved, the presence of a surface excess is confirmed by RBS. As a real-space technique, the data interpretation is much less ambiguous than for neutron reflectivity. From these concentration-depth profiles, values for the surface excess were calculated as 7.2, 7.1 and 10.4 nm for films spun from solutions containing 8, 10 and 12 % solute respectively. Although there is very little change in the surface excess in the two thinner films, there is a modest increase in z^* for the thickest film, and thus these measurements follow a qualitatively similar trend to the NR data. It is interesting, however, that the extent of surface segregation as determined by RBS is much lower than that measured by NR, from which z^* was determined to be 11.1 and 42.8 nm for films spun from solutions containing 8 and 12 wt.% total solute respectively. Although RBS has a much lower resolution, this alone is not enough to explain the substantial difference in the surface excess values obtained using RBS and NR as the film containing 10 wt.% SDS in a film spun from solution containing 12 wt.% total solute exhibits a surface excess 4 times greater than that obtained by RBS. The lower extent of surfactant segregation in the vitrified films observed by RBS is also reflected in the significantly higher concentration of SDS observed in the

bulk film. These differences between the depth profiles obtained using the two techniques are likely to be indicative of migration occurring after spin-coating, which is prevented from occurring by vitrification of the samples measured by RBS. These measurements therefore provide evidence for the gradual (minutes to hours) migration of dSDS to the surfaces of plasticised films.

4.2.3 Film Surface Topography

Specular neutron reflectivity is only capable of probing the z-direction of the film. It is of interest to understand how the PVA film topography changes upon incorporation of SDS, and whether the change in depth profile with surfactant concentration can be related to effects on film surface structures. Atomic force microscopy is a useful tool for identifying any surface features, which could help to gain insight into the lateral surfactant distribution on the surface. AFM can capture a number of surface properties, but in this study the height maps will be primarily considered. Adhesion is another property that can be useful in understanding the film surface, which records the pull-off force for the probe on the sample. In the case of assessing the effect of incorporating a stickier additive, for example oligomers into polymers,[178] adhesion measurements can give a good idea of the lateral distribution of the additive. However, in the case of SDS incorporation into PVA it is not obvious which of the two components is tackier, and therefore whether surfactant-rich domains would produce a higher or lower adhesion.

Height maps were obtained for $1\,\mu m^2$ areas of films spin-cast from aqueous solution of 4 wt.% total solute concentration, producing samples approximately 70 nm thick, containing SDS as the only additive. These are shown in Figure 4.15. From these images, it is immediately apparent that, while the surface of the pure PVA film is very smooth, incorporation of SDS leads to the formation of surface features, which become more prominent and better-defined as loading increases from 2 to 20 wt.%. This can also be seen in Fig. 4.16, which compares typical cross sections of the sampled film areas with increasing SDS loading, illustrating the presence of a significant unevenness of the surface when [SDS] $\geq$ 10 wt.%.

Figure 4.15 also shows the captured adhesion maps. Again, from these images, the appearance of surface features can be identified upon SDS incorporation, which become more prominent as additive concentration increases. In the case of adhesion measurements, the scale is arbitrary, but is consistent between samples as the same probe was used for each measurement, and thus the films can be reliably compared.

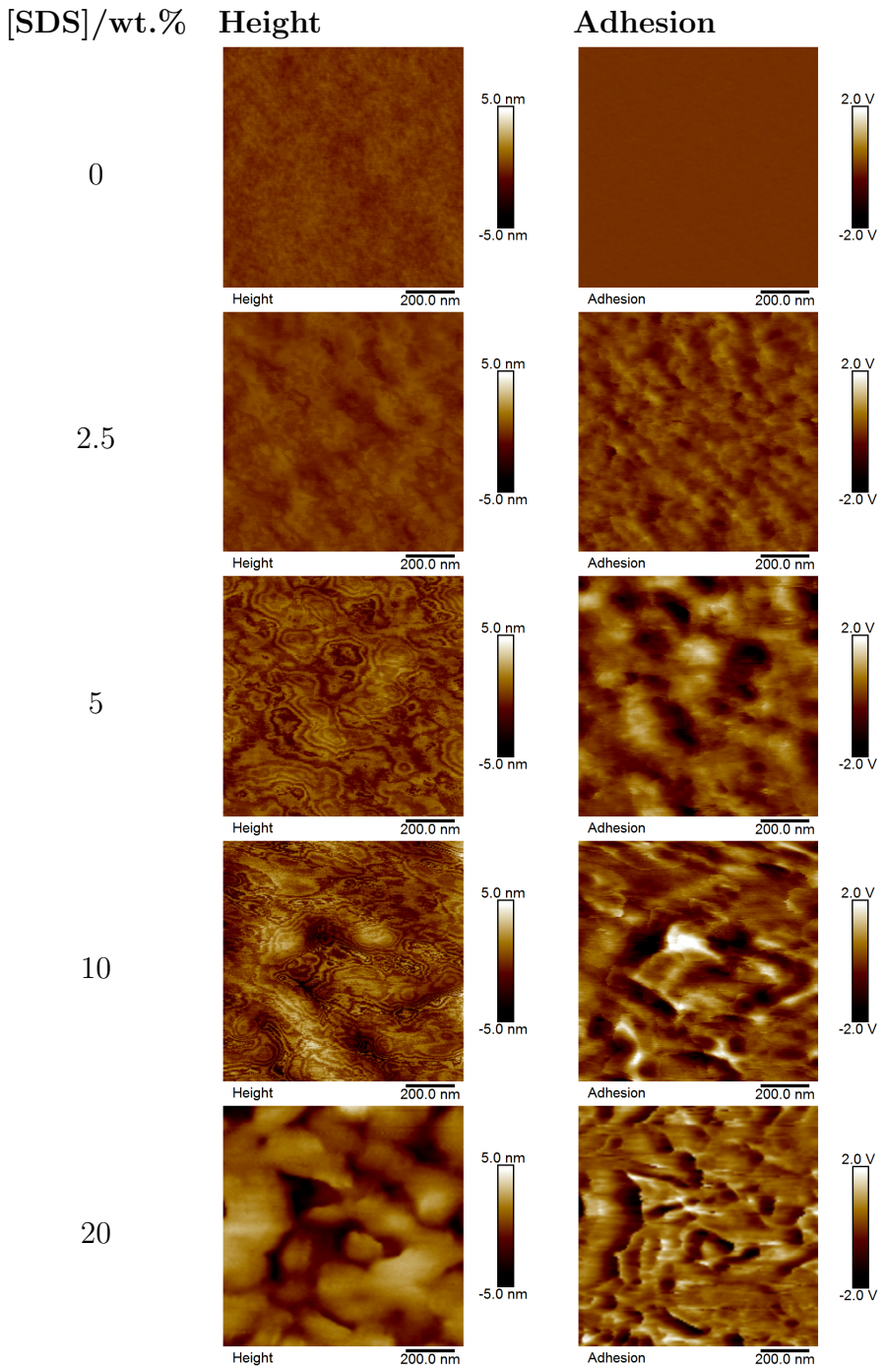

Figure 4.15: Height and adhesion maps for binary PVA/SDS films.

Comparison of the height and adhesion maps shows that the regions of greatest adhesion generally correspond to the least prominent areas of the film. Based on the increasing SDS concentration on the surface as surfactant loading increases, as observed by NR, it is plausible that the increasing adhesion as SDS concentration increases suggests that the surfactant-rich domains produce the greatest adhesion, and it is therefore the polymer-rich domains that comprise the surface of the most prominent regions of film. However, the surface adhesion cannot be considered

quantitatively due to the uncertainty in the contact area of the probe and the film surface. Additionally, it is possible that the apparent adhesion will coincide with concave surface features simply because there is more contact with the probe when it fits into these holes.

Surface roughness of the height maps can be used to quantitatively assess the effect of surfactant concentration on film topography. Average roughness, R_a, root mean square roughness, R_q, and maximum roughness, R_{max}, will be considered, which are discussed more extensively in Chapter 3. These three parameters are plotted against surfactant loading in binary films in Figure 4.17. Error bars represent the standard error in the average result taken from at least 5 areas of film. From this plot, it is clear that there is a significant increase in all three roughness parameters with SDS concentration, although this increase is distinctly non-linear for R_{max}, where a substantial increase is observed upon increasing [SDS] from 2.5 to 5 wt.%, which is followed by a modest increase in R_{max} as [SDS] is further increased to 20 wt.%.

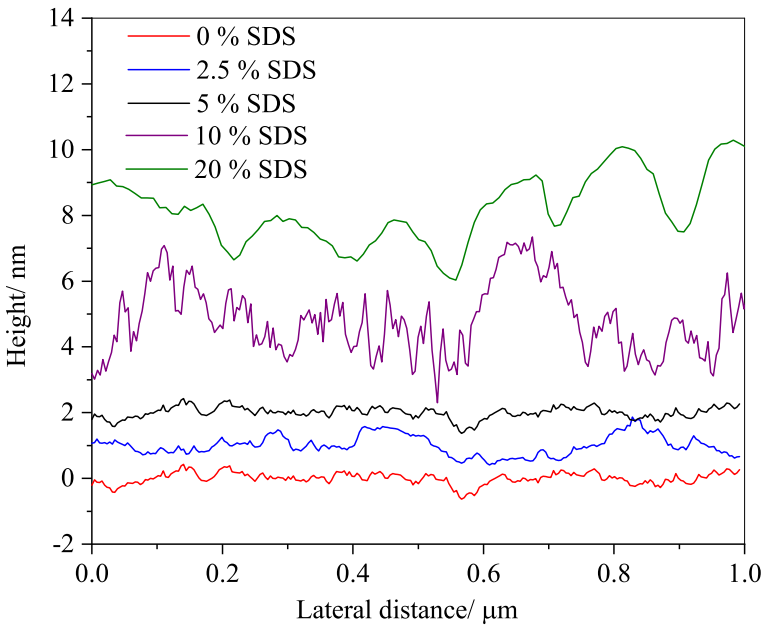

Figure 4.16: Example cross sections of binary PVA/SDS films with increasing surfactant concentration. Cross sections of films containing 2.5-20 wt.% SDS are offset for clarity.

AFM was also used to assess the change in surface topography of plasticised PVA films with SDS loading. As for the NR experiments, glycerol was incorporated as a model plasticiser with a fixed loading of 20 wt.%. Example height maps of plasticised PVA films containing 0, 5, 10 and 20 wt% SDS are shown in Fig. 4.18 and typical cross sections for these films can be seen in Fig. 4.19. Fig. 4.18 also includes the adhesion maps for films containing 5 and 10 wt.%

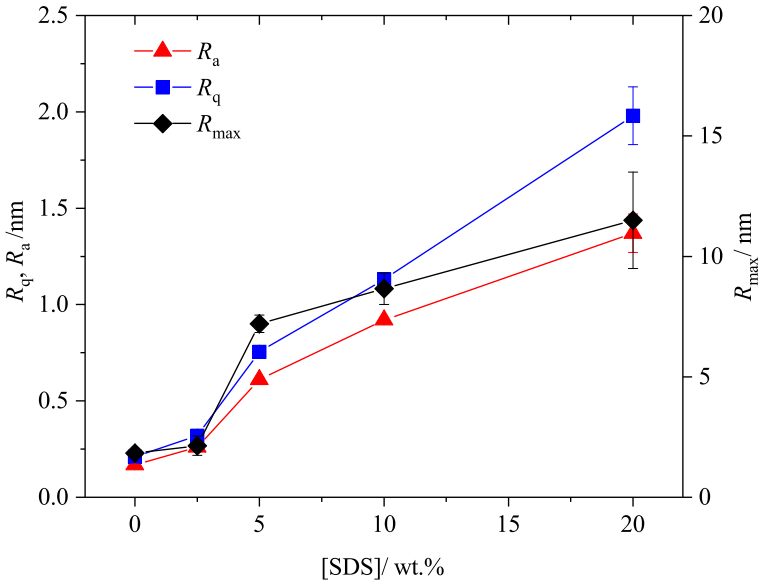

Figure 4.17: Change in average roughness, root mean square roughness and maximum roughness of binary PVA films with surfactant loading.

SDS, although the scanned regions of the films containing 0 % and 20 % SDS were found to be featureless in adhesion. It should be noted that due to the presence of larger-scale surface features, images of 5 µm were captured for plasticised films containing SDS (in contrast to the binary films containing SDS and the plasticised film in the absence of SDS, where 1 µm areas of film were captured). Although the Bragg sheet present in the off-specular reflectivity reveals in-plane surface structures of lengthscales $\sim$ 4.1 nm, these are impossible to resolve on AFM scans because they are not larger than the AFM tip diameter ($\sim$ 10 nm), and thus the focus here is on the larger scale surface structures. As for the binary films, SDS inclusion results in the presence of distinct surface features, compared to the PVA/glycerol film, although little obvious difference can be identified from the films containing 5, 10 and 20 wt.% SDS. For 10 and 20 wt.%, these structures resemble connected domains, that are on the order of 1 nm higher than the remaining sample surface. This is reflected in the values for surface roughness (plotted in Fig. 4.20), which shows an increase in all three roughness parameters upon inclusion of 5 wt.% SDS, but no further change (outside the uncertainty in the measurements) upon increasing SDS concentration to 20 wt.%. This is different to the behaviour of the binary films. Comparison of the height and adhesion maps for films containing 5 and 10 wt.% SDS reveals that the most prominent structures on the film surface have greater adhesion than the surrounding material. This is in contrast to observations of the binary films, and suggests that

these elevated regions are rich in the tackier plasticiser and surfactant. It can also be seen that the variation in adhesion across the film is substantially less for the film containing 5 wt.% SDS than 10 wt.% SDS, contrasting with the behaviour observed in the height maps. It is likely that the regions of greater adhesion are caused by the presence of glycerol on the surface. This is consistent with the slight enrichment of glycerol observed for the thinner films. Even in the absence of significant glycerol surface enrichment, the adhesion of the polymer-rich regions is nonetheless expected to be greater in the presence of plasticiser. When the surfactant concentration is low, and no complete surfactant-glycerol structures are able to form, this could lead to regions of glycerol-plasticised PVA on the surface. At higher loadings however, when more extensive surfactant-glycerol nanostructures are able to form on the surface, the surface of the film is likely to be occupied almost exclusively by SDS, giving rise to the lower adhesion observed across the surface; when the surface is dominated by SDS tailgroups, the glycerol at the exterior surface will be negligible.

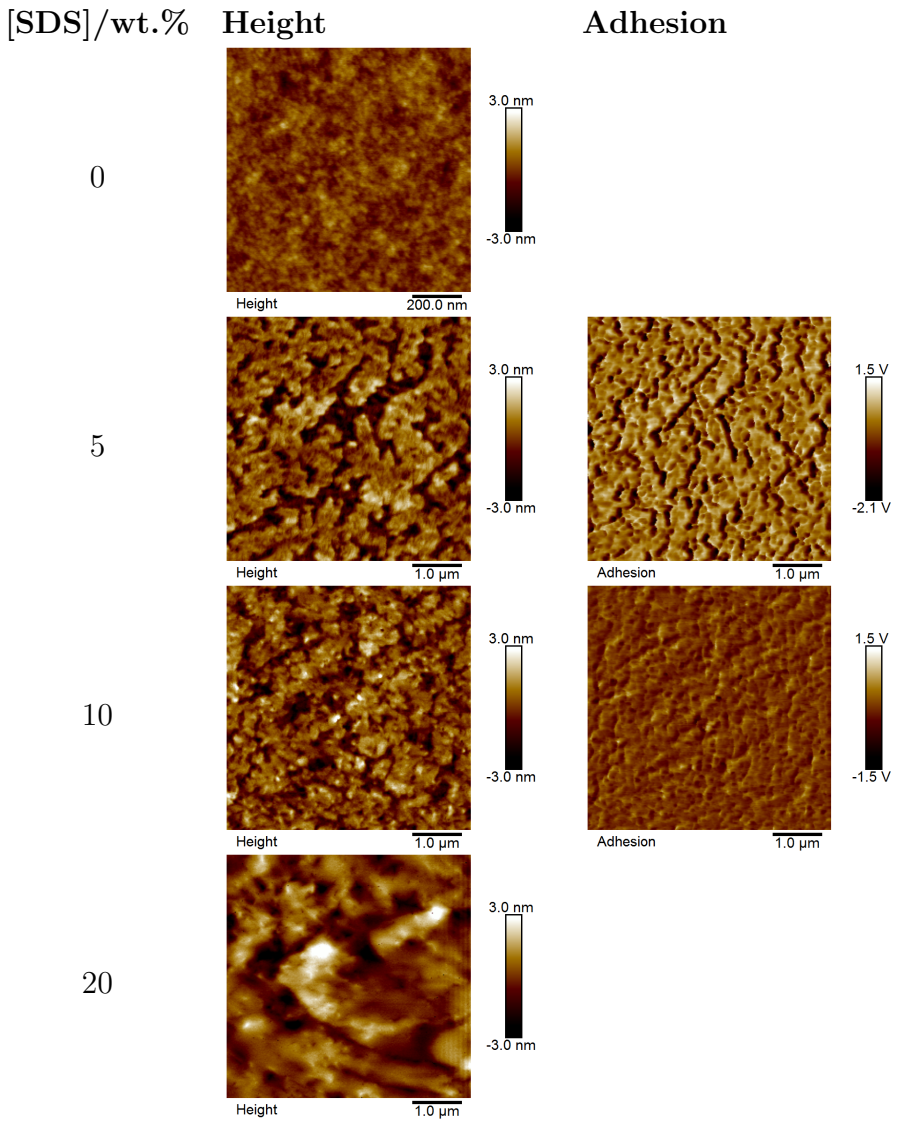

Figure 4.18: Height and adhesion maps for plasticised PVA/SDS films.

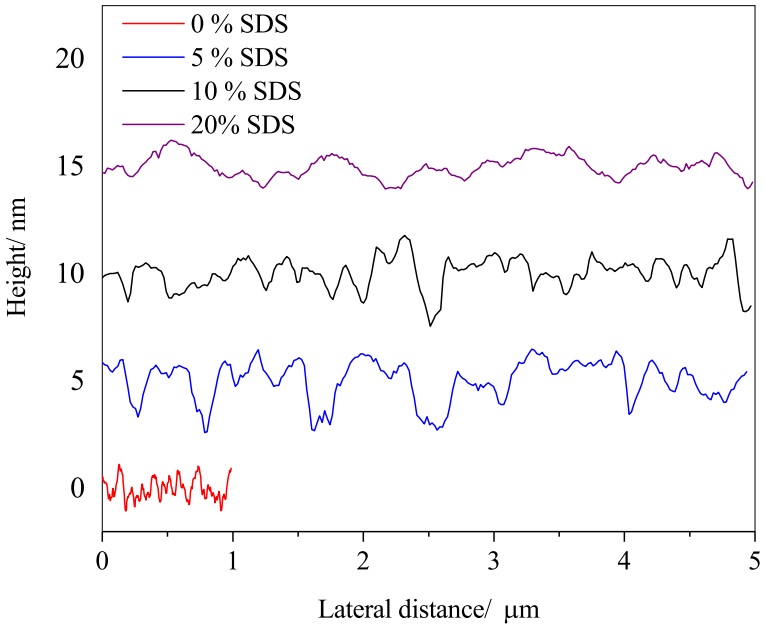

Figure 4.19: Example cross sections of plasticised PVA/SDS films (incorporating 20 wt.% glycerol) with increasing SDS concentration.

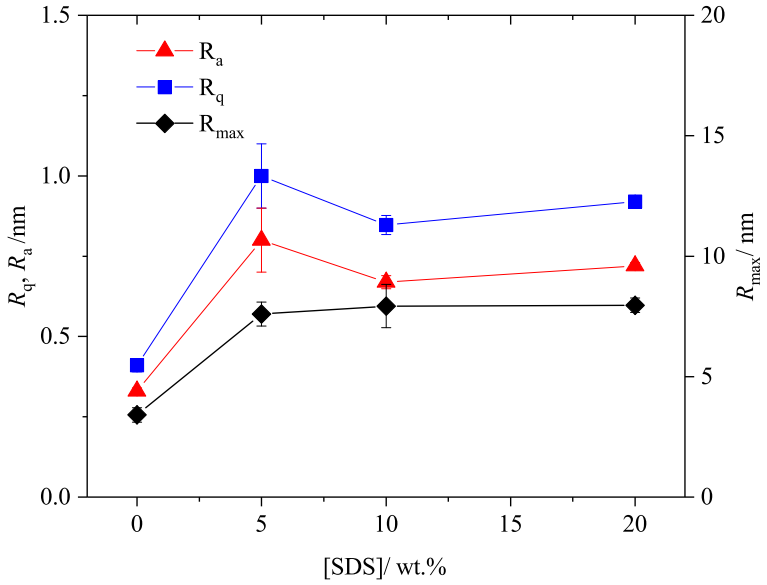

Figure 4.20: Change in average roughness, root mean square roughness and maximum roughness of plasticised PVA films with SDS concentration.

4.3 Discussion

4.3.1 Surfactant Distribution in Binary and Plasticised Films

SDS was shown to segregate extensively from unplasticised PVA films. In the film containing 5 wt.% dSDS, it appears that the surface does not consist of a layer of pure surfactant, but instead comprises a thin (3.5 nm) layer of PVA enriched in surfactant, or alternatively an incomplete and patchy wetting layer. This is likely due to the limited availability of surfactant in this thin film. In the thin unplasticised film containing 10 wt.% dSDS, however, it is clear that a full wetting layer is able to form. The thickness of this layer, 4.5 nm, is much greater than the average length of an SDS molecule, calculated by Sammalkorpi et al.[179] to be 1.36 ± 0.07 nm, suggesting the surface adsorption of multiple surfactant layers during the drying process.

In order to rationalise and understand this segregation, the surface energies of the respective components should be considered, as spontaneous surface segregation would be expected for the component with the lower surface energy. Values for the surface energy of PVA from 37 to 59 mN m^{-1} have been reported, varying with molecular weight and degree of hydrolysis.[180–183] However, the polymers most closely resembling that used for this study have surface tension reported to be ~40 mN m^{-1}. As reported values for the surface energy of pure SDS range from 48.4 to 52.5 mN m^{-1},[184] all of which are greater than the surface tension of PVA, no spontaneous surfactant segregation may be expected based on these values alone. However, it is likely to be of greater value to consider the surface activity of components in aqueous solution. This will be addressed thoroughly in Chapter 5, alongside the role of the compatibility of film components.

Although glycerol shows no surface activity when present as the only additive in PVA films,[168] it has a profound effect on the segregation of SDS. In the presence of glycerol, surfactant segregation was enhanced significantly, evident by an increase in both the thickness of the surface layer and the surfactant volume fraction in this layer. This was accompanied by a decrease in the concentration of surfactant in the bulk, subsurface layer. It can be seen that in the thin, plasticised film containing 10 wt.% dSDS, $\phi_{b(\mathrm{dSDS})} = 0.025$, corresponding to a dSDS concentration of 2.3 wt.%. (The significant surface excess means that even though the concentration of dSDS in the bulk film is low, the total amount of dSDS reflects the composition of the 10 wt.% dSDS solution used to spin cast the film.) This is greater than the total SDS concentration incorporated into the film containing

2 wt.% dSDS, which can still be seen to exhibit a surface excess, with a very limited concentration remaining in the bulk film. The increase in $\phi_{b(\mathrm{dSDS})}$ with total SDS concentration could therefore suggest that some surfactant becomes kinetically trapped in the bulk film during the spin-casting of films with higher surfactant loading, and that these films are therefore not at equilibrium. On the other hand, the lack of change of $\phi_{b(\mathrm{dSDS})}$ in the binary films suggests that this concentration of surfactant may be more readily accommodated by the polymer, and thus there may a greater compatibility of the polymer and surfactant in the absence of plasticiser. This will be explored more extensively in the next chapter.

Upon increasing film thickness, multiple repeating layered structures on the film surface were resolved by NR, even when only a low concentration of surfactant was present. This behaviour, where a substantial amount of additive precipitates on the film surface, is referred to as blooming. In thin films, blooming was only observed for high concentrations of SDS.[174] As discussed in reference 174, the thickness of these layers corresponds very well to surfactant bilayers, separated by layers of glycerol molecules. Despite being measured on separate films, the SLD profiles measured with the two different deuterium labelling regimes fit together very well. The remarkably consistent values for the thicknesses of these repeating layers provide strong evidence for a multi-layered surface structure in thick PVA/SDS/glycerol films, with the only significant variation being in the number of stacked layers. The films fitted with repeating multilayers could therefore be represented by the structure indicated in Fig. 4.21. This layering of multiple smectic surfactant/plasticiser layers, has not been observed for other surfactants in PVA.[168] However, the behaviour of SDS correlates with its strong tendency to form bilayers and stacked structures in other media.[185–187] For example, Coiro et al.[185] report the presence of SDS lamellae of thickness $\approx$ 4 nm, separated by a polar slab in concentrated aqueous solutions. As glycerol is also highly polar, and capable of interacting favourably with the surfactant head groups, it is therefore perhaps unsurprising that this is the thermodynamically favourable conformation adopted by the segregated surfactant, necessitating the limited segregation of glycerol molecules. Auvray et al.[187] have measured the phase behaviour of SDS in non-aqueous solvents including glycerol. Although they observed that the lamellar phase forms only above 104 °C, with SDS crystals present in the solvent at lower temperatures, the presence of PVA could nonetheless drive the formation of these SDS/glycerol layers as surfactant is excluded from the bulk polymer.

This spontaneous structuring does suggest that the formation of smectic layers is likely to be thermodynamically favourable, as exclusion of the surfactant from

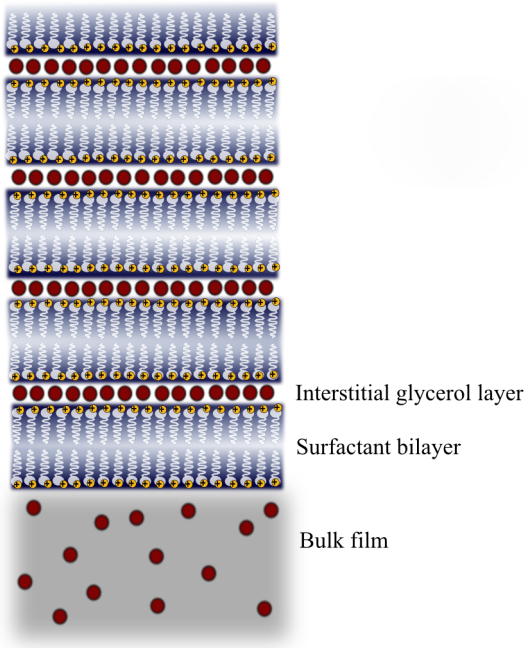

Figure 4.21: Diagram of the structure of the surface excess in thick, plasticised PVA/SDS films.

the bulk film into an ordered, stable structure without perturbing the polymer chains enables the system to minimise its free energy. However, further insights into whether this enhancement of segregation by glycerol is kinetically or thermodynamically driven can be gained by assessing how the film thickness affects the surface excess and fraction of segregated surfactant in plasticised films.

If the plasticiser enhancement of the surface excess is thermodynamically driven, the surface excess would be defined by the solubility limit in the bulk film. It would therefore be expected that increasing the total amount of surfactant (by increasing film thickness) would increase the surface excess, while the concentration of surfactant accommodated in the subsurface region would remain constant.

On the other hand, if equilibration is kinetically limited, with the presence of glycerol increasing the mobility of components during spin casting, ultimately enabling a greater proportion of surfactant to arrange itself on the surface during the relatively quick drying times, it is likely that the structure and size of the surface excess would remain constant with film thickness. The surface excess would then be defined by the rate of migration in the drying film and bulk concentration would therefore change as the ratio between solutes remains constant but total amount of surfactant increases.

From the volume fraction-depth profiles determined by NR, it is clear that there is a significant increase in the surface excess of dSDS with film thickness,

as well as surfactant concentration. This therefore strongly suggests that the enhancement of the SDS surface excess by glycerol is driven by the thermodynamically favourable structuring of the surface excess into stable smectic layers. Specific factors responsible for surfactant segregation will be considered in greater depth in Chapter 5.

The substantial quantitative differences in the depth profiles obtained using NR and RBS suggest that the mobility of additives after the spin-coating of the films could have a major role in the distribution of film components. This is likely to be due to the presence of residual water. It is worth noting that, with a slightly lower surface energy, the deuterated surfactant (used in NR) may have a greater tendency to segregate than the fully hydrogenated surfactant (used in RBS). However, this effect is likely to be small. Additionally, the fact that the depth profiles of d-glycerol in thick PVA/SDS/glycerol films show large regions of depleted SLD on the surface, corresponding to surfactant, confirms that the hydrogenated surfactant still exhibits extensive segregation. The substantial differences in quantitative values obtained with NR and RBS make it most likely that RBS measurements were taken on films in a state of incomplete equilibration, and further surface structure rearrangement occurs during the relatively long time required for sample alignment and data collection for the former technique.

4.3.2 Impact of Surfactant and Plasticiser Inclusion on PVA Film Topography

AFM can be used to relate the surfactant depth profiles to the film topography. From the dSDS depth profiles determined from NR, it can be seen that increasing both SDS concentration and total film thickness results in an increase in surface excess. For each film, the low overall film roughnesses observed by AFM supports the simple interpretation of the specular neutron reflectivity. From the variation in roughness parameters with SDS concentration, it is clear that this increase in z^* is accompanied by a substantial increase in surface roughness. From Fig. 4.17, the greatest increase in roughness occurs upon increasing SDS concentration from 2.5 to 5 wt.%. No NR data was obtained for binary films with [SDS] <5 wt.%. However, based on the observation that the presence of glycerol promotes SDS segregation, and the depth profile of dSDS in a plasticised film containing 2 wt.% surfactant reveals only a slight surface excess, very low amounts of segregation would be expected in the binary film. This would result in a film surface of similar roughness to that of a pure PVA film. Figure 4.2 shows that there is extensive surfactant segregation from binary films containing 5 wt.% dSDS, which results

in the substantial increase in roughness observed by AFM. A slight increase in roughness is found when 10 wt.% SDS is incorporated compared to 5 wt.%. From NR the thickness of this layer in the film containing 10 wt.% is similar to that of the film containing 5 wt.% SDS, although the concentration of SDS is higher as it approaches more complete wetting in the former film, resulting in a modest increase in roughness. This increase in roughness should be expected as the segregation of a single, solid additive results in the presence of defects in the solid adsorbed layer.

In contrast to the binary films, there is negligible increase in film roughness of plasticised films above an SDS loading of 5 wt.%. This could be linked to the formation of a highly structured surface excess in the presence of plasticiser. The stacking of SDS bilayers in plasticised films with high SDS concentration has been found,[174] and this has indeed also been observed for thick films of lower SDS concentration. With 5 wt.% SDS adequate to form a wetting layer of surfactant on the film surface in the presence of plasticiser, and any additional surfactant leading to the formation of additional surfactant bilayers separated by glycerol, it is reasonable to suggest that this would lead to an even surfactant layer on the film surface. Therefore, following the formation of a wetting layer, any increase in the concentration of SDS has little effect on the surface roughness. The observed features in the height maps are likely to be defects in the lamellar-structured surface excess.

Considering the SLD profiles obtained alongside the AFM height maps, it is likely that the repeating smectic layers extensively cover the surface, but there are defects that could consist of areas of fewer numbers of stacked layers. This is analogous to lipid-surfactant layers containing defects, that are routinely studied using NR.[188,189] For plasticised films containing SDS, $R_q < 1$ nm. This is substantially less than the thickness of a surfactant bilayer (≈ 4 nm). However, the maximum roughness of ≈ 8 nm, is approximately equal to the thickness of the surface excess layer of these films as determined by NR, suggesting that even without a high level of structuring of the surface layer, as observed for the thin films, the segregated layer is patchy.

4.4 Chapter Conclusions

In this chapter, the segregation behaviour of the anionic surfactant SDS has been explored. Extensive segregation in binary films, leading to wetting layers of SDS, was observed from surfactant depth profiles obtained using neutron reflectivity. This segregation was found to increase in the presence of glycerol, and in thick

films the plasticiser enables the formation of stacked structures of alternating glycerol and surfactant layers on the surface, which could be identified by determining the depth profiles of both dSDS and d-glycerol.

By studying the effect of film thickness, it can be concluded that the observed enhancement of the surface excess by glycerol is thermodynamically driven by the formation of the stable smectic layers on the surface, as the thickness of the surface layer (and thus number of repeating layers) is related to the total amount of surfactant present, not simply the surfactant concentration relative to PVA. This has significant implications for the thick ($\sim 70\,\mu m$) industrial films, which are often similarly plasticised, as incorporation of a very low concentration of additive could eventually lead to a substantial surface excess and therefore significantly impact the properties of the film.

Determination of the distribution of SDS using Rutherford backscattering, after immediately vitrifying samples following spin-coating, revealed the same qualitative trend as determined by NR, with an increase in surface excess observed with increasing film thickness. However, values for the surface excess were substantially lower than those determined by NR, which strongly suggests that equilibrium structures are not obtained immediately during the spin-coating.

Although the off-specular reflectivity has indicated that there is some lateral structuring on the plasticised film in addition to the formation of alternating surfactant/plasticiser layers parallel to the surface, AFM has also revealed some longer-range surface structures, which are likely to indicate defects in the repeated surface structure such as patches of fewer repeating layers. However, the consistency of the average and maximum roughness values throughout the surfactant concentration range suggests that the size and number of these defects are similar at each SDS loading. In contrast to the evenly stacked layers present on the surface of the plasticised films, the huge increase in roughness of binary films with SDS concentration suggests that the NR profiles correspond to the presence of uneven wetting layers of almost pure SDS.

Thorough characterisation of the distribution of components in model systems is the first step in understanding the segregation behaviour of additives in PVA. By contributing the extensive characterisation of this model system to those previously characterised, the aim is to build a more complete picture of the behaviour of surfactants in PVA, and use these observations to understand the role of different factors in segregation. This will be considered more extensively in the next chapter.

Chapter 5

Solution State Studies: Rationalising Segregation Observed in Model Systems

5.1 Chapter Introduction

Both the model films used in this work and the complex industrial films are prepared from aqueous solutions of polymer and additives. It is therefore of interest to better understand the interactions between components in solution, as their solution properties are likely to influence the final structure and nature of interactions in the film. Although the interactions between polymers and surfactants have been extensively studied in solution[51,52,65,173,190,191] (as discussed in greater detail in Chapter 2), on the whole this research has largely focused on the effect of small amounts of polymer on the micellisation behaviour of surfactants and their aggregation with the polymer below the critical micelle concentration (CMC). Conversely, solutions used for film preparation, either model spin-cast films or thick commercial films, contain very high concentrations of polymer and lower amounts of surfactant additives. Although the surfactant:polymer ratio is generally low, the relatively high total solute concentration in these solutions makes the concentration of surfactant significantly greater than the CMC. In this chapter two main driving forces for surface segregation will be assessed: surface energy and compatibility. By assessing these in turn, the aim is to be able to begin to make justified predictions of the segregation behaviour in polymer/additive films, based on their experimentally-accessible solution behaviour. The solution behaviour of film components of the two systems previously studied[147,168] (containing the cationic surfactant, CTAB and the non-ionic surfactant, $C_{12}E_5$) as

well as the SDS system from Chapter 4 will be assessed, and discussed in the context of their observed segregation behaviour.

5.2 Results and Discussion

5.2.1 Role of Surface Energy in Segregation

One likely driving force for migration is the surface energy differences between components; as discussed in Chapter 2, the component with the lowest surface energy should be enriched at the surface of the mixture. In the case of films prepared from aqueous solutions, the surface tension of solutions of each solute is therefore useful in understanding the surface activity of different components. Additionally, measuring the surface tension of mixed solutions can help gain insight into the drying process and aid in understanding the interactions between components in solution. Surface tension has been widely used to explore the nature of polymer surfactant interactions,[51–53] and a greater understanding of the interactions in these systems can be used to relate the solution properties to the properties of the solution-cast or spin-cast films, aiding the identification of driving forces for segregation, and ultimately assisting in predicting and controlling this behaviour.

The solute concentration used to spin-cast model films is high, relative to the CMC of the surfactant species. However, in order to explore the interactions between components of the model films, particularly via surface tension measurements, lower solute concentrations must be used, both to reduce excessive viscosity and to ultimately aid transferability to the industrial systems where, although total solute concentration in the aqueous solutions used for film preparation is very high, additive concentration is much lower than in these simple model systems.

5.2.1.1 Surface Tension of Individual Film Components

The surface tension of the pure film components in aqueous solution was first considered in order to characterise the surface activity of individual species in dilute solution. Plots of the surface tension of aqueous solutions of each of the solutes are shown in Fig. 5.1.

The surface tension behaviour of PVA was characterised using solutions of the same polymer used for film preparation (30-70 kg mol^{-1}, 87-90 % DH). There is a linear decrease in surface tension with ln[PVA/wt.%], up to a transition at 3 wt.%, indicative of some association of the polymer in solution above this concentration.

The observed surface tension of these solutions shows very similar behaviour to that observed by Tadros,[65] who used PVA with a molecular weight of 42 kg mol^{-1} and a DH of 88 %. Although the concentration at which this transition occurs differs slightly (0.7 % (w/v)), this could be attributable to the difference in molecular weight. Additionally, although the degree of hydrolysis is very similar to that used in this study, the distribution of the remaining acetate groups is likely to significantly affect both the surface adsorption and the micellisation of the polymer. Blocky polymers are likely to be more effective at lowering the surface tension and forming micelles than polymers where residual acetate groups are evenly distributed throughout the chain.

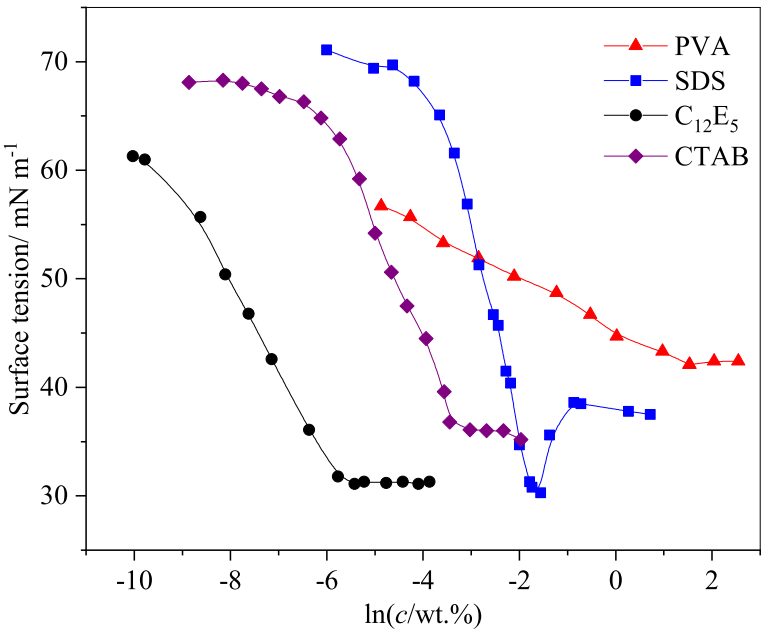

Figure 5.1: Surface tension of aqueous solutions of each of the pure solutes. Lines are a guide to the eye.

The Gibbs adsorption equation can be used to determine the surface excess (Γ) of a solute (Equation 5.1), using the gradient of the linear section of the plot of surface tension (γ) against the natural logarithm of concentration (c). R and T represent the molar gas constant and absolute temperature respectively. Here, the surface excess is defined as $\Gamma = z^*/V_m$, where V_m is the effective volume of the adsorbing molecule. Although n is equal to 1 for nonionic surfactants, the rigorous thermodynamic treatment requires the term $n = 2$ for a 1:1 electrolyte, such as SDS, in the absence of extra electrolytes. However, the point should be raised that, while this factor is widely accepted in the literature, the factor $n = 2$ suggests equal contribution of the anion and cation to the surface tension, whereas in reality they differ hugely in both size and surface activity.[192] Nevertheless, Tajima et al.[193] found that the Gibbs adsorption for SDS is valid for $n = 2$, with

the authors using activity in place of concentration.

The surface excess represents the excess of solute per unit area over what would be present if the bulk concentration prevailed all the way to the surface. However, it is important to note that this equation is only valid for ideal solutions, where the activity coefficient is 1 and thus the activity is equal to the concentration. In this case, as the concentration range for these surfactants in the region below the CMC is very low, replacing the activity with concentration is a reasonable approximation. The area per molecule on the surface of the solution is then related to Γ by Equation 5.2.

$$\Gamma = -\frac{1}{nRT}\left(\frac{d\gamma}{d\ln c}\right)_T \tag{5.1}$$

$$A = \frac{1}{\Gamma N_A} \tag{5.2}$$

It is possible to using the Gibbs adsorption equation at 20 °C, to determine Γ_{PVA}. This yielded a value of 0.47± 0.01 µmol m^{-2}, corresponding to a molecular area, A_{PVA}, of $3.50 \pm 0.09\,\mathrm{nm}^2$. However, it has been previously determined that when applied in this form, the Gibbs adsorption equation strongly overestimates the surface concentration of polymers, due to their polydisperse nature, and thus this value should be treated with caution.[31]

This surface tension measurement of SDS solutions, illustrated in blue in Fig. 5.1, shows behaviour in agreement with reports in the literature,[184,194] dropping sharply towards the CMC. of 0.14 wt%. The dip in surface tension observed between 0.15 and 0.25 wt.% SDS has also been extensively reported and is attributable to contamination with traces of dodecanol from SDS hydrolysis.[195]

Using the Gibbs adsorption equation at 20 °C, Γ_{SDS} in solution in the absence of PVA was determined to be 3.8 ± 0.1 µmol m^{-2}. This is consistent with that obtained by Hines et al.[196] using neutron reflectivity (3.9 µmol m^{-2}). The calculated surface excess corresponds to an area of 0.44 ± 0.01 nm^2 per SDS molecule on the surface.

Pentaethylene glycol monododecyl ether ($C_{12}E_5$) (Fig. 5.2) is a nonionic surfactant. As with SDS, it has a 12-carbon hydrophobic tail, but has a much larger, uncharged headgroup consisting of 5 ethylene glycol units.

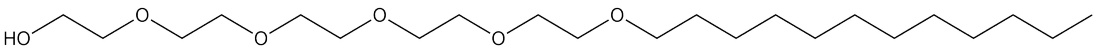

Figure 5.2: Structure of pentaethylene glycol monododecyl ether.

The surface tension behaviour of aqueous $C_{12}E_5$ solutions reveals a CMC at 3.0×10^{-3} wt.%. This is broadly consistent with values reported in the literature,

which, although significantly variable, include 2.9×10^{-3} wt.%,[197] 6.8×10^{-5} M (2.8×10^{-3} wt.%)[198] and 5.7×10^{-5} M (2.3×10^{-3} wt.%).[199] Applying the Gibbs adsorption equation to data in Fig. 5.1 shows that pure aqueous $C_{12}E_5$ solutions show a surface excess, $\Gamma_{C_{12}E_5}$, of $3.31 \pm 0.06\,\mu\text{mol m}^{-2}$, corresponding to a molecular area, $A_{C_{12}E_5}$, of $0.50 \pm 0.02\,\text{nm}^2$.

The final surfactant that will be considered in this chapter is cetyl trimethyl ammonium bromide (CTAB). The structure of this cationic surfactant is shown in Fig. 5.3. The molecule has a 16-carbon hydrophobic tail group and a quaternary ammonium headgroup.

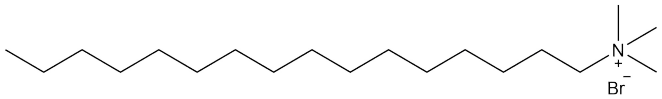

Figure 5.3: Structure of cetyl trimethyl ammonium bromide.

The measured surface tension of CTAB solutions is represented by the purple data points in Fig. 5.1. The CMC of 0.032 wt.% lies comfortably within the range of previously reported critical micelle concentrations for CTAB of 0.027-0.034 wt.% ($0.8 - 0.98 \times 10^{-4}$ M).[200–202] From these measurements Γ_{CTAB} was determined to be $2.19 \pm 0.08\,\mu\text{mol m}^{-2}$, corresponding to a value for A_{CTAB} of $0.76 \pm 0.03\,\text{nm}^2$.

Based on the surface tension behaviours of solutions of each solute, it is clear that although both the polymer and surfactants are surface active, at all concentrations relevant for spin-coating ($\geq$4 wt.%) (which is above the transition points for all components), the surface tension of all surfactant solutions are lower than that of the PVA solution.

It has been previously reported that CTAB shows no surface segregation in spin-cast, non-plasticised PVA films, and is instead evenly distributed throughout the entire film.[168] Upon glycerol incorporation, however, extensive CTAB segregation to both the air and substrate interfaces occurs. This qualitatively follows the same trend observed with the PVA/SDS system. On the other hand $C_{12}E_5$ was shown to exhibit substantial segregation in PVA, and form wetting layers in non-plasticised films.[168] However, $C_{12}E_5$ exhibits much less extensive segregation than SDS, with a greater concentration of the non-ionic surfactant accommodated in the bulk PVA film. The segregation of $C_{12}E_5$ in PVA is somewhat suppressed in the presence of glycerol, with a reduced surface excess forming in the plasticised films. This contrasts with the behaviour of SDS.

Therefore, even taking into account the differences in concentration of the polymer and surfactant in typical solutions used for spin casting, (i.e. 3.6 wt.%

PVA and 0.4 wt.% additive), differences in surface energy of film components cannot alone explain the previously observed different segregation behaviours.[168] If surface energy differences alone determined segregation behaviour, all three surfactants would be expected to exhibit substantial surface excesses, but CTAB shows no surface excess in binary films. If the extent of segregation was dependent only on the reduction in free energy achieved by the surfactant occupying the surface it would be expected that segregation increases in the order SDS < CTAB < $C_{12}E_5$.

Therefore, to better understand the interactions in solution during the drying process the surface tension of mixed solutions containing both polymer and surfactant should be considered. In this way the impact of PVA on surfactant surface activity can be assessed. Tadros[65] has previously studied the effect of PVA on the surface tension of CTAB, finding that at low PVA (< 0.1 wt.%) concentrations the surface activity of the surfactant decreases (the minimum surface tension reached increases) and the CMC becomes ill-defined. This is shown in Fig. 5.4. At PVA concentrations greater than 0.1 wt.%, surface tension merely decreases with increasing surfactant concentration, with no apparent CMC, and surface tension does not reach values as low as in the case of the pure surfactant solution, even at very high CTAB concentrations. Although there are differences in the exact resin used by this study, these findings suggest that the favourable interactions between the polymer and cationic surfactant reduces the surface-energy driving force for the surfactant to segregate, so that less free energy reduction would be achieved by the preferential adsorption of CTAB to the surface. This is in fact consistent with the absence of surfactant segregation observed in the binary PVA/CTAB system. However, it should be noted that the distribution of CTAB in PVA was determined using Rutherford backscattering, which has a lower resolution than NR. Although it would be expected that even partial monolayer coverage should fall within the detection threshold, a very small surface excess of CTAB could have been too little to resolve by this technique. It is therefore not possible to say unequivocally that CTAB shows no surface activity in PVA.

Fig. 5.5 shows the effect of PVA on the surface tension behaviour of SDS and $C_{12}E_5$ solutions. In order to clearly see the effect of PVA on the surface activity of the surfactants, a range of polymer concentrations was used from 0.01 to 0.5 wt.%, (all significantly lower than the 4 wt.% used for film preparation), kept constant throughout the entire surfactant concentration range.

In the case of SDS, although PVA dramatically reduces the surface tension at very low surfactant concentration, presumably due to the adsorption of polymer to the surface of the solution, the surface tension at higher concentrations (rele-

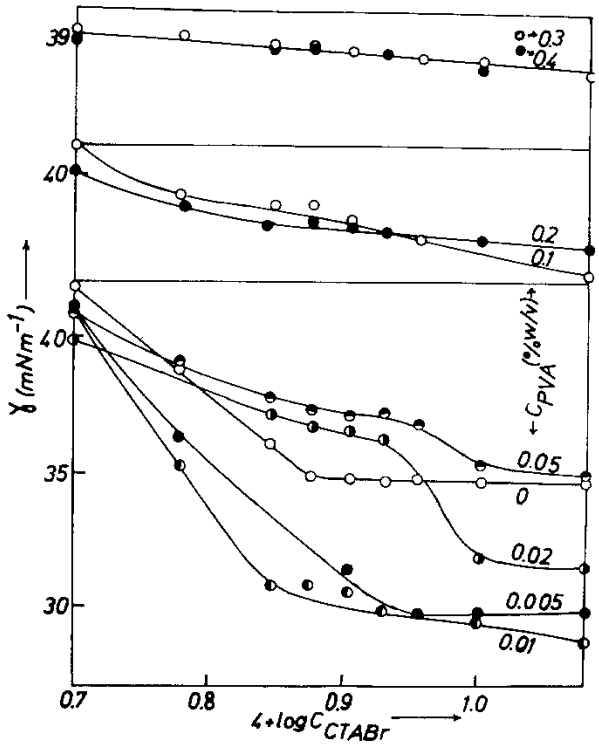

Figure 5.4: Surface tension of CTAB with different PVA concentrations. Reproduced with permission from reference 65.

vant for the spin-coating of films) is higher than that for the solutions containing only SDS, indicating that the PVA suppresses the surface activity of SDS (note this figure is not plotted on a log scale). Although the surfactant is ionic, the nonionic nature of the polymer means that the interactions between components are relatively weak, leading to the absence of any noticeable transitions corresponding to aggregation of the polymer and surfactant. This is perhaps surprising given that noticeable transition points have been previously observed in the case of SDS interacting with poly(ethylene oxide)[51] and poly(vinylpyrrolidone),[52,173] despite the nonionic nature of these polymers. In the presence of PVA the CMC is no longer identifiable, with the surface tension merely decreasing gradually with concentration, as observed by Tadros[65] in the case of the PVA/CTAB mixtures. In contrast to the PVA/CTAB system, however, the minimum surface tension reached is as low as the pure surfactant solution. At the highest surfactant concentrations, which are most relevant for film preparation, the value for surface tension for all PVA concentrations is approximately equal to that in the absence of polymer, suggesting that even though surfactant surface activity is somewhat suppressed at intermediate concentrations, SDS is still the more surface active component at the higher concentrations. Therefore, despite the interactions be-

tween species, enrichment of SDS on the film surface should reduce the surface free energy of the system and thus be favourable.

PVA has a lesser effect on the surface tension of $C_{12}E_5$ solutions than on SDS solutions. Although there is a substantial reduction in surface tension at the lowest $C_{12}E_5$ concentration due to the surface adsorption of PVA, there is no significant suppression of surfactant surface adsorption, even up to 0.4 wt.% polymer, and the CMC can still be clearly identified. Apart from very low concentrations of surfactant, the presence of PVA has negligible effect on the surface tension of $C_{12}E_5$ solutions. This can be rationalised by considering the much weaker interactions present between non-ionic surfactants and polymers, which has been extensively reported.[190,191] This demonstrates that $C_{12}E_5$ remains the most surface active component in the mixed system, meaning segregation to the film surface is favourable, which is indeed observed. Although the surface tension results can account for the $C_{12}E_5$ behaviour, the suppression of SDS surface activity by the polymer highlights the importance of looking beyond simply the differences in surface energy of the pure components in solution in order to rationalise or predict segregation behaviour in other model polymer/surfactant systems.

5.2.1.2 Influence of Glycerol on Surface Tension of Surfactant Solutions

As it has been observed that plasticiser inclusion has a significant impact on the surfactant distribution in spin-cast films in all three of the model film systems studied, in order to thoroughly investigate the role of surface energy in surfactant segregation, the study of the surface tension of film components was extended to explore the interactions between surfactant and glycerol in solution. The surface tension of aqueous glycerol solutions are shown in Fig. 5.6. Takamura et al.[203] previously reported an almost linear decrease in the surface tension of aqueous solutions with glycerol content at 20 °C. However, in this current work (Fig. 5.6) recording the surface tension of solutions using the du Noüy ring method revealed a greater deviation from linearity, although there is a smooth, gradual decrease from the surface tension of pure water to the surface tension of pure glycerol. As glycerol is not surface active, the reduction in surface tension with glycerol incorporation is due to a change in solvent properties. Although glycerol does give rise to some surface tension reduction, it is the least surface active solute and at all concentrations the surface tension of glycerol solutions is much higher than both PVA and SDS solutions. Surface energy alone is therefore unlikely to be responsible for segregation of the plasticiser observed in the presence of SDS

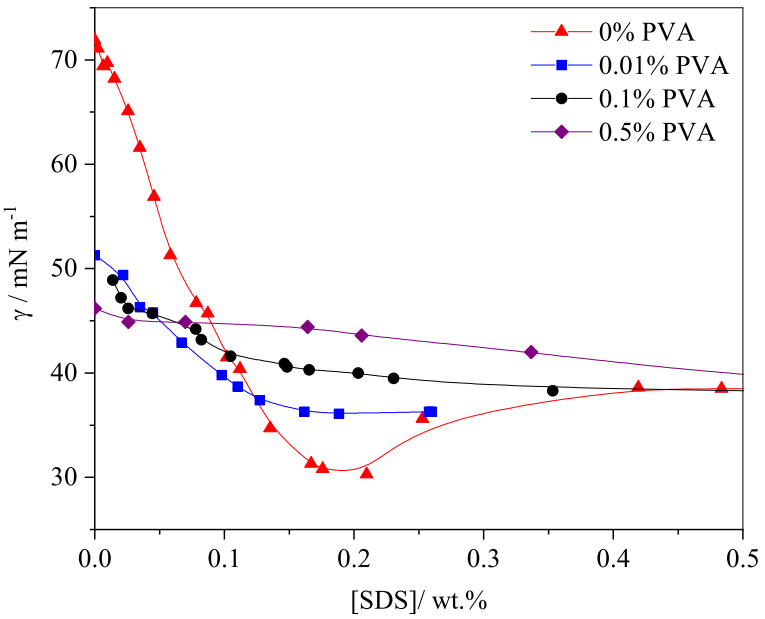

(a) SDS

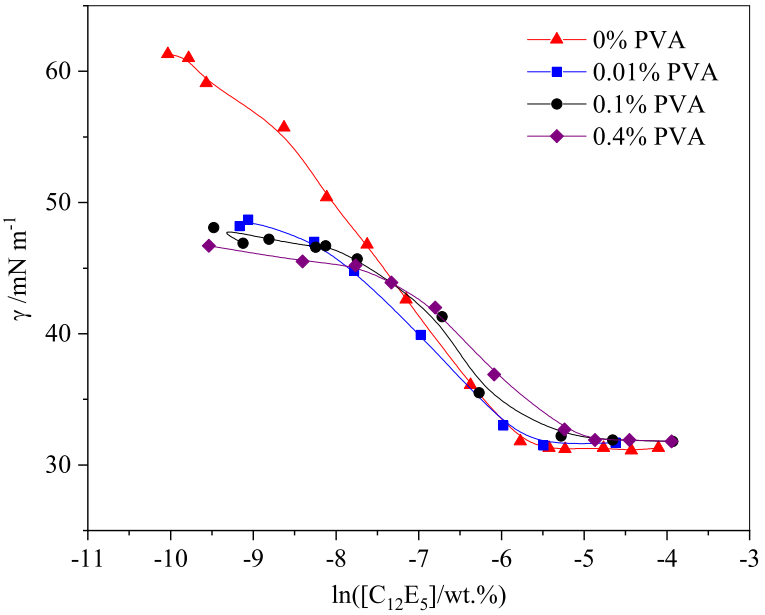

(b) $C_{12}E_5$

Figure 5.5: Effect of PVA inclusion on surface tension of surfactant solutions.

or $C_{12}E_5$. This is also logical given that if this were the case, glycerol would also be expected to segregate in the presence of CTAB, which was not observed by ion beam analysis.[168]

The effect of glycerol on the behaviour of surfactants in solution has been previously reported. Hamel et al.[204] observed an increase in the CMC of CTAB, DTAB and TTAB (analogues of CTAB with 12 and 14 carbons in the alkyl chain respectively) with glycerol concentration, which was attributed to the combination of two factors. First, the presence of glycerol causes a reduction of the

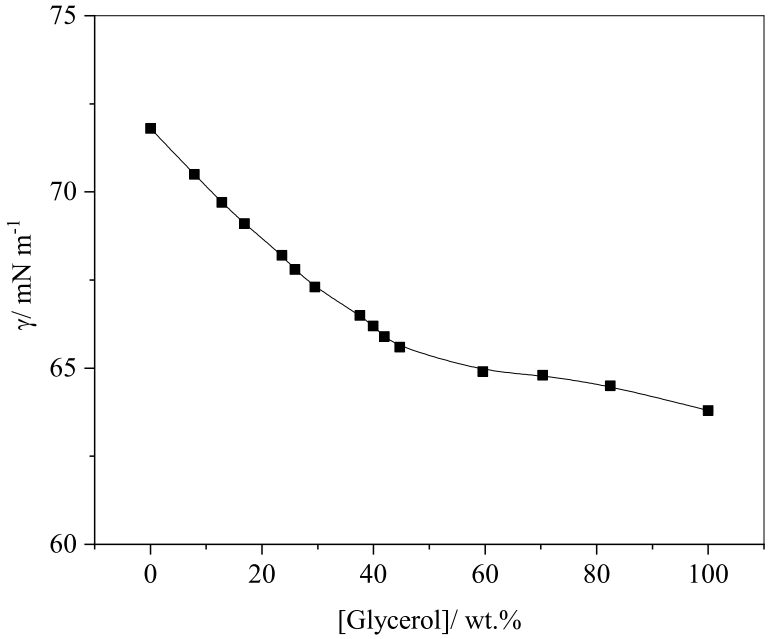

Figure 5.6: Surface tension of aqueous glycerol solutions.

cohesive energy density of the solvent system, increasing the solubilising ability of the solvent system. Second, the co-solvent decreases the dielectric constant of the solution, which favours the mutual repulsion of the ionic head group in the micelle and opposes micellisation. D'Errico et al.[205] also investigated the effect of glycerol on CTAB by analysing the changes in surfactant self-aggregation as a function of glycerol concentration, using surface tension to determine the CMC of the surfactants and static fluorescence quenching to determine aggregation numbers. The authors first found that the CMC of CTAB is affected by the presence of glycerol only when glycerol concentration is above 30 wt.% of the total solution. The area per surfactant molecule was found to increase with glycerol concentration, indicating less dense packing at the air-solution interface. They also showed that the mean aggregation number decreases with increasing glycerol concentration. These observations were interpreted to be a result of an indirect solvent-mediated mechanism. As glycerol lowers the dielectric constant of the medium, the addition of glycerol enhances electrostatic interactions in solution, which oppose the surfactant self-aggregation and cause a slight decrease in the CMC. The increased electrostatic repulsion between the head groups also increases the curvature of the micelle, which results in the observed decrease in aggregation number. The observed decrease in surface activity of CTAB in the presence of glycerol means that surface energy alone cannot explain the segregation of CTAB from PVA films in the presence of plasticiser.

As discussed in Chapter 4, neutron reflectivity revealed a lamellar structure

comprising SDS and glycerol layers on the surface when large quantities of surfactant were present, suggesting a synergistic effect in the adsorption of SDS and glycerol at the PVA-air interface. To fully explore surface energy as a driving force for segregation, the interactions between these species in solution should be investigated. The surface tension behaviour of mixed solutes for this model system was therefore measured. Glycerol was incorporated into SDS solutions at fixed loadings from 6-42 wt.%. The effect of glycerol incorporation on the surface tension of SDS solutions is shown in Figure 5.7. It is apparent that glycerol incorporation enhances the reduction in surface tension achieved by SDS at low concentrations, up to the CMC of the surfactant, showing that the presence of glycerol enhances the efficiency of the surfactant adsorption. At the higher concentrations that are most relevant for the spin-casting or solution-casting of model films, however, glycerol causes no further reduction in surface tension of the SDS solutions (to spin cast a film containing 10 wt.% SDS from a solution with 4 wt.% total solute, ln([SDS]/wt.%) = -0.9). Increasing glycerol concentration can be seen to slightly decrease the CMC, and the dip attributed to dodecanol contamination is much smaller. This could be indicative of the presence of glycerol precluding the efficient packing of the monolayer of SDS and dodecanol. The Gibbs adsorption equation was applied to determine the SDS surface excess at each glycerol loading, which is illustrated in Fig. 5.8. There is an almost linear decrease in the SDS surface excess with glycerol concentration, which is likely to be due to the co-adsorption of glycerol and surfactant onto the solution surface. This means that the solution surface activity of film components cannot alone explain the enhancement in film surface excess in this model system in the presence of glycerol, but the adsorption of glycerol to the solution surface is consistent with the formation of mixed surface layers suggested by NR.

The surface tension behaviour of the three-solute solutions can be assessed in order to consider how glycerol inclusion affects the surface tension behaviour of SDS when it has already been significantly suppressed by the PVA. Fig. 5.9 shows that glycerol incorporation into SDS solutions containing 2 fixed concentrations of PVA has a negligible effect on the surface tension throughout the whole surfactant concentration range. Therefore, these experiments clearly show that surface energy alone is insufficient to explain the plasticiser enhancement of the surface excess in PVA/SDS films.

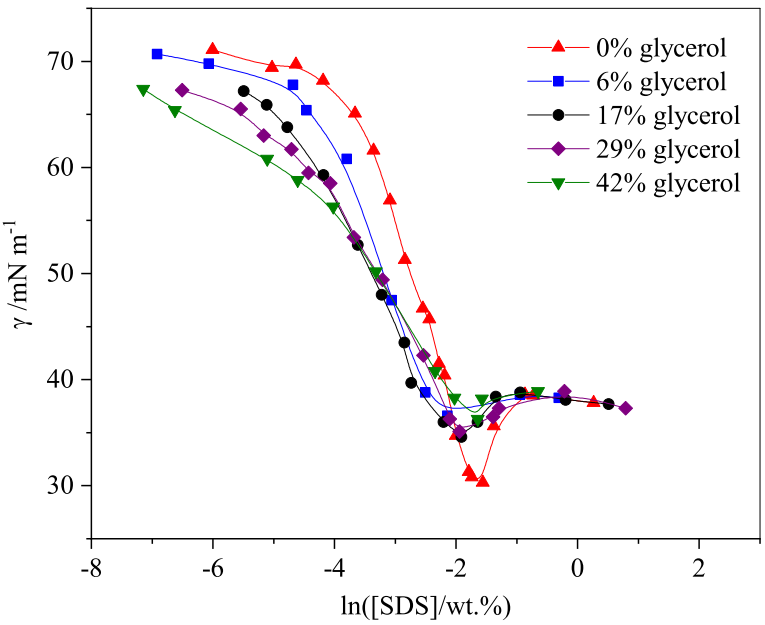

Figure 5.7: Surface tension of aqueous SDS solutions in the presence of 0, 6, 17, 29 and 42 wt.% glycerol.

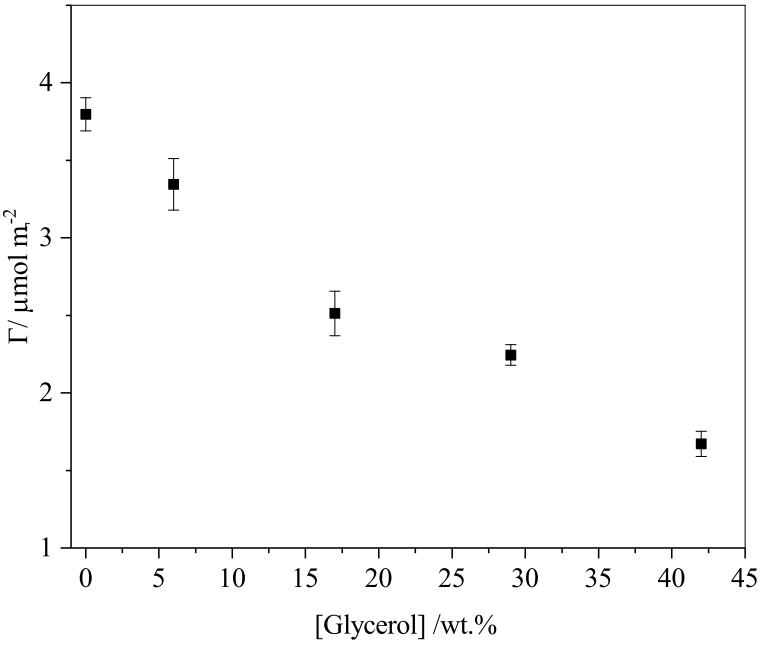

Figure 5.8: Influence of glycerol concentration on the solution surface excess of SDS.

5.2.2 Role of Compatibility in Segregation

It is also important to explore the link between the compatibility of film components and their wetting behaviour in films. There have been a number of theoretical approaches to understand compatibility of different species, including modified Flory Huggins theories and solubility parameters (Chapter 2).[119,120,123,124] Insight into the compatibility of different film components can also be gained experimen-

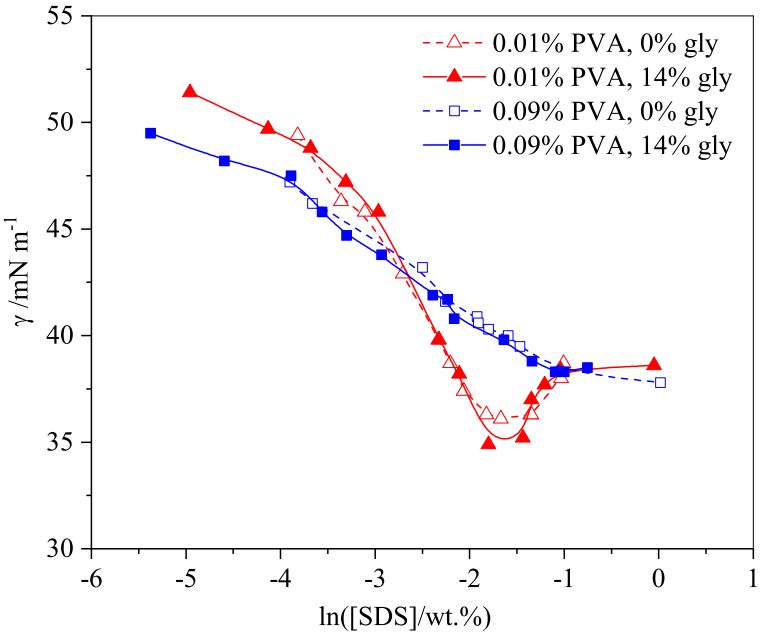

Figure 5.9: Effect of glycerol on SDS surface tension behaviour in the presence of PVA.

tally by exploring the phase behaviour of model systems. The aim of the work in this section is therefore to demonstrate an experimentally facile method, capable of determining compatibility of model systems, that can be used to rationalise and ultimately aid in predicting segregation in other systems.

As both the simple spin-cast films and the industrial films are prepared from aqueous solution, the phase behaviour of the polymer/surfactant/water system should be assessed. This can be done by tracking the composition during solution casting of a thick film on a glass slide, and visually identifying phase separation from the clouding of the film. Phase diagrams were determined at 40 °C in order to reduce time for the water evaporation so that measurements for each polymer/surfactant system can be collected within an hour. This is reasonable as the phase diagrams of CTAB[206] and SDS[207] in water show no phase change between 20 and 40 °C. Although this approach is experimentally accessible, it is not appropriate for non-ionic surfactants including $C_{12}E_5$ as these possess a temperature-dependent cloud point. The cloud point is the temperature at which liquid-liquid phase separation occurs, when the temperature-sensitive hydrogen bonding between the solvent and the oxygen atoms of the hydrophilic tail are insufficient to solubilise the hydrophobic region of the surfactant. At this temperature the surfactant separates into a surfactant rich phase and an aqueous phase containing nonionic surfactant at a concentration close to the CMC.[208] The temperature at which clouding occurs is strongly dependent on the presence

of additives, and their concentration,[209] and could therefore plausibly be used to study polymer-surfactant compatibility. However, using the simple experimental approach of tracking composition during the solution casting of a film to assess phase behaviour would be severely limited by both its temperature sensitivity and the difficulty in judging the liquid-liquid phase separation in a film.

Using the method described above, ternary phase diagrams for the non-plasticised and plasticised PVA/surfactant/water systems were constructed to identify phase transitions associated with the drying of the solution-cast films. In order to construct the plasticised phase diagrams, the PVA:glycerol ratio was fixed at 4:1, and treated as a single psuedocomponent throughout.

The SDS/PVA/water phase diagrams are presented in Fig. 5.10. The single phase, compatible region is represented by black data points and the phase separated, clouded region, where surfactant crystallisation is apparent, is represented by the red data points. First considering the non-plasticised phase diagram, it is apparent that there is very limited compatibility in the absence of water. This extremely limited compatibility is also clear in the plasticised phase diagram. In fact, there is a significant decrease in the size of the one-phase region when PVA is replaced by a PVA/glycerol mixture. The observed enhancement of SDS surface excess in spin-cast films upon glycerol incorporation is therefore consistent with this decrease in compatibility, and phase separation of the system.

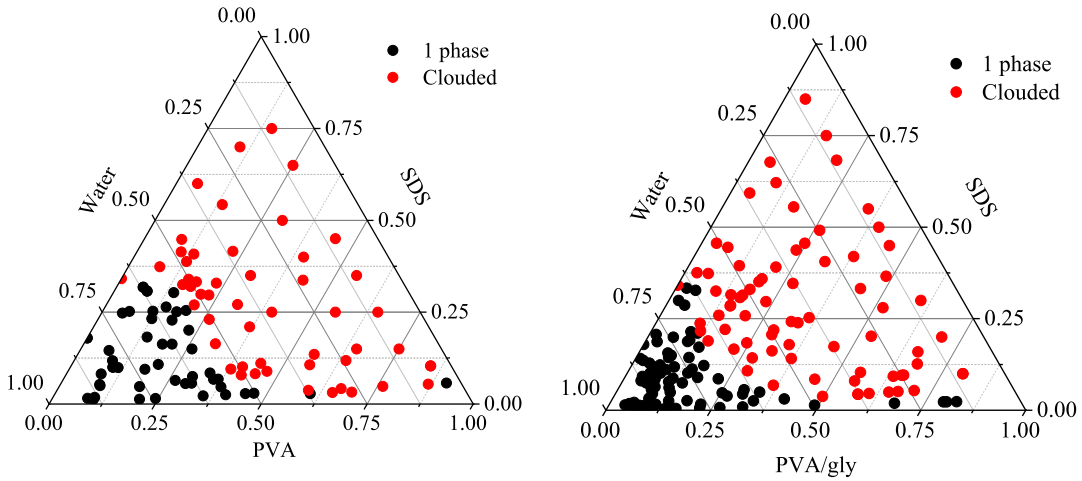

(a) PVA/SDS/water

(b) PVA/gly/SDS/water

Figure 5.10: Phase diagram of the non-plasticised (5.10a) and plasticised (5.10b) PVA/SDS/water systems, in units of mass fraction.

The constructed phase diagrams of non-plasticised and plasticised PVA/CTAB/water system are shown in Fig. 5.11. In contrast to the SDS system, there is an extended one-phase region in the non-plasticised system, where polymer and surfac-

tant are compatible in the absence of water. This is also true for the plasticised system, although substantially less CTAB can be incorporated in the PVA film in the absence of water before phase separation occurs. Given the fact that CTAB has a longer hydrocarbon tail, the significantly higher compatibility of CTAB over SDS is perhaps surprising, as it would be expected to interact unfavourably with the hydrophilic polymer. Tadros,[65] showed that in dilute solution there is a significant interaction between the PVA and CTAB, where polymer binds surfactant in solution via hydrophobic bonding of the surfactant tails and the hydrophobic part of the polymer chain, forming a charged complex. It is therefore plausible that this interaction could be reflected by a favourable interaction in the solid state.

It could be suggested that the absence of CTAB segregation is largely a kinetic effect, where the surfactant, which is solid in the pure state, with its bulky headgroup as a result of its association with the Br^- ion, is unable to migrate to the surface during spin-casting, and thus remains trapped in the bulk film. The segregation apparent in the presence of glycerol could then be explained in terms of the glycerol increasing the mobility of the film components, preventing the CTAB from becoming kinetically trapped in the bulk PVA, and permitting it to localise on the surface. However, the extensive one-phase region of CTAB and PVA in the absence of water suggests that the even distribution of CTAB in PVA films is the result of its compatibility, in conjunction with there being little surface energy reduction from the segregation of the surfactant to the surface (5.2.1). The decrease in the size of the one-phase region in the presence of glycerol (Fig. 5.11b), shows that CTAB is less compatible in the plasticised films. This incompatibility, alongside its greater mobility, could allow for the segregation observed in plasticised films.

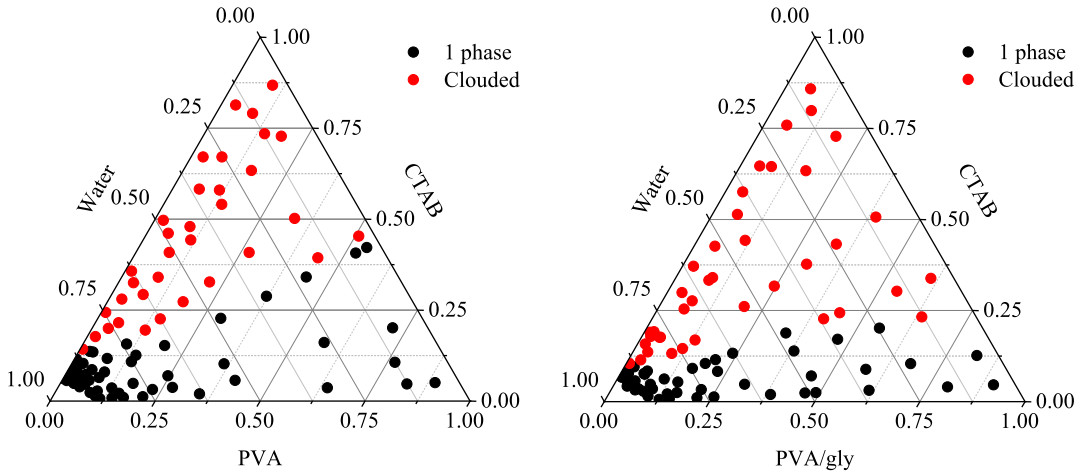

(a) PVA/CTAB/water **(b)** PVA/gly/CTAB/water

Figure 5.11: Phase diagram of the non-plasticised (5.11a) and plasticised (5.11b) PVA/CTAB/water systems, in units of mass fraction. In the plasticised system the PVA/glycerol ratio was fixed at 8:2.

5.3 Chapter Conclusions

In this chapter, surface energy and compatibility have been assessed as driving forces for additive segregation, that can be used to rationalise the behaviour in the PVA/SDS system, as well as some previously characterised model systems. Considering the surface activity of individual film components can provide a useful indicator of the preference of additives to segregate, but, by itself, is limited as consideration of the interactions between the film components may be necessary. Surface energy arguments alone are insufficient to predict the enhancement of the surface excess of CTAB and SDS by glycerol.

Compatibility of bulk systems can be an useful indicator for the segregation behaviour of additives in spin-cast films. This experimentally simple method of determining phase behaviour via solution casting is capable of delivering insights into compatibility, corroborating the observed segregation behaviour in spin-cast films. These initial studies show promise in their transferability to other systems. Based on the significant role of compatibility in the segregation behaviour of surfactant systems, this very simple experimental protocol could have a useful role to play in making initial predictions about segregation in a range of systems.

Taken together, an understanding of the surface tension behaviour of solutions of film components (and the interactions between components) and their compatibility in bulk systems holds promise in being a powerful tool in the prediction of segregation in polymer/additive systems. The insights gained in this chapter will be taken forward in an attempt to rationalise segregation observed

in other model film systems, and test the validity of these conclusions.

Chapter 6

Segregation of Amine Oxide Surfactants in PVA Films

6.1 Chapter Introduction

In this chapter, the segregation behaviour of another class of surfactant will be characterised in order to develop a fuller picture of surfactant segregation in PVA. Amine oxides are particularly interesting because of their small but highly polar headgroup. They are also widely used in industry, notably as a key component of hand dish washing products such as FAIRY.[210] Compared to other surfactants of the same chain length such as SDS and $C_{12}E_5$ they are more hydrophilic, due to the unusually high dipole moment of the -NO group of 4.38 D.[211] In solution this surfactant exists in equilibrium between the protonated (neutral) form and the deprotonated (cationic) form. The position of this equilibrium is dependent on the pH of the solution. The two specific amine oxide surfactants that will be studied in this chapter are *N*,*N*-dimethyldodecylamine *N*-oxide (DDAO) and *N*,*N*-dimethyltetradecylamine *N*-oxide (DTAO), which differ by a single -C_2H_4 group. The generic structure of these surfactants is shown in Fig. 6.1.

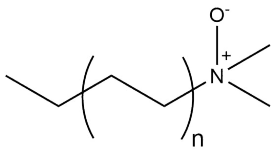

Figure 6.1: Structure of the amine oxide surfactants studied in this chapter. For DDAO and DTAO, n is 5 and 6 respectively.

As in Chapter 4, NR with deuterium labelling is used to identify surfactant segregation in spin cast PVA films. The more complex plasticised system will also be considered in order to determine the effect of glycerol on the distribution of

amine oxides and compare this behaviour to previously studied systems. Surface tension measurements are used to compare the surface adsorption in solution with that identified in the solid polymer, and also to assess the role of surface energy in the surfactant distribution. The phase behaviour of the PVA/amine oxide/water system is also assessed in order to gain insights into the compatibility of these components. Finally, small angle neutron scattering on solution cast films is employed to better understand this compatibility, and the bulk organisation of the PVA/surfactant film. By undertaking these solution-state studies, the aim is to assess how well the conclusions reached in Chapter 5 can be used to rationalise observed segregation in other systems.

6.2 Results

6.2.1 Distribution of *N*,*N*-dimethyldodecylamine *N*-oxide in PVA films

Neutron reflectivity was used to determine the depth profiles of DDAO in spin-cast PVA films. In order to fairly compare the surfactant behaviour in a range of model systems containing the different classes of surfactant, the same resin used in previous systems, with a molecular weight range of 30-70 kg mol^{-1} and a degree of hydrolysis of 87-90 %, was used to prepare the films. The obtained reflectivity data could be fitted well to a three-layer model, consisting of a thin surfactant-rich layer at the film-air interface, a bulk polymer-rich layer, and a layer of higher SLD corresponding to silicon oxide on the substrate. Using the same method described in Chapter 4, the SLD profiles were converted into concentration-depth profiles of the deuterated surfactant. The depth profiles obtained from the binary films are shown as the solid lines in Fig. 6.2. It should be noted that reflectivity for the film containing 2 wt.% DDAO was collected using only the two smallest angles, and is therefore missing the data at high Q. As a result, a slight increase in reflectivity can be identified at $Q \approx 0.2$ Å^{-1}, which would normally not be apparent upon stitching the data with that from the highest angle.

From these depth profiles, a very similar surface composition can be identified for all surfactant concentrations. In order to quantitatively compare these profiles, the volume fraction ($\phi_{\mathrm{DDAO},1}$) and thickness (d_1) of the surface layer of surfactant (determined from the fitted parameters) are included in Table 6.1. These values can be seen to be consistent for each surfactant loading in binary films, with the exception of the lowest loading of 2 wt.%. The thickness of the layers are all consistent within the precision of the measurement (∼0.5 nm),

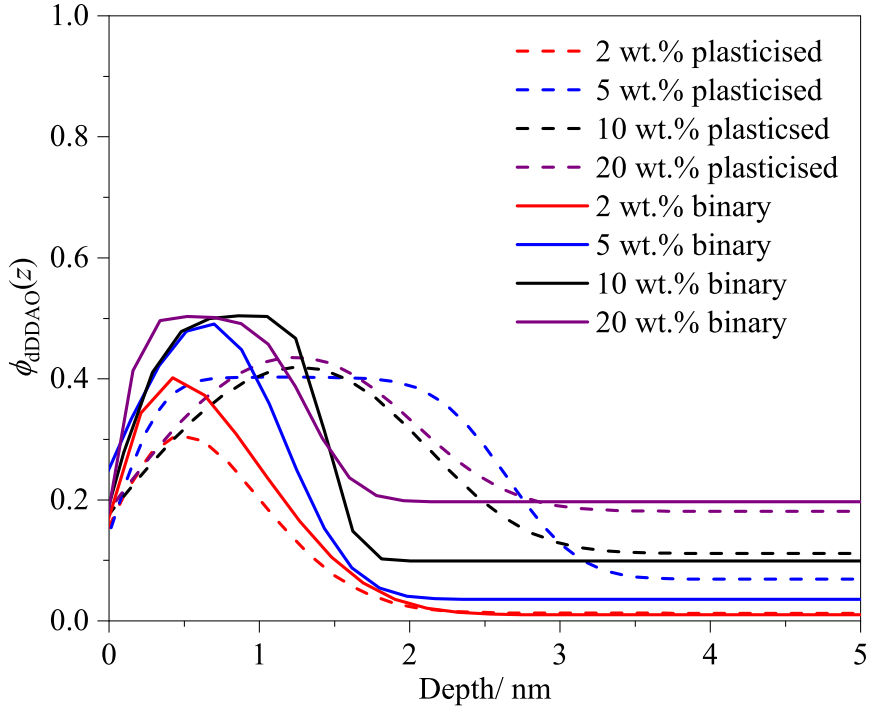

(a) Concentration-depth profiles.

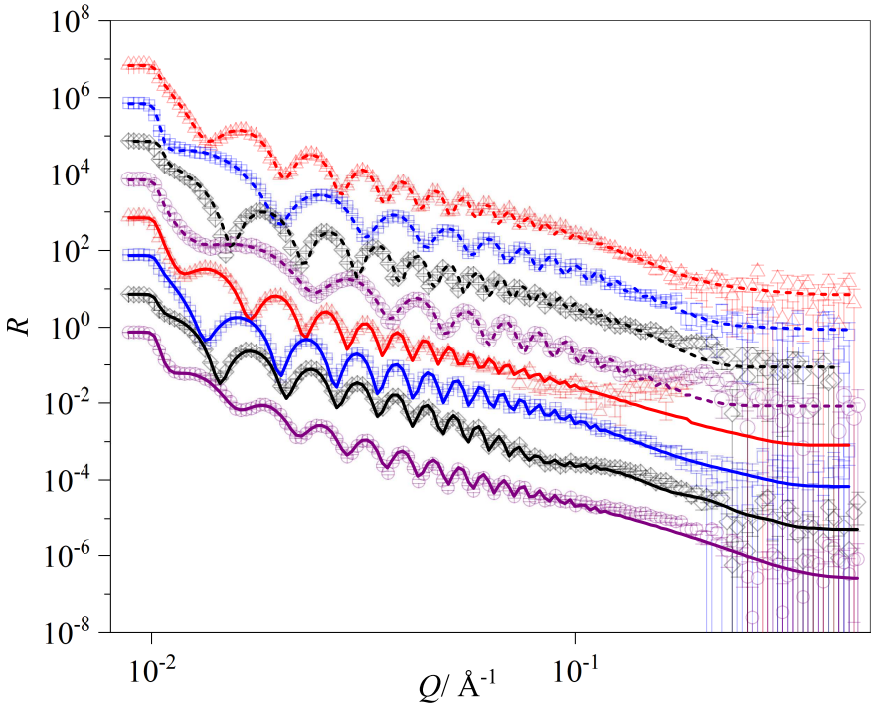

(b) Reflectivity data and fits.

Figure 6.2: Concentration-depth profiles 2-20 % DDAO in binary and plasticised PVA films, and neutron reflectivity data and fits. Fits for data from non-plasticised films are shown as solid lines, with fits for data from plasticised films shown as dashed lines. Reflectivity data offset by factors of 10 for clarity, using the same colour scheme as for the derived profiles.

with this thickness corresponding well to a surfactant monolayer adsorbed onto the surface. The surface excess, defined by Equation 4.3, was also calculated. These values are also included in Table 6.1. In the binary films, little change in the surface excess with surfactant loading can be identified due to the large uncertainties associated with this measurement which result from significant error propagation of each of the fitted parameters (errors in each value were determined by adding the uncertainties of the parameters necessary for calculation of the value in quadrature).

NR was also used to explore the effect of the inclusion of glycerol as a model plasticiser on the distribution of deuterated DDAO in PVA films. The glycerol loading was fixed at 20 wt.% and the surfactant concentration was varied from 2 to 20 wt.%. Using the same method as for the PVA/SDS/glycerol model system the concentration-depth profile of the deuterated surfactant was obtained by assuming an even distribution of glycerol throughout the film. These depth profiles are shown as the dashed lines in Fig. 6.2.

For all surfactant loadings, the concentration of dDDAO in the surface layer is slightly reduced upon glycerol incorporation. Table 6.1 also includes the obtained values for the volume fractions of DDAO in the surface layer of plasticised films, ($\phi_{\mathrm{DDAO},1}$) and the thickness of the surface layer, d_1, alongside the surface excess, z^*. It can be seen that, as observed with the binary films, surfactant volume fraction and the thickness of the surface layer is very similar for all surfactant loadings above 2 wt.%, with both sets of values consistent for each loading within the uncertainty of the fitted parameters. In the case of plasticised films, the consistent structure of the surface layer, regardless of the surfactant loading (with the exception of 2 wt.%), results in a general decrease in the surface excess as the bulk surfactant volume fraction increases.

Table 6.1: Thickness of surface layer (d_1), surfactant volume fraction in the surface layer ($\phi_{\mathrm{DDAO},1}$) and surface excess (z^*) in binary and plasticised films containing dDDAO.

[dDDAO]/wt.%	$\phi_{\mathrm{DDAO},1}/10^{-2}$		d_1/nm		z^*/nm	
	Binary	Plast.	Binary	Plast.	Binary	Plast.
2	50±20	49±6	1.0±0.4	0.9±0.1	0.4±0.3	0.3±0.1
5	60±10	40±3	1.1±0.5	2.6±0.3	0.5±0.3	0.8±0.2
10	60±10	50±10	1.4±0.3	2.1±0.4	0.5±0.1	0.6±0.2
20	56±10	48±3	1.2±0.3	2.0±0.2	0.5±0.2	0.4±0.1
40	54±3	-	1.3±0.2	-	0.24±0.06	-

6.2.1.1 Interfacial Surfactant Adsorption

Comparison of the fitted parameters (included in Appendix B) reveals that depth profiles of samples containing dDDAO appear to have a thicker silicon oxide layer adjacent to the substrate than would be expected (approximately 25 Å, measured by ellipsometry for representative silicon blocks). This observation strongly suggests adsorption of the deuterated surfactant to the substrate interface. The SLD of the deuterated surfactant is similar to that of the silicon oxide, and so adsorption of an additional surfactant layer would manifest itself in a thickening of the third layer in this 3-layer model.

To test this hypothesis, reflectivity data for binary film containing 5 wt.% dDDAO was fitted using a 4 layer model, including an additional layer to account for surfactant absorption to the substrate interface. Although this does result in a slight improvement in the χ^2 values, the other fitted parameters (thickness and SLD of surface and bulk layers) are consistent within the uncertainty of these values. Due to the similar SLD of the enriched layer of deuterated surfactant and the silicon oxide there is a uncertainty in the thickness of this surfactant layer as these two components cannot be distinguished. Therefore, in order to avoid over-parameterisation, the reflectivity data for these systems is fitted using a three layer model, although the thickness of the silicon oxide layer can reasonably be increased due to the presence of surfactant. The increase in thickness of the silicon oxide layer is of the order of (but not greater than) that of a surfactant monolayer. The similarity of the profiles obtained using 3 and 4 models is illustrated in Fig. 6.3.

Table 6.2: Concentration of deuterated DDAO in the solutions used for spin-casting and volume fraction and weight percentage of surfactant in the spin-cast film.

	$[\text{DDAO}]_{\text{sol}}$/wt.%	$\phi_{\text{dDDAO(tot)}}/10^{-2}$	$w_{\text{dDDAO(film)}}$/wt.%
Binary	2.0 ± 0.5	1.4 ± 0.2	1.3 ± 0.2
	5.0 ± 0.5	4.2 ± 0.4	3.9 ± 0.3
	10.0 ± 0.5	10.5 ± 0.2	9.8 ± 0.1
	20.0 ± 0.4	21.2 ± 0.2	19.9 ± 0.2
	40.0 ± 0.4	35.6 ± 0.1	33.8 ± 0.1
Plasticised	2.0 ± 0.5	1.7 ± 0.1	1.6 ± 0.1
	5.0 ± 0.5	8.6 ± 0.4	7.9 ± 0.3
	10.0 ± 0.4	11.9 ± 0.4	10.9 ± 0.3
	20.0 ± 0.4	19.1 ± 0.2	17.7 ± 0.2

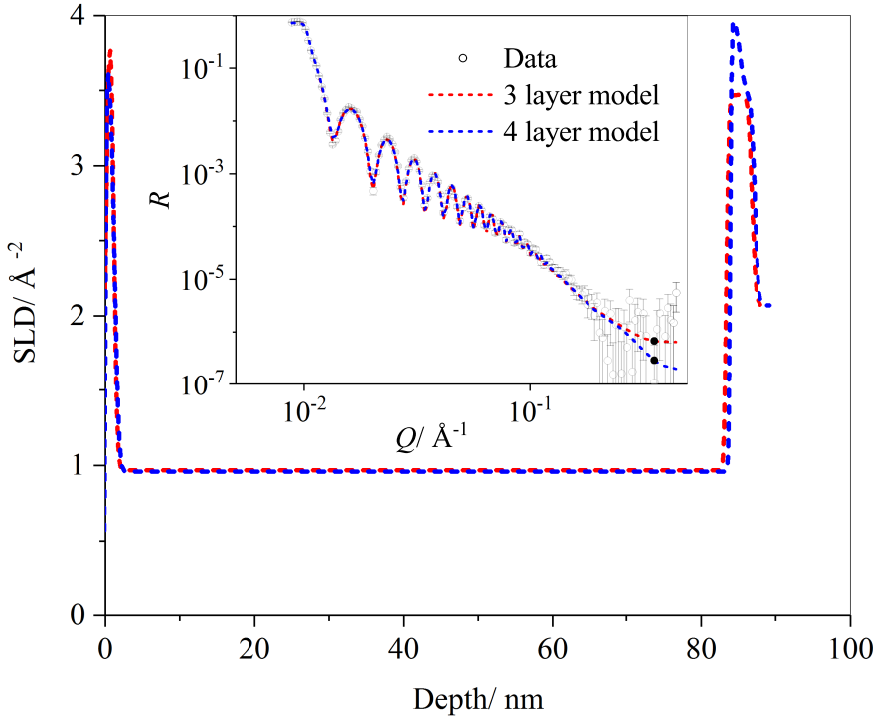

Figure 6.3: SLD-depth profiles obtained from reflectivity data for a film containing 5 wt.% dDDAO fitted with a 3 layer model and 4 layer model (red and blue dashed lines respectively). Data and fits are shown in the inset.

6.2.1.2 Plasticiser Distribution in the Presence of Amine Oxide Surfactants

Further insight into the distribution of components in the plasticised films can be gained by collecting reflectivity data with another contrast. In order to identify any impact of amine oxide surfactants on the distribution of glycerol throughout the film, the SLD-depth profiles of films consisting of PVA, deuterated glycerol and hydrogenated DDAO were obtained. These are illustrated in Fig. 6.4. There is much less contrast in SLD between PVA and the hydrogenated surfactant than between d-glycerol and the hydrogenated components, and so the NR signal is almost entirely dominated by the depth distribution of the plasticiser. However, an accurate conversion of SLD to $\phi_{\mathrm{Gly}}(z)$ cannot be made and the surface excess of glycerol cannot be accurately determined in this three-component system as the distribution of the surfactant is not even and the concentrations of each of the hydrogenated components, and thus their contribution to the SLD, in the surface layer are unknown. (Unlike with the other contrast, the SLDs of the two hydrogenated components differ significantly). However, the minimum and maximum concentration of glycerol on the surface can be determined by assuming the remaining surface is fully occupied by PVA (minimum), and fully occupied

by hDDAO (maximum), which have SLDs of 0.75 $\times 10^{-6}$ and -0.20 $\times 10^{-6}$ Å^{-2} respectively. The SLD of the surface layer in the presence of 5 wt.% DDAO of 3.3 $\times 10^{-6}$ Å^{-2} therefore corresponds to $0.61 \leq \phi_{\mathrm{Gly}} \leq 0.69$, with the spread in values due to the uncertainty the conversion of SLD to $\phi_{\mathrm{Gly}}(z)$. The difference between the values for the minimum and maximum volume fraction of glycerol on the surface is actually less than the uncertainty arising from the fitted parameters.

The surface layer of higher SLD therefore reveals some segregation of the deuterated glycerol. Previous work has confirmed that no segregation of glycerol occurs in pure PVA/glycerol films.[147,168] The increased concentration of glycerol on the surface therefore strongly suggests the co-adsorption of DDAO and plasticiser into a monolayer on the film surface. Comparison of the SLD and thickness of this layer (Table 6.3) shows that, in the same manner as the surfactant distribution, the segregation of glycerol is consistent, regardless of the surfactant loading in the film. This further supports the hypothesis that z^* is independent of $\phi_{\mathrm{DDAO,tot}}$. In contrast to the behaviour of the surfactant, however, there is no evidence for glycerol enrichment at the substrate interface.

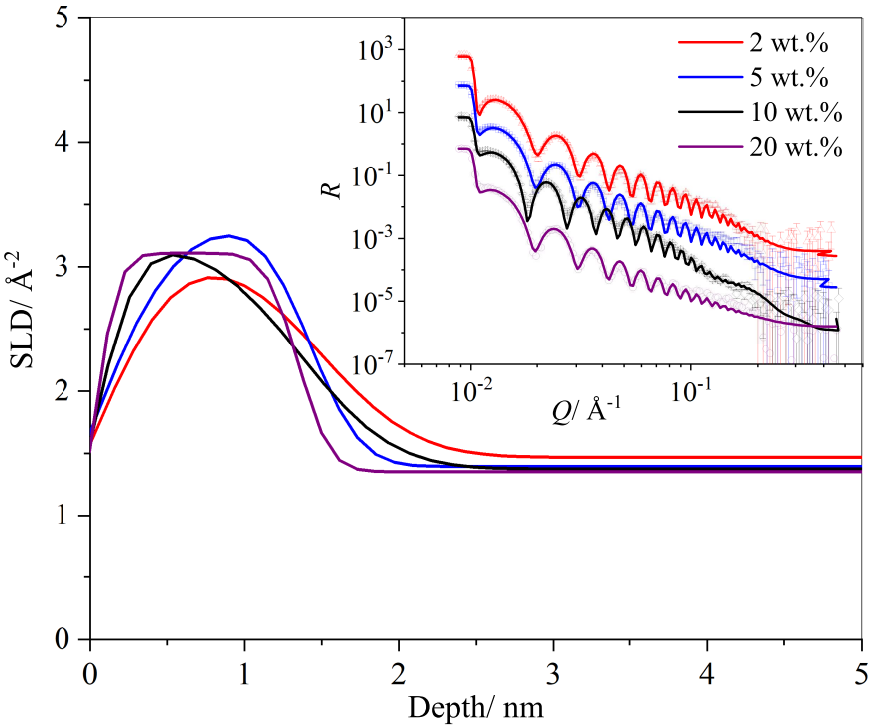

Figure 6.4: SLD-depth profiles obtained from reflectivity data for films containing 2-20 wt.% hDDAO with 20 wt.% d-glycerol. Data and fits are shown in the inset.

Table 6.3: SLD and thickness (d_1) of the surface layer of films containing 20 % d-glycerol and 2-20 wt.% hDDAO.

$[DDAO]_{sol}$/wt.%	SLD_1/ 10^{-6} Å^{-2}	d_1/ nm
2	3.3±0.6	1.5±0.6
5	3.3±0.5	1.4±0.3
10	3.2±0.6	1.3±0.4
20	3.1±0.4	1.3±0.3

6.2.1.3 Impact of Surfactant Tail Length on Amine Oxide Distribution

The effect of the hydrophobicity of the surfactant on the segregation behaviour was assessed by comparing the distribution of *N*,*N*-dimethyldodecyl amine *N*-oxide with *N*,*N*-dimethyltetradecyl amine *N*-oxide (DTAO) (12 and 14 carbons in the chain respectively), in both binary and plasticised films. At a 20 wt.% surfactant loading, DTAO exhibits very similar segregation behaviour to DDAO, where a surfactant rich layer is present on the surface, the thickness of which corresponds well to a surfactant monolayer, with the remaining surfactant evenly distributed throughout the bulk of the film (Fig. 6.5). The fitted parameters for the surface layer (ϕ_1 and d_1) and calculated surface excess are compared for the two surfactants in Table 6.4. As observed for DDAO, plasticisation results in a decrease in the surface volume fraction of DTAO and an increase in thickness of this layer, with no overall change in the surface excess. There is no measurable change in the thickness of the surface layer upon increasing the number of carbons in the alkyl chain from 12 to 14. There is, however, a significant increase in the surfactant volume fraction in the surface layer, and, as a result, a corresponding increase in the surface excess.

Table 6.4: Surfactant volume fraction in the surface layer (ϕ_1), thickness of the surface layer (d_1) and surface excess (z^*) for 20 wt.% dDDAO and 20 wt.% dDTAO in binary and plasticised PVA films.

Surfactant	$\phi_1/10^{-2}$		d_1/nm		z^*/nm	
	Binary	Plast.	Binary	Plast.	Binary	Plast.
DDAO	56±10	48±3	1.2±0.3	2.0±0.2	0.5±0.2	0.4±0.1
DTAO	78±6	61±4	1.5±0.2	1.6±0.2	0.8±0.1	0.6±0.1

For both surfactants, the obtained depth profiles show behaviour remarkably similar to that typically observed for surfactants in solution, with a monolayer adsorbed to the solution-air interface and the remaining surfactant present as aggregates in solution. Based on the assumption that this profile does indeed

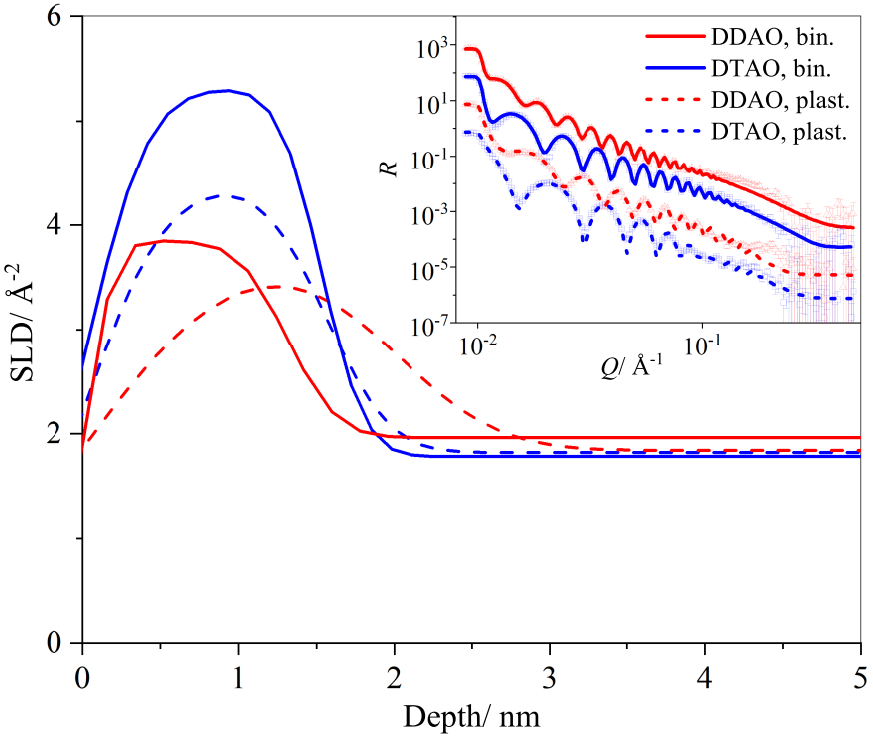

Figure 6.5: Comparison of the SLD-depth profiles of PVA films containing dDDAO and dDTAO. Data and fits are shown in the inset.

reflect an adsorbed pure monolayer on the surface, rather than a layer of PVA enriched in surfactant, it is possible to determine the area per molecule from the reflectivity fitted by modelling the adsorbed layer as a single uniform layer. The area per molecule, A, can be calculated using Equation 6.1

$$A = \frac{\sum m_i b_i}{\rho \tau} \tag{6.1}$$

where ρ is the scattering length density, τ is the layer thickness and $\sum m_i b_i$ is the total scattering length for the surfactant, with m_i being the number of atoms of scattering length b_i. The coherent scattering lengths of each isotope present in the surfactants are tabulated below (Table 6.5).

Table 6.5: Coherent scattering lengths of isotopes present in the surfactant molecules comprising the surface monolayer.

Atom	b_i/ 10^{-5}Å
H	-3.74
D	6.67
C	6.65
N	9.36
O	5.80

There are additional considerations in calculating the area per molecule in plasticised films. It is apparent from Figure 6.4 that glycerol is also enriched in the surface monolayer, co-adsorbed with the surfactant, which will therefore contribute to the SLD of this layer. However, with the assumption that this surface monolayer in plasticised films contains only surfactant and glycerol, an approximation can be made. The SLD contribution from the hydrogenated component (glycerol) is calculated from the SLDs of the surface monolayer of the two contrasts via simultaneous equations and subtracted, to leave a corrected value for the SLD which arises solely from the deuterated component, and can be used to determine the area per molecule. Without making this correction in the SLD to account for the presence of glycerol in the surface layer, the calculated area per molecule is lower but generally within the uncertainty of the corrected value, demonstrating that the presence of the hydrogenated component has very little effect on the calculated area per molecule. The surfactant molecular areas in each of the films containing *N*,*N*-dimethyldodecylamine *N*-oxide (binary and plasticised) calculated using Equation 6.1 are compared in Table 6.6.

Table 6.6: Area per dDDAO and dDTAO molecule in the surface layer of binary and plasticised films.

[dDDAO]/wt.%	A/nm^2		
	Binary	Plasticised(uncorrected)	Plasticised(corrected)
2	0.7±0.3	0.8±0.2	0.9±0.2
5	0.5±0.2	0.29±0.06	0.35±0.09
10	0.5±0.1	0.33±0.09	0.4±0.1
20	0.5±0.2	0.34±0.05	0.40±0.07
40	0.5±0.1	-	-
[dDTAO]/wt.%	A/nm^2		
	Binary	Plasticised(uncorrected)	Plasticised(corrected)
20	0.36±0.06	0.42±0.05	-

For dDDAO, the area per molecule is unchanged with surfactant loading, suggesting that the structure of the monolayer is identical, irrespective of the total amount of surfactant present in the bulk of the film. For the plasticised films, the area per molecule is again unchanged with surfactant concentration, with the exception of the film containing 2 wt.% dDDAO, which is significantly larger. This suggests that there is less than full coverage at 2 wt.% surfactants but at higher loadings, the monolayer formed is identical, regardless of the surfactant concentration. Due to the large uncertainties associated with the values for molecular area in the binary films, the effect of plasticisation on the area per surfactant molecule in the surface monolayer is unclear, but appears to be small.

6.2.2 Film Surface Topography

As described in Chapter 4, assessing the height maps of the film surface, and considering the roughness of the film in conjunction with the measured depth profiles, can reveal information about the nature of the segregated layer, such as the presence of defects. Height maps of representative regions of non-plasticised spin-cast films with areas of $2\,\mu m^2$ are shown in Figure 6.6. By eye, there is very little change in the surface when DDAO concentration is increased from 5 to 20 wt.%. Upon increasing DDAO concentration to 40 wt.%, however, the surface features become larger and more pronounced. Nevertheless, as the scale bar only ranges from -1 nm to 1 nm, the film is still very smooth. This contrasts the behaviour observed with non-plasticised PVA/SDS films, which show a huge increase in surface roughness as additive concentration increases (which are presented with scale bars ranging from, -5 to 5 nm, Chapter 4). The smoothness of these PVA/DDAO films, and general consistency of surface features with increasing surfactant loading, can also be clearly seen by comparing cross sections (Fig. 6.7).

Figure 6.8 shows a plot of R_a, R_q and R_{max}. It can be seen that there is no significant increase in average film roughness upon DDAO incorporation throughout the entire surfactant concentration range (even including the pure PVA film). Up to a concentration of 5 wt.%, R_{max} also remains consistent with that of the pure PVA film. However, as the concentration is increased further there is a substantial increase in R_{max} with [DDAO]. Despite this, the low and consistent values for average roughness show that the surface monolayer, identified from the depth profiles obtained using neutron reflectivity, is very even across the surface.

6.2.3 Solution Properties of Amine Oxide Surfactants

The segregation behaviour of these amine oxide surfactants in PVA films is different to that previously observed in any PVA/surfactant system.[168,174] However, this behaviour is analogous to that of surfactants in solution. Surface tensiometry was used to characterise the behaviour of the amine oxide surfactants in water. Figure 6.9 shows that the surface tension of DDAO and DTAO solutions decrease to critical micelle concentrations of 0.024 and 0.0051 wt.% respectively (1.1 and 0.20 mM). These values are similar to, but both slightly lower than those reported by Birnie et al.[212] (1.7 and 0.27 mM for DDAO and DTAO respectively).

As discussed in Chapter 5, the Gibbs adsorption equation enables the determination of the amounts of adsorbed surfactant from surface tension measurements.[213] Values for the surface excess, Γ, of the surfactant in solution are

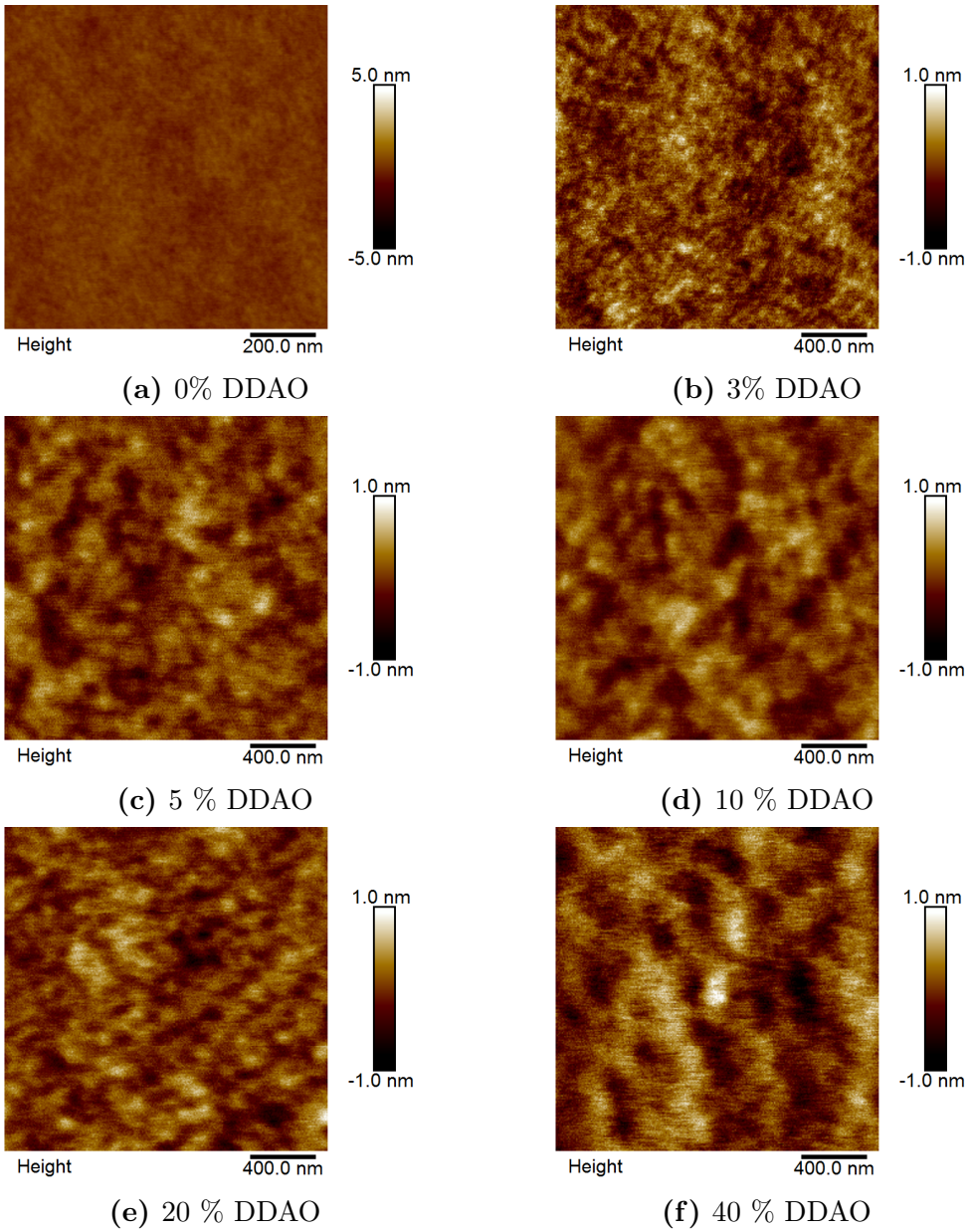

(a) 0% DDAO **(b)** 3% DDAO

(c) 5 % DDAO **(d)** 10 % DDAO

(e) 20 % DDAO **(f)** 40 % DDAO

Figure 6.6: Height maps of non-plasticised PVA/DDAO films.

included in Table 6.7

Comparison of the obtained area per molecule in solution with the area per molecule on the polymer surface, determined from the fitted reflectivity data (Table 6.7) shows that DTAO occupies a smaller area per molecule than DDAO both in solution and in the film. Additionally, although there are fairly large uncertainties associated with these measurements, the area per molecule on the film and solution surface are remarkably consistent for both surfactants.

The effect of plasticiser inclusion on the surface tension of solutions of the amine oxide surfactants is shown in Figure 6.9. The surface excesses of DDAO and DTAO were determined at glycerol concentrations of 0, 20 and 40 wt.%.

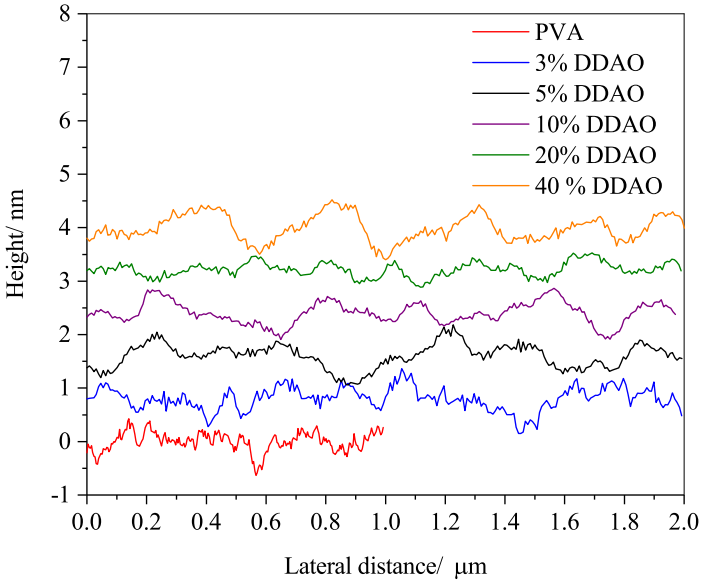

Figure 6.7: Example cross sections of PVA films containing 0-40 wt.% DDAO. Profiles are offset for clarity.

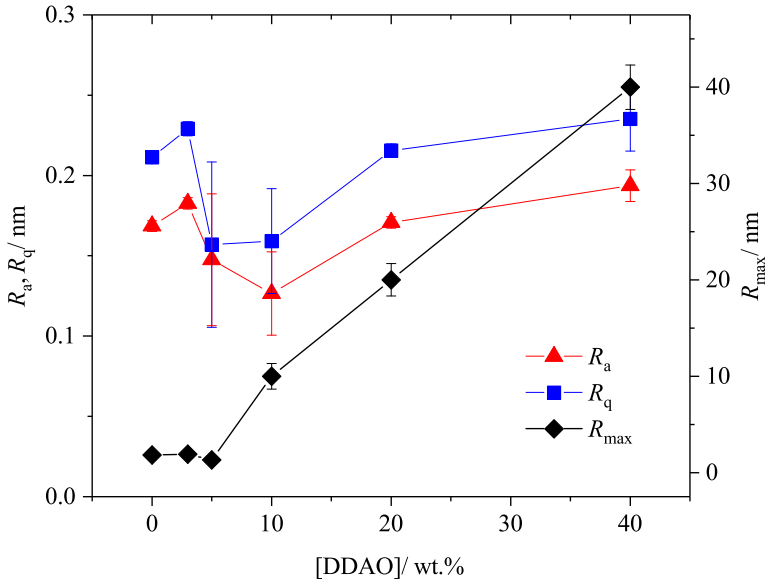

Figure 6.8: Change in average roughness, root mean square roughness and maximum roughness of PVA films with DDAO loading.

These values are included in Table 6.7 and illustrated in Fig. 6.10 (values marked with an asterisk represent values that have not been corrected for the presence of hydrogenated glycerol in the surface layer). As previously stated, DTAO occupies a lower area per molecule than DDAO. Upon incorporation of 20 wt.% glycerol

the molecular area of both surfactants on the solution surface is unchanged. In contrast, upon incorporation of 40 wt.% glycerol the two surfactants have the same molecular area, as a result of the increase in area per DDAO molecule and decrease in area per DTAO molecule.

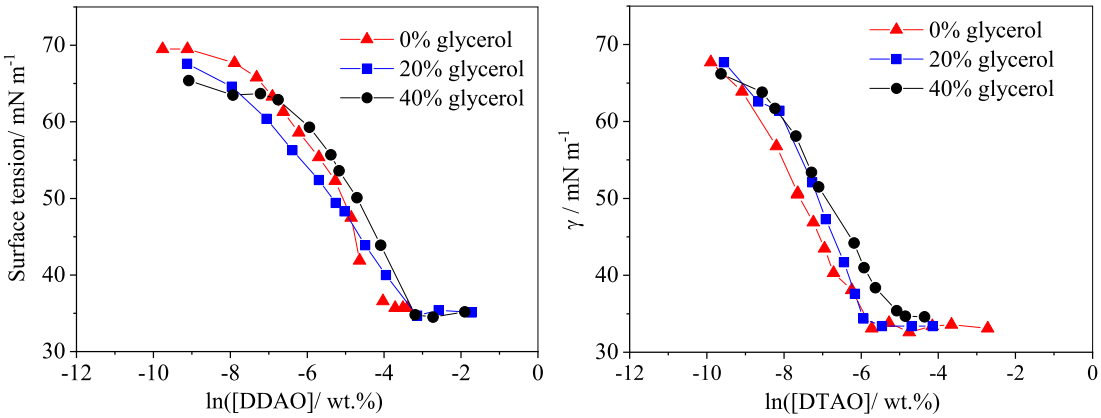

(a) DDAO **(b)** DTAO

Figure 6.9: Surface tension of aqueous solutions of amine oxide surfactants in the presence of 0, 20 and 40% glycerol.

The values of the surfactant surface excesses at the air-water interface of the solution can be compared with the determined surface excesses in the plasticised film. Despite the excellent agreement between the surface excess in solution and film for binary films, it is inconsistent and outside of the range of uncertainty for plasticised films/solution of the same glycerol loading (20 wt.%). However, the decrease and increase in A_{surf} of DDAO and DTAO respectively in solution with 40 wt.% glycerol qualitatively follows the same trend observed in the film, although a greater concentration of glycerol in solution is required to bring about this effect. Interestingly, the values of A_{surf} in plasticised films are consistent for DDAO and DTAO, and are also consistent with the values determined for both surfactants in solution with 40 wt.% glycerol.

Table 6.7: Comparison surface excess (Γ) and area per molecule of DDAO and DTAO in PVA films and on the water surface.

DDAO	Γ/μmol m^{-2}		A/nm^2	
	Solution	Film	Solution	Film
Binary	2.90±0.09	3.3±0.7*	0.57±0.02	0.5±0.2*
Plasticised	4.89±0.06	4.1-4.7*	0.58±0.01	0.35-0.40*
[3] DTAO	Γ/μmol m^{-2}		A/nm^2	
	Solution	Film	Solution	Film
Binary	4.9±0.3	4.6±0.5	0.34±0.02	0.36±0.04
Plasticised	5.0±0.1	4.0±0.5*	0.33±0.01	0.42±0.05*

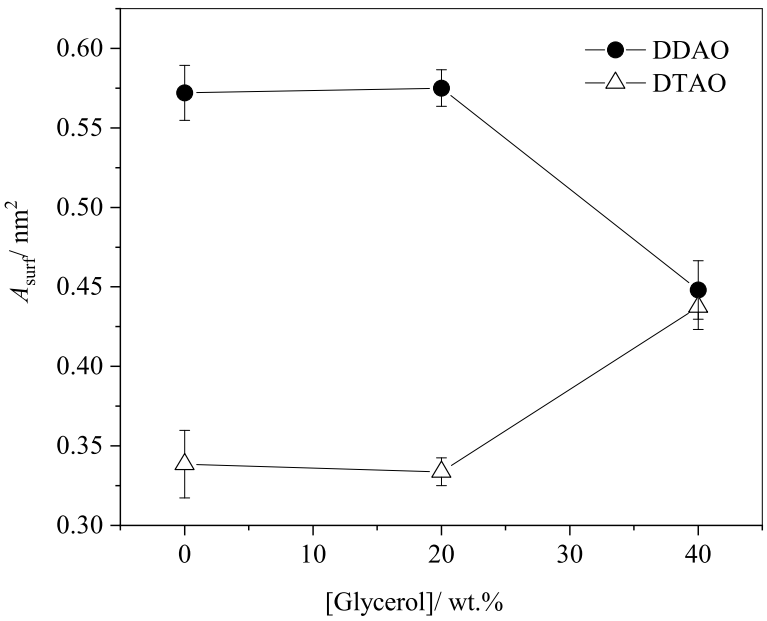

Figure 6.10: Change in molecular area of DDAO and DTAO on the solution surface with glycerol concentration.

6.2.4 Compatibility of the PVA/Amine Oxide Surfactant System

6.2.4.1 Phase Behaviour

Compatibility has been previously demonstrated to have a high influence on surfactant segregation, and ternary phase diagrams have been shown to provide a good indication of the compatibility of the PVA/water/surfactant systems. As for the PVA/SDS and PVA/CTAB systems discussed in Chapter 5, PVA/water/amine oxide surfactant phase diagrams were constructed by determining points at which the system clouds during solution-casting. The ternary phase diagrams for the PVA/DDAO/water and PVA/DTAO/water systems are shown in Fig. 6.11. It can be seen that all compositions relevant for the formation of spin-cast films are well into the one-phase region; in the absence of water over 50 wt.% surfactant can be incorporated before phase separation occurs. There is little difference in the phase behaviour of DDAO and DTAO, which is reflected in their very similar depth profiles and segregation behaviour. This shows that the significant increase in hydrophobicity with the extra -C_2H_4 group in DTAO leads to no obvious change in compatibility with PVA. Damas et al.[64] reported that the -CH_2OH groups of non-ionic polyol surfactants interact unfavourably with PVA, with the -CH_2 groups of the surfactant interacting favourably with the polymer in solution. It could therefore be expected that DTAO would be more compatible with PVA than DDAO, which is not observed.

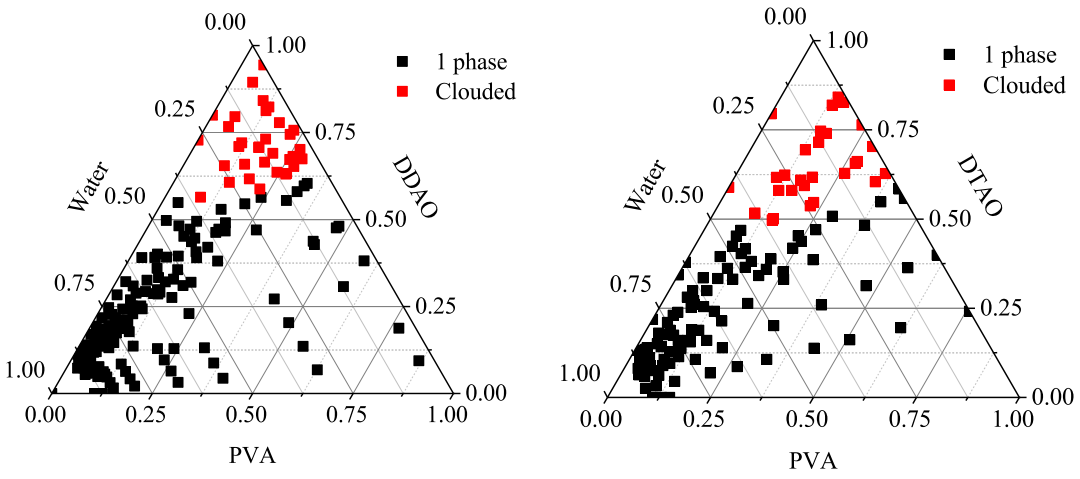

(a) DDAO **(b)** DTAO

Figure 6.11: Ternary phase diagrams of the binary DDAO/PVA and DTAO/PVA systems, in units of mass fraction.

6.2.4.2 Aggregation of Surfactant in the PVA Matrix: A SANS Study

Based on this phase behaviour analysis, amine oxide surfactants have been shown to exhibit substantially higher compatibility with PVA than any other surfactant studied so far. Small angle neutron scattering can provide further insight into the structures present in polymer samples, and thus can be used as a tool to better understand the nature of the surfactant aggregates. Data was collected on PVA films containing amine oxides and/or glycerol in varying ratios. In contrast to neutron reflectivity, SANS measures organisation in the bulk. Therefore, in order to ensure that the samples scattered enough for measurement, the films were solution-cast at 40 °C (rather than spin-cast) to give films approximately 70 µm thick, much thicker than the 70 nm thick films produced by spin-coating and actually of very similar thickness to the industrial films in soluble unit-dose applications. An important point to note is that the much longer time for the solution-cast film to dry (on the order of tens of minutes rather than seconds) means that it is likely that equilibrium structures will have had longer to develop, whereas spin-cast films may contain surfactant kinetically trapped in non-equilibrium structures. This is addressed more thoroughly in Chapter 7.

The SANS data for binary and plasticised films containing dDDAO and dDTAO at concentrations ranging from 0-40 wt.% are shown in Figures 6.12 and 6.13 respectively. All samples scatter strongly, exhibiting a large peak in scattering intensity at $Q \approx 0.055$ Å^{-1}. Because the size of this peak increases with surfactant concentration, it strongly suggests the aggregation of the deuterated surfactant within the samples.

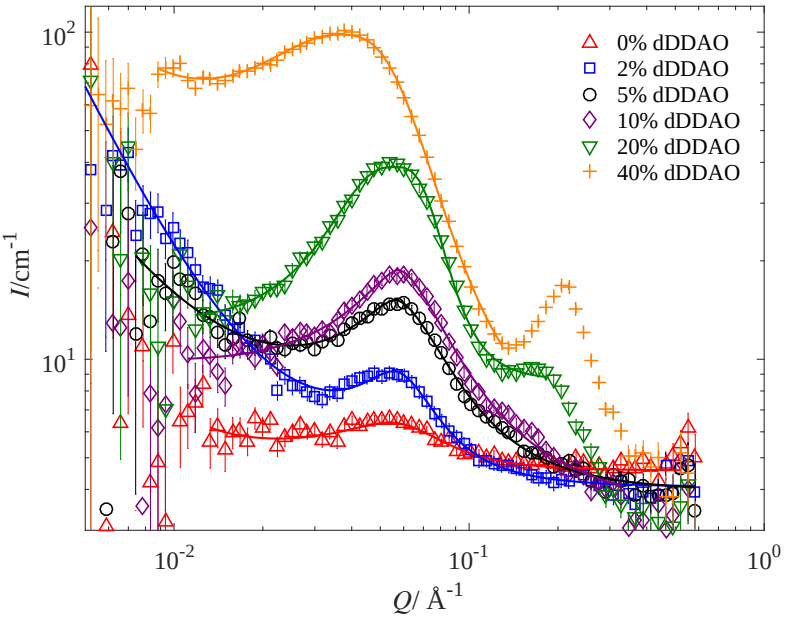

(a) dDDAO

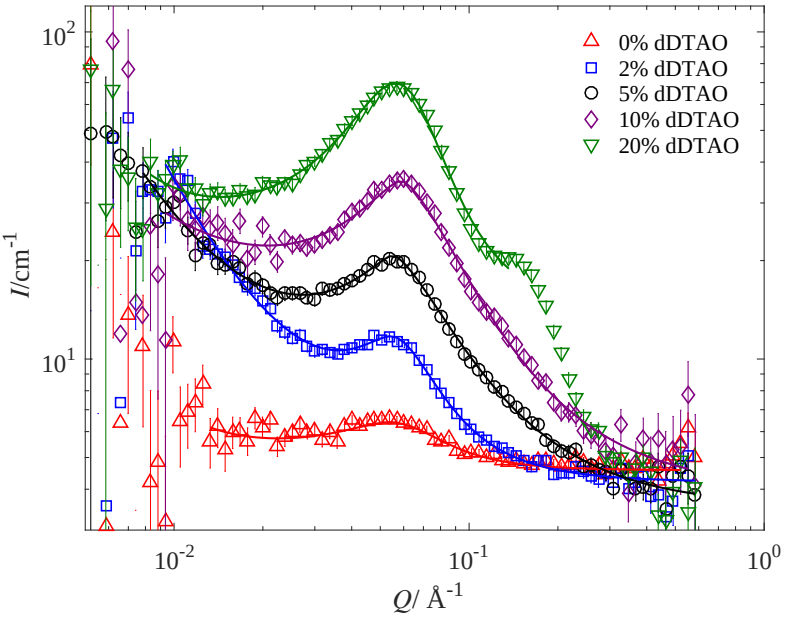

(b) dDTAO

Figure 6.12: SANS data for the binary PVA/DDAO and PVA/DTAO systems. Solid curves are fits using the broad peak model.

The peak at $Q \approx 0.055$ Å^{-1} is present in all samples, including pure PVA. This is therefore likely to be due to scattering from the interface between the amorphous and crystalline domains of the polymer, with contrast in the pure PVA arising due to the density differences of the two regions. The position of this peak in pure PVA ($Q_0 = 0.054$ Å^{-1}) is largely unchanged upon incorporation

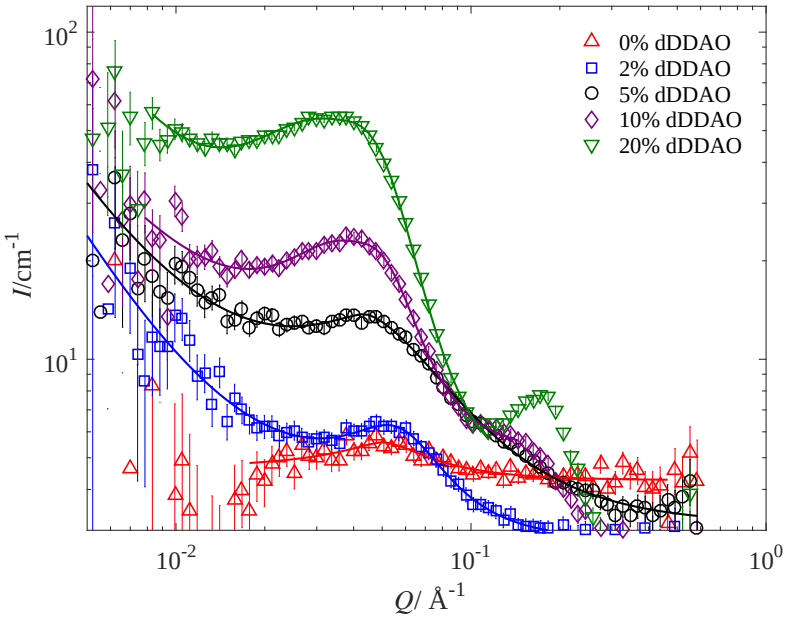

(a) dDDAO system

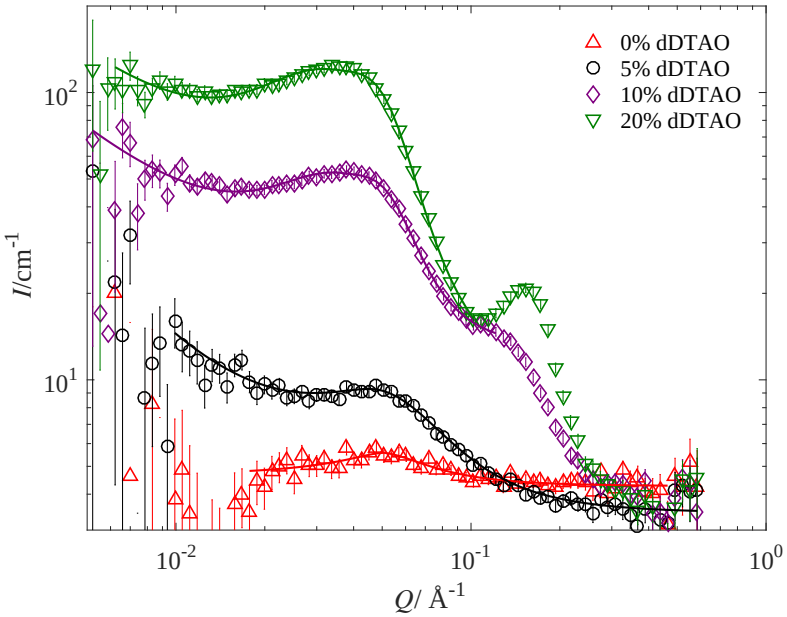

(b) dDTAO

Figure 6.13: SANS data for the plasticised (20 % glycerol) PVA/DDAO and PVA/DTAO systems. Solid curves are fits using the broad peak model.

of either 20 % d-glycerol ($Q_0 = 0.057$ Å^{-1}) (Fig. 6.14) or up to 20 % deuterated amine oxide surfactants ($Q_0 = 0.054 - 0.059$ Å^{-1}), strongly suggesting that scattering from the same structures is measured. However, intensity is significantly greater in the latter system due to the increased contrast between amorphous and crystalline domains as a result of a higher concentration of additive with a

greater SLD.

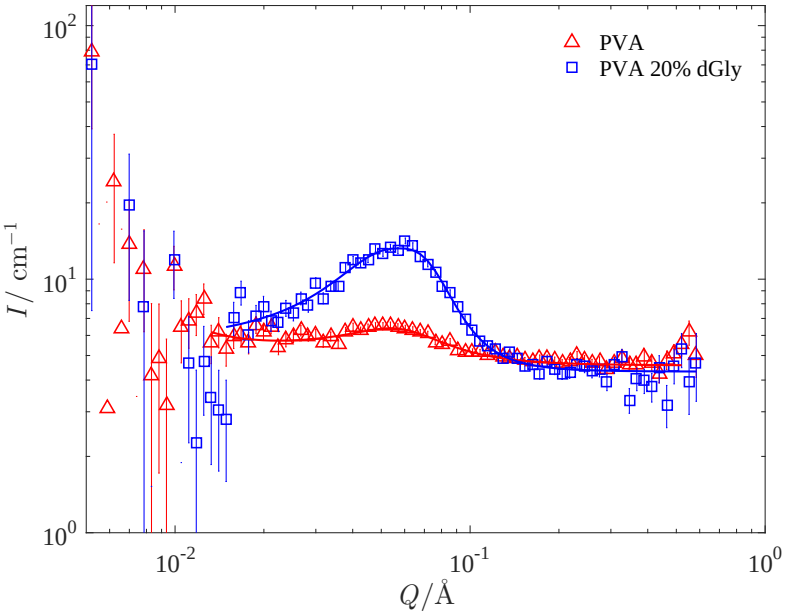

Figure 6.14: SANS data for pure PVA and PVA containing 20 wt.% d-glycerol. Solid curves are fits using the broad peak model.

The SANS data with a single peak could be captured well by a broad peak model, that can be used to identify the peak position, and thus the distance between scattering inhomogeneities. In this model, the scattering intensity, $I(Q)$, is calculated as:

$$I(Q) = \frac{A}{q^n} + \frac{C}{1 + (|Q - Q_0|\xi)^m} + B \tag{6.2}$$

where A is the Porod law scale factor, n is the Porod exponent, C is the Lorentzian scale factor, m is the exponent of Q, ξ is the screening length and B is the flat background. A limited range of the data containing a secondary peak at higher Q was also fitted with this simple model in order to extract the positions of the primary peak. Fitted parameters are included in Appendix C. From the peak positions, determined from Q_0, the characteristic distance corresponding to this peak, d_0, can be calculated using Equation 6.3. The variation in d_0 for binary and plasticised films containing dDDAO and dDTAO is shown in Fig. 6.15.

$$Q = \frac{2\pi}{d} \tag{6.3}$$

First considering the binary films, it can be seen that in the concentration range of 2-20 % surfactant, there is very little difference in the spacing between the regions occupied by DDAO and DTAO, and there is no significant change in

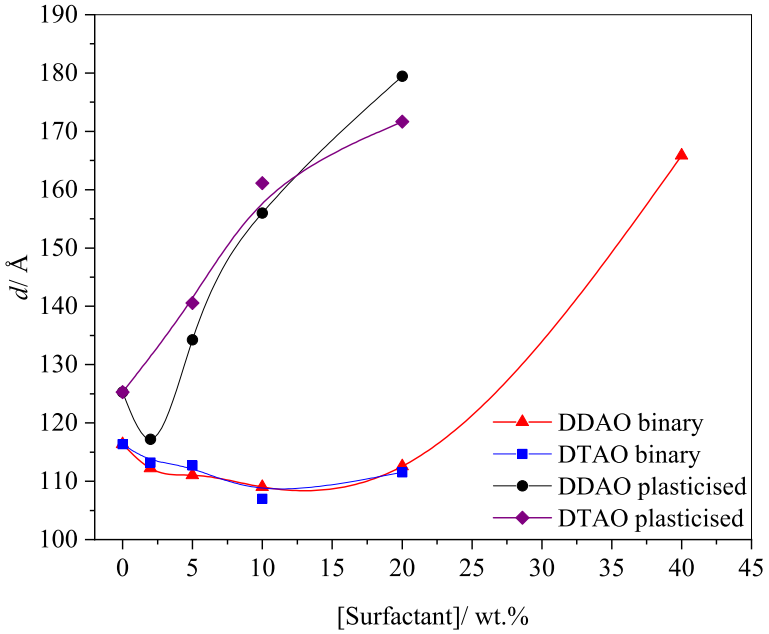

Figure 6.15: Spacing between scattering structures in binary and plasticised PVA films containing DDAO and DTAO, determined from peak positions of SANS data. Curves are a guide to the eye.

d_0 with surfactant concentration. Upon incorporation of 40 % DDAO, however, there is a substantial increase in d_0. There is no difference between the values for DDAO and DTAO, and thus this feature is not directly related to surfactant molecular structure.

In the case of the plasticised films, there is again very little difference between the spacing between scattering structures in PVA films containing DDAO and DTAO at each concentration. However, in contrast to the binary films, there is a general increase in d_0 with surfactant concentration.

At high surfactant loadings (20 % DDAO and 10 % DTAO) a secondary peak at higher Q appears (denoted Q_1). This is likely to be due to the structuring of the surfactant within the surfactant-rich domains, such as the formation of micelles. The position of this secondary peak is consistent with that previously observed for DDAO in solution, which has been consistently modelled as prolate ellipsoids.[214–216] The peak position is also related to the spacing, d, of the scattering inhomogeneities by Equation 6.3. Based on $Q_1 \approx 0.15$ Å^{-1}, determined from the data corresponding to PVA containing 40 % DDAO, the secondary peak corresponds to a distance, d_1, of 41 Å. This correlates well with the length of a fully extended DDAO bilayer.[217] Although a value for d_1 cannot be accurately determined from the SANS data on binary films, comparison of the secondary peak positions (Q_1) for DDAO and DTAO in plasticised PVA films reveals that $Q_{1\,\mathrm{DDAO}}$ (0.19 Å^{-1}) > $Q_{1\,\mathrm{DTAO}}$ (0.15 Å^{-1}), which reflects the larger size of the

aggregates formed from the surfactant with the larger hydrocarbon tail.

6.3 Discussion

6.3.1 Distribution of Components in PVA/Amine Oxide Surfactant Films

Surface enrichment: Adsorption of Surfactant to the Film-Air Interface

Neutron reflectivity has revealed that the amine oxide surfactants exhibit segregation behaviour in PVA unlike any previously studied model surfactant. DDAO shows some surface activity in PVA, forming a surfactant monolayer layer on the surface, but the majority of the surfactant is evenly distributed throughout the bulk film. Although surfactant multilayer adsorption has been previously observed with $C_{12}E_5$[168] and SDS,[174] this is the first system where the adsorption is restricted to a single monolayer.

Surface energy has been previously suggested to be largely responsible for segregation; comparison of the surface activity of the components in aqueous solution was able to rationalise the extensive segregation of SDS and $C_{12}E_5$ from PVA (Chapter 5). In this chapter, tensiometry has shown that the amine oxide surfactants have the lowest surface tension in solution of all components in the model film system. Therefore, based on the previous arguments presented in Chapter 5, it would be favourable for them to segregate more extensively to the surface, with the amount of segregated additive dependent on the total amount of surfactant present. Although very little surfactant is actually observed to segregate, and the amount of segregated surfactant is independent of the total amount present in the system, the substantially lower surface tension of DDAO and DTAO in solution compared to PVA is likely to lead to the formation of the surface monolayer in the solid films as this is sufficient to reduce the surface energy of the system. This corroborates the findings presented in Chapter 5, although for this to be unequivocally concluded, the interaction between PVA and surfactants in solution should be more thoroughly investigated.

The role of the entropic penalty associated with the deformation of large polymer molecules at the surface should also be considered in the context of rationalising the observed segregation of the smaller surfactant molecules. It is plausible that a monolayer of surfactant remaining on the solution surface throughout the spin-coating process, resulting in its presence on the the dry film, reduces the surface free energy for this reason. A single monolayer of the

relatively short chain surfactant on the surface is sufficient to reduce the entropic penalty from long PVA chains occupying the surface in restricted configurations, if the monolayer makes the interface more diffuse. If this was the sole factor responsible for the observed segregation of the amine oxide surfactants, however, an enrichment of glycerol on the surface of PVA films would be expected in the absence of surfactant, which has not been observed.[168] Furthermore, a sharp interface between the monolayer and the PVA would not be expected as this would again result in a conformational entropy penalty.

Guided by the insights gained from Chapter 5, compatibility arguments will therefore also be considered in order to rationalise the observed depth profiles of the amine oxides. Based on the minimal segregation observed even with very high surfactant concentration, it is probable that most of the surfactant is present in the bulk film due to its high solubility in the PVA matrix. This was confirmed by obtaining phase diagrams of the PVA/amine oxide/water systems, which reveal that a substantial amount of surfactant can be incorporated into the PVA matrix in the absence of water without phase separation occurring. Amine oxide surfactants are extremely hydrophilic, with their high hydrophilicity compared to other surfactants of the same chain length attributable to the strength of the dipole in the N-O bond of the amine oxide. This property could act to make them very compatible with the host polymer.[218] It is therefore likely that the strength of their interaction with hydroxyl groups in the PVA matrix can compensate for the free energy penalty of having the component with a lower surface free energy dispersed throughout the bulk.

The association of polymers and surfactants in solution to form polymer-bound micelles has been thoroughly documented, and it is well-established that non-ionic and cationic micelles do not associate greatly with hydrophilic polymers.[219] Additionally, although Brackman et al.[220] reported the stabilisation of micelles of DDAO in the cationic form by the hydrophobic polymers poly(vinyl methyl ether) and poly(propylene oxide), no-association between these polymers and the neutral form of DDAO was identified in solution. Association of neutral DDAO with polymers has been shown to occur only when the polymer is sufficiently hydrophobic.[45,219] Indeed DDAO showed no association with the relatively hydrophilic polymer poly(ethylene oxide). In the current work with PVA, with the solutions at the natural pH, the surfactants are almost exclusively in the neutral form, and therefore little interaction with the hydrophilic PVA in solution would be expected. However, this does not preclude the possibility of the amine oxide surfactants interacting favourably with hydroxyl groups present in amorphous regions of the solid film matrix.

Influence of Plasticiser on Surface Properties of Three-Component Films

The replacement of some PVA with glycerol can have a significant impact on surfactant and plasticiser distribution in PVA films due to the competing compatibilities of the three components.[168,174] However, in this model system there is surprisingly little difference in the segregation of the amine oxide upon glycerol incorporation other than a slight thickening of the surface layer, and an increased area per surfactant molecule for DDAO. The adsorption of glycerol onto the surface over a similar lengthscale to the thickness of the adsorbed surfactant layer indicates the co-adsorption of this species with the surfactant into a more diffuse monolayer, but no other surface enrichment.

It was previously reported that incorporating glycerol into a film containing CTAB results in segregation of the surfactant that was not observed in the binary film. This was suggested to be a result of glycerol out-competing CTAB for sites in the amorphous regions of the matrix.[168] In Chapter 4, it was illustrated that glycerol enables the formation of thermodynamically stable stacked SDS/glycerol layers on the film surface, allowing even more SDS to segregate than was observed in binary films. The behaviour of the amine oxide system, however, contrasts both of these previously observed behaviours, with the measured depth profiles suggesting a very high compatibility of the amine oxide with the matrix, even in the presence of plasticiser. This is likely due to the hydrophilicity of the surfactant.

Interfacial Adsorption

The thick region of high SLD ($\sim$3.8 $\times 10^{-6}$ Å^{-2}) on the substrate interface apparent in the SLD-depth profiles of films containing deuterated surfactant is strongly indicative of interfacial surfactant adsorption. Although neutron reflectivity is not capable of resolving the nature of the structures at the interface of these films spun onto a silicon substrate due to the similar SLD of the silicon oxide and the deuterated surfactant, there has been substantial evidence for the formation of structures on solution-substrate interfaces. When reflectivity data for a PVA/DDAO film was fitted with a 4-layer model, to include an additional surfactant-rich layer adjacent to the substrate, the thickness of the interfacial layer was found to be 13$\pm$10 Å, which could correspond to a number of different structures, which have been probed theoretically experimentally.[221–224] The huge uncertainty in this value is a result of the difficulty in resolving the interfacial surfactant from the SiO_x. It was previously reported that treating structured surfactant films as a bilayer generally results in a good fit to reflectivity data.[224]

This surfactant rich layer present adjacent to the silicon substrate could therefore correspond either to a monolayer, as observed on the surface, a bilayer-type structure consisting of a surfactant headgroup closest to the hydrophilic substrate, a tail region, and another headgroup region adjacent to the bulk polymer film, or a more complex structure such as cylindrical aggregates, as observed in the case of nonionic DTAO on the mica-solution interface by Kawasaki et al.[225] The evidence from NR suggests that, similarly to the behaviour observed in solution, structures are forming on the film-substrate interface. They are not multilayered, however, and are therefore consistent with the single-phase behaviour of the surfactant in the bulk. Although the nature of these aggregates will not be considered further, this presents convincing evidence that the behaviour of the surfactant in the solid film reflects that in solution.

6.3.2 Structure of the Surface Monolayer: DDAO vs. DTAO in Film and Solution

It is particularly noteworthy that the surfactant exhibits identical behaviour when water is replaced by a solid polymer, given the significant differences in surface tension of pure water and pure PVA. Although a range of surface energy values for PVA have been reported, from 37-59 mN m^{-1} [180,181,226] depending on the degree of hydrolysis and molecular weight, all are higher than the surface tension of the surfactant solutions above the CMC.

When discussing the nature of the surfactant behaviour both in the film and in solution, it is important to acknowledge the equilibrium between the protonated and unprotonated forms of the surfactant. The equilibrium constant, K_a is defined as

$$K_a = \frac{[(CH_3)_2RNO^-]\,[H^+]}{[(CH_3)_2RNOH]}. \tag{6.4}$$

The pK_a can be written in terms of the degree of ionisation of the micelle, α_M

$$pK_a = pH + \log[\alpha_M/(1-\alpha_M)]. \tag{6.5}$$

At neutral pH, the amine oxides are almost exclusively in the neutral form, although the presence of the cationic species should be considered. The pK_m value can be defined as the intrinsic proton dissociation constant of the micelle, rather than the single surfactant molecules. This is known to be greater than that of the single surfactant molecule.[227,228] It is particularly relevant that Maeda et

al.[218] have shown that DDAO and DTAO have significantly different pK_m values; $pK_{m(\mathrm{DDAO})}$ (5.89) is smaller than $pK_{m(\mathrm{DTAO})}$ (6.30), meaning that a higher concentration of the cationic species of DTAO is likely to be present in solution than in the corresponding DDAO solution. This is thought to be a result of the different shapes of the largely non-ionic micelles; DDAO has been shown to form spherical micelles, whereas DTAO forms rod-like micelles. Although these pK_m values were taken in solutions containing 1 M NaCl, it was determined that the salt concentration has no significant effect on pK_m. The degree of protonation therefore affects both the solution and surface properties of the surfactant, including CMC, aggregation number, and aggregate shape. This is due to the well-known hydrogen bonding between cationic and non-ionic amine oxide groups,[229] the likely formation of hydrogen bonds between two neighbouring cationic groups,[230] and the dipole-dipole interactions between the nonionic species.[218] Solutions for both surface tension measurements and spin-casting were used at natural pH, above pH 7, and the proportion of cationic surfactant is therefore very low.

Analysis of the Gibbs isotherms, however, has shown that DTAO occupies a significantly smaller area per molecule than DDAO. As the area per molecule on the surface is highly sensitive to the degree of ionisation (α) of the surfactants, it is probable that the lower area per molecule is due to the slightly greater degree of ionisation of DTAO (although a substantially greater degree of ionisation would lead to a greater molecular area due to greater headgroup repulsion). However, the dissociation constants of the surfactant monomers are not identical to that in the micelle as the introduction of charges is generally more favoured on the micelle surface. Despite this, it is plausible that even a slightly higher concentration of the cationic surfactant in DTAO solutions would result in the formation of strong hydrogen bonds on the surface between the cationic and non-ionic headgroups, leading to the formation of dimers and decreasing the average area per headgroup. This effect is then replicated in the solid film, where the area per molecule is greater for DDAO than DTAO, with values consistent with those of the area on the solution surface. This suggests that the nature of interactions is consistent when the bulk is water or solid PVA.

Influence of Glycerol on Surfactant Molecular Area

At the highest concentration, the presence of glycerol has the opposite effect on the areas of the DDAO and DTAO molecules both in the film and solution. With a pK_a of 14.4,[231] the incorporation of glycerol into the mixtures is expected to have a negligible increase in the proportion of the cationic species from that of the binary solutions. It could therefore be suggested that it is the interaction

between the surfactant head groups and the plasticiser molecules that affects the area per molecule on the surface. This should be addressed by considering the nature of the interactions between the surfactant and glycerol.

The effect of glycerol on surfactant behaviour has been addressed in a number of systems including ionic and nonionic surfactants,[204,205,232] although there have been no reported studies on the effect of co-solutes such as glycerol on the surface tension or micellisation behaviour of amine oxide surfactants. In general two different mechanisms for the action of co-solvents such as glycerol on the micellisation of surfactants have been suggested. The first is an indirect mechanism, where the additive changes the properties of the aqueous medium, in particular the dielectric constant, which impacts the electrostatic interaction in solution. This is generally accepted in the case of ionic surfactants. The second is a direct mechanism, where the additive replaces some of the water molecules that hydrate the surfactant. D'Errico et al.[205] investigated the effects of glycerol on the cationic surfactant, CTAB and the non-ionic ethoxylated surfactant Brij 58. Although the CMC of CTAB is affected by the presence of the co-solute only above 30 wt.% glycerol, above this concentration the area per surfactant molecule was found to increase almost linearly with the glycerol concentration. The average area per Brij 58 molecule on the surface was also found to follow a generally linear increase with concentration. In both of these systems the authors found no evidence of a direct interaction between the surfactant and glycerol molecules. However, different behaviour could be reasonably expected of the amine oxide surfactants studied in this work due to the strong N-O dipole and ability to form strong hydrogen bonds with the additive.

It is surprising that in solutions containing 40 wt.% glycerol, the molecular areas of DDAO and DTAO are equal, given that this necessitates a decrease in molecular area for the former surfactant and increase in molecular area for the latter. This suggests that at this high glycerol concentration, the interactions between individual surfactant alkyl chains are not the dominating factor. It is therefore likely that the glycerol-surfactant monolayer is controlled by the hydrogen bonding between glycerol and amine-oxide groups, rather than the presence of any cationic-nonionic hydrogen bonds, which leads to identical structures of the monolayers. This argument can therefore be used to rationalise the respective increase and decrease in A_{surf} of DTAO and DDAO with glycerol concentration; it is plausible that the strength of hydrogen bonds between glycerol and the surfactant headgroup are stronger than the dipole-dipole interactions between the non-ionic headgroups predominantly present in the DDAO solution/film, which leads to a contraction of the monolayer. Conversely, the glycerol-surfactant hy-

drogen bonds are likely weaker than those present between cationic/non-ionic headgroups in the DTAO solution/film and so the plasticiser acts to preclude the formation of the hydrogen bonded dimers and overall increase molecular area.

The lack of change of molecular area in solution for both surfactants when glycerol content is increased from 0 to 20 wt.% is surprising. This behaviour suggests that in this system, the monolayer is unaffected by the co-solute at this loading as there is no co-adsorption of glycerol in solution. (This is in contrast to the solid film, where enrichment of d-glycerol to the surface of PVA containing 20 wt.% d-glycerol is apparent, Fig. 6.4). This argument can be used to explain the observations in both solution and films. However, the inconsistency of the values for A_{surf} between solution and film in the presence of 20 wt.% glycerol suggests a subtle difference in the behaviour of surfactants when water is replaced by a solid polymer; in the presence of the PVA much lower loading of glycerol is required for its co-adsorption to the surface.

6.3.3 Compatibility of the PVA/Amine Oxide System

Having discussed the nature of the monolayer on the surface of the PVA film, it is worth now considering the nature of the surfactant aggregates in the bulk of the film, where the majority of the additive is localised. The high compatibility of the PVA/amine oxide surfactant system, as revealed by the ternary phase diagram, was previously discussed in terms of its role in the resulting surfactant distribution in spin-cast films. The high compatibility of the amine oxides with PVA can also be corroborated with findings from small angle neutron scattering. First, SANS demonstrates that these molecules are localised in specific regions already present in the polymer. As it is clear from the SANS data that the surfactants localise in the same region as glycerol, a commonly used plasticiser, it is probable that DDAO and DTAO are localised in the amorphous regions of the polymer. To confirm this, the effect of DDAO on the glass transition temperature of PVA films was measured using DMA (Fig. 6.16). A representative plot of the DMA data used to determine the T_{g} is included in Appendix D. If the additive localises in the amorphous regions, a change in glass transition temperature would result, whereas this would not be expected should the additive localise exclusively in the crystalline regions. From the clear decrease in T_{g} with DDAO concentration it can be concluded that the amine oxides do indeed occupy the amorphous regions, and contribute to the plasticisation of the PVA.

The lack of change in d_0 upon increasing the concentration of both DDAO and DTAO from 0 to 20 % (Fig. 6.12) suggests that these additives can be incor-

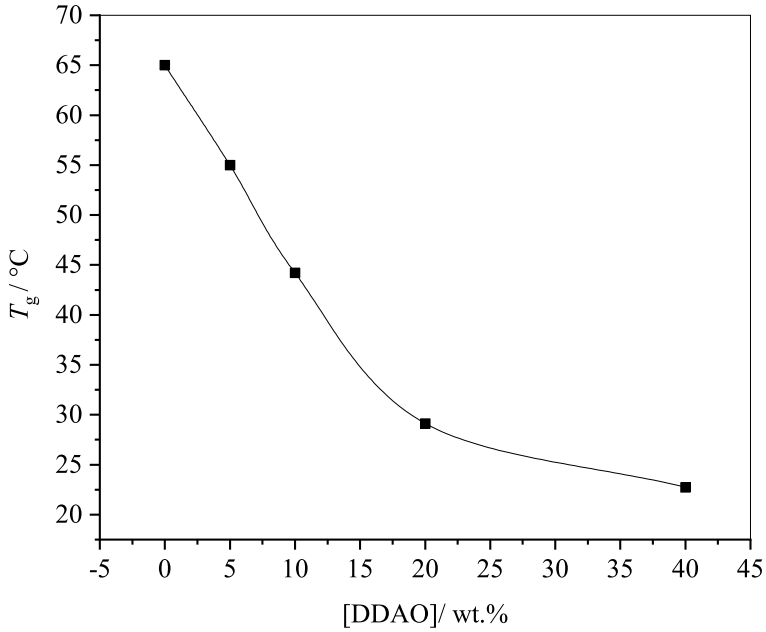

Figure 6.16: Change in T_g of PVA with DDAO concentration.

porated at a high loading without substantially changing the overall structure of the polymer. At the very high loading of 40 % DDAO, however, an increase in the size of the amorphous domains must occur to accommodate the surfactant, leading to an increase in d_0. In contrast to the binary films, in the case of the plasticised films, where 20 % glycerol is additionally incorporated, as little as 5 % surfactant causes a substantial increase in d_0, which increases almost linearly with additive concentration. This likely indicates that the preferential occupation of both surfactant and plasticiser in the amorphous domains causes an increase in size of these regions and a resulting greater spacing between them.

From Figure 6.17, it can be seen that the peak in $I(Q)$ for a film containing 20% dDDAO shows a greater scattering intensity than a film containing 20 % d-glycerol, therefore suggesting that surfactant localises more specifically in the amorphous regions than glycerol. To determine whether this is indeed due to the increased aggregation of the amine oxide in the amorphous regions of the PVA, rather than simply being a result of the difference in contrast between PVA and d-glycerol and PVA and dDDAO, SANS data was acquired for a film containing DDAO contrast matched to d-glycerol (4.91 $\times 10^{-6}$ Å^{-2}). The comparison of the SANS data for these samples is shown in Fig. 6.17. It can be clearly seen that although the intensity of the peak at $Q \approx 0.055$ Å^{-2} decreases upon replacing dDDAO with DDAO contrast matched to d-glycerol due to the decreasing contrast between the PVA matrix and the additive, it is still significantly higher than for the peak from the sample containing d-glycerol. This confirms that there is

a higher concentration of the surfactant additive aggregating in these domains than plasticiser, or at least sharper interfaces at the polymer-rich domains.

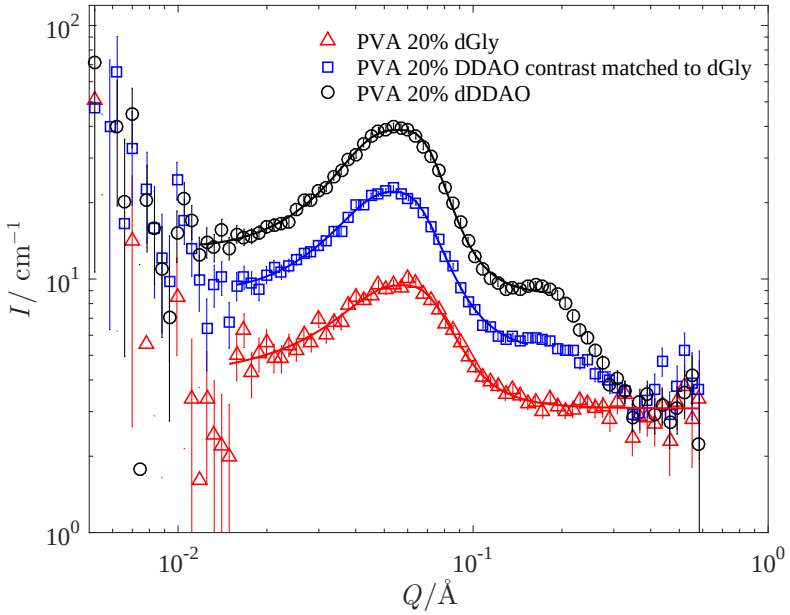

Figure 6.17: Comparison of SANS data for PVA films containing 20 wt.% d-glycerol, 20 wt.% dDDAO and 20 wt.% (h/d)-DDAO, contrast matched to d-glycerol.

6.4 Chapter Conclusions

In this chapter, a new model PVA/surfactant system has been characterised in films and solution. Two amine oxide surfactants have been shown to exhibit segregation behaviour in PVA remarkably similar to their behaviour in water, showing consistent molecular areas in solution and in the film. Neutron reflectivity has shown that the surface structure of the films is consistent, regardless of surfactant loading.

This is the only polymer/surfactant system observed where the surfactant acts similarly to its behaviour in aqueous solution. This has been attributed to the small amine oxide group which affords the surfactant a high level of compatibility with the polymer matrix. The head group is also capable of strong dipole-dipole bonds with adjacent head groups, resulting in the favourable formation of a monolayer on the surface.

Comparison of the molecular areas of DDAO and DTAO shows that the longer chain surfactant has a lower molecular area, which is attributed to the higher degree of ionisation and hence stronger inter-head group interactions. This could also be a result of the stronger tail-tail attraction due to the extra -C_2H_4 in

the hydrocarbon chain, and slightly lower surface energy as indicated by surface tensiometry. The nature of the intermolecular interactions in the monolayer can be used to justify the effect of the incorporation of glycerol on the molecular areas of DDAO. Although there are some subtle differences between the surfactant behaviour in solution and in the film, the remarkable and unprecedented similarity between the systems demonstrates the importance of the interactions between the headgroups.

Consideration of the solution properties of the amine oxide surfactants shows that the conclusions presented in Chapter 5 can be confirmed in this system, as the observed depth profiles appear to be a balance of surface energy and compatibility factors. First, the very low surface tension of the amine oxide surfactant compared to PVA can lead to a preferential adsorption to the surface. Second, the high compatibility of the PVA/amine oxide system as determined by its phase behaviour and specific localisation in the amorphous regions of the polymer, reflects the lack of extensive segregation as observed in other surfactant systems. The corroboration of these findings with the conclusions of Chapter 5 illustrates the value of the solution state studies in allowing predictions of surfactant segregation in other systems to be made.

Chapter 7

Impact of Temperature on Film Additive Distribution

One of the underlying questions throughout this work is whether additives are capable of migrating over time. To what extent is equilibrium reached in the initial spin-casting process? Is there scope for further segregation, and how does this depend on the nature of the additive? These questions were first hinted at in Chapter 4, where subtle differences in surfactant distribution were identified when the films were immediately vitrified after spin-casting rather than measuring under ambient conditions. In this chapter, this question is explored more extensively. For three model systems (SDS, $C_{12}E_5$ and DDAO in PVA) the effect of ageing films at elevated temperature on the surfactant distribution is investigated, in order to provide insights into the mobility of these additives and its implications for the properties of industrial films.

7.1 Protocol

In order to determine whether additive migration occurs upon heating the films, neutron reflectivity was used to quantify the depth profiles of deuterated additives in the same spin cast films, at a number of temperature increments. For each model system, the loading of deuterated surfactant was fixed at 10 wt.%. Each film was spin-cast from a solution containing 4 wt.% total solute to produce $\sim$ 70 nm thick samples, in order to obtain reflectivity with resolvable Kiessig fringes. By repeatedly measuring a single film for each surfactant, this eliminates any ambiguity arising from slight variations of total film thickness or additive concentration in different films of the same composition. Measurements were carried out at 25, 45, 65 and 85 °C. Films were subsequently allowed to cool back to 25 °C and reflectivity data was obtained again.

7.2 Results

7.2.1 Effect of Temperature on SDS Distribution

7.2.1.1 Binary Films containing SDS

PVA films containing dSDS as the only additive were first investigated. As in the previous chapters, reflectivity data was collected over a range of $0.01 < Q < 0.3$ Å^{-1}, which was used to obtain a SLD-depth profile, that could be converted to a volume fraction-depth profile as described in Chapter 4 (Equation 4.2). The obtained volume fraction-depth profiles for the film obtained at 25 °C (before heating), 45, 65, 85 and 25 °C (re-cooled) are shown in Fig. 7.1.

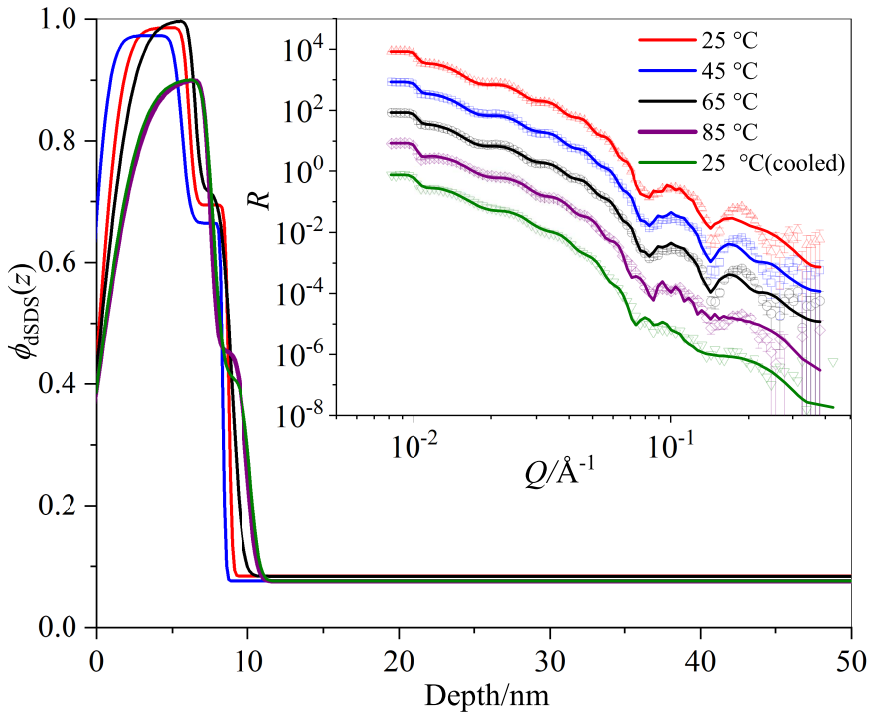

Figure 7.1: Depth profiles of 10 wt.% dSDS in non-plasticised PVA films at 25 °C, after heating to 45, 65 and 85 °C and upon cooling to 25 °C. Neutron reflectivity data and fits are shown in the inset, with data offset for clarity.

For each temperature, the reflectivity data can be fitted with a four-layer model, consisting of two layers comprising a surface excess, a bulk, subsurface polymer layer and the SiO_x layer. This is in contrast to the profiles presented in Chapter 4, where the reflectivity data of a binary PVA/dSDS film could be adequately fitted using a three-layer model, with all features adequately captured by treating the surface excess as a single layer. The surface excess, z^*, and fraction of segregated surfactant, f, have been calculated at each temperature. These values are included in Table 7.1.

Table 7.1: Surface excesses (z^*) and fraction of segregated surfactant (f) in binary films containing 10 wt.% dSDS.

T/°C	z^*/nm	f
25	6.5 ± 0.5	0.58 ± 0.06
45	6.4 ± 0.5	0.60 ± 0.06
65	6.9 ± 0.5	0.60 ± 0.06
85	6.2 ± 0.4	0.61 ± 0.06
25 (cooled)	6.1 ± 0.4	0.61 ± 0.06

Considering first the profile obtained from the film measured at 25°C, the top surface layer consists of almost pure dSDS, and it is apparent that there is a wetting layer of the surfactant. The thickness of this layer is much thicker than a bilayer of SDS. The second layer is also rich in surfactant, but can be seen to contain a significant amount of the (lower SLD) hydrogenated polymer. The subsurface film is fitted with a single layer. Although the volume fraction of this layer is quite high ($\phi_{\text{dSDS}} \approx 0.08$, corresponding to 8.8 wt.%), particularly when compared to that in the Chapter 4, where $\phi_{\text{dSDS}} \approx 0.03$, the uncertainty in the concentration of the bulk layer, as determined using NR is typically quite large. The value for the volume fraction of 0.08 reported here is likely greater than the true value, given that the values for z^* and f determined in this film at 25°C are also substantially higher than the values presented in Chapter 4 for a thin film containing 10 wt.% dSDS.

From Fig. 7.1, it can be seen that the a feature at $Q \approx 0.2$ Å^{-1} is not captured well by this model. It should be noted that in contrast to the features observed at high Q in the thick, plasticised films (Chapter 4), these are not Bragg peaks, and therefore not necessarily indicative of a repeating structure on the surface. However, since the feature is at relatively high Q, it corresponds to a feature on a relatively short lengthscale. Although it is not as well-defined as the Bragg peaks seen in Chapter 4 for plasticised films, it is still likely to arise from the internal structure of the adsorbed layer, since the feature occurs at about the same Q. Despite these fringes being poorly captured by the fit, the good fit of this model to the reflectivity data over the low Q range show the successful characterisation of the overall larger scale features of the total adsorbate thickness and density.

Upon heating to 45 °C and subsequently 65 °C, the reflectivity data can be fitted using a similar 4-layer model, with little change in concentration or thickness of each of the layers observed. Within the uncertainty of these values, there is no change in either z^* or f. This, alongside the very similar shape of the profiles at these temperatures, indicates little change in the distribution of surfactant throughout the film.

Upon heating to 85 °C, however, a more significant change in the surface excess of the film occurs. Although the data is still fitted using the same 4-layer model, the concentration of dSDS in the two surface layers comprising the surface excess is substantially lower. A slight broadening of the surface excess layers can also be identified in Fig. 7.1, reflecting a roughening of this layer. This can also be inferred from the raw reflectivity data; the fringes at higher Q (0.16 Å^{-1}) becomes slightly flattened out at 85 °C, indicating an increase in roughness. The suppressed feature at 0.16 Å^{-1} does not recover upon cooling the film, suggesting that the internal structure of the adsorbed layer is irreversibly altered. Despite the slight change in the shape of the volume fraction-depth profile, the values in Table 7.1 reveal no significant change in the surface excess or fraction of segregated surfactant upon heating to 85 °C. This therefore suggests a rearrangement of the surface occurs, rather than further additive migration into or from the subsurface film. When the film is cooled back to 25 °C, there is very little change in the volume fraction-depth profile or z^* and f values, compared to the film at 85 °C, indicating that the changes in surface excess upon heating to 85 °C are irreversible.

7.2.1.2 Plasticised Films containing SDS

The change in the distribution of dSDS upon heating plasticised films was subsequently investigated. As in previous chapters, glycerol was used as a model plasticiser, with its loading fixed at 20 wt.%. As described in Chapter 4, after fitting the reflectivity data to a SLD-depth profile, this can be converted into a volume fraction-depth profile by assuming an even ratio of the two hydrogenated components. The obtained volume fraction-depth profiles, alongside the reflectivity data and fits, are presented in Fig. 7.2. In this case a significant ($>$ 10 nm) decrease in film thickness was observed to occur upon heating from 25 °C to 45 °C, and there is a further slight decrease in film thickness upon heating to 65 °C. This is almost certainly due to a loss of glycerol from the film over time as it has previously been determined that glycerol can be significantly volatile in thin films.[147] To illustrate the variation in film thicknesses, the depth profile of the whole film (from air interface to substrate) is included in Fig. 7.2. It should be noted, therefore, that the second "peak" in the concentration profile corresponds to the silicon oxide layer on the substrate, and not a layer enriched in surfactant. Assuming an even distribution of glycerol throughout the plasticised film, z^* and f can be calculated. These values are reported in Table 7.2.

The film measured at 25 °C is qualitatively consistent with the plasticised film containing 10 wt.% dSDS presented in Chapter 4. As for the film in Chapter

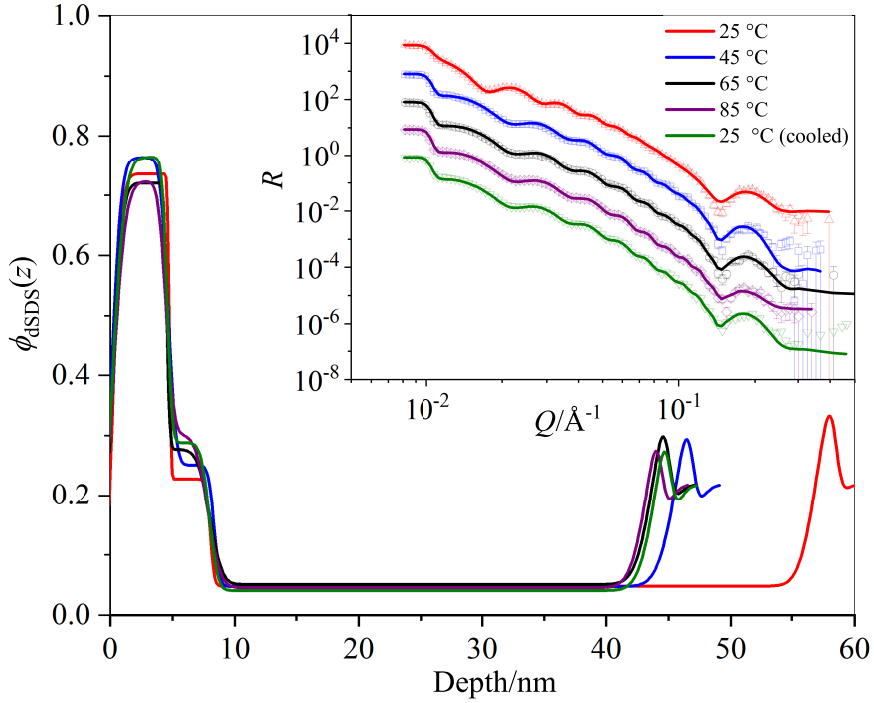

Figure 7.2: Depth profiles of 10 wt.% dSDS in PVA films containing 20 wt.% h-glycerol at 25 °C, after heating to 45, 65 and 85 °C and upon cooling to 25 °C. Neutron reflectivity data and fits are shown in the inset, with data offset for clarity.

Table 7.2: Surface excesses (z^*) and fraction of segregated surfactant (f) in plasticised films containing 10 wt.% dSDS.

T/°C	z^*/nm	f
25	3.6 ± 0.4	0.58 ± 0.06
45	3.9 ± 0.4	0.66 ± 0.07
65	3.6 ± 0.4	0.63 ± 0.06
85	3.6 ± 0.4	0.65 ± 0.07
25 (cooled)	3.8 ± 0.4	0.69 ± 0.07

4, reflectivity data was fitted with a four-layer model. However, the values for z^* and f differ slightly; although z^* is slightly higher than that previously reported, f is substantially lower. One likely reason for this is the large uncertainty in the SLD of the layer corresponding to the bulk film. Although the degree of segregation could also be affected by the total film thickness, if this was the case a lower value for z^* would be expected here, due to the significantly lower total film thickness compared to that in Chapter 4. The total volume fraction of dSDS in the film measured at 25 °C, prior to heating, was calculated to be 0.11, which corresponds to 10.7 wt.%, and is therefore representative of the solution used to spin cast the film. It is interesting to note that f is very similar to the value obtained for the binary film (Section 7.2.1.1) as glycerol was previously shown

to enhance segregation in PVA (Chapter 4). Although the influence of glycerol on SDS distribution is most apparent at higher loadings of SDS (including the 20 wt.% loading studied in Chapter 4), the similar values for f in binary and plasticised films observed here could nevertheless indicate some development in the surface before first reflectivity was first collected (at 25 °C).

Upon heating the film incrementally to 85 °C, very little change in the reflectivity data and obtained volume fraction profile of the surfactant can be identified. This is is reflected by the lack of change in z^* and f. This contrasts with the behaviour of the non-plasticised film, where a slight change in structure of the surface excess layer was observed to occur. This is likely to be, at least in part, due to the action of the plasticisers leading to the film already being close to equilibrium structure at 25 °C.

It is also worth determining the change in plasticiser distribution upon heating the film. SLD-depth profiles obtained from films containing 10 wt.% hSDS and 20 wt.% d-glycerol determined from reflectivity measured at 25 and 85 °C are included in Fig. 7.3. The slight decrease in film thickness and decrease in SLD of the bulk film are indicative of loss of d-glycerol from the film. It can be seen, however, that the surface layer remains enriched in d-glycerol after heating, although the concentration of the plasticiser at the surface decreases slightly. This is likely to be a result of heating directly from 25 to 85 °C, which gives less cumulative time for evaporation of the plasticiser, leading to some retention of d-glycerol in the film. This observed surface enrichment of glycerol supports the idea that glycerol is somewhat bound to the surfactant headgroups and is thus more readily lost from the bulk of the film than the adsorbed layer environment.

7.2.2 Effect of Temperature on $C_{12}E_5$ Distribution

7.2.2.1 Binary Films containing $C_{12}E_5$

The effect of heating PVA films containing $C_{12}E_5$ was subsequently studied. The distribution of this surfactant in non-plasticised films at each temperature can be assessed by their volume fraction-depth profiles (Fig. 7.4). Here both the full depth profile (from air interface to the substrate) and a depth profile of the surface region of film are included.

A model consisting of 5 layers was required to adequately fit the entire Q range of the reflectivity at each temperature. These correspond to two layers for the surface excess, enriched in deuterated surfactant, a bulk film layer, a layer of surfactant enriched at the substrate interface, and finally a layer corresponding to silicon oxide on the substrate. This interfacial segregation of the surfactant, in

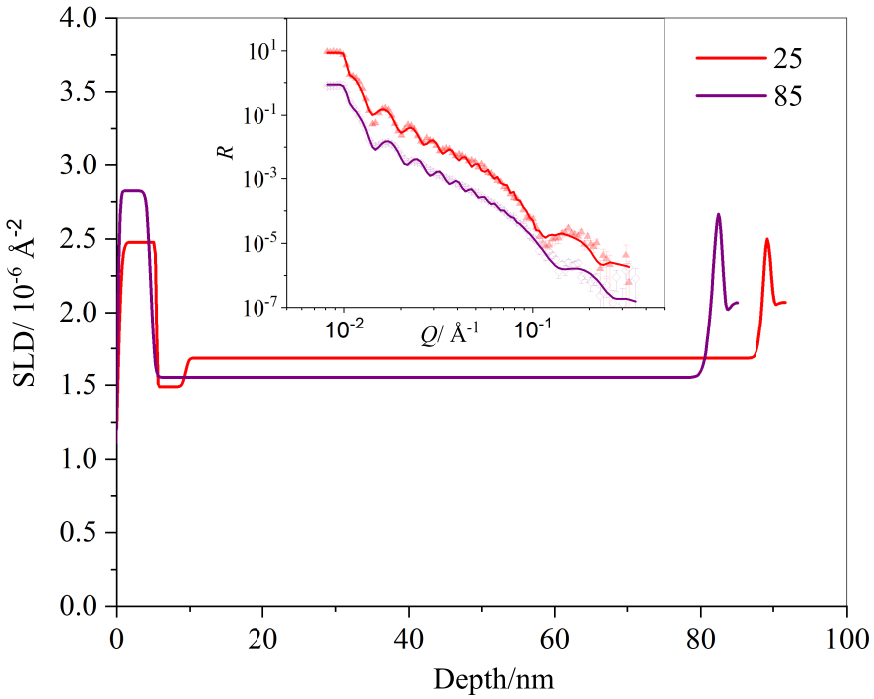

Figure 7.3: SLD-depth profiles of PVA films containing 10 wt.% hSDS and 20 wt.% d-glycerol at 25 °C and after heating to 85 °C. Neutron reflectivity data and fits are shown in the inset, with data for 25 °C offset for clarity.

addition to the surface segregation, has been previously reported.[168] However, as the silicon oxide has a similar SLD to the deuterated surfactant it is difficult to resolve these two layers in order to accurately quantify the interfacial segregation.

From the full depth profile, a slight decrease in film thickness can be observed at each temperature increase. As no plasticiser is present in this film, this decrease in thickness is likely to indicate loss of the surfactant itself. Alternatively, a decrease in thickness could be the result of the loss of residual water from the film, although if this were the case, a decrease in the thickness of the binary dSDS/PVA film would also be expected. As water has a low SLD (-5.6×10^{-7}Å^{-2}), its loss from the bulk film should lead to an increase in the SLD of this layer, which would appear as an increase in $\phi_{C_{12}E_5}$. However the uncertainty in the SLD of the bulk layer is typically too high to quantify dehydration in this way.

From the depth profile of the surface region of the film (7.4b), it is apparent that the surfactant distribution changes upon heating the film. The surface excess and fraction of segregated surfactant are reported in Table 7.3. There is little change in the depth profile (and thus z^* and f) upon heating from 25 °C to 45 °C. Upon heating further to 65 °C, the thickness of two surface layers remains constant but the surfactant volume fraction on the surface drops slightly, appearing to drop again after heating to 85 °C. A much more substantial change in the

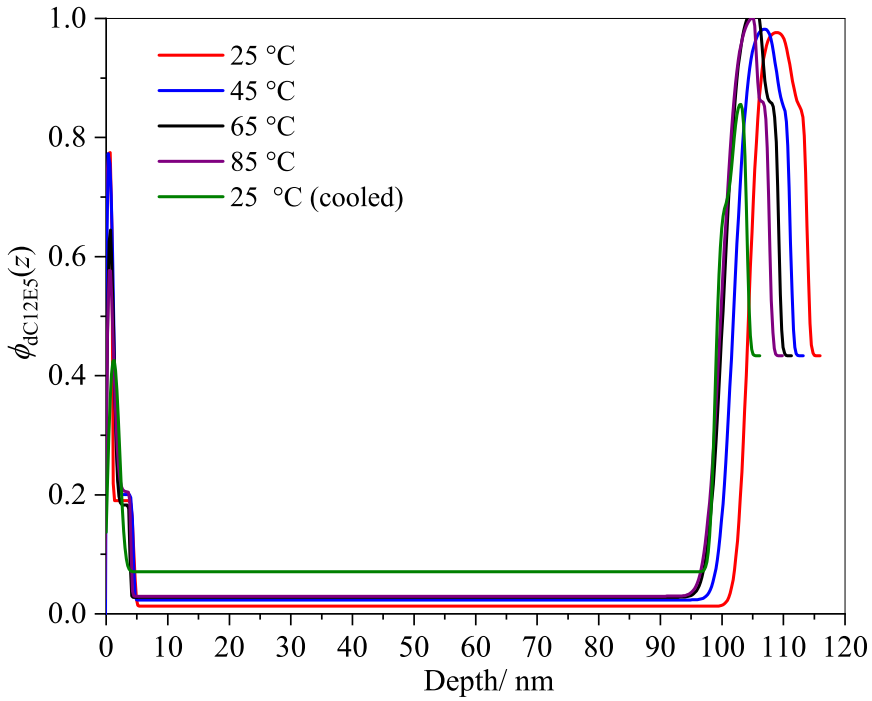

(a) Full film depth profile.

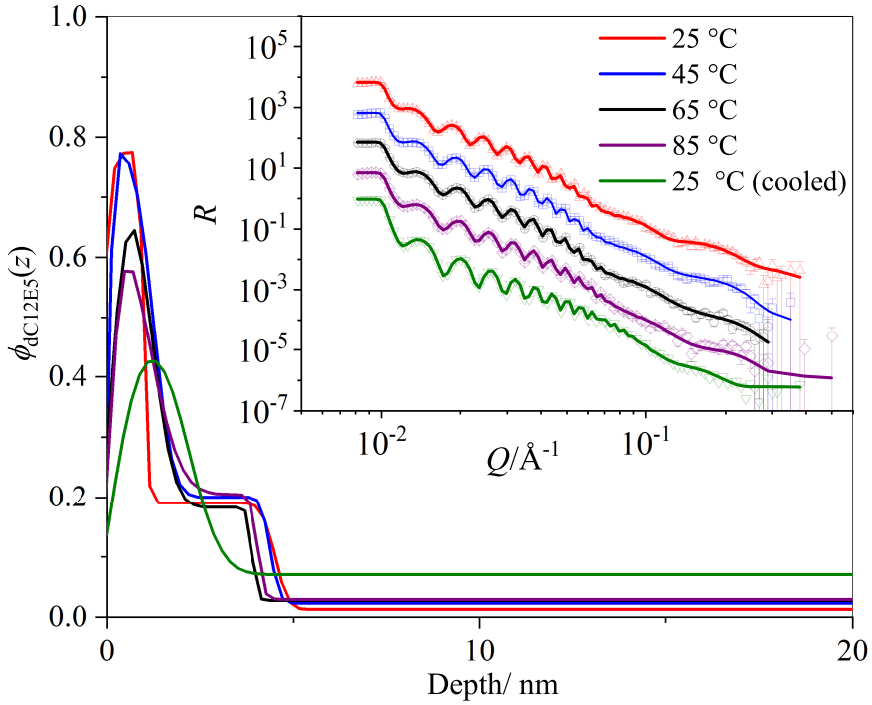

(b) Surfactant distribution at the film surface.

Figure 7.4: Depth profiles of 10 wt.% $dC_{12}E_5$ in non-plasticised PVA films at 25 °C, after heating to 45, 65 and 85 °C and upon cooling to 25 °C. Neutron reflectivity data and fits are shown in the inset of 7.4b, with data offset for clarity.

depth profile can be seen after allowing the film to cool back to 25 °C. In this case the reflectivity data can be fitted using a 4-layer model, with a single layer found

to be capable of capturing the surface excess. The thickness of this layer is lower than that of the two surface layers determined at all other temperatures, and the volume fraction of surfactant in this layer is also lower. In addition, it can be seen that volume fraction of surfactant in the bulk film layer is greatly increased, relative to the concentration in this layer at every other temperature measured. Although the SLD of this layer can typically have a large uncertainty associated with it, the substantial increase in $\phi_{b(C_{12}E_5)}$ suggests that this is not only a result of the uncertainty in the fitted parameter. It is clear, however, that the decrease in surface excess apparent in the film measured after cooling to 25 °C is not adequate to cause such an increase of surfactant volume fraction in the bulk film. It is therefore necessary to consider the interfacial segregation of the surfactant more carefully. From the full depth profiles (Fig. 7.4a), it can be seen that the thick, surfactant-rich layer adjacent to the silicon oxide clearly identifiable in the films measured at 25, 45, 65 and 85 °C is barely present in the profile determined after the film was cooled, suggesting the migration of surfactant from the substrate to the bulk film. From this profile, although it is hard to resolve interfacial $C_{12}E_5$ from the silicon oxide, it is also clear that the extent of segregation at the substrate is much greater than that at the air-film interface. Therefore, although difficult to quantify, this should not be neglected by considering only z^* and f, which are calculated based only on the $C_{12}E_5$ segregated to the air-film interface.

Table 7.3: Surface excesses (z^*) and fraction of segregated surfactant (f) in plasticised films containing 10 wt.% $dC_{12}E_5$.

T/°C	z^*/nm	f
25	1.4 ± 0.2	0.91 ± 0.09
45	1.4 ± 0.2	0.86 ± 0.09
65	1.1 ± 0.1	0.80 ± 0.08
85	1.1 ± 0.1	0.79 ± 0.07
25 (cooled)	0.7 ± 0.1	0.70 ± 0.07

7.2.2.2 Plasticised Films containing $C_{12}E_5$

The change in the distribution of $C_{12}E_5$ in plasticised films upon heating will now be assessed. The volume fraction depth profiles for the surfactant obtained from reflectivity measured at 25, 45, 65 and 85 °C and after cooling back to 25 °C are included in Fig. 7.5.

The z^* and f values for $C_{12}E_5$ for the plasticised film at each temperature are presented in Table 7.4. In accordance with previously published results,[168] comparison of Table 7.3 and 7.4 reveals a lower extent of $C_{12}E_5$ segregation in

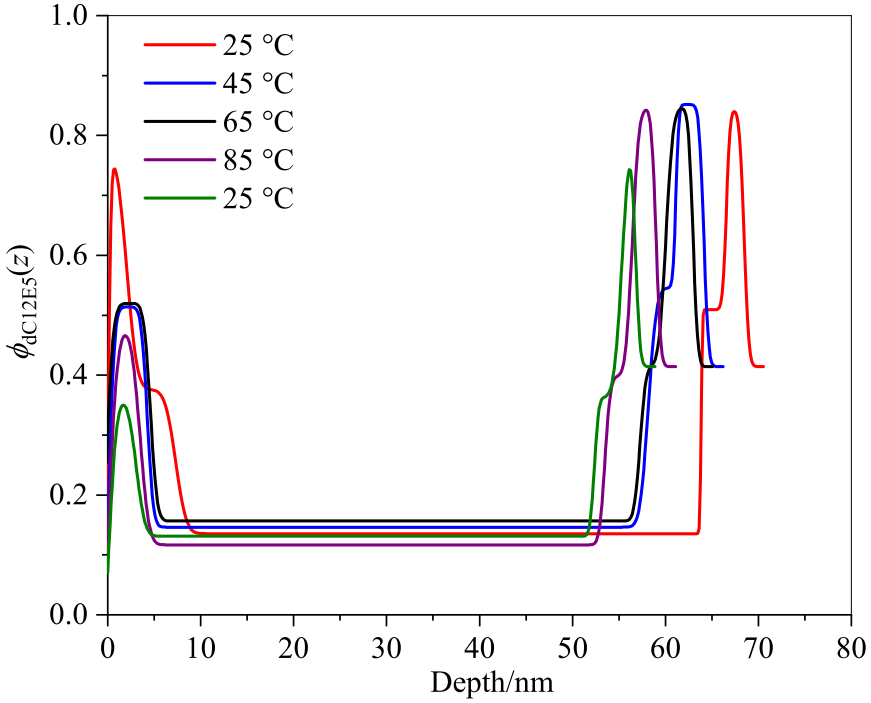

(a) Full film depth profile.

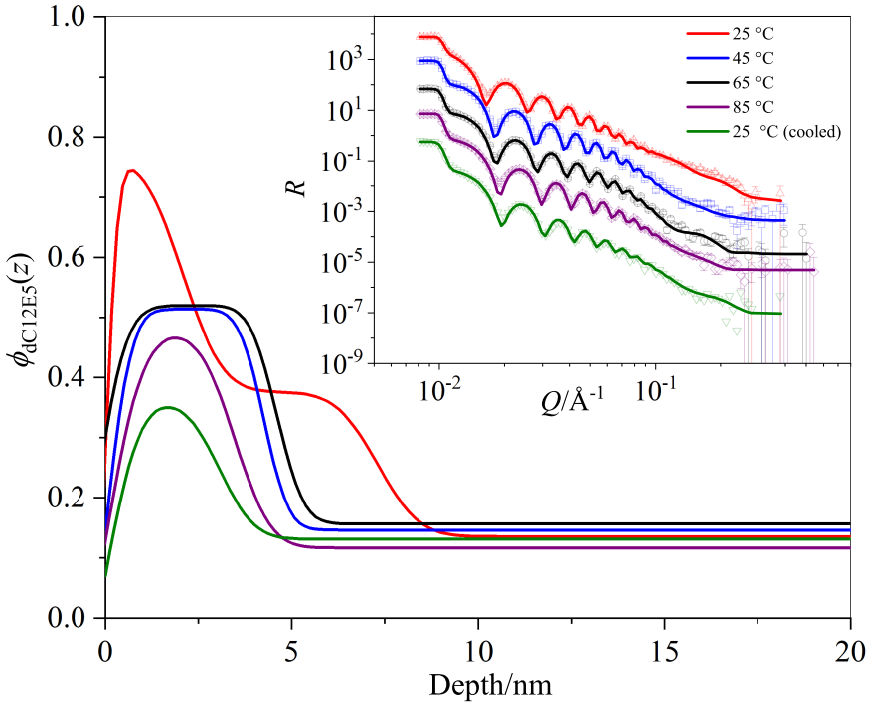

(b) Surfactant distribution at the film surface.

Figure 7.5: Depth profiles of 10 wt.% $dC_{12}E_5$ in PVA films containing 20 wt.% h-glycerol at 25 °C, after heating to 45, 65 and 85 °C and upon cooling to 25 °C. Neutron reflectivity data and fits are shown in the inset of 7.5b, with data offset for clarity.

the plasticised film.

First considering the whole depth profile (from the air to substrate interface),

Table 7.4: Surface excesses (z^*) and fraction of segregated surfactant (f) in plasticised films containing 10 wt.% $dC_{12}E_5$.

T/°C	z^*/nm	f
25	2.5 ± 0.2	0.22 ± 0.03
45	1.4 ± 0.2	0.30 ± 0.04
65	1.6 ± 0.2	0.15 ± 0.02
85	1.0 ± 0.1	0.14 ± 0.02
25 (cooled)	0.5 ± 0.1	0.07 ± 0.02

a decrease in film thickness upon heating the film can be identified. This is likely to be due to loss of glycerol, as observed for the SDS system. However, the loss of $C_{12}E_5$ observed from the binary film means that this depth profile could be complicated by the loss of both molecules, to different extents, over time and upon heating.

Although the reflectivity measured at 25 °C (before heating) was fitted with a 5-layer model with two layers comprising the surface excess region, upon heating to 45 °C, a 4-layer model, with the surface excess region comprising a single layer, could adequately fit the entire Q range. At 45 °C, the volume fraction of the surfactant on the surface can be seen to decrease, and the additional decrease in thickness of the surface region results in a decrease in z^* and f (Table 7.4). The depth profile then remains almost identical upon further heating to 65 °C . However, a further decrease in the surface excess is apparent at 85 °C (although due to the accompanying decease in total film thickness this does not correspond to a significant change in f). A further decrease in the surface excess can be identified when the film is cooled back to 25 °C although, again, any differences in f are within the uncertainty of this calculated value.

As for the binary film, it is clear that interfacial surfactant segregation is also significant for the plasticised film, as indicated by the presence of an additional layer of high SLD adjacent to the silicon oxide layer. Although precise quantification of interfacial segregation is not possible due the difficulty in resolving the two layers on the substrate, by eye it can be identified that the amount of interfacial surfactant decreases at each temperature increment.

Finally, the effect of heating the plasticised films containing $C_{12}E_5$ on the distribution of d-glycerol was assessed. Figure 7.6 shows the SLD-depth profile of the film measured at 25 and 85 °C. Only a slight decrease in film thickness occurs upon heating the sample, which is accompanied by a slight decrease in the SLD of the bulk film, suggesting some plasticiser loss. At 25 °C, there is some substantial enrichment of d-glycerol on the surface, in agreement with Briddick et al.,[168] and this surface layer is largely unchanged after heating to 85 °C. As

for the film containing SDS, the retention of d-glycerol in the film is likely to be because the film was heated straight from 25-85 °C, and thus the experiment was conducted over a shorter timescales.

It is clear that heating a film containing SDS has a very different effect to heating the film containing $C_{12}E_5$. However, it should also be considered that the quality of the fits on the $C_{12}E_5$ films is much higher than the SDS films. As the reflectivity models assume uniform, flat layers, this suggests that the $C_{12}E_5$ films can be characterised by much more even layers, with the SDS films containing a greater degree of lateral unevenness across the film, particularly upon heating.

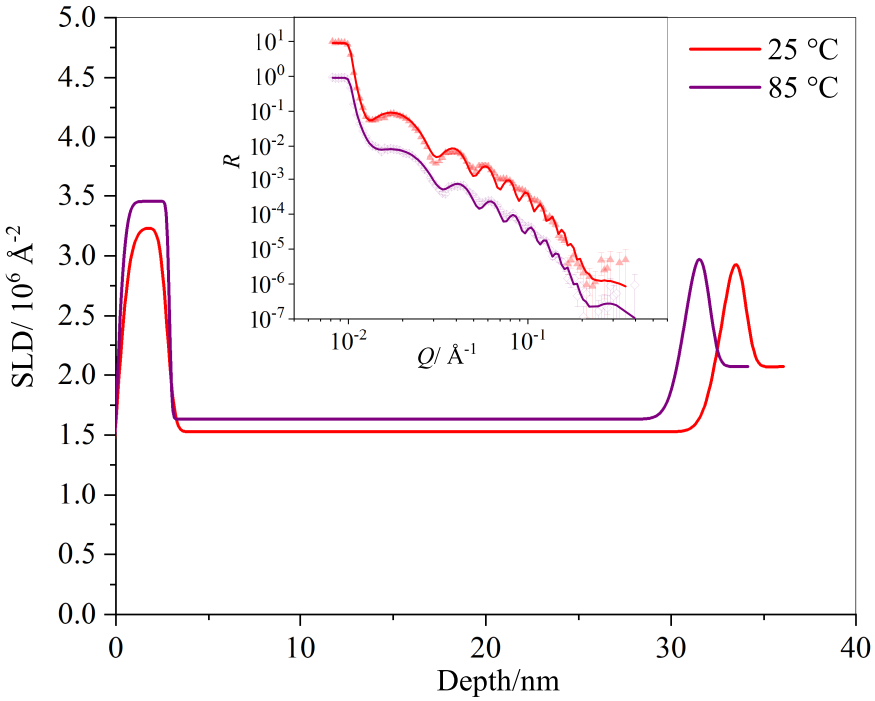

Figure 7.6: SLD-depth profiles of PVA films containing 10 wt.% $hC_{12}E_5$ and 20 wt.% d-glycerol at 25 °C and after heating to 85 °C. Neutron reflectivity data and fits model are shown in the inset, with data for 25 °C offset for clarity.

7.2.3 Effect of Temperature on DDAO Distribution

7.2.3.1 Binary Films containing DDAO

The final model system that will be explored contains the zwitterionic surfactant DDAO. The volume fraction-depth profiles of the surfactant in a non-plasticised film obtained from the reflectivity data acquired as 25, 45, 65 and 85 °C, and after cooling back to 25 °C are shown in Fig. 7.7.

In this system, a thin layer of segregated surfactant at the air-film interface can be identified at 25 °C , corresponding well to the thickness of a surfactant

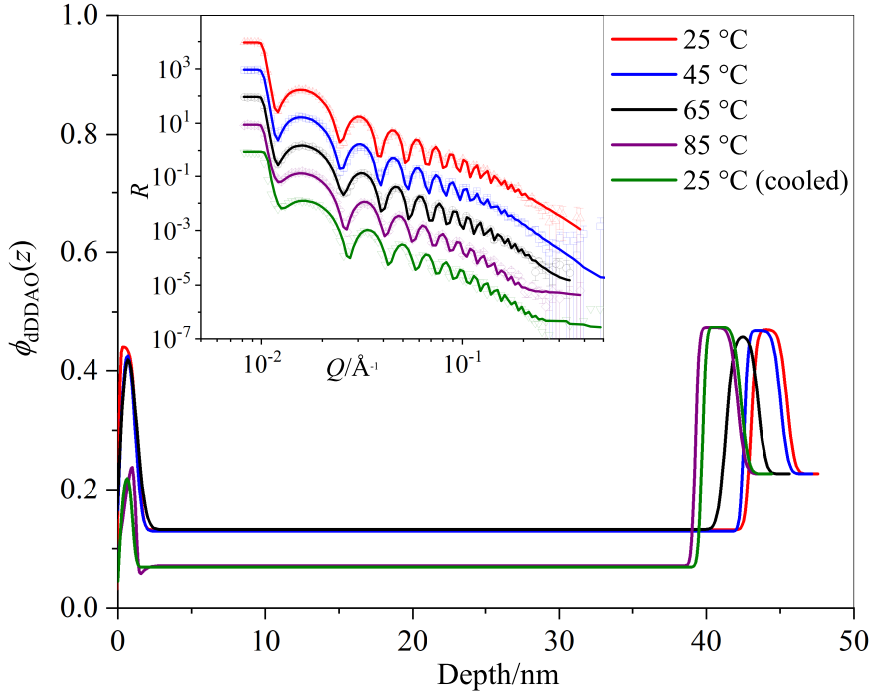

Figure 7.7: Depth profiles of 10 wt.% dDDAO in non-plasticised PVA films at 25 °C, after heating to 45, 65 and 85 °C and upon cooling to 25 °C. Neutron reflectivity data and fits are shown in the inset, with data offset for clarity.

monolayer, and in agreement with the findings reported in Chapter 6. NR also reveals evidence for the adsorption of DDAO at the substrate interface, as the layer adjacent to the substrate ($\sim$ 4 nm) appears to be somewhat thicker than would be expected for silicon oxide ($\sim$ 2.4 nm). This depth profile remains almost identical upon heating to 45 and 65 °C, with only a slight decrease in overall film thickness observed when the film is heated to 65 °C. However, upon heating to 85 °C, a substantial loss in surfactant concentration both in the surface layer and bulk film is also immediately apparent. A significant drop in SLD of the bulk and surface layers occurs, although the surface excess remains present, and is of very similar thickness to that identified in the film at lower temperatures. This substantial drop in SLD of the surface and bulk film is accompanied by a decrease in the total thickness of the film. This therefore initially appears to indicate the evaporation and loss of additive. However, it is important to explore and discount, if appropriate, other possible explanations.

In particular, it is important to consider that the obtained concentration-depth profiles are determined from an SLD profile based on the NR fits. SLD can be simply converted into volume fraction using on Equation 4.2. Immediately attributing the decrease in SLD upon heating and ageing this film to additive loss would therefore assume that the SLD of the PVA and deuterated additive

remain constant throughout this process. The validity of this assumption should be explored.

The SLD of a material is defined by the coherent scattering lengths of its constituent elements, b_i, and its molar volume, v_m (Equation 7.1). The molar volume is itself related to the density of the material, D, and its molar mass, M, by Equation 7.2.

$$\rho = \frac{\Sigma_{i=1}^{n} b_i}{v_m} \tag{7.1}$$

$$v_m = \frac{M}{D} \tag{7.2}$$

Although the coherent scattering lengths of the elements do not change during this process, it is plausible that the density of one or more of the film components changes during the ageing process, particularly as the film is heated through the glass transition of the polymer. It therefore may not be valid to assume that the molar volume and thus SLD remain constant. It can be seen from Fig. 7.7 that the significant "loss" occurs upon heating from 65 to 85 °C, through the T_g, where the dynamics in the amorphous region become faster, and the mobility of the additive could increase significantly.

To explore this possibility, the SLDs of both PVA and DDAO should be considered. First, it is possible that the density of the PVA decreases upon heating through the T_g, which would decrease its SLD, and therefore the observed SLD. However, if this were the case, it would be expected to reverse upon cooling, which is not observed. It would also be expected to occur in other model systems.

Second, it is also possible that the density of the deuterated DDAO could decrease if some reorganisation occurs upon heating through the T_g. In Chapter 6, the SANS data of solution-cast films containing amine oxides shows that the surfactant is aggregated in well-defined regions, corresponding to the amorphous regions of the polymer. In the case of the spin-cast films used for NR, the film dries much faster and so it is possible that surfactant is trapped out of equilibrium since the glass transition temperature is somewhat above room temperature (Fig. 6.16). Then, as polymer chains become more mobile, the surfactant molecules could reorganise and aggregate in the amorphous regions, as observed for the thicker solution cast films. If this latter state has a lower density than the surfactant distribution following spin-casting, this could result in a decrease in the observed SLD of this film. To illustrate this possibility numerically, for the bulk PVA film containing 10 wt.% dDDAO to give an SLD of 1.5 $\times 10^{-6}$Å^{-2}, (observed in Fig. 7.7) the density of the surfactant would be 1.2 g cm^{-3}. For the SLD of

this layer to reduce to 1.2 $\times 10^{-6}$ Å^{-2} after heating to 65 °C, the density would need to reduce to 0.8 g cm^{-3}. This is a substantial decrease in density, and it is extremely questionable whether this rearrangement to an aggregated state of significantly lower density is favourable.

The probability of additive loss from the film should therefore be considered. Although with a melting point of 132-133 °C[233] and a boiling point of 260 °C,[234] it would not be expected that this additive is highly volatile, glycerol (with a boiling point of 290 °C[146]) has been observed to evaporate. The loss of other high-boiling point additives, including $C_{12}E_5$ at room temperature, has also previously been observed.[147] TGA was therefore used to assess the thermal behaviour of DDAO, alongside other additives. Pure samples of DDAO, $C_{12}E_5$, SDS and glycerol were initially heated from 20 °C to 85 °C at a rate of 1 °C min^{-1}. This temperature range reflects that experienced by the spin-cast films during the neutron reflectivity experiment. TGA was also performed on the pure additives whilst heating samples to 400 °C in order to determine if there is any further additive volatility. The TGA traces are shown in Figure 7.8.

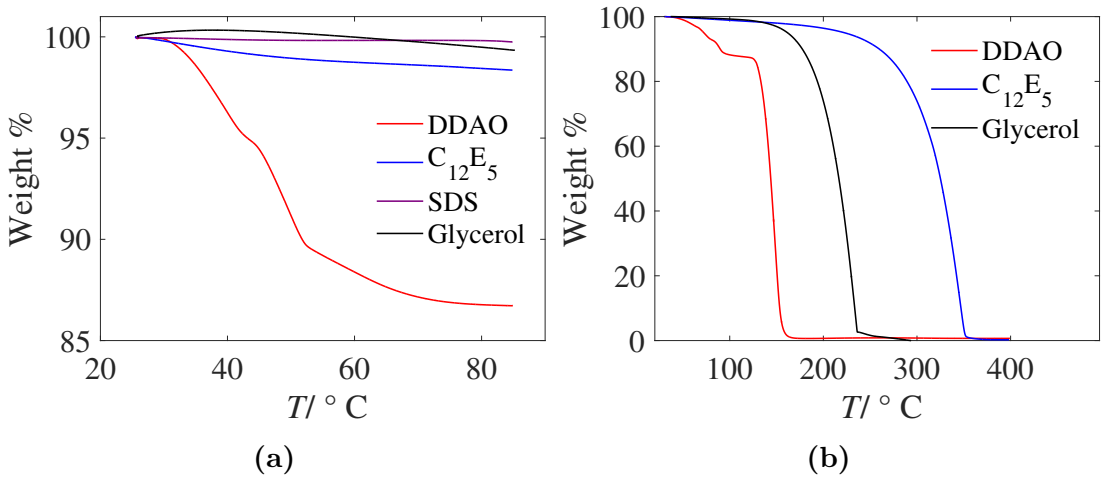

Figure 7.8: TGA traces of the pure additives. 7.8a shows the thermal behaviour of additives heated to 85 °C at a rate of 1 °C min^{-1}, and 7.8b shows the additives heated to 400 °C at a rate of 10 °C min^{-1}.

Upon heating the pure additive samples to 85 °C, a 13 % loss in mass of the amine oxide occurs. This is substantially lower than degree of mass loss observed in the spin-cast films upon heating to 85 °C (Figure 7.7), which suggest that 48 % of the surfactant is lost; ϕ_{DDAO} drops from 0.14 to 0.075 (12.2 to 6.3 wt.%). However, it is apparent from the TGA that there is a greater amount of DDAO loss than any of the other additives. Heating to 400 °C revealed the complete loss of DDAO by 160 °C. A likely reason for this DDAO loss from films at temperatures significantly below its reported boiling point is the increased exposed surface area

of the films compared to the pure additive, which is particularly significant if the enthalpy of vaporisation of the additive is fairly low (although no value for this could be found). To attempt to confirm that substantial DDAO loss could occur during the heating of the spin-cast film, PVA/surfactant samples were solution cast into DSC pans in an oven thermostatted to 40 °C, in an attempt to avoid additive loss during solution casting, and then mass loss was measured while samples were heated to 80 °C and then held at 80 °C for 1 hour. At the end of this isotherm, however, it is clear from the $\gg$10 wt.% mass loss that a significant amount of water remains in the sample after solution-casting which is lost from the film during the isotherm, and is impossible to distinguish from additive loss. This is consistent with the measured water content of samples that will be discussed in Chapter 9. These TGA curves are included in Appendix F.

It should be noted that the amine oxide surfactants are highly hydrophilic.[218] Some of the observed mass loss in the TGA of the pure additive samples could therefore be due to evaporation of water already bound to the surfactant, prior to dissolving it to make the mixed solutions. This is also something to consider with the spin-cast films: heating to 85 °C could cause loss of any residual water. However, the negative SLD of water (-5.6×10^{-7}Å^{-2}) means that loss of water would cause an increase in the SLD of the film. As the opposite is in fact observed upon heating the film, this suggests that water loss is not significant as the thin samples aid water loss during casting.

One limitation with these TGA experiments is that the surface area of the sample is much lower than that of the spin-cast films. This has two implications: first, the amount of water trapped in the TGA sample is much higher than in the film and second, the higher surface area of the film would lead to a greater evaporation of volatile components. Due to the limitation of running TGA of these systems, it can therefore not be unequivocally confirmed that DDAO loss occurs during the temperature exposure of the spin-cast films. However, the greater loss of DDAO compared to other investigated additives, which reveal no substantial change in SLD upon heating the film, alongside the entropic unfavourability of the rearrangement of surfactant into lower-density structures inside the film suggest that additive loss from this system is the most plausible explanation.

As for the previous model systems, the surface excess and fraction of segregated surfactant can be obtained from the depth profile. These are tabulated below (Table 7.5). Values for $\phi_{\mathrm{DDAO,tot}}$ are also included in order to assess the extent of additive loss.

Table 7.5: Surface excesses (z^*), fraction of segregated surfactant (f) and total surfactant volume fraction ($\phi_{\mathrm{DDAO\,tot}}$) in binary films containing 10 wt.% dDDAO.

T/°C	z^*/nm	f	$\phi_{\mathrm{DDAO\,tot}}$
25	0.37 ± 0.05	0.06 ± 0.01	0.14 ± 0.02
45	0.40 ± 0.05	0.07 ± 0.01	0.14 ± 0.02
65	0.40 ± 0.05	0.07 ± 0.01	0.14 ± 0.02
85	0.13 ± 0.03	0.05 ± 0.01	0.08 ± 0.02
25 (cooled)	0.13 ± 0.03	0.05 ± 0.01	0.08 ± 0.02

7.2.3.2 Plasticised Films containing DDAO

Volume fraction-depth profiles of dDDAO in plasticised films at 25, 45, 65 and 85 °C and 25 °C (cooled back down) are included in Fig. 7.9.

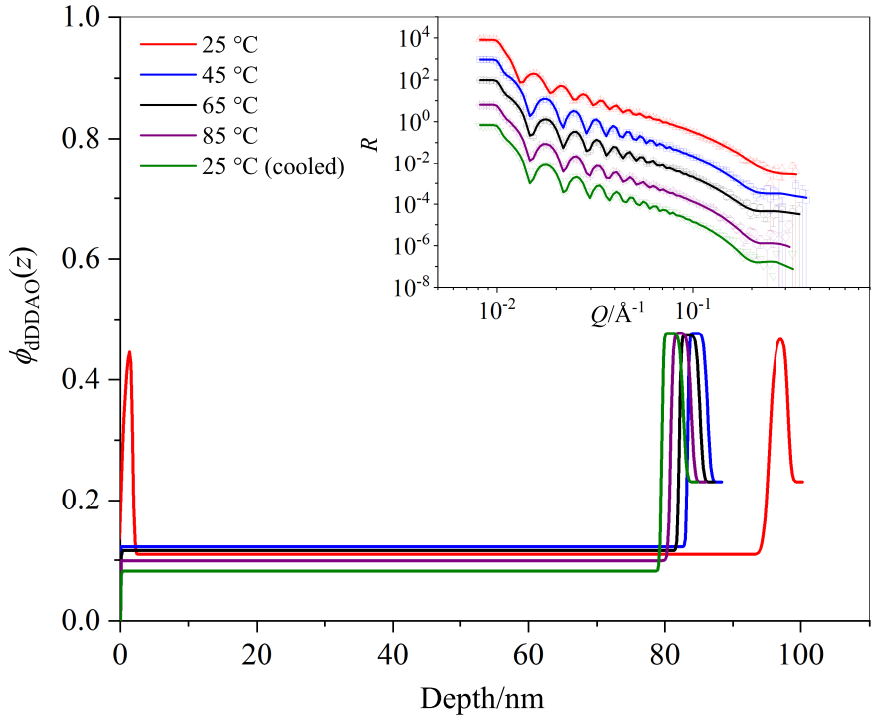

Figure 7.9: Depth profiles of 10 wt.% dDDAO in PVA films containing 20 wt.% h-glycerol at 25 °C, after heating to 45, 65 and 85 °C and upon cooling to 25 °C. Neutron reflectivity data and fits are shown in the inset, with data offset for clarity.

Although at 25 °C, a layer of segregated surfactant is present on the film surface, consistent with the findings reported in Chapter 6, upon heating the film to 45 °C, the surface excess disappears, leaving a film that has an even distribution of surfactant throughout.

Loss of additive from the plasticised film is also apparent. As was found for the film containing $C_{12}E_5$, the volatility of both glycerol and DDAO (as apparent from the binary film) means it can be difficult to know the exact composition of

the film at each temperature.

In this plasticised film, upon heating from 25 to 45 °C a significant decrease in film thickness (> 10 nm) occurs, although the SLD of the bulk film layer remains unchanged. This indicates the loss of glycerol. Upon heating further, a small decrease in film thickness occurs ($\sim$ 1 nm at each temperature step). The decrease in total thickness is accompanied by a decrease in SLD of the bulk film layer. Therefore, this is likely to be a result of the loss of dDDAO, as the loss of hydrogenated plasticiser would not decrease the SLD of the film. Indeed, it could increase the SLD very slightly, although as the SLD of h-glycerol (0.61 $\times 10^{-6}$ Å^{-2}) is very similar to the SLD of PVA (0.75 $\times 10^{-6}$ Å^{-2}), this effect would likely be negligible.

Although it is likely that DDAO is lost from the binary film upon heating, a surface monolayer is apparent at each temperature. Therefore it could be suggested that the disappearance of the monolayer upon heating the plasticised film cannot be attributed to additive loss from the film. It is unlikely that the DDAO on the surface would spontaneously migrate into the bulk film upon heating to 45 °C. It is therefore plausible that the absence of surface monolayer resolved by NR could be a result of the rearrangement of an evenly mixed surfactant/plasticiser monolayer into smaller patches on the surface, which would not be detectable by specular reflectivity. This could potentially be confirmed using AFM. Indeed, depth profiling a polybutadiene film with a squalane monolayer on the surface using ion beam analysis, revealed the presence of phase-separated regions of squalane which were undetectable by NR.[235]

The SLD-depth profiles of a film containing 10 wt.% dDDAO and 20 wt.% d-glycerol at 25 and 85 °C are shown in Fig. 7.10. In contrast to the findings in Chapter 6, no enriched glycerol layer is present on the surface of the plasticised film containing DDAO at 25 °C. Instead, the reflectivity data could be fitted with a surface layer of a lower SLD than the bulk film, indicative of glycerol depletion on the surface. When the film is heated to 85 °C, substantial glycerol loss is apparent, from both the decrease in total film thickness and decrease in SLD of the bulk film. At this temperature, the reflectivity could be fitted to a two layer model, with layers corresponding to the film and the silicon oxide. It should be noted that the SLD of the film was determined to be $\sim$ 0.7 $\times 10^{-6}$ Å^{-2}, very similar to the SLD of PVA, suggesting that the plasticiser has been completely lost from the film. This is also consistent with the film becoming 20 % thinner upon heating.

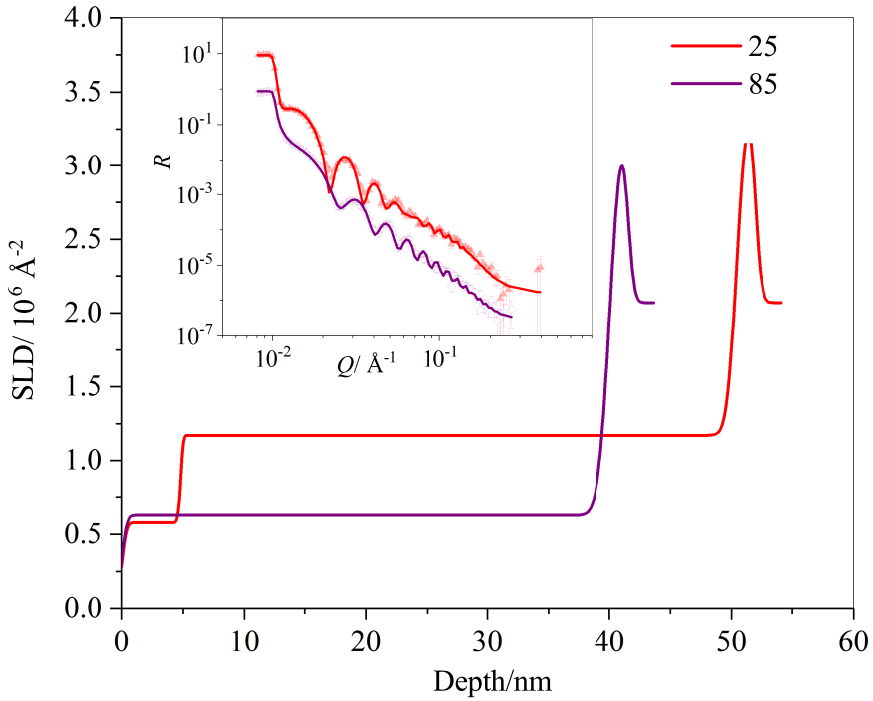

Figure 7.10: SLD-depth profiles of PVA films containing 10 wt.% hDDAO and 20 wt.% d-glycerol at 25 °C and after heating to 85 °C. Neutron reflectivity data and fits are shown in the inset, with data for 25 °C offset for clarity.

7.3 Discussion

In-situ neutron reflectivity measurements at elevated temperature have revealed a rich range of behaviours of surfactant additives. Although it is apparent that surfactant and/or plasticiser migration occurs within the films, in many films there is an accompanying loss of additive which must also be considered.

The experimental approach used throughout this chapter neglects any potential migration during the measurement occurring below 25 °C. As NR measurements for previous chapters were measured using a sample stage with no temperature control, at a temperature of ∼20 °C, there is potential for development of the surface structure or additive migration (either into or out of the film) to occur as the film is first heated from room temperature (∼20 °C) to 25 °C. This is likely to be particularly significant in the case of the plasticised films, which has been shown by DMA to have a T_g of 23 °C. It is also possible that the surfactant additives are capable of lowering the glass transition temperature from the value of 65 °C for the pure PVA. This should be borne in mind when considering slight differences in surfactant distribution measured at 25 °C to that determined in previous chapters.

Additionally, due to variable times for sample alignment and measurement, the time that the films were held at each temperature cannot be completely

controlled. It is therefore difficult to decouple the effects of temperature and time on additive loss, and thus differences in the extent of glycerol loss, for example, in different films should be expected. As differences in depth profiles of PVA/SDS/glycerol films obtained from NR (where the sample was under ambient conditions) and RBS (where the sample was vitrified immediately after spinning) have indicated the migration and surface development in the time shortly after spin coating (Fig. 6.16), the age of the film is likely to be important. Although the migration on this timescale cannot be probed using NR, this highlights the importance of time, as well as temperature, on surfactant distribution.

The effect of temperature on the distribution of film components in each of the model systems will now be discussed in greater detail.

7.3.1 Effect of Temperature on SDS Distribution

Non-plasticised PVA/SDS films show no significant change in the surface excess or fraction of segregated surfactant over time upon heating the film. However, there was some change in the shape of the surface excess region of the concentration profile upon heating to 85 °C. As the glass transition temperature of this non-plasticised PVA resin has been measured to be 65 °C (Chapter 9), it is likely that above this temperature the surfactant and polymer will have sufficient mobility to allow rearrangement of the surface. The melting point of pure SDS (204-207 °C)[236] is much higher than the maximum temperature of the film (85 °C), and so the lack of shift in the overall surfactant distribution is consistent with strongly segregated, nearly pure SDS, that does not migrate because it is solid.

The broadening of the surface excess layer, combined with the overall decrease in surfactant volume fraction is therefore likely to be due to a change in surfactant structuring and morphology at the surface. Changes in surfactant structures upon heating has been previously reported. For example, Auvray et al.[187] noted the increase in SDS lattice spacing in ethylene glycol with temperature. However, as specular NR is only capable of measuring the vertical distribution of surfactant, it cannot be unequivocally concluded that the change in volume fraction-depth profile is due to the structural re-organisation of the SDS on the surface. Nevertheless, based on the broadening of the surface excess layer and increase in interfacial roughness of the obtained volume fraction-depth profiles, it is likely that this is the result of the rearrangement of surfactant into aggregates.

The fact that the reflectivity for the binary SDS film could only be adequately fitted using 2 layers to capture the surface excess (and therefore using a 4-layer model), in contrast to the 3-layer model successfully used in Chapter 4, could also

indicate development of the surface below 25 °C. However, based on these experiments alone it could not be postulated whether this would arise from migration from the bulk film, or simply a rearrangement of the segregated surfactant.

Although NR is not well-suited to the characterisation of rough interfaces, the good fit to the low Q region using this model means that the thickness and SLD of the surface layer can be accurately obtained, and thus the consistency of the surface excess at each temperature can be identified with a high level of confidence.

The behaviour of this surfactant is likely to be consistent with the work of Dulal et al.[68] who studied the behaviour of the slip additive erucamide in high density polyethylene. The authors identified the accumulation of the additive at 38 °C, and the formation of plate-like crystal structures, which when heated further (to 50 °C) formed in raised compositions, leaving some of the polymer uncovered. This resulted in a change in the surface characteristics and morphology. They also used contact angle analysis to show that the hydrophobic hydrocarbon chains were oriented towards the air interface. Although no contact angle analysis has been performed on these PVA/surfactant systems to confirm the orientation of the surfactant tails towards the air interface (which is difficult due to the water solubility of the PVA), this probable arrangement is likely to have significant implications for the wetting behaviour of the film, and thus on the sealing ability of commercial films.

There is little change in the volume fraction-depth profile in the plasticised films. Although there is no extensive stacking of surfactant and plasticiser layers in this thin film, there is still likely to be a favourable interaction between the SDS and glycerol. Glycerol increases the mobility of the film components during the later stages of spin-casting and, as a result, upon heating the film there is little rearrangement of the already stable surface structures, which are likely close to equilibrium structure. Another possibility that would explain the differences between binary and plasticised films upon heating, is that the surface layer of surfactant on the surface contains some polar solvent around the headgroups. This may be driven off by heating, causing the observed restructuring of the surfactant. When water is bound to the surfactant head groups (in binary films), this could be lost at elevated temperatures. However, the higher boiling point of glycerol (290 °C[146]) means that if glycerol replaces water molecules in binding to the headgroups in plasticised films, the structure is more resilient with respect to heating. Nevertheless, glycerol has been previously be shown to evaporate from spin-cast PVA films under atmospheric conditions, with glycerol content in the film equilibrating after approximately 1 week.[147] The loss of glycerol is linked

to both elevated temperature and time after spin-casting, and as it is difficult to control the amount of time the films are held at each temperature, decoupling the roles of time and temperature in additive loss would require more experiments. However, although it is apparent that glycerol is lost from the film over time, determining the distribution of d-glycerol in the film at 25 and 85 °C revealed that the enrichment of plasticiser at the surface remained upon heating, and that the plasticiser was mainly lost from the bulk film, which is also indicative of the high stability of the surfactant/plasticiser structures on the surface.

The substantial loss of plasticiser is in part likely to be due to the low crystallinity of this PVA resin; with a DH of 87-90%, the presence of acetate groups reduces the extent of hydrogen bonding between adjacent polymer chains (this will be considered in greater depth in Chapter 9). As diffusion occurs primarily in the amorphous domains of a semi-crystalline polymer,[237] this lower crystallinity could result in the significant loss of glycerol observed. Additionally, glycerol has a lower affinity for the acetate groups due to their inability to hydrogen bond, which could also lead to its lower affinity for the polymer and thus increased migration from the film.

7.3.2 Effect of Temperature on $C_{12}E_5$ Distribution

$C_{12}E_5$ was found to exhibit very different behaviour to SDS upon heating a non-plasticised film. First, it is apparent that this surfactant is sufficiently volatile to be partially lost from the film upon heating. The loss of this surfactant from PVA films over time has been previously observed,[147] and it is clear that heating the film increases this additive loss. Second, some migration of $C_{12}E_5$ from both the film-air interface and the film-substrate interface is clear. Although small changes in the surface excess occur upon heating from 25-65 °C, the greatest decreases in surface and interfacial excesses, and the largest increase in SLD of the bulk film layer occur after the film was heated to 85 °C and subsequently cooled to 25 °C. This provides strong evidence for migration as a result of the increase in polymer and surfactant mobility as the film is heated above the glass transition temperature. The substantial differences in the depth profiles of the film measured at 85 °C and after cooling to 25 °C are likely to be a result of it being held at 85 °C, where further migration can occur, rather than it being the cooling process driving migration into the bulk film. This highlights the difficulty arising from the inability to decouple the roles of time and temperature in additive migration.

The decrease in surfactant segregation with increasing temperature, and mi-

gration of $C_{12}E_5$ into the bulk film indicates that this surfactant could be kinetically trapped on the surface of the spin-cast film, suggesting that the depth profiles measured at room temperature do not represent an equilibrium system, with the surfactant concentration in the bulk film unrepresentative of the solubility of the surfactant with the polymer. Additionally, the high concentration of $C_{12}E_5$ in the bulk film measured at 25 °C after being heated to 85 °C demonstrates that this higher surfactant concentration in the subsurface film is thermodynamically stable; as the film cools very gradually to 25 °C (∼1 hour), it would be very unlikely for surfactant to be kinetically trapped in the bulk film. The increasing equilibrium solubility of $C_{12}E_5$ in PVA with temperature is surprising, however, given that nonionic surfactants become less soluble with increasing temperature in hydrogen bonding solvents such as water.

The migration of additives from the surface into the bulk film has previously been reported.[68] For example, although the behaviour of the slip additive erucamide at elevated temperature varies, (it has been found to either be lost from the film, undergo chemical change or decomposition or migrate back into the film), Shuler et al.[238] found that in a trilayer film comprising two layers of linear low-density polyethylene and a skin layer consisting of a polyolefin plastomer incorporating the erucamide, the additive migrated back into the film from the surface upon heating. This was observed for the $C_{12}E_5$ in PVA.

In plasticised films, there is also a substantial decrease in the interfacial excesses of $C_{12}E_5$ upon heating from 25 to 85 °C. However the biggest change in the volume fraction-depth profile occurs upon heating from 25 to 45 °C. This correlates well with heating the film through the glass transition of plasticised PVA, where polymer and surfactant mobility increases significantly, facilitating the migration of the surfactant into the film, and the additive loss through evaporation.

Although migration from the interfaces to the bulk film occurs in the plasticised film, this is to a lesser extent than in the non-plasticised film, as indicated by the lack of significant increase in the SLD of the bulk film. A likely reason for this is the presence of glycerol, which occupies the amorphous regions of the polymer, out-competing $C_{12}E_5$, which instead remains localised on the surface.

From the SLD-depth profiles of films containing d-glycerol and $hC_{12}E_5$, only a slight loss of glycerol can be identified upon heating from 25 to 85 °C. This shows the importance of time rather than temperature in plasticiser loss from films. From these profiles, it is also apparent that it is favourable for glycerol to co-adsorb with the surfactant at the surface, even after the mobility of film components has increased above the glass transition, and surfactant segregation

has somewhat decreased. This highlights the favourable interactions between the two additives on the surface.

7.3.3 Effect of Temperature on DDAO Distribution

In films containing DDAO, the change in volume fraction-depth profile is dominated by the unexpected loss of the surfactant as the film is heated.

In the binary film, surfactant loss was mostly found to occur upon heating from 65 to 85 °C. It should be noted that despite a large drop in total dDDAO content in the film, a monolayer of surfactant remains on the film surface at each temperature. This could be favoured in order to avoid the entropic penalty that would result from having a long polymer molecule localised on the surface.[113,239] However, should this be the case, it would be expected that in PVA/glycerol films, in the absence of surfactant, a layer of glycerol should be present on the surface, which has not been observed.[168] Therefore, the persistence of this surfactant layer could instead be enthalpically driven, and due to the favourable reduction in surface energy.

In plasticised films, DDAO loss was found to occur at each temperature increment. This is therefore consistent with additive loss occurring only when sufficient mobility is attained after heating above the glass transition temperature. In contrast to the non-plasticised film, after heating above 25 °C the surface monolayer of surfactant appears to be no longer present, as the depth profiles reflect an even distribution of surfactant throughout the whole film. This could be a result of the high compatibility of the amine oxide surfactant for PVA (Chapter 6); the surface monolayer of surfactant may be kinetically trapped after the fast spin-coating, and upon heating the plasticised film, sufficient additive mobility is achieved for the surfactant to re-disperse into the bulk. However, it is interesting that this is not observed for the non-plasticised film. The exact distribution of surfactant cannot be predicted from these experiments alone, but is likely to be governed by balance of entropic and enthalpic factors, including surface energy and compatibility.

It can be seen that after heating the film containing hDDAO and d-glycerol to 85 °C all glycerol had evaporated from the film. This is probably due to the length of time the film was aged at high temperature as the film was heated to 85 °C immediately after measurement at 25 °C, but reflectivity data of the heated film was not collected for $\sim$ 4 hours. As a result, it cannot be determined whether there would have been any glycerol enrichment of the surface.

7.4 Chapter Conclusions

In this Chapter, the effect of temperature on the distribution of three surfactant additives in PVA films was investigated. Understanding the effect of heating these model films was complicated by the difficulty in decoupling the effect of temperature and time, which is particularly relevant in the loss of additives from the films. Nevertheless, a range of additive behaviours was identified.

In the SDS system, no change in the amount of segregated surfactant occurs upon heating and ageing the film. However, in binary films, a increase in interfacial roughness of the surface excess layer indicates a rearrangement of surfactant structures on the surface. No change at all is apparent when heating the plasticised film.

$C_{12}E_5$ is the only surfactant observed to migrate into the bulk PVA film upon heating. In the non-plasticised films, there is a significant decrease in the size of the surface and interfacial excesses. When glycerol is present, although analysis is complicated by the loss of two components from the film, a reduction in the surface excess is again indicative of surfactant migration into the bulk film. This is less significant than in the non-plasticised film, probably due to the glycerol competing for the amorphous regions in the polymer that the surfactant would otherwise localise in.

Finally, the DDAO system exhibits the most significant surfactant loss upon heating through the glass transition of PVA. The greater volatility of DDAO compared to the other additives studied was confirmed by TGA. Despite the significant loss of DDAO from films in the absence of plasticiser, a monolayer of surfactant remains on the surface of the film upon heating. This is in contrast to its behaviour in plasticised films, where an even surfactant distribution throughout the whole film was identified upon heating above 25 °C.

Although further experiments are required to fully resolve the relationship between time and temperature in the distribution of these additives, these findings suggest that changes in film surface structure upon ageing will have significant implications for film surface properties such as hydrophilicity, and thus their sealing ability in commercial systems. Additionally, this work has touched upon the importance of surfactant diffusion through the PVA, which is likely to be relevant for the mobility of encapsulated components in unit-dose detergents.

Chapter 8

Segregation Synergy of Mixed Surfactant Systems in PVA Films

8.1 Chapter Introduction

Having thoroughly characterised the segregation behaviour of a number of model film systems comprising a single surfactant (Chapters 4 and 6), and rationalised their behaviours using surface energy and compatibility arguments, in this chapter more complex model systems will be considered.

Mixtures of surfactants can be non-ideal, and properties of mixtures can differ from those of the individual species. Depending on the nature of the surfactants, the interactions between them can lead to synergism or antagonism. Many industrial formulations contain mixtures of surfactants, either to exploit this synergistic behaviour or to provide different types of performance in a single formulation (for example cleaning plus fabric softening).[240] By probing segregation behaviours in films containing multiple surfactant species, this takes the model systems closer to the complex formulations used in industry, enabling a fuller understanding of the driving forces for segregation.

Three model systems will be considered here: SDS/DDAO, $C_{12}E_5$/DDAO and SDS/$C_{12}E_5$. The segregation of SDS and DDAO has been thoroughly discussed in earlier chapters, and the behaviour of $C_{12}E_5$ have been reported in a previous publication.[168] The three selected surfactants exhibit very distinct segregation behaviours in PVA, and are also affected by the presence of plasticiser to different extents. Probing the distribution of each additive in the film should therefore highlight any synergism between surfactants in the segregation from PVA films.

To complement the depth profiling of the films, the interactions between components in solution will be probed via surface tension experiments. Through this,

the aim is to better understand the role of surface energy in segregation in more complex systems.

The interactions between surfactant molecules are influenced by the nature of the headgroup. Therefore, in this study, the use of surfactants with the same 12-carbon hydrophobic tail should enable the nature of interactions between headgroups to be assessed.

8.2 Results

8.2.1 Vertical Depth Distribution in Mixed-Surfactant Films

8.2.1.1 SDS/DDAO

The first model system contains the anionic surfactant SDS and the zwitterionic amine oxide surfactant DDAO. Their individual segregation behaviours are covered in detail in Chapters 4 and 6 respectively.

The simpler, non-plasticised system will be initially considered. By contrast matching all components except one to the SLD of the PVA resin (0.75 $\times 10^{-6}$ Å^{-2}), the volume fraction-depth profile of a single (deuterated) component in the film can be isolated. Table 8.1 shows the respective amounts of deuterated and hydrogenated additives required to contrast match to PVA.

Table 8.1: Mass of hydrogenated and deuterated additives required to contrast match to PVA (giving a total additive mass of 0.1 g).

Additive	Mass deuterated/ g	Mass hydrogenated/ g
Glycerol	0.034	0.966
SDS	0.069	0.931
DDAO	0.153	0.847
$C_{12}E_5$	0.181	0.819

For the SDS/DDAO model system, two contrasts were used in order to identify how the incorporation of SDS affects the distribution of dDDAO, and how the incorporation of DDAO affects the distribution of dSDS. The obtained volume fraction-depth profiles are shown in Figures 8.1 and 8.2 respectively. To quantify the effect of a secondary surfactant additive on the distribution of a deuterated surfactant, the surface excess, z^*, and fraction of segregated surfactant, f, are calculated and tabulated (Tables 8.2 and 8.3), in the same way as in earlier chapters.

In this set of experiments, the total surfactant loading in each sample was fixed at 10 wt.%. In order to vary the ratio of two surfactant species, this therefore

necessitates the variation of the concentration of the deuterated species, which will itself directly impact the surface excess. The fraction of segregated surfactant, accounting for variation in film thickness and overall surfactant concentration, will therefore be used as the primary means of assessing the impact of a secondary surfactant on segregation behaviour. In order to simplify interpretation of the depth profiles in these more complex systems, the effect of SDS on the distribution of dDDAO will first be considered before assessing the effect of contrast matched (cm) DDAO on the distribution of dSDS.

As discussed in detail in Chapter 6, in the absence of any additional surfactant, dDDAO forms a single monolayer on the surface of the PVA film, with the remaining additive evenly distributed throughout the bulk film. This is illustrated by the red curve in Fig. 8.1. From this figure, it can be seen that upon incorporation of contrast matched SDS (at two different loadings), the dDDAO surface layer is significantly broadened over a lengthscale much greater than a single monolayer. The concentration of dDDAO in this layer is also substantially reduced. Instead of a monolayer, the surface region of the depth profile now comprises a thick layer of PVA enriched in surfactant. To quantitatively assess the effect of SDS loading on dDDAO distribution, the surface excess (z^*) and fraction of segregated surfactant (f) are reported in Table 8.2. Although the variation in the concentration of dDDAO means that a clear trend cannot be easily discerned from z^*, the change in f with dDDAO/SDS ratio clearly shows that SDS strongly promotes dDDAO segregation, with the higher SDS concentration causing a much higher fraction of the amine oxide to enrich the surface. As previously observed for films containing dDDAO as the only surfactant, the film containing 2.5 % contrast matched SDS showed significant segregation of the amine oxide at the substrate interface. However, this is harder to quantify due the difficulty in resolving interfacial surfactant from the silicon oxide. This interfacial segregation was less apparent in the film containing 7.5 % contrast matched SDS and only 2.5% dDDAO.

Table 8.2: Surface excess (z^*) and fraction of segregated surfactant (f)for binary and plasticised PVA films containing dDDAO and contrast matched SDS.

	Binary		Plasticised	
	z^*/nm	f	z^*/nm	f
10 wt.% dDDAO	0.5 ± 0.1	0.06 ± 0.01	0.6±0.2	0.06 ± 0.01
7.5 wt.% dDDAO, 2.5 wt.% cmSDS	1.4 ± 0.1	0.30 ± 0.02	0.7 ± 0.1	0.30 ± 0.05
2.5 wt.% dDDAO, 7.5 wt.% cmSDS	0.5 ± 0.1	0.9 ± 0.1	2.1 ± 0.1	0.4 ± 0.1

Having established this trend, it is worthwhile quantitatively comparing the effect of SDS inclusion on f, compared to a film containing the same concentration

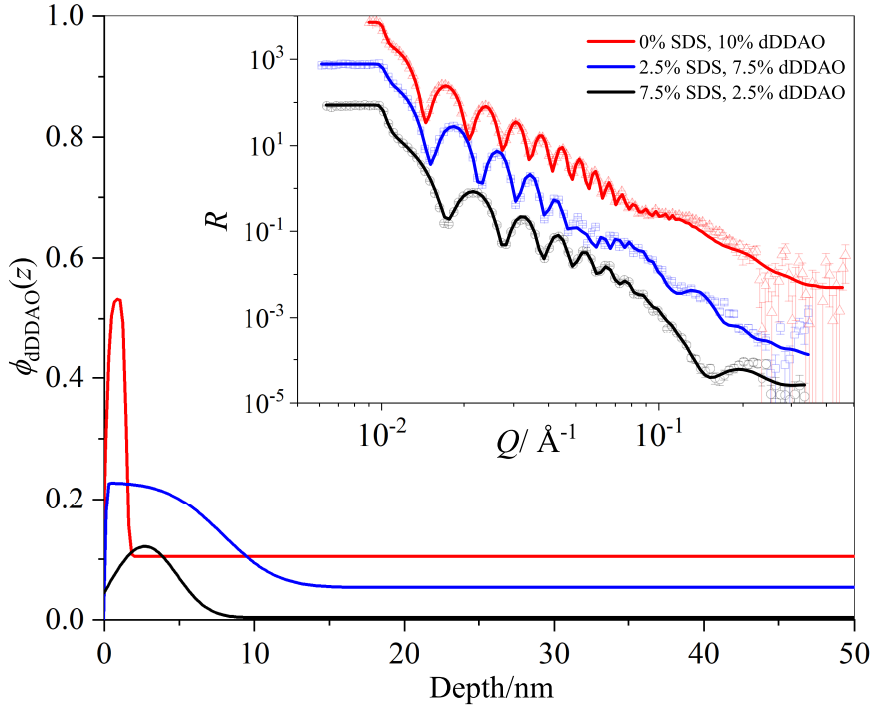

Figure 8.1: Volume fraction-depth profiles of dDDAO in PVA films with a total surfactant loading of 10 wt.%, with varying ratios of dDDAO and contrast matched SDS. Neutron reflectivity data and fits (offset for clarity) are shown in the inset.

of the dDDAO with no additional surfactant. In Chapter 6, it was shown that the surface excess remains constant at ∼0.5 nm for all loadings of dDDAO in binary films. Expressing these values as fractions of the total surfactant present comprising the surface excess gives $f_{\mathrm{DDAO}} = (0.06 \pm 0.01)$ and $f_{\mathrm{DDAO}} = (0.30 \pm 0.05)$ for films containing 5 and 2 wt.% dDDAO respectively. Although these loadings do not exactly match the concentrations of dDDAO in the mixed surfactant films, by considering the values for f of (0.30 ± 0.02) and (0.9 ± 0.1) for films containing 7.5 wt% dDDAO (plus 2.5 wt.% SDS) and 2.5 wt% dDDAO (plus 7.5 wt.% SDS) respectively, it is clear that the reduction in dDDAO concentration alone cannot account for the substantial increase in efficiency of adsorption.

The effect of DDAO on dSDS segregation will now be considered. As discussed in Chapter 4, in non-plasticised films SDS forms a thick surface excess layer, with a low surfactant concentration in the bulk film. This is illustrated by the red line in Figure 8.2. For this contrast, only one measurement of a mixed surfactant film could be taken due to the formation of visible crystals of surfactant in solutions containing a higher concentration of dSDS. Although the surfactant concentrations are much greater than the CMC, and thus the formation of other liquid crystalline phases is possible, the solute concentration is no higher than in the single surfactant systems. This observable crystallisation could be sugges-

tive of an increase in Krafft temperature (T_k), the temperature below which the surfactant solubility is less than the CMC, of one of the surfactants. However in previous studies, T_k in binary surfactant mixtures in solution has been found to be lower than that of the respective single components.[241] In these mixed surfactant systems, micelle formation is increasingly favoured, which lowers the CMC and reduces the monomer concentration that is able to form crystals.[242] Summerton et al.[243] studied crystallisation in the mixed SDS/DDAO system, finding that increasing the concentration of DDAO lowers the concentration of SDS monomers, due to mixed micelle formation, consequently reducing the drive for SDS crystallisation. The opposite effect is observed in this current work, and therefore the possibility of DDAO increasing the Krafft temperature of SDS should be discounted. Nevertheless, as no SDS crystallisation has been observed in its pure solutions (Chapter 4), it is likely that in this case, DDAO crystallisation is observed, as the Krafft point of DDAO could be elevated by increasing ionic strength due to the high concentration of SDS. This has been extensively observed for surfactants in the presence of salts.[244,245]

It should be noted that this crystallisation was not observed for the other contrast (hSDS and dDDAO), raising the question of whether equilibrium has been reached in the mixed surfactant solutions before spin-casting. However, detailed consideration of crystallisation kinetics is beyond the remit of this thesis, but could form part of a future work extension.

From Figure 8.2, it is immediately apparent that the film containing 2.5 wt.% dSDS (and 7.5 wt.% cm-DDAO) exhibits a much lower surface excess compared to the film containing 10 wt.% dSDS; although the thickness of the surface layer is similar for the two films, the concentration of dSDS in this layer is much lower in the presence of DDAO. It should be noted that fitting the data for this film to this simple 3-layer model does not capture the feature at $Q \sim 0.2$ Å^{-1}. However, the good fit throughout the lower Q range means that an accurate picture of the thickness and concentration of the total thickness of surface layer can be attained.

To determine whether the lower extent of segregation can be accounted for simply by the lower concentration of deuterated surfactant in this film, f values should again be compared (Table 8.3). The decrease in f from 0.3 to 0.1 upon DDAO incorporation confirms that segregation is inhibited in the latter film.

As for the previous contrast, it should also be confirmed that this observed trend is a direct result of the incorporation of the amine oxide, and not merely due to the reduction in dSDS concentration. The reflectivity data from a spin-cast film of PVA containing 2.5 wt.% dSDS as the only additive was therefore collected and fitted. The obtained volume fraction-depth profile, yielded an f

value of 0.6, substantially higher than the value of 0.1 obtained from the film containing 2.5 wt.% dSDS and 7.5 wt.% DDAO. This confirms that the presence of DDAO strongly suppresses SDS segregation. These reflectivity data and fits, alongside the corresponding depth profiles, are included in Appendix A.

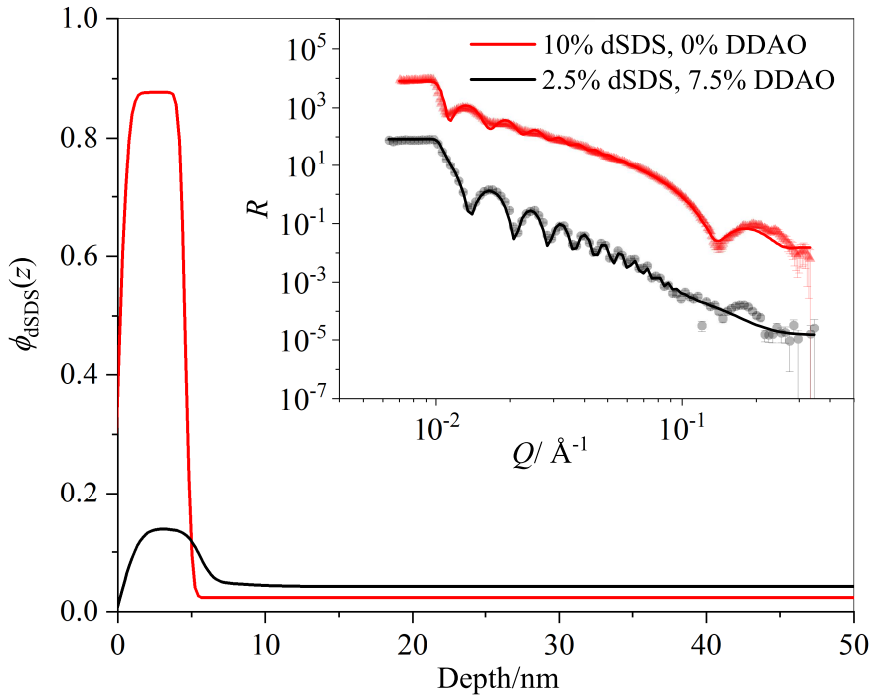

Figure 8.2: Volume fraction-depth profiles of dSDS in PVA films with a total surfactant loading of 10 wt.%, with varying ratios of cmDDAO and dSDS. Neutron reflectivity data and fits (offset for clarity) are shown in the inset.

Table 8.3: Surface excess (z^*) and fraction of segregated surfactant (f) for binary and plasticised PVA films containing dSDS and cmDDAO.

	Binary		Plasticised	
	z^*/nm	f	z^*/nm	f
10 wt.% dSDS	3.4 ± 0.1	0.3 ± 0.1	5.5 ± 0.1	0.9 ± 0.1
7.5 wt.% dSDS, 2.5 wt.% cmDDAO	-	-	2.44 ± 0.07	0.47 ± 0.04
2.5 wt.% dSDS, 7.5 wt.% cmDDAO	0.42 ± 0.03	0.11 ± 0.02	0	0

Superimposing the depth profiles can be used to better assess the distribution of components in these multi-surfactant systems. It should be noted that as the distribution of only one component can be measured, each profile corresponds to a different spin-cast film, which may vary in total film thickness and additive concentration. The superimposed depth profiles can therefore only approximately reflect the concentration of the two surfactants at the surface. The superimposed depth profiles of dDDAO and dSDS in non-plasticised films is shown in Fig. 8.3. From this figure, it can be seen that the thickness of the surface excess

regions of the two surfactants differ substantially, despite the thickness of the two films being similar (72 nm and 78 nm for the films containing dDDAO/cm-SDS and dSDS/hDDAO respectively). Although the thicknesses of the surface excess regions of these two films appears to be different, the use of a third contrast, in which both surfactants are deuterated would be required to be confident in resolving the relative positioning of these layers.

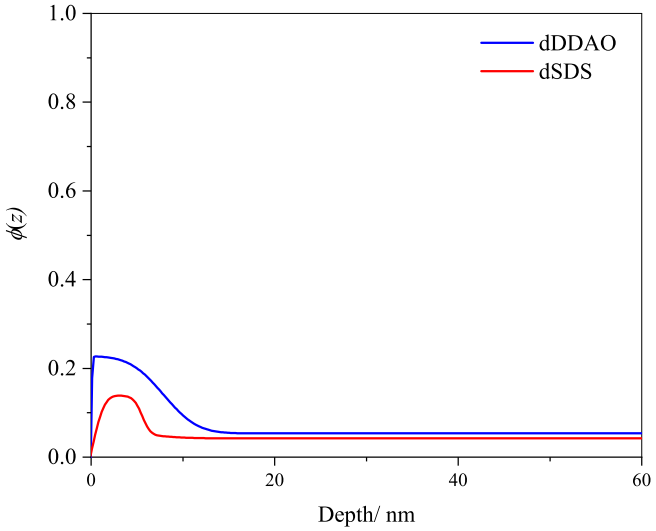

Figure 8.3: Superimposed volume fraction-depth profiles of dDDAO (7.5 wt.%) and dSDS (2.5 wt.%) in unplasticised PVA.

As it has been found that incorporation of a model plasticiser (glycerol) can significantly impact surfactant distribution in single-surfactant systems, the effect of plasticisation on the distribution of the components in films containing multiple surfactants was subsequently studied. In these systems, all components except one were again contrast matched to the SLD of PVA. This approach removes the need to assume an even distribution of glycerol throughout the film to obtain a surfactant volume fraction-depth profile (the approach taken in Chapters 4 and 6). In all films the loading of contrast-matched glycerol is fixed at 20 wt.%.

To assess the effect of multiple surfactants on their distribution in plasticised films, an identical approach was taken to that for the binary films, whereby the effect of cmSDS on dDDAO distribution, and the effect of cmDDAO on dSDS distribution were considered. The obtained depth profiles for these two contrasts are presented in Figures 8.4 and 8.5 respectively, with determined values for z^* and f reported in Tables 8.2 and 8.3 respectively. In the non-plasticised films, SDS significantly promotes the segregation of DDAO, while DDAO strongly suppresses SDS segregation, and it can be seen that these trends are consistently reproduced in the plasticised system. First considering the dDDAO/SDS contrast, SDS incorporation causes an overall increase in the fraction of segregated

dDDAO. However, this is a lesser effect than in the non-plasticised films, as there is no significant broadening of the surface layer upon incorporation of 2.5 wt.% cmSDS, and the extent of segregation in the presence of 7.5 wt.% cmSDS is significantly lower in the plasticised film than in the non-plasticised film. Second, considering the dSDS/DDAO contrast, it can be seen that DDAO incorporation causes a substantial reduction in f, to an even greater extent than in the non-plasticised film. Indeed, in the presence of 7.5 wt.% DDAO, no surface layer enriched in dSDS is observed at all, with the dSDS uniformly distributed throughout the entire film.

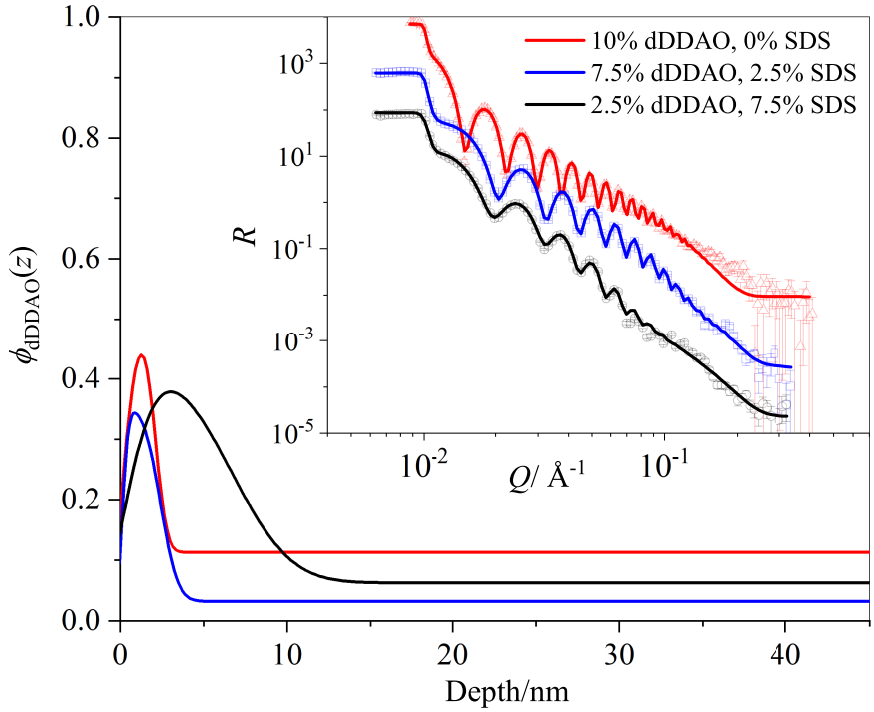

Figure 8.4: Volume fraction-depth profiles of dDDAO in PVA films with 20 wt.% h-glycerol and a total surfactant loading of 10 wt.%, with varying ratios of dDDAO and cmSDS. Neutron reflectivity data and fits (offset for clarity) are shown in the inset.

Finally, the effect of including two surfactants on the segregation of the plasticiser in this model system will be assessed. To briefly summarise, although no glycerol segregation occurs in pure PVA films, the presence of surfactant can have a significant impact on its distribution in the film: SDS and glycerol were found to bloom into stacked bilayer structures at high surfactant concentrations (although when this film structure was fitted using a single surface excess layer, it corresponds to a layer substantially depleted in glycerol, relative to the subsurface film). Glycerol was also found to co-adsorb into the DDAO monolayer at all DDAO loadings. These depth profiles, alongside the depth profiles of d-glycerol in the presence of DDAO/SDS mixtures are included in Figure 8.6. Here it can

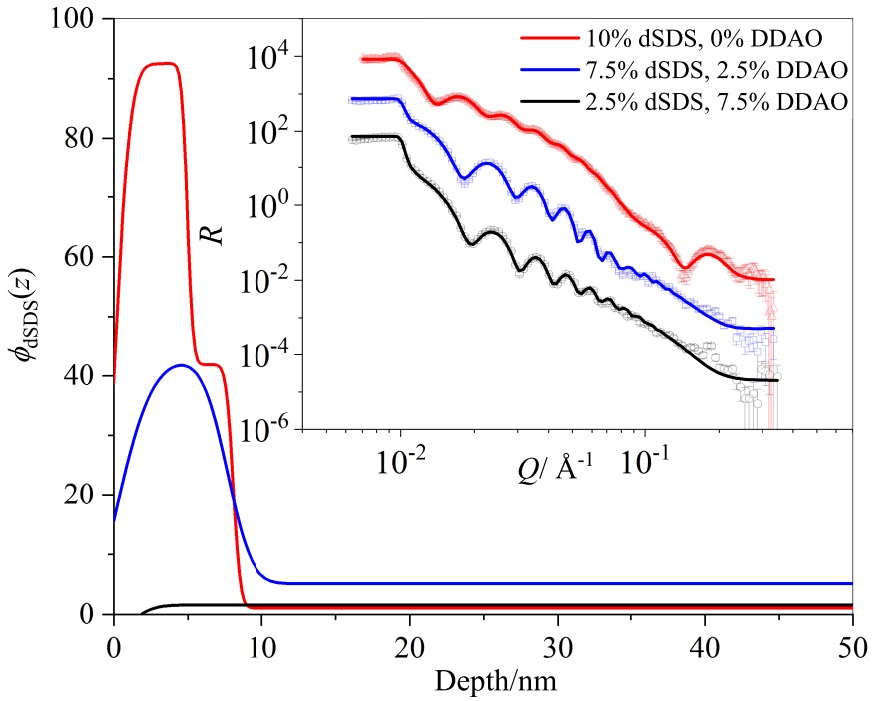

Figure 8.5: Volume fraction-depth profiles of dSDS in PVA films with 20 wt.% h-glycerol and a total surfactant loading of 10 wt.%, with varying ratios of dSDS and cmDDAO. Neutron reflectivity data and fits (offset for clarity) are shown in the inset.

be seen that when the films contain 2.5 % SDS and 7.5 % DDAO, glycerol is excluded from the surface. When the film contains a 7.5 wt.% SDS (and 2.5 wt.% DDAO), the glycerol distribution is even throughout the whole film. This suggests that the distribution of glycerol is linked to that of the anionic surfactant; when SDS segregation is sufficiently suppressed, exhibiting only a slight surface excess, glycerol segregation is not favoured.

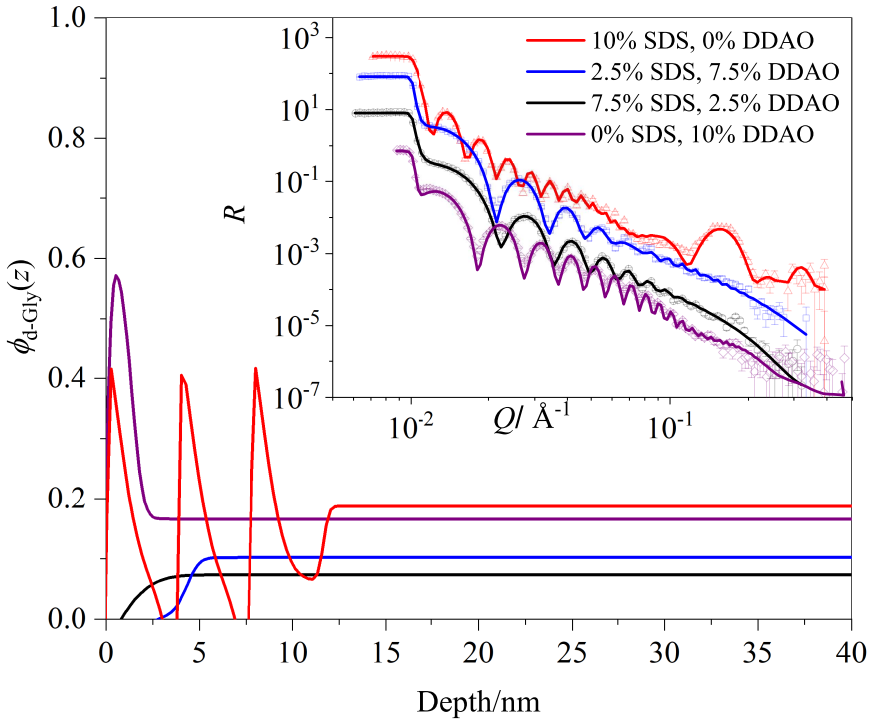

Figure 8.6: Volume fraction-depth profiles of d-glycerol in PVA films with 20 wt.% d-glycerol and a total surfactant loading of 10 wt.%, with varying ratios of SDS and DDAO. Neutron reflectivity data and fits (offset for clarity) are shown in the inset.

8.2.1.2 $C_{12}E_5$/DDAO

The second model system consists of DDAO and the non-ionic surfactant $C_{12}E_5$. $C_{12}E_5$ has been previously reported to show substantial surface and interfacial segregation, with the lengthscales of the enriched layers significantly greater than a monolayer.[168] The depth profile of 10 wt.% $C_{12}E_5$ in the absence of any additional additive is shown in red in Figure 8.7.

The impact of DDAO on the distribution of $dC_{12}E_5$ will first be assessed. It is clear from the depth profiles presented in Figure 8.7 that there is no enhancement of segregation of $dC_{12}E_5$ upon inclusion of cmDDAO. In fact, from comparison of f values in Table 8.4, it can be seen that there is a decrease in f upon incorporation 2.5 wt.% cmDDAO, and a further decrease in the presence of 7.5 wt.% cmDDAO.

As with the previous model system, it is worth confirming that this effect is a result of the incorporation of the secondary surfactant, rather than due to the changing dDDAO concentration alone. From an additional measurement on a film containing 2.5 wt.% $dC_{12}E_5$ as the only additive, f was found to have a value of 0.3 ± 0.1. The extremely low degree of $C_{12}E_5$ segregation in the film containing 2.5 wt.% $dC_{12}E_5$ and 7.5 wt.% DDAO ($f = 0.05$) means that this

effect can therefore be confidently attributed to the presence of the secondary surfactant.

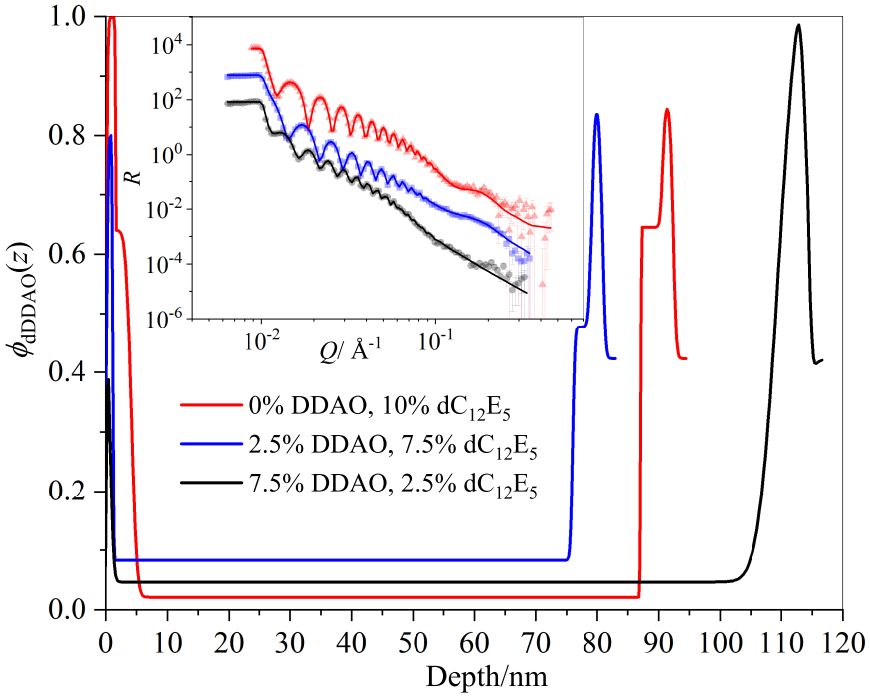

Figure 8.7: Volume fraction-depth profiles of $dC_{12}E_5$ in PVA films with a total surfactant loading of 10 wt.%, with varying ratios of $dC_{12}E_5$ and cmDDAO. Neutron reflectivity data and fits (offset for clarity) are shown in the inset.

Turning to the second contrast, the depth profiles of dDDAO in the presence of $cmC_{12}E_5$ are presented in Figure 8.8. Determined values for z^* and f are included in Table 8.5. In contrast to the previous model system (SDS/DDAO), $C_{12}E_5$ causes no enhancement of the segregation of dDDAO. Upon incorporation of 2.5 wt.% $C_{12}E_5$ the surface excess layer can still be seen to correspond to the thickness of a single monolayer. There is even a reduction in ϕ_{dDDAO} in this layer, which corresponds to a greater area per molecule occupying the surface in a monolayer (Chapter 6). When the concentration of $C_{12}E_5$ is increased further, the dDDAO surface excess disappears completely, and the depth profile comprises a uniform distribution of dDDAO throughout the entire film.

In Chapter 6, it was shown that varying the DDAO concentration had little effect on its volume fraction in the surface layer (and thus its molecular area in a monolayer). Therefore, variation in DDAO concentration alone cannot explain the reduction in ϕ_{dDDAO} in the film containing 7.5 wt.% dDDAO and 2.5 wt.% $C_{12}E_5$. A film containing 2 wt.% DDAO as the only additive was reported to have a surface excess (z^*) of 0.4 nm (Table 6.1) corresponding to an f value of 0.3. This confirms that the complete absence of a surface excess in the equivalent

mixed surfactant film is a result of the nonionic surfactant acting to suppress the segregation of the zwitterionic surfactant.

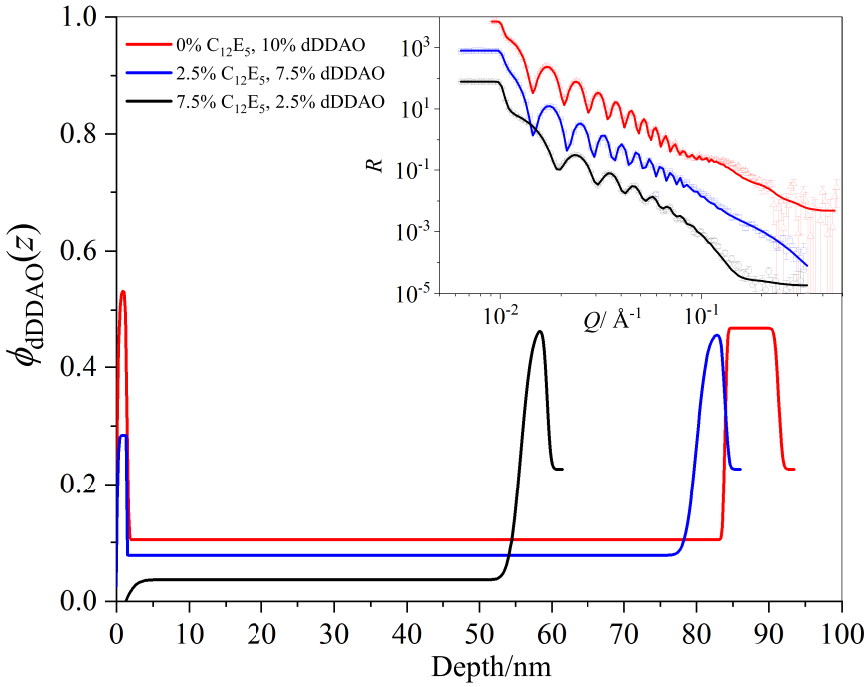

Figure 8.8: Volume fraction-depth profiles of dDDAO in PVA films with a total surfactant loading of 10 wt.%, with varying ratios of $cmC_{12}E_5$ and dDDAO. Neutron reflectivity data and fits (offset for clarity) are shown in the inset.

Table 8.4: Surface excess (z^*) and fraction of segregated surfactant (f) for binary and plasticised PVA films containing $dC_{12}E_5$ and cmDDAO.

	Binary		Plasticised	
	z^*/nm	f	z^*/nm	f
10 wt.% $dC_{12}E_5$	4.7 ± 0.1	0.7 ± 0.1	3.5 ± 0.1	0.5 ± 0.1
7.5 wt.% $dC_{12}E_5$, 2.5 wt.% hDDAO	1.6 ± 0.1	0.2 ± 0.05	0.96 ± 0.04	0.2 ± 0.05
2.5 wt.% $dC_{12}E_5$, 7.5 wt.% hDDAO	0.3 ± 0.1	0.05 ± 0.02	0.12 ± 0.03	0.05 ± 0.02

Table 8.5: Surface excess (z^*) and fraction of segregated surfactant (f) for binary and plasticised PVA films containing dDDAO and $cmC_{12}E_5$.

	Binary		Plasticised	
	z^*/nm	f	z^*/nm	f
10 wt.% dDDAO	0.5 ± 0.1	0.06 ± 0.01	0.6 ± 0.2	0.06 ± 0.01
7.5 wt.% dDDAO, 2.5 wt.% $hC_{12}E_5$	0.28 ± 0.08	0.04 ± 0.01	0.23 ± 0.07	0.05 ± 0.01
2.5 wt.% dDDAO, 7.5 wt.% $hC_{12}E_5$	0	0	0.08 ± 0.04	0.06 ± 0.01

To illustrate the distribution of the two surfactants in the non-plasticised film, a superposition of the depth profiles in films containing 7.5 wt.% dDDAO and 2.5 wt.% $dC_{12}E_5$ is shown in Fig. 8.9.

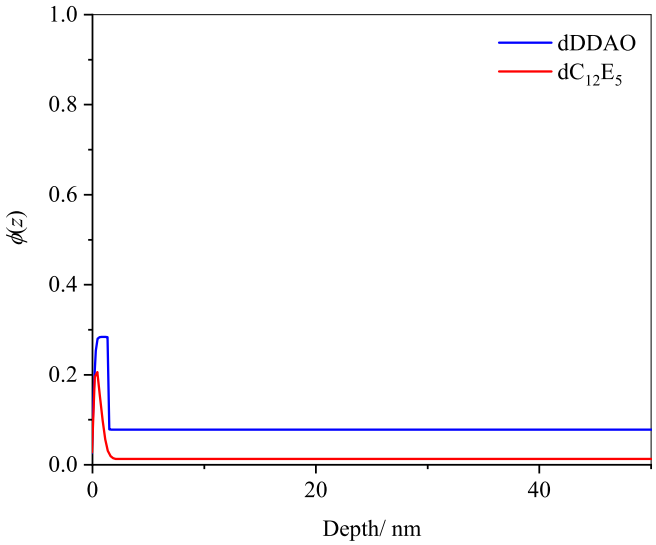

Figure 8.9: Superimposed volume fraction-depth profiles of dDDAO (7.5 wt.%) and $dC_{12}E_5$ (2.5 wt.%) in a non-plasticised PVA film.

It can been seen that the two surfactants segregate over approximately the same lengthscale. Additionally, it is clear that the volume fractions of DDAO and $C_{12}E_5$ in the surface layer do not account for the entire volume. This layer therefore consists of polymer enriched in surfactant, rather than a layer consisting exclusively of surfactant.

The distribution of DDAO and $C_{12}E_5$ in mixed-surfactant, plasticised films was subsequently assessed. The effect of DDAO incorporation on the distribution of $dC_{12}E_5$ will first be considered. In this case, determination of f is complicated by the interfacial segregation of the nonionic surfactant; the SLD of $dC_{12}E_5$ is close to that of the silicon oxide on the substrate, and so the two layers are difficult to resolve precisely in order to quantify an interfacial excess. This can be seen in the full concentration-depth profiles (Fig. 8.10). Therefore, to allow comparison, the reported f values only account for the fraction of surfactant comprising the surface excess (at the film-air interface). Considering both interfaces, the total fraction of segregated additive is, in reality, higher than these reported values. Here it can be seen that DDAO causes a substantial reduction in $dC_{12}E_5$ surface segregation. Indeed, in the film containing 2.5 wt.% $dC_{12}E_5$ and 7.5 wt.% cmDDAO, there is no surface excess at all, although an interfacial excess can be identified from the depth profile.

When assessing the effect of $C_{12}E_5$ incorporation on the distribution of dDDAO, a trend in f (Table 8.5) is much harder to distinguish in the plasticised films than in the non-plasticised films. However, from the profiles (Fig. 8.11), it can be seen that when the non-ionic surfactant is included, the concentration of dDDAO in

the surface layer decreases, as observed in the absence of glycerol.

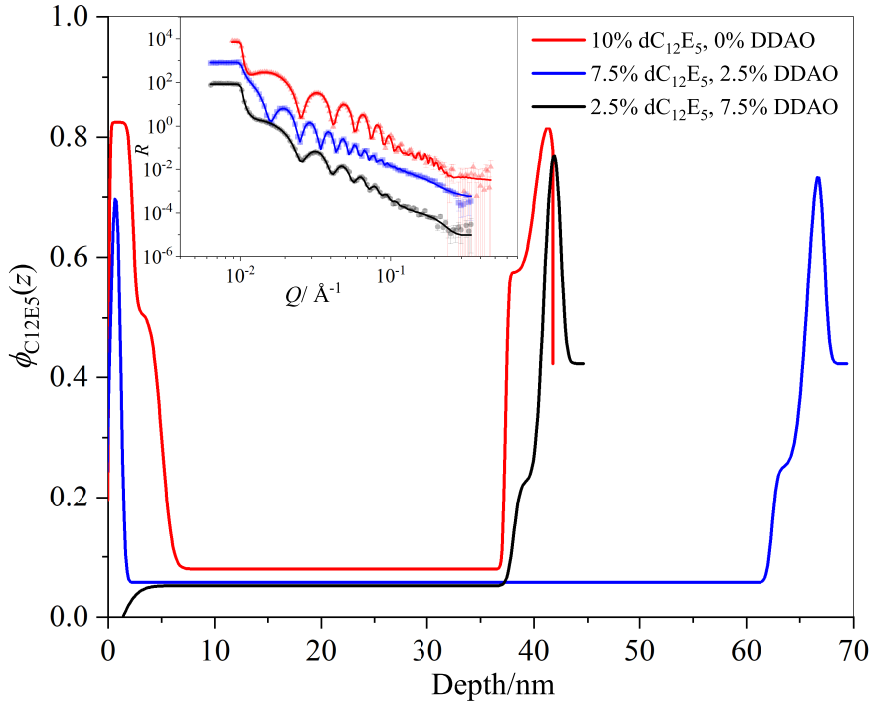

Figure 8.10: Volume fraction-depth profiles of $dC_{12}E_5$ in PVA films containing 20 wt.% h-glycerol and a total surfactant loading of 10 wt.%, with varying ratios of $dC_{12}E_5$ and cmDDAO. Neutron reflectivity data and fits (offset for clarity) are shown in the inset.

The effect of two interacting surfactant species on the segregation of the plasticiser will now be assessed. This is shown in Fig. 8.12.

Briddick et al.[168] previously identified a slight surface excess of d-glycerol in the presence of 10 wt.% $C_{12}E_5$, and, as previously discussed, a slight surface excess of d-glycerol is also observed in the presence of DDAO. However, in the presence of both surfactants, no segregation of glycerol can be identified. This suggests that as the segregation of both surfactants is reduced in this mixed surfactant system, glycerol segregation is also suppressed. Differences in the glycerol volume fraction in the bulk (and the substantially lower volume fraction than would correspond to 20 wt.%) are likely to be a result of the loss of glycerol from the film.

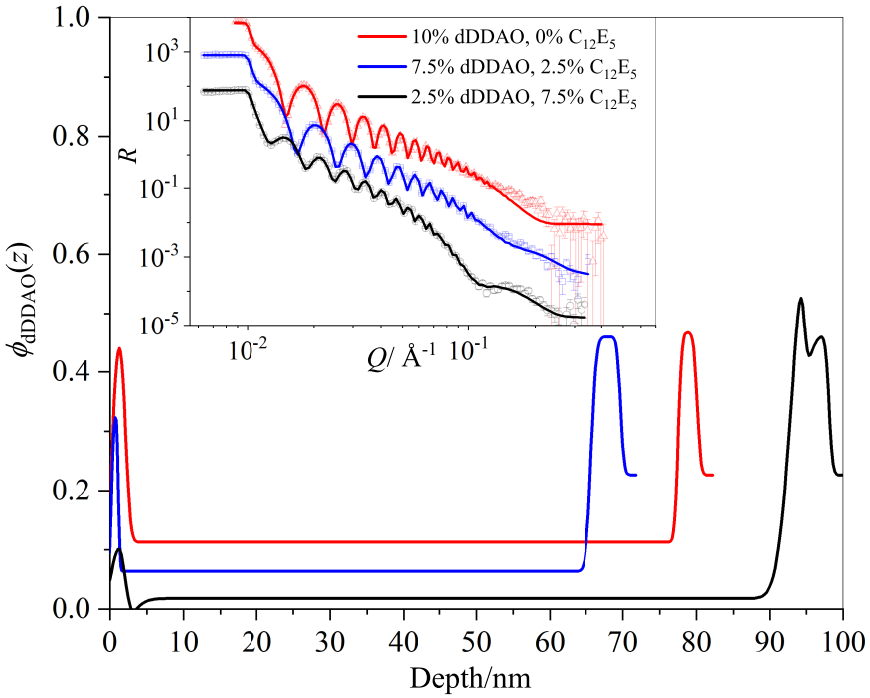

Figure 8.11: Volume fraction-depth profiles of dDDAO in PVA films with 20 wt.% h-glycerol and a total surfactant loading of 10 wt.%, with varying ratios of cm$C_{12}E_5$ and dDDAO. Neutron reflectivity data and fits (offset for clarity) are shown in the inset.

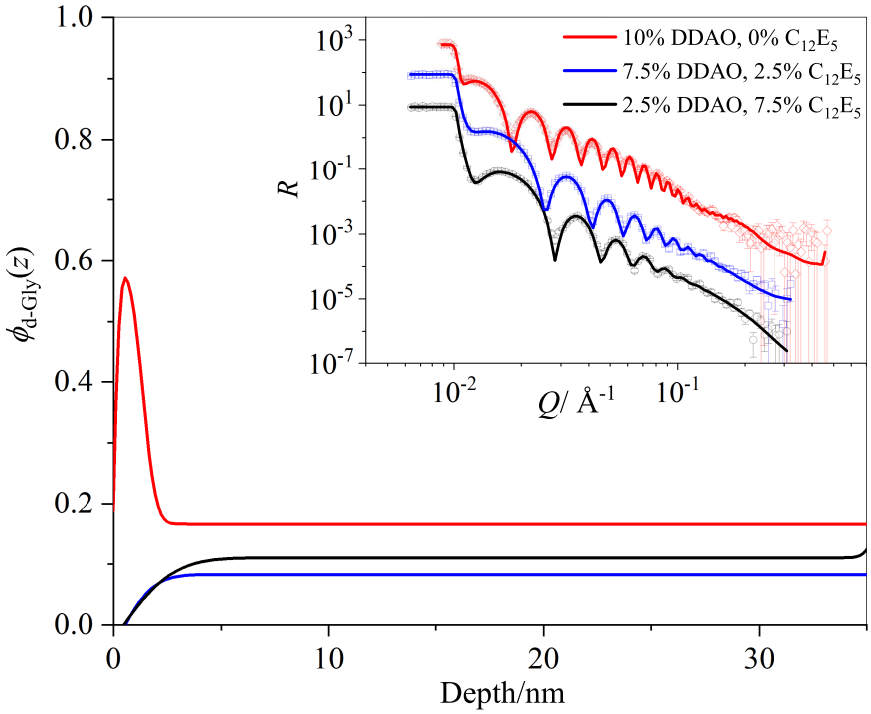

Figure 8.12: Volume fraction-depth profiles of d-glycerol in PVA films with 20 wt.% d-glycerol and a total surfactant loading of 10 wt.%, with varying ratios of $C_{12}E_5$ and DDAO. Neutron reflectivity data and fits (offset for clarity) are shown in the inset.

8.2.1.3 SDS/$C_{12}E_5$

In this final model system, films containing mixtures of SDS and $C_{12}E_5$ will be explored. First considering the effect of $C_{12}E_5$ inclusion on the distribution of dSDS in non-plasticised PVA, Figure 8.13 reveals a substantial suppression of SDS segregation in the presence of the nonionic surfactant. The values in Table 8.6 show that f decreases from 0.9 in the absence of $C_{12}E_5$, to 0.2 when there is a 1:3 ratio of dSDS to cm$C_{12}E_5$. To eliminate the possibility of this being attributable to differences in dSDS concentration, f for mixed surfactant systems was compared to those determined from binary dSDS/PVA films of the corresponding dSDS concentrations. The values of f of 0.8 ± 0.1 and 0.6 ± 0.1 for films containing 7.5 wt.% and 2.5 wt.% dSDS respectively, show that although the loading of the anionic surfactant itself does affect f, this is not to a great enough extent to account for the reduction of f to 0.6 ± 0.1 and 0.2 ± 0.1 for films containing 7.5 and 2.5 wt.% dSDS respectively, when total surfactant loading is made up to 10 wt.% with $C_{12}E_5$.

The effect of SDS on the distribution of $dC_{12}E_5$ shows a much less clear trend. Although the depth profiles in Figure 8.14 show an obvious decrease in the size of the surface excess upon SDS incorporation, the similar values for f (within the uncertainty of the measurements) show that this can be accounted for by the changing concentration of $dC_{12}E_5$ as the ratio between surfactants in the mixed system is varied.

Table 8.6: Surface excess (z^*) and fraction of segregated surfactant (f) for binary and plasticised PVA films containing dSDS and cm$C_{12}E_5$.

	Binary		Plasticised	
	z^*/nm	f	z^*/nm	f
10 wt.% dSDS	3.4 ± 0.1	0.3 ± 0.1	5.5 ± 0.1	0.9 ± 0.1
7.5 wt.% dSDS, 2.5 wt.% cm$C_{12}E_5$	2.81±0.08	0.6 ± 0.1	3.3 ± 0.1	0.8 ± 0.1
2.5 wt.% dSDS, 7.5 wt.% cm$C_{12}E_5$	1.4 ± 0.2	0.2 ± 0.05	0.3 ± 0.1	0.3 ± 0.1

Table 8.7: Surface excess (z^*) and fraction of segregated surfactant (f) for binary and plasticised PVA films containing $dC_{12}E_5$ and cmSDS.

	Binary		Plasticised	
	z^*/nm	f	z^*/nm	f
10 wt.% d-$C_{12}E_5$	4.7 ± 0.1	0.7 ± 0.1	3.5 ± 0.1	0.5 ± 0.1
7.5 wt.% $dC_{12}E_5$, 2.5 wt.% cmSDS	3.9 ± 0.1	0.5 ± 0.1	1.2 ± 0.1	0.4 ± 0.1
2.5 wt.% $dC_{12}E_5$, 7.5 wt.% cmSDS	1.3 ± 0.1	0.5 ± 0.1	1.2 ± 0.1	0.5 ± 0.1

As for the previous systems, the relative concentrations of the two surfactants can be assessed by superimposing their depth profiles. This is illustrated for a film containing 7.5 wt.% SDS and 2.5 wt.% $C_{12}E_5$ in Fig. 8.15.

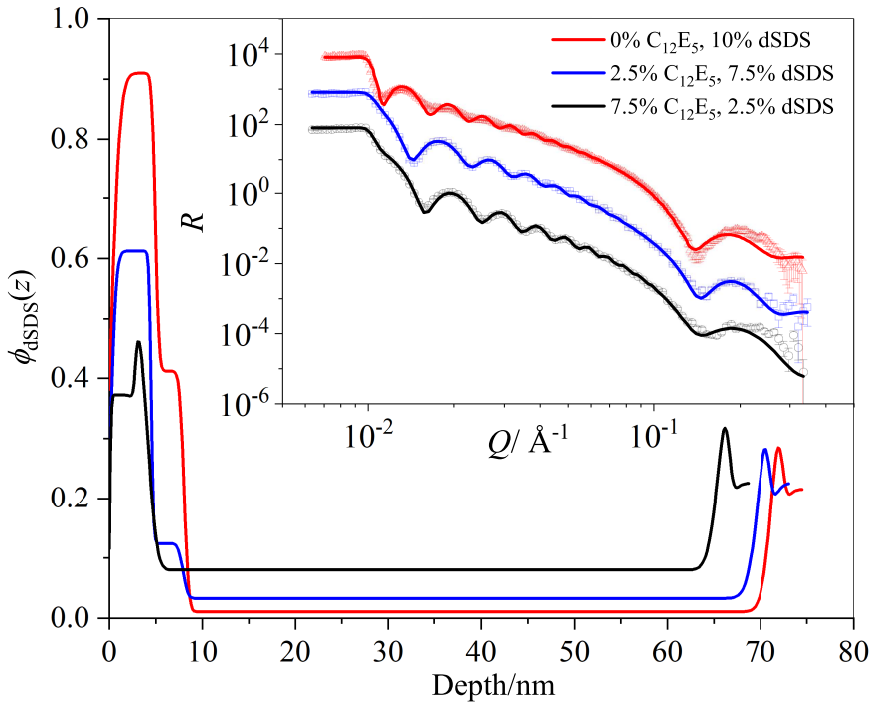

Figure 8.13: Volume fraction-depth profiles of dSDS in PVA films with a total surfactant loading of 10 wt.%, with varying ratios of cm$C_{12}E_5$ and dSDS. Neutron reflectivity data and fits (offset for clarity) are shown in the inset.

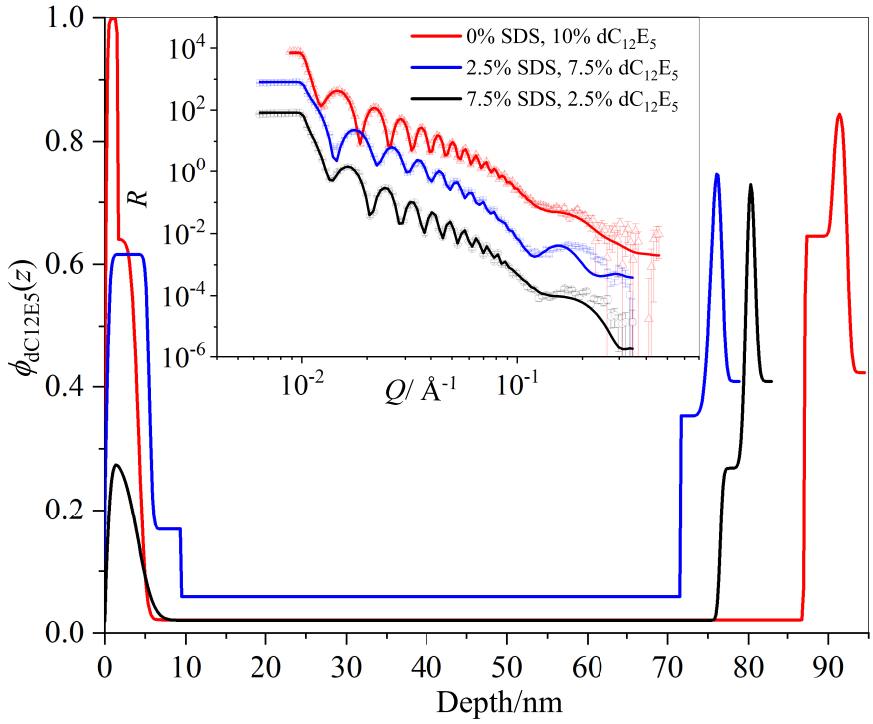

Figure 8.14: Volume fraction-depth profiles of $dC_{12}E_5$ in PVA films with a total surfactant loading of 10 wt.%, with varying ratios of $dC_{12}E_5$ and cmSDS. Neutron reflectivity data and fits (offset for clarity) are shown in the inset.

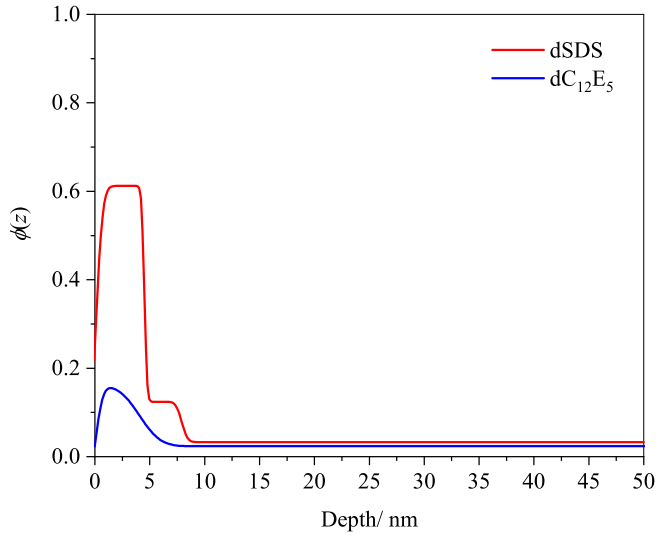

Figure 8.15: Superimposed volume fraction-depth profiles of dSDS (7.5 wt.%) and $dC_{12}E_5$ (2.5 wt.%) in non-plasticised PVA.

It can be seen that the $C_{12}E_5$ and SDS segregate over a similar lengthscale on the surface. Although it appears that the concentration of these surfactants in the surface layer do not give a total volume fraction of 1, in this case it is likely that the surface layer consists almost exclusively of surfactant.

The influence of glycerol on the surfactant segregation in this model system will now be considered. The depth profiles of dSDS in the plasticised, mixed surfactant films are shown in Figure 8.16. The values in Table 8.6 show that incorporation of $C_{12}E_5$ causes a suppression of the dSDS segregation, as observed for the non-plasticised films. In contrast to the non-plasticised films, however, the inclusion of SDS causes a substantial reduction in $dC_{12}E_5$ segregation in plasticised films (Fig. 8.17).

The effect of two surfactants on the distribution of d-glycerol will now be assessed. Concentration depth profiles of d-glycerol in films containing SDS and $C_{12}E_5$ are shown in Fig. 8.18. It can be seen that the reflectivity data contains a feature at high Q, analogous to that present in the data for the film containing 10 wt.% hSDS and 20 wt.% d-glycerol. As for the film containing SDS as the only surfactant, the reflectivity could be fitted using a multilayer model for the surface region, comprising thick regions of hydrogenated material separated by thin layers rich in deuterated glycerol.

However, as the concentration of SDS was decreased, and the concentration of $C_{12}E_5$ was increased, the distribution of glycerol throughout the film was found to be even. As found for the SDS/DDAO system, it appears that glycerol segregation is closely linked to the distribution of pure SDS.

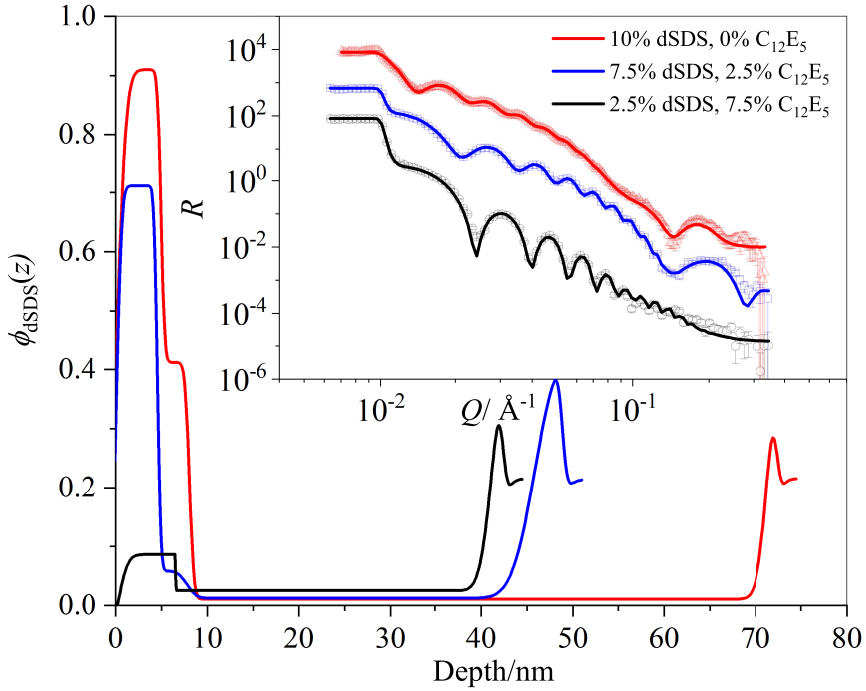

Figure 8.16: Volume fraction-depth profiles of dSDS in PVA films with 20 wt.% h-glycerol and a total surfactant loading of 10 wt.%, with varying ratios of $cmC_{12}E_5$ and dSDS. Neutron reflectivity data and fits (offset for clarity) are shown in the inset.

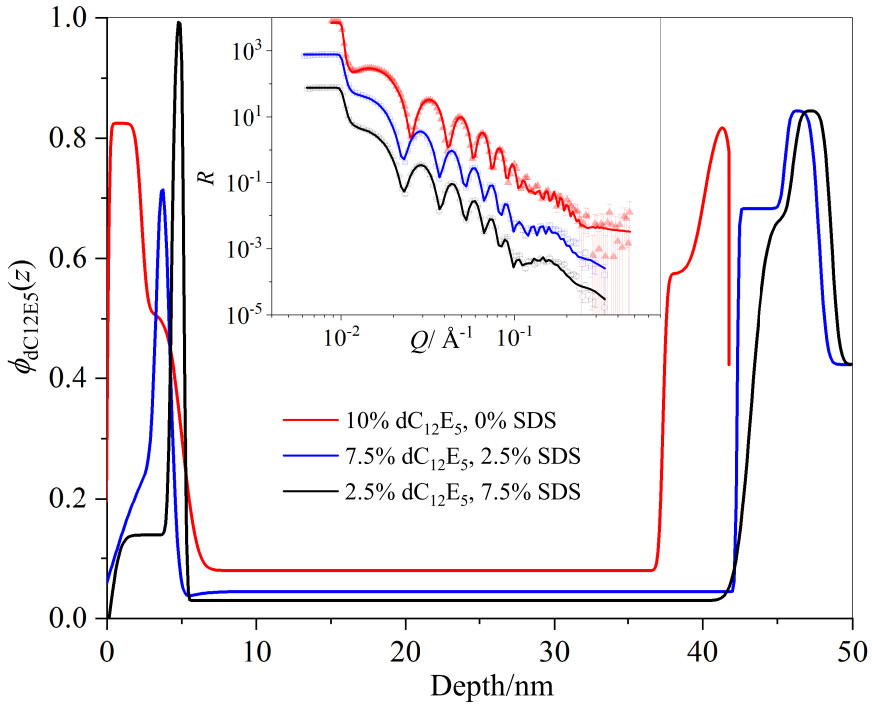

Figure 8.17: Volume fraction-depth profiles of $dC_{12}E_5$ in PVA films with 20 wt.% h-glycerol and a total surfactant loading of 10 wt.%, with varying ratios of $dC_{12}E_5$ and cmSDS. Neutron reflectivity data and fits (offset for clarity) are shown in the inset.

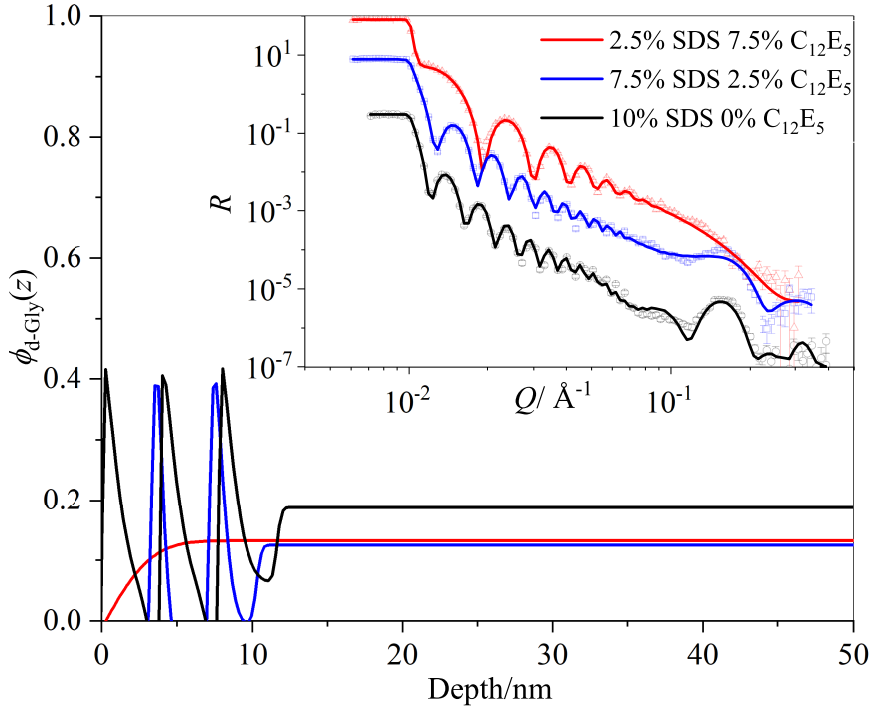

Figure 8.18: Volume fraction-depth profiles of d-glycerol in PVA films with 20 wt.% d-glycerol and a total surfactant loading of 10 wt.%, with varying ratios of $C_{12}E_5$ and SDS. Neutron reflectivity data and fits (offset for clarity) are shown in the inset.

8.2.2 Surface Tension of Mixed Surfactant Systems

In Chapter 5, surface tension experiments were used to provide insight into the role of the surface energy of film components in the segregation observed in spin-cast films. In this section, surface tension will be used to better understand the interactions between different surfactants in solution, and identify any synergism in surface adsorption, which could ultimately be related to the observed distribution of surfactants in PVA. In solution, mixtures of different surfactants can exhibit synergism or antagonism. Mixtures of charged and uncharged surfactants generally show synergism, due to the interaction between different headgroups. However, mixtures of surfactants with different tail groups, for example mixtures of hydrocarbon and perfluorinated chains, can show antagonism due to demixing, which results in the formation of two different kinds of micelles.[246] In this study, binary mixtures of surfactants with the same 12-carbon hydrocarbon chains will be considered, to reflect the polymer/surfactant systems studied in the solid state.

At the CMC, surfactants undergo cooperative self-association, forming micelles. In mixed surfactant systems, both ideal and non-ideal mixing contributions may occur. As the hydrophobic effect which drives micellisation is not specific to the headgroup of the surfactant, even in the absence of favourable interactions, combinatorial entropy favours the formation of randomly mixed aggregates. This

leads to the ideal mixing behaviour. However, electrostatic interactions between different head groups provide the base for the non-ideal component of mixing, and the interactions between surfactant molecules have been shown to be influenced by the nature of the headgroup.[240]

It is possible to use data from the surface tension behaviour of mixed surfactant solutions to evaluate the interaction between surfactant species in the mixed micelles. Mixtures of two surfactants can exhibit synergy (whereby the mixture shows greater surface activity than that attainable with the individual surfactants of the mixture at the same concentration) if they attract each other sufficiently.

According to the pseudophase separation model,[240] the CMC of a binary surfactant system is related to the CMCs of the individual surfactant species by Equation 8.1,

$$\frac{1}{\mathrm{CMC}} = \frac{y_1}{f_1\,\mathrm{CMC}_1} + \frac{(1-y_1)}{f_2\,\mathrm{CMC}_2}. \tag{8.1}$$

where y_i is the mole fraction of the ith component in the mixed surfactant system, and f_i is the activity coefficient of this component in micelles. The activity coefficients can be related to the interaction parameter, β.

$$\ln f_1 = (1-x_1)^2\beta \quad \text{and} \quad \ln f_2 = x_1^2\beta \tag{8.2}$$

Hua and Rosen[247] have shown that the condition for synergism due to mixed micelle formation and mixed monolayer formation is determined solely by the value of the relevant β parameters and the properties of the individual surfactants. A negative value for β indicates an attractive interaction between the two surfactants, whereas a positive value indicates overall repulsion. This parameter could therefore be used to assess interactions in solution, which are likely to be important in the structure of films spin-cast from aqueous solution.

In this section, in order to assess the effect of a second surfactant on the surface tension of a primary surfactant, the concentration of the second species is kept constant while the surface tension of a broad range of concentrations of the first surfactant is measured. This enables determination of the concentration of both surfactant species at which micellisation occurs, and permits the effect of one surfactant on the surface excess of another to be identified in some systems.

8.2.2.1 SDS/DDAO

The surface tension behaviour of mixed SDS/DDAO solutions will first be considered. Surface tension as a function of DDAO concentration in the presence of

different (fixed) SDS concentrations is shown in Fig. 8.19. Every SDS concentration shown is below the CMC of the pure SDS.

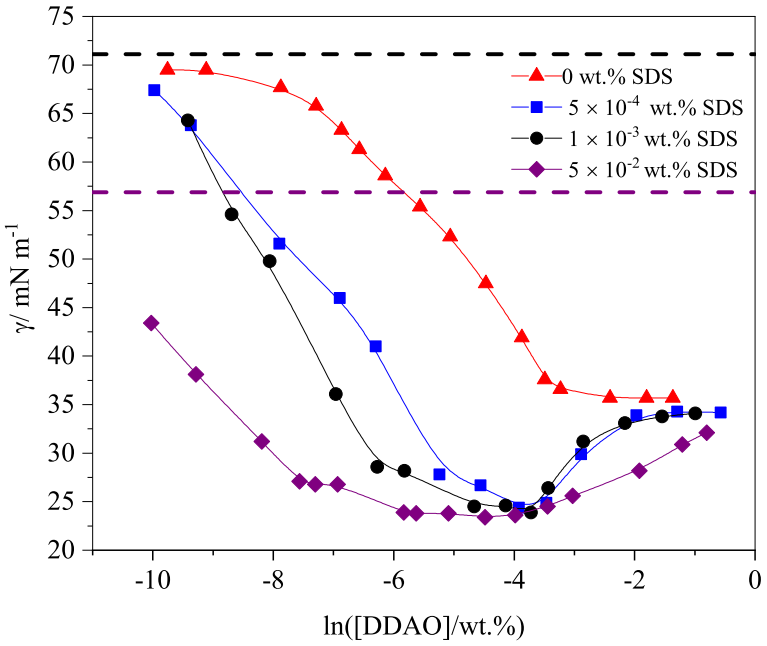

Figure 8.19: Effect of SDS incorporation on the aqueous surface tension behaviour of DDAO. Lines are a guide for the eye. Dashed black and purple lines represent the surface tension of 1 $\times 10^{-3}$ and 5×10^{-2} wt.% SDS solutions respectively, in the absence of DDAO.

In the presence of SDS it can be seen that there is a significant decrease in the surface tension of the solutions at each DDAO concentration, compared to that of the pure DDAO solutions, indicating a strong synergistic effect. The CMC also becomes less clearly identifiable from the break point in the surface tension plot, although appears to shift to lower concentration with increasing SDS concentration.

Goloub et al.[248] have studied the effect of SDS on the surface tension of DDAO solutions buffered to pH 8 (where almost all surfactant molecules are neutral), similarly observing a decrease in surface tension of DDAO solutions and a decrease in DDAO concentration at the CMC in the presence of SDS. They obtained a value for the β parameter of -7.0. This large, negative value indicates strong attractive interactions between the surfactants.

In this work, in order to accurately represent the solutions used to spin-cast the polymer/surfactant films, surfactant solutions are not buffered. Based on the pK_m (intrinsic proton dissociation constant of the micelle) of DDAO (5.89, Chapter 6), it is likely that, in the absence of additional solutes, the surfactant would be overwhelmingly in the neutral, unprotonated form. However, zwitterionic surfactants, such as DDAO, may exhibit specific interactions in mixtures with either

cationic or anionic surfactants, due to their capability to either accept or donate the proton on the head group. This results in the formation of ion pairs with an oppositely charged ionic surfactant. In the protonated form, DDAO would be strongly stabilised by binding to the anionic surfactant. This means that, in this system, the deprotonation of DDAO requires much higher pH than that required to deprotonate pure DDAO, and thus the DDAO is no longer exclusively in the unprotonated state. The formation of strong ion pairs, and presence of SDS in the mixed micelles, can therefore rationalise the strong synergistic reduction in CMC for the mixed DDAO/SDS system.

Interestingly, in the presence of SDS, at higher DDAO concentrations there is an increase in the surface tension, approaching the limiting surface tension of pure DDAO solutions. Although this was not apparent in the work of Goloub et al.,[248] this is likely due to the narrower range of DDAO concentrations used in their study. This observation suggests that at high DDAO concentrations (above the CMC), the surfactant monolayer on the surface comprises mostly DDAO. However, given that the formation of ion pairs with SDS is favourable, this is unexpected. One possibility is that the surface of the solution was not at equilibrium when the surface tension measurement was made, and some replacement of DDAO with SDS occurs over longer timescales ($\sim$ minutes). However, this is unlikely, given that at higher concentration molecules have less far to travel in order to approximate their equilibrium formation. Another possibility, therefore, is that the composition of the adsorbed layer at high concentrations is different from that at low concentrations, as micelles can provide an environment that can sequester a surface active component from the solution surface. If micelles are able to lower their free energy by solubilising a surface active component, this can compensate the cost in increasing the surface tension. Indeed, this effect is observed in the surface tension plot of SDS contaminated with dodecanol (Chapter 5).

It is worth considering the limitation in taking static surface tension measurements, using the du Noüy ring method, and it should therefore also be noted that the surface tension measurements at lower concentrations may also not represent a surface at equilibrium. However, the reduction from the surface tension of pure water to $<$30 mN m^{-1} nevertheless indicates very efficient surfactant adsorption. Although dynamic surface tension measurements would be required to fully understand the properties of the surface, in the context of this thesis, these measurements are significant; during the spin-casting process, solution is applied to the silicon block which is stationary for $<$ 30 s prior to spinning. As a result, these (potentially) non-equilibrium surface tension measurements are rep-

resentative of the solution surface during film preparation. This is particularly significant given that the concentrations of surfactant in solutions used to spin cast the films are above the CMC.

It is possible to use the Gibbs adsorption equation to assess the effect of SDS incorporation on the surface excess of DDAO. These values are included in Table 8.8. Typical fitting regions from which values for the surface excess are obtained are included in Fig. 8.20. Quoted uncertainties are taken from the uncertainty in the gradient of this fit.

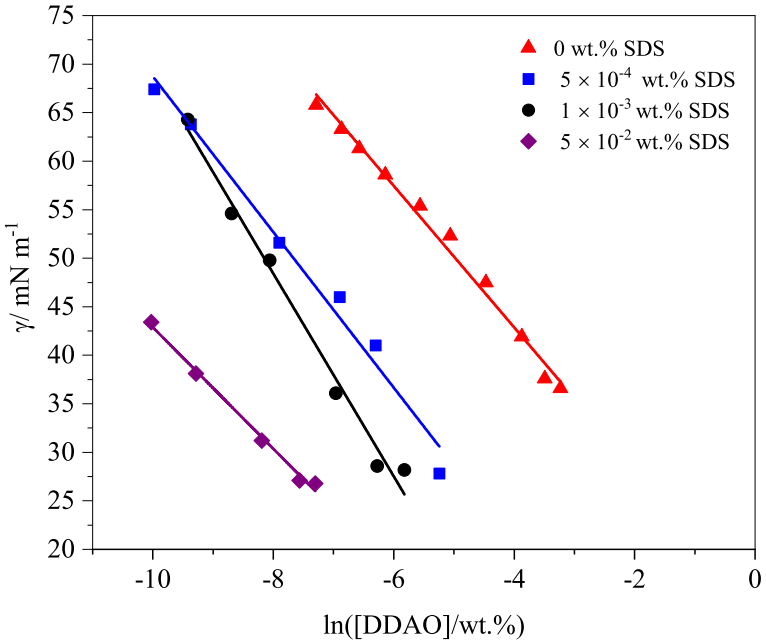

Figure 8.20: Gibbs plots used to determine the maximum surface excess of DDAO in the presence of different concentrations of SDS.

Table 8.8: Limiting values for the surface excess of DDAO in the presence of different concentrations of SDS.

[SDS]/wt.%	$\Gamma/10^{-6}$ mol m^{-2}
0	2.90 ± 0.09
5×10^{-4}	2.9 ± 0.1
1×10^{-3}	4.0 ± 0.3
5×10^{-2}	2.65 ± 0.04

Despite the general shift of the curve to lower surface tensions, the surface excess of DDAO is fairly consistent at each SDS loading, with the exception of 1×10^{-3} wt.%. This suggests that the presence of SDS has little impact on the maximum packing density of DDAO.

The effect of DDAO on the surface tension of SDS solutions is shown in Fig. 8.21. It should be noted that each DDAO concentration studied is lower than

the CMC of pure DDAO. By fixing the concentration of DDAO and assessing the change in surface tension with SDS concentration, a greater range of concentrations of the two species can be probed. This shows very different behaviour to the reverse case (Fig. 8.19). Here a strong synergistic effect in surfactant adsorption is immediately apparent, as at all concentrations of DDAO, the surface tension of the SDS solutions is dramatically reduced to values lower than the surface tension achieved by the pure SDS solution above the CMC. At each DDAO concentration, the surface tension is much lower than would be expected should each surfactant contribute to the reduction in surface tension to the same extent as in the single component solutions. At the lowest DDAO concentration (7×10^{-4} wt.%), the surface tensions of the mixed solutions are still much lower than at the CMC of this surfactant.

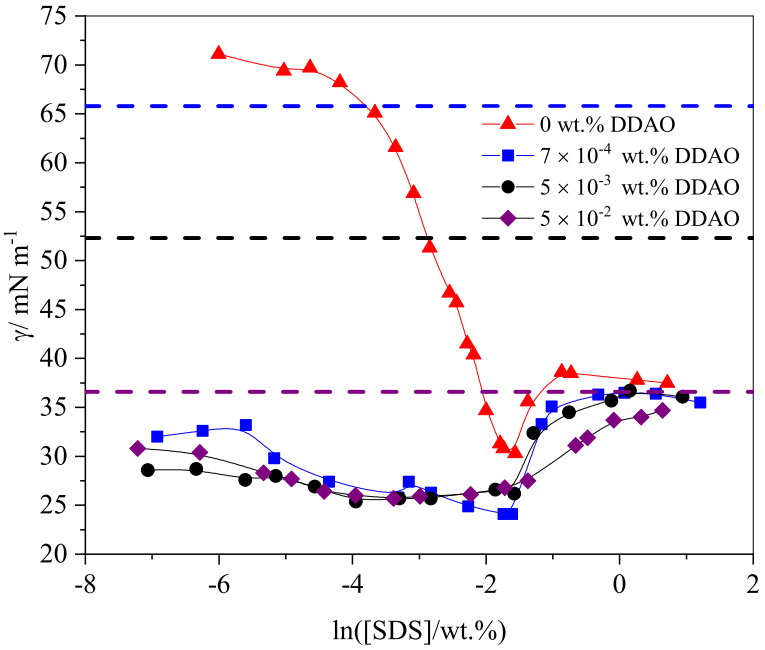

Figure 8.21: Effect of DDAO incorporation on the aqueous surface tension behaviour of SDS. Lines are a guide for the eye. Dashed blue, black and purple lines represent the surface tension of solutions of 7×10^{-4}, 5×10^{-3} and 5×10^{-2} wt.% DDAO solutions respectively, in the absence of SDS.

As previously stated, it is likely that the interaction between the headgroups, and formation of ion pairs, are responsible for this surface tension reduction, apparent even at very low total surfactant concentration. The significant contamination of the SDS with dodecanol should perhaps also be acknowledged here. It is plausible that the low surface tension apparent at low loadings of all surfactant is related to the adsorption of both surfactants and the dodecanol. However, the composition of the surface cannot be determined from surface tension measurements alone. Nevertheless, in the context of this project, the surface tension

behaviour at high surfactant concentrations is more relevant.

As observed in Fig. 8.19, at concentrations above the CMC of pure SDS solutions, the surface tension of mixed solutions can be seen to increase with SDS concentration, approaching the value of the surface tension of pure SDS solutions. Again, this suggests that when [SDS] is substantially greater than [DDAO], the surface monolayer is dominated by SDS. As this would suggest that ion pair formation between the two species is more important in the bulk than on the surface monolayer, it is reasonable to suggest that, again, the surface adsorbed DDAO is sequestered into the micelles.

8.2.2.2 $C_{12}E_5$/DDAO

The surface tension behaviour of the mixed $C_{12}E_5$/DDAO system will now be considered. The effect of $C_{12}E_5$ on the surface tension of DDAO solutions is shown in Fig. 8.22. Here, 4×10^{-3} wt.% is a higher concentration of $C_{12}E_5$ than its CMC, but all other $C_{12}E_5$ concentrations are below the CMC.

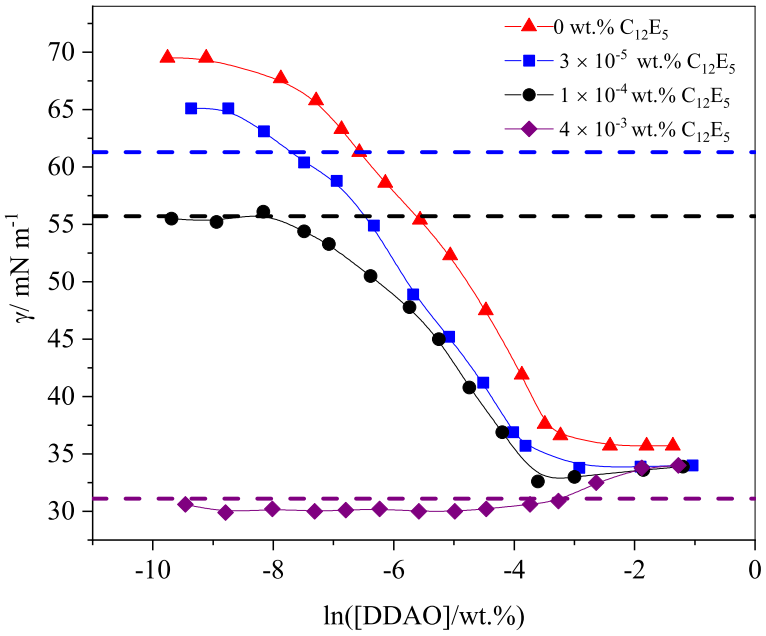

Figure 8.22: Effect of $C_{12}E_5$ incorporation on the aqueous surface tension behaviour of DDAO. Lines are a guide for the eye. Dashed blue, black and purple lines represent the surface tension of of 3 $\times10^{-5}$, 1 $\times10^{-4}$ and 4×10^{-3} wt.% $C_{12}E_5$ solutions respectively, in the absence of DDAO.

It can be seen that in the presence of 3×10^{-5} and 1×10^{-4} wt.% $C_{12}E_5$, there is a decrease in the surface tension of the mixed solutions throughout the DDAO concentration range, up to the CMC. The surface tension above the CMC is then only slightly lower in the presence of $C_{12}E_5$. A slight decrease in the CMC can also be identified. In this case, there is no obvious synergism, as the

reduction in surface tension of water at most DDAO concentrations, seems to be close to a linear addition of the reduction of surface tension achieved by each solute individually. On close inspection, the surface tension of the mixed systems is actually higher than would be expected should each solute contribute to the same extent to the reduction in surface tension as in their single-solute solutions. This antagonism in surfactant adsorption is likely to be a result of the weaker attraction between the headgroups of the non-ionic and zwitterionic surfactant (which is mostly uncharged at natural pH).

In the presence of 4×10^{-3} wt.% $C_{12}E_5$, the surface tension of the mixed solutions is consistently low ($\sim$30 mN m^{-1}) throughout the concentration range of DDAO below the CMC. This concentration of $C_{12}E_5$ is above its CMC in the absence of additional solutes, and therefore the surface appears to be saturated with $C_{12}E_5$. Above the CMC of the mixed solutions, however, there is a slight increase in surface tension, approaching the value of the surface tension of solutions of high DDAO concentration in the absence of additional solute. As for the previous system discussed, this could be a result of DDAO exclusively occupying the surface at high [DDAO], which is particularly likely when DDAO concentration is high enough that these aggregates dominate in the bulk, solubilising any $C_{12}E_5$ that would be on the surface.

Goloub at al.[248] probed the effect of DDAO on the surface tension of $C_{12}E_6$ solutions. Despite the slight change in headgroup on the nonionic surfactant (with $C_{12}E_6$ possessing one extra -CH_2CH_2O group), they report very similar behaviour to that presented here, with a slight decrease in the CMC of $C_{12}E_5$ with DDAO concentration. At pH 8, they determined the interaction parameter, β, of the two surfactants to be -1.0. The negative value is indicative of attractive interactions between the surfactants, although this interaction is weaker than that between SDS and DDAO.

The change of surfactant surface excess upon incorporation of a second surfactant can be identified using the Gibbs adsorption equation. The effect of $C_{12}E_5$ concentration on the surface excess of DDAO is shown in Table 8.9. From this, it can be seen that although the $C_{12}E_5$ causes a reduction in surface tension, it causes no significant change in the surface excess of the DDAO.

The effect of DDAO (at concentrations below its CMC) on the surface tension of $C_{12}E_5$ is shown in Fig. 8.23. Here, behaviour is very similar to that shown in Fig. 8.22, with a decrease in surface tension with DDAO concentration, a slight decrease in slope of the linear region, and a decrease in the CMC of $C_{12}E_5$. In this case, it can be seen that there is a greater reduction in surface tension than that attainable with the two surfactants in the mixture individually, indicative

Table 8.9: Limiting values for the surface excess of DDAO in the presence of different concentrations of $C_{12}E_5$.

$[C_{12}E_5]$/wt.%	$\Gamma/10^{-6}$ mol m^{-2}
0	2.90 ± 0.09
3×10^{-5}	2.9 ± 0.1
1×10^{-4}	2.7 ± 0.1

of synergy between the additives. This is in accordance with Rosen,[249] who observed that zwitterionic surfactants with no net formal charge show only weak interactions with non-ionic surfactants, although when the zwitterionic species is capable of forming a species with a net charge, the interaction may become strong enough for the system to exhibit synergy at neutral pH.

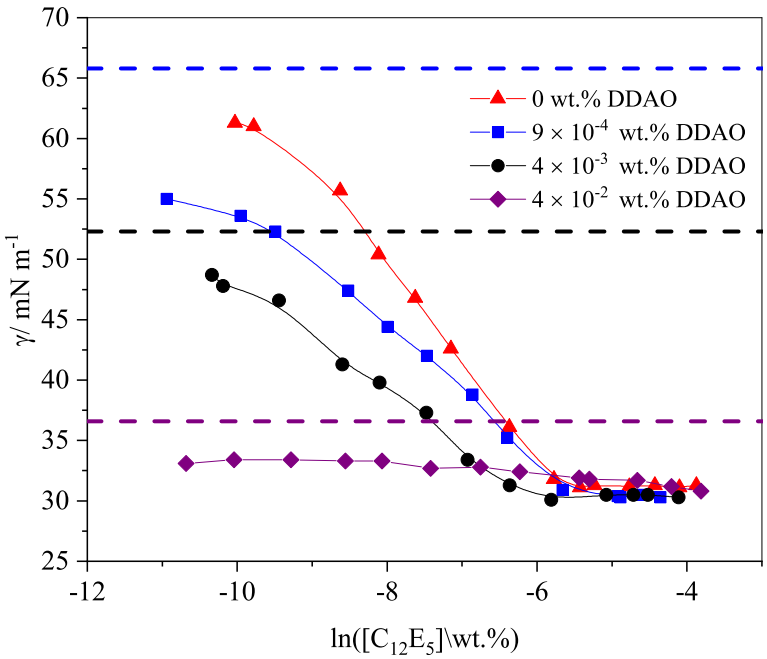

Figure 8.23: Effect of DDAO incorporation on the aqueous surface tension behaviour of $C_{12}E_5$. Lines are a guide for the eye. Dashed blue, black and purple lines represent the surface tension of solutions of 9×10^{-4}, 4×10^{-3} and 4×10^{-2} wt.% DDAO solutions respectively, in the absence of $C_{12}E_5$.

The change in $C_{12}E_5$ surface excess, calculated using the Gibbs adsorption equation, with DDAO concentration is shown in Table 8.10. This shows that in this $C_{12}E_5$ concentration range, DDAO inclusion reduces $\Gamma_{C_{12}E_5}$ as a result of the co-adsorption of the two surfactants in the monolayer.

A β parameter of -1.0 for the interaction of DDAO with $C_{12}E_6$ at pH 8 has been previously reported.[248] This suggests a favourable interaction between the two surfactants. Assuming that at the natural pH measured, DDAO is exclusively in the nonionic (unprotonated) state, and the presence of an additional ethoxy

Table 8.10: Limiting values for the surface excess of $C_{12}E_5$ in the presence of different concentrations of DDAO.

[DDAO]/wt.%	$\Gamma/10^{-6}$ mol m^{-2}
0	3.16 ± 0.06
9×10^{-4}	2.25 ± 0.06
4×10^{-3}	1.98 ± 0.09

group in $C_{12}E_6$ has little effect on the interactions with DDAO, it is likely that the interactions in this system are also attractive.

8.2.2.3 SDS/$C_{12}E_5$

Finally, the surface tension of the mixed SDS/$C_{12}E_5$ system will be assessed. The effect of incorporating various concentrations of $C_{12}E_5$ on the surface tension of SDS solutions is shown in Fig. 8.24. Here, a decrease in surface tension throughout the whole $C_{12}E_5$ concentration range can be identified, although the shape of the curve is similar for all SDS concentrations, with a clear CMC exhibited. Comparing the surface tension of the single component solutions, to the values obtained in the mixed solutions suggests that there is no large synergistic effect in the surface tension reduction. As for the previous model system, when the concentration of $C_{12}E_5$ is greater than its CMC in the single component solution, the surface tension is dominated by its adsorption to the surface at low [SDS]. However, a gradual increase in the surface tension with [SDS] suggests the co-adsorption of both species. Again this is likely to be a result of the more surface active component being sequestered by micelles above the CMC.

The effect of incorporating various concentrations of SDS on the surface tension of $C_{12}E_5$ solutions is shown in Fig. 8.25. Upon SDS incorporation there is a slight decrease in the surface tension of the $C_{12}E_5$ solutions throughout the concentration range below the CMC, although this reduction is somewhat less than would be observed should the SDS contribute as much to the surface tension reduction as in solutions with SDS as the only additive. In addition, the CMC can be observed to shift slightly to lower concentrations.

These results show a similar trend to that observed by Goloub et al.[248] in the case of $C_{12}E_6$ in the presence of SDS and additional salt. However, in contrast to their work, although the values of surface tension above the CMC are unchanged from pure $C_{12}E_5$ upon addition of 8×10^{-4} and 6×10^{-3} wt.% SDS, when 5×10^{-2} wt.% SDS is incorporated, the surface tension above the CMC is slightly higher.

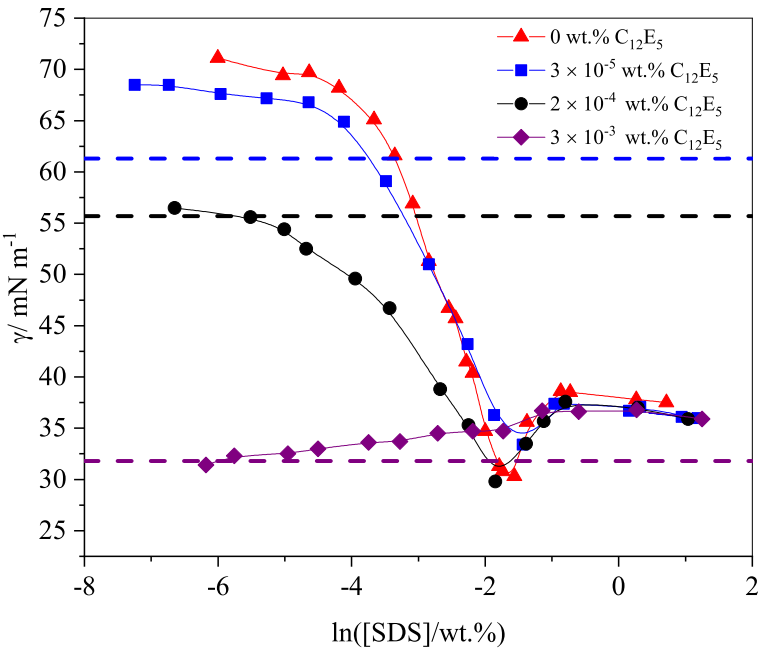

Figure 8.24: Effect of $C_{12}E_5$ incorporation on the aqueous surface tension behaviour of SDS. Lines are a guide for the eye. Dashed blue, black and purple lines represent the surface tension of of 3 $\times 10^{-5}$, 2×10^{-4} and 3×10^{-3} wt.% $C_{12}E_5$ solutions respectively, in the absence of SDS.

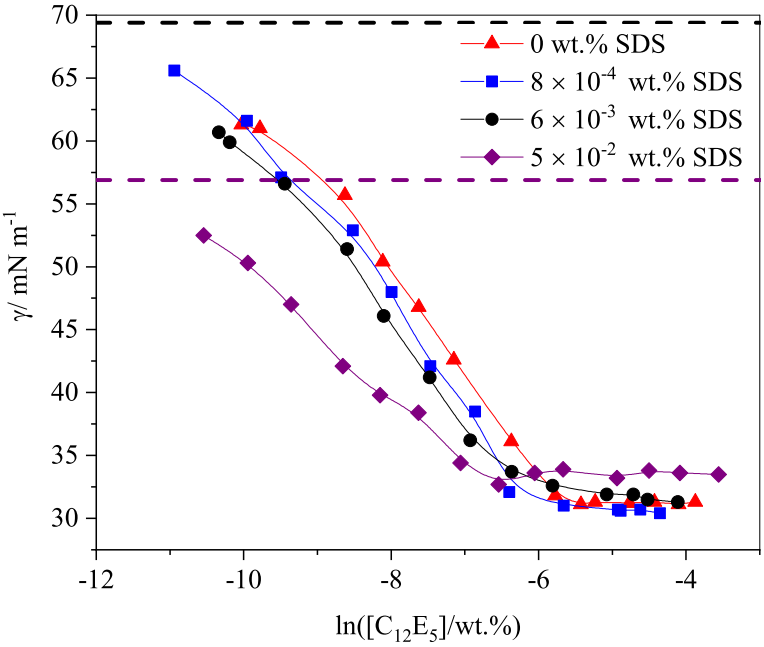

Figure 8.25: Effect of SDS incorporation on the aqueous surface tension behaviour of $C_{12}E_5$. Lines are a guide for the eye. Dashed black and purple lines represent the surface tension of solutions of 6×10^{-3}, and 5×10^{-2} wt.% SDS solutions respectively, in the absence of $C_{12}E_5$.

Goloub et al.[248] reported β parameters for the $C_{12}E_5$/SDS system in the presence of different electrolytes, ranging from $\beta = -3.4$ for 0.1 M NaCl to $\beta = -4.3$ for 1M CsCl solution. These negative values show that the net interactions in the mixed micelles are attractive, despite synergy between the two components not being easily identifiable from Fig. 8.24.

As for the previous model systems, the Gibbs adsorption equation can be used to assess the effect of $C_{12}E_5$ on the surface excess of SDS, and vice versa (Tables 8.11 and 8.12). It can be seen that the surface excess of both surfactants decreases in the mixed system, indicating the co-adsorption of the two species in the surface monolayer.

Table 8.11: Limiting values for the surface excess of $C_{12}E_5$ in the presence of different concentrations of SDS.

[SDS]/wt.%	$\Gamma/10^{-6}$ mol m^{-2}
0	3.16 ± 0.06
8×10^{-4}	3.2 ± 0.1
6×10^{-3}	3.0 ± 0.1
5×10^{-2}	2.10 ± 0.07

Table 8.12: Limiting values for the surface excess of SDS in the presence of different concentrations of $C_{12}E_5$.

[$C_{12}E_5$]/wt.%	$\Gamma/10^{-6}$ mol m^{-2}
0	3.8 ± 0.1
3×10^{-5}	2.60 ± 0.1
2×10^{-4}	1.9 ± 0.1

8.3 Discussion

8.3.1 Surfactant Distribution in Multiple-Component Systems

The segregation behaviour of the mixed surfactant systems studied using neutron reflectivity can be summarised as follows:

1. DDAO/SDS: In both non-plasticised and plasticised films, DDAO strongly suppresses the segregation of SDS, while SDS promotes the segregation of DDAO.

2. $C_{12}E_5$/DDAO: DDAO significantly suppresses $C_{12}E_5$ segregation and $C_{12}E_5$ suppresses DDAO segregation in non-plasticised films. In the presence of glycerol, DDAO suppresses $C_{12}E_5$ segregation, although $C_{12}E_5$ has little effect on DDAO segregation.

3. SDS/$C_{12}E_5$: In non-plasticised and plasticised films containing SDS and $C_{12}E_5$, segregation of both surfactants is reduced compared to films containing a single surfactant.

In model systems containing a single surfactant, segregation behaviour was explained and interpreted by considering the surface energy of film components as well as their compatibility with the host polymer. Interactions between plasticiser, polymer and surfactant have also been shown to be important in influencing surfactant distribution. Here these arguments will be extended to the more complex systems in an effort to rationalise the observed depth profiles. Three factors that should therefore be considered are the order of compatibilities with PVA, the order of surface tensions and any possible interactions between additives. To summarise briefly:

Most compatible DDAO > $C_{12}E_5$ > SDS **Least compatible**

Highest surface tension SDS > DDAO > $C_{12}E_5$ **Lowest surface tension**

8.3.1.1 SDS/DDAO

The SDS/DDAO system will first be considered. When DDAO is the sole additive in a film, the formation of a single monolayer on the surface was attributed to a lowering of the free energy of the system, but the even distribution of the remaining surfactant revealed its high compatibility with PVA. As SDS has a higher surface tension than DDAO, when considering the components individually, the inclusion of SDS presents no further driving force for DDAO to segregate. With the lower aqueous surface tension, there is a greater preference for DDAO to occupy the surface, than SDS. It is therefore plausible that this effect can be, at least in part, responsible for the suppressed segregation of SDS, compared to its behaviour as the only surfactant in films.

Incompatibility of SDS with PVA has been identified as the main factor responsible for its extensive segregation (Chapter 4). The significant reduction in f in the presence of DDAO therefore suggests some increase in SDS compatibility as a result of interaction with the second surfactant. One possibility is that the interactions between the headgroups of the two surfactants lead to the formation

of structures that can localise more favourably within the amorphous regions of polymer matrix. This potential favourable interaction between surfactants could also play a role in the enhanced segregation of DDAO, and its presence in a thick surface excess layer, rich in both surfactants.

Another contributing factor that should not be neglected is the entropy of mixing. While SDS is extremely incompatible with PVA, DDAO is very compatible with the polymer. Segregation of a single surfactant species on the film surface would be entropically unfavourable, although with two surfactants comprising the surface excess, the entropy of mixing increases, decreasing the free energy of the system. This mixing necessitates an increase in the segregation of DDAO, with the layer enriched in this surfactant expanding from a monolayer (in the single surfactant film) to the thickness of multiple surfactant molecules.

There are some significant differences observed in the surfactant segregation in this system when experiments were repeated in the presence of glycerol. First, when the ratio of dDDAO to SDS is 3:1, the thickness of the surface excess layer corresponds to a monolayer, suggesting very little influence of SDS on the segregation of dDDAO. From the depth profile of the other contrast for this film (ratio of DDAO to dSDS is 3:1) no segregation of SDS is observed at all. This supports the argument that the lower aqueous surface tension of DDAO leads to its occupation of the surface instead of SDS, reducing segregation of the latter surfactant. This also again implies that interactions between the two surfactant species promote compatibility of SDS with the matrix. In Chapter 4, it was suggested that the enhancement of the surface excess of SDS in the presence of glycerol is thermodynamically driven. As glycerol segregation only occurs when the SDS:DDAO ratio is high, it is apparent that glycerol segregation is closely linked to the anionic surfactant, and thus DDAO also suppresses glycerol segregation in this mixed system.

8.3.1.2 $C_{12}E_5$/DDAO

To interpret the observed depth profiles in the model system comprising $C_{12}E_5$ and DDAO, surface energy arguments should again be considered. In this case, $C_{12}E_5$ has the lower aqueous surface tension and so has a greater preference to occupy the surface than DDAO. This can explain the change in distribution of dDDAO upon $C_{12}E_5$ incorporation to the film. At a 3:1 ratio of dDDAO:$C_{12}E_5$, the significant decrease in the volume fraction of dDDAO in the surface layer (and hence greater area per DDAO molecule) is likely to be a result of the co-adsorption of the more surface active non-ionic species. Increasing the concentration of $C_{12}E_5$ further so the dDDAO:$C_{12}E_5$ ratio becomes 1:3, there is no enrichment of the

surface with dDDAO.

Now considering the distribution of $dC_{12}E_5$, the thickness of the surface layer is consistent with that of DDAO, confirming the co-adsorption of the two surfactant species. The observation that DDAO acts to significantly suppress $C_{12}E_5$ segregation suggests that compatibility also plays a role in these surfactant distributions. As for the previous model system, it is plausible that, particularly with the high compatibility of DDAO with PVA, interactions between the head groups of the two surfactant species could act to promote the compatibility of $C_{12}E_5$ with the matrix. In addition, the high solubility of DDAO in PVA may also provide an environment capable of accommodating the tailgroups of $C_{12}E_5$ that is otherwise absent. The entropy of mixing is also likely to be significant here; localisation of a single surfactant on the surface would be less entropically favourable than its distribution throughout the bulk film.

Upon inclusion of glycerol, very similar effects are observed as in the non-plasticised films. Again, the reduction of ϕ_{dDDAO} in the surface monolayer is consistent with the co-adsorption of $C_{12}E_5$ due to its lower aqueous surface tension. One subtle difference is that there is still some dDDAO present in the surface layer of the film (albeit at a very low concentration). Additionally, in contrast to the non-plasticised film, no surface excess of $C_{12}E_5$ is apparent, despite its low surface tension. However, this could be due to the difficulty in identifying the surface layer with a low concentration of deuterated additive due to the low contrast between the layers. As glycerol shows some segregation in the single-surfactant films containing $C_{12}E_5$ and DDAO, the lack of plasticiser segregation in the mixed surfactant system, in conjunction with the overall reduction in surfactant segregation, again demonstrates that surfactant and plasticiser segregation are closely linked.

8.3.1.3 SDS/$C_{12}E_5$

In the final model system, containing $C_{12}E_5$ and SDS, both surfactants are highly incompatible with PVA, exhibiting substantial surface excesses in their respective single-surfactant films. In this system, it was found that the segregation of both surfactant species is reduced, compared to the films containing one surfactant. However, whereas a strong reduction in SDS segregation is observed in the presence of $C_{12}E_5$, SDS only causes a modest suppression of the nonionic surfactant. Again, it should be noted that the interfacial segregation of $C_{12}E_5$ makes accurate calculation of the total fraction of segregated surfactant more difficult, and here only the surfactant segregated to the film-air interface is considered in the calculation.

Surface energy should first be assessed as a driving force for segregation. $C_{12}E_5$ has the lower aqueous surface tension, and therefore it is thermodynamically favourable for this species to occupy the surface. When considering the first model system (SDS/DDAO) it was suggested that the lower surface energy of DDAO excludes some SDS from the surface, thereby suppressing segregation. This argument could also be applied here. In fact, the even greater difference in aqueous surface tension between $C_{12}E_5$ and SDS, could lead to this being a more significant effect than for the first model system. Compatibility of the surfactants with the matrix also has a significant role to play in the distribution of components throughout the film. Although both species exhibit low compatibility with PVA, it is plausible that interactions between headgroups of the two surfactants enable the formation of structures that can occupy regions of the polymer matrix more favourably.

In the presence of glycerol, the same trend is observed as in the non-plasticised films, with the suppression of segregation of both surfactants observed. Despite the lower aqueous surface tension of $C_{12}E_5$, the low concentration of this additive adjacent to the air-film interface indicates that it is the SDS that is predominantly enriched on this surface, although the nonionic surfactant does still exhibit extensive segregation from the bulk film.

In the presence of low concentrations of $C_{12}E_5$, it appears that glycerol is still capable of forming some stacked structures with surfactant, as previously observed for films containing SDS as the only surfactant. A Bragg peak is apparent in the reflectivity data for the film containing 7.5 wt.% SDS. As this is indicative of a repeating structure, this suggests that even with 2.5 wt.% $C_{12}E_5$ incorporated, in the presence of glycerol the surface excess is arranged into repeating layered structures. This Bragg peak is located at $Q \sim 0.2$ Å^{-1}, consistent with the position of the Bragg peak from the plasticised film containing SDS as the only surfactant. This indicates that, at a low concentration, the non-ionic surfactant does not significantly perturb the stacking of the SDS/glycerol structures, described in Chapter 4. Taking this in conjunction with the low concentration of $C_{12}E_5$ in the near surface region of the film, suggests that compatibility, and the favourable formation of thermodynamically stable stacked structures of plasticiser and SDS, dominates over surface energy arguments in determining the vertical distribution of the two surfactant species in this film. As the concentration of SDS is decreased and the concentration of $C_{12}E_5$ is increased, the plasticiser does not segregate to the surface, again demonstrating the strong coupling of SDS and glycerol segregation.

8.3.2 Solution Behaviour of Mixed Surfactant Systems

Studies on mixed surfactant systems are usually concerned with the onset of micelle formation and therefore on interactions at and below the CMC. However, by probing a broader range of concentrations, above the CMC, and considering the surface tension at high surfactant concentrations, the effect of a secondary surfactant species on surface tension, and therefore the role of surface energy on driving segregation in more complex systems can be understood. In particular, this can aid understanding on the species present on the solution surface, which may correlate with the surface of the spin-cast film.

For each model system studied, interactions between species in solution are apparent. These will be discussed in greater depth in the following sections.

8.3.2.1 SDS/DDAO

In this model system, DDAO was found to suppress the segregation of SDS, whereas SDS was found to promote the segregation of DDAO in the PVA film. The attractive interaction between these two surfactants, identified in solution, combined with the high incompatibility of SDS with PVA (Chapter 5) and the high compatibility of DDAO with PVA (Chapter 6) is likely to result in an "average" compatibility of the two additives with the matrix, and thus the suppressed segregation of SDS and promoted segregation of DDAO.

Surface tension experiments (Fig. 8.19 and 8.21) showed that at high DDAO concentration, DDAO competes with the adsorption of SDS to the surface (at least on the timescales relevant for measuring surface tension, or for spin-coating), which could also contribute to the lower SDS segregation observed in the presence of DDAO. When considering the reverse case, it is apparent the high SDS concentrations only suppresses the adsorption of DDAO to the surface at high surfactant concentrations, relevant after solvent loss during spin-coating. This could also plausibly contribute to the observed suppression and enhancement of the segregation of SDS and DDAO respectively.

8.3.2.2 $C_{12}E_5$/DDAO

Neutron reflectivity revealed that $C_{12}E_5$ segregation was significantly suppressed in the presence of DDAO. In this mixed system, DDAO also segregated to a lesser extent, with no surface excess apparent in the presence of high concentrations of $C_{12}E_5$ concentration. Although this can be rationalised to some extent in terms of the surface energies of the pure components, assessing the surface tension of the mixed components can also aid in better understanding the interaction between

the two surfactants.

The findings of Goloub et al.[248] show that an attractive interaction is likely present between these surfactants, albeit to a lesser extent than in the DDAO/SDS system. These favourable interactions could therefore lead to the highly compatible DDAO promoting the compatibility of the $C_{12}E_5$ with the PVA.

As only a surface monolayer of DDAO forms in the simple PVA/DDAO films, the synergistic adsorption of the two surfactants apparent from the surface tension experiments shows that the $C_{12}E_5$ and DDAO co-adsorb onto the surface of the solution in order to effect a greater reduction in surface tension. The necessary replacement of some DDAO by $C_{12}E_5$ is therefore likely to result in the overall reduced segregation of DDAO in the mixed system.

8.3.2.3 SDS/$C_{12}E_5$

Neutron reflectivity has revealed that segregation of both SDS and $C_{12}E_5$ is reduced in the mixed system, compared to in the single-surfactant systems. Although surface tension showed little synergism in the surface adsorption of the two surfactants in solution, from the work of Goloub et al.[248] the interaction between the two species is attractive. The Gibbs adsorption isotherms also revealed that both species are present on the solution surface. Similarly to the previous two systems, the favourable interaction between the surfactants may mean that this results in an "average" compatibility with PVA. Although this could be expected to cause an increase in the extent of $C_{12}E_5$, its higher compatibility with PVA means that segregation of the non-ionic surfactant is likely to be largely related to the monolayer on the surface of the solution. Therefore the co-adsorption of the two surfactants in the mixed solution and the replacement of $C_{12}E_5$ with SDS could plausibly lead to suppression of the non-ionic surfactant.

8.4 Chapter Conclusions

In this chapter, the distribution of multiple surfactants in PVA films was assessed in order to better understand the role of different factors in segregation. It is clear from the insights in this chapter that in mixed systems, the presence of multiple additives has a significant influence on segregation behaviours, resulting in different depth profiles from those of the single surfactants systems. This is true for the three model systems studied. The explanation of segregation behaviours in each of the mixed systems can be summarised in terms of three effects:

1. Surface energy

2. Entropy of mixing

3. Compatibility

Looking at the surface tension behaviour of the mixed systems can help to better understand the interactions between the different species. From these results, it is significant that the surface energy of each component cannot be considered independently when attempting to predict segregation in multi-surfactant systems.

By assessing these findings in the context of a previously reported study,[248] it is likely that the interactions between surfactants in each of the model systems studied is attractive. This favourable interaction could therefore plausibly contribute to the increased compatibility of surfactants with PVA observed in the presence of another surfactant, and the suppression of segregation of both surfactants.

Surface tension has therefore offered insights into into each of the model systems. Although there are limitations in this approach, such as the neglect of interactions with the polymer in solution, it is clear that an understanding of the nature and strength of interactions between different additives can prove informative in ultimately understanding and predicting segregation in more complex film systems.

Chapter 9

Properties of the PVA Matrix

Some of the work comprising this chapter has been published as: Fong, R.J.; Robertson, A.; Mallon, P.E.; Thompson, R.L. "The Impact of Plasticizer and Degree of Hydrolysis on Free Volume of Poly(vinyl alcohol) Films." *Polymers*, 10, 1036, 2018.[250]

Thanks must go to Gary Oswald for running the XRD measurements, and Alex Robertson for running the DMA measurements included in this chapter.

9.1 Chapter Introduction

In earlier chapters, it was demonstrated that the presence of plasticiser in PVA films, and its interaction with other molecules such as surfactants, can bring about a surprisingly rich range of segregation behaviours of model film components.[168,174] However, the complex nature of the interactions between film components means that predicting the migration and adsorption of different species to interfaces is difficult, even in simple models for complex formulations. It is therefore of interest to better understand the effect of film composition on the properties of the polymer matrix in order to ultimately better predict and control small molecule segregation and migration. Developing this understanding could also assist with the correlation of the properties of the material with film permeability and transport properties, which is particularly important in the context of the diffusion and migration of encapsulated detergent components through the film. In this chapter, positron annihilation lifetime spectroscopy (PALS) is assessed as a tool to understand the behaviour of plasticisers in PVA at a molecular level, which is supported by macroscopic studies of the polymer matrix by XRD and DMA.

PALS can be used to probe free volume size distributions and concentrations in polymers by measuring the time difference between the emission of a positron

from a radioactive source and its subsequent annihilation. The details of this technique are described in greater depth in Chapter 3. PALS is a highly valuable technique in providing information on the polymer free volume and its relationship with various properties. These include permeability, the glass transition, crystallisation, dynamics, and the chemical environment of free volume cavities. PALS has been widely used in the study of polymeric systems at a molecular level, and can be used to quantitatively assess the effect of plasticisation on free volume. Although the plasticisation of amorphous polymers has been predominantly investigated,[251,252] there have been some cases of the use of PALS to investigate the plasticisation of semi-crystalline polymers, including poly(ethylene oxide)[253,254] and poly(vinyl chloride).[255,256]

Although the plasticisation of PVA has been widely studied,[11,18,19,257] PALS has not been implemented to study its effect on free volume properties. There have been a number of PALS studies of unplasticised PVA,[20,258–260] including the incorporation of non-plasticising additives and the properties of nanocomposites,[261–264] but most have focused on the effect of the chemical environment on the yield of positronium formation, rather than on the free volume properties of the materials.[265–267] In this chapter, PALS is used to assess the effect of the degree of hydrolysis and plasticiser incorporation on the free volume properties of solution-cast PVA films, and explore the relationship between free volume and bulk properties such as crystallinity and glass transition temperature, T_g, which were characterised by XRD and DMA respectively. By investigating the plasticisation of PVA and the influence of degree of hydrolysis (DH), the aim is to gain insights into the polymer-additive interactions.

9.2 Results

9.2.1 Influence of Plasticisation on PVA Properties

9.2.1.1 Influence of Plasticisation on Free Volume

To investigate the effect of plasticisation on the free volume properties of PVA, two model plasticisers were used: glycerol and propylene glycol. The concentrations of both additives were varied from 0 to 50 wt.%. Following preparation of the samples (as detailed in Section 3.13), PALS was used to determine the effect of plasticiser inclusion on the cavity radius, R, and on the o-Ps intensity, which can be linked to the void concentration in the absence of any chemical effects.

All PALS results could be satisfactorily fitted using three-lifetime analysis. As described in greater depth in Section 3.13, these lifetimes are attributable to

annihilation of the para-positronium (p-Ps), the "free" positron, and the ortho-positronium (o-Ps) respectively.

Figure 9.1 shows the impact of propylene glycol on the cavity radius, R, and intensity of the o-Ps component, I_3, in PVA. The linear increase in R with propylene glycol loading throughout the whole concentration range shows the increasing cavity radius upon plasticiser inclusion. There is a very modest decrease in I_3 with propylene glycol concentration. Although this parameter is generally associated with the concentration of free volume voids, in this case the decrease in I_3 is unlikely to suggest that the number of voids decreases as the plasticiser loading increases. A decrease in I_3 with plasticiser concentration has been previously reported in a number of studies.[254,268] In some cases the decrease in I_3 has indeed been attributed to a hole-filling mechanism, whereby the plasticiser molecules occupy the cavities, rather than increasing their size or creating new ones, reducing the overall void concentration.[251] However, the clear increase in cavity radius with propylene glycol concentration suggests that this is not the case in this system and that there must be another effect. Instead, this decrease in I_3 is likely to be the result of the inhibition of o-Ps formation by the plasticiser. Although Equation 3.33 could be used to calculate the fractional free volume, the use of the determined positron parameters (τ_3, I_3) to calculate free volume can only be justified when void concentration is the sole factor governing o-Ps intensity, and any possible chemical effects capable of affecting the probability of o-Ps formation can be neglected.[269]

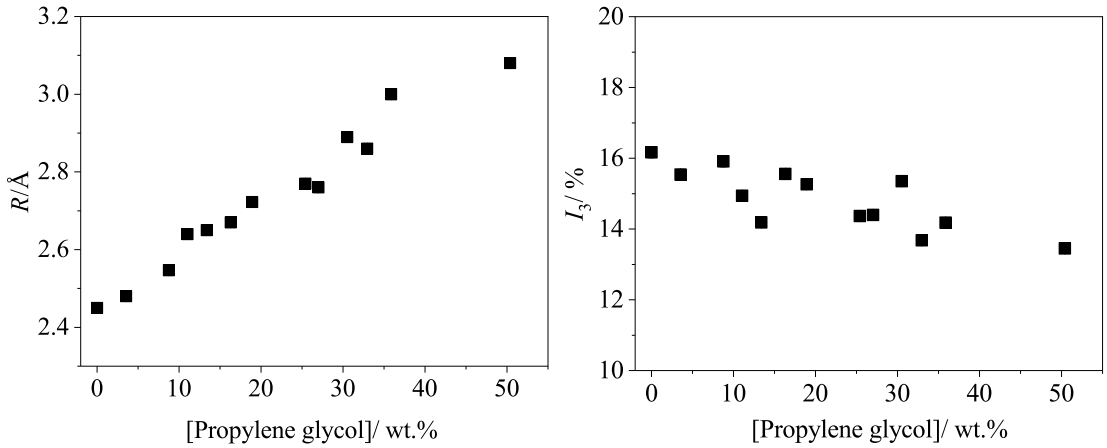

(a) Cavity radius **(b)** o-Ps intensity

Figure 9.1: (a) cavity radius (R) and (b) o-Ps intensity (I_3) in vacuum-dried, solution-cast PVA films as a function of propylene glycol concentration. Error bars are within the size of the data points.

The effect of plasticisation by glycerol on the free volume properties of PVA was subsequently investigated. As glycerol is very hygroscopic, it is also impor-

tant to consider the impact of water on the plasticised PVA films. The presence of water, and thus relative humidity, significantly affects the mechanical properties of PVA and its blends.[270] The impact of water inclusion on the plasticisation of PVA by glycerol was therefore also assessed by comparing air-dried and vacuum-dried films in order to link this to its macroscopic free volume properties. The preparation of these vacuum-dried glycerol-plasticised PVA films is consistent with the preparation of the films containing propylene glycol. Figure 9.2 shows the impact of glycerol concentration on the free volume properties (R and I_3) of PVA, and the effect of the presence of water in the film on these parameters. The water content of the films after air-drying for 24 h, prior to drying under vacuum, (hollow symbols) was determined by thermal gravimetric analysis (TGA) to be 8 wt.% (Figure 9.3).

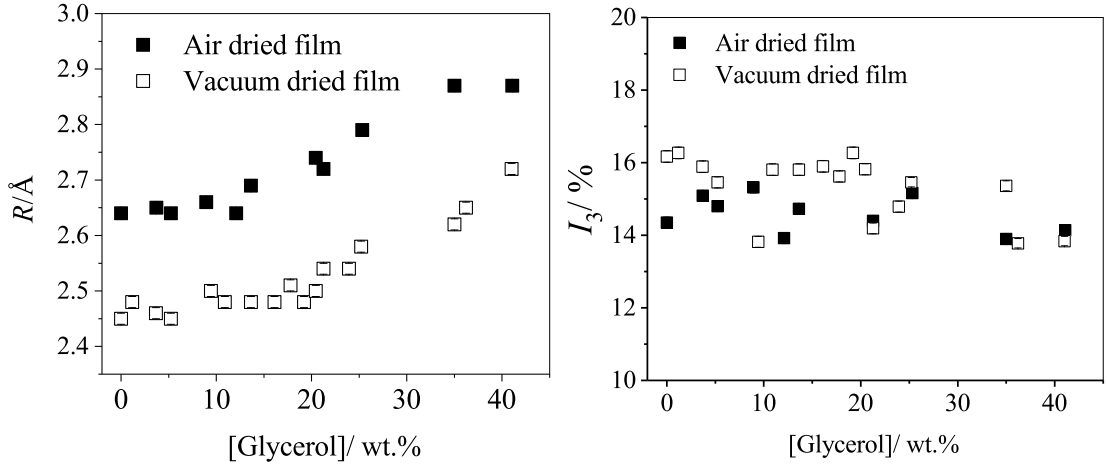

(a) Cavity radius **(b)** *o*-Ps intensity

Figure 9.2: Cavity radius (R) (a) and *o*-Ps intensity (I_3) in air dried and vacuum-dried, solution-cast PVA films as a function of glycerol concentration. Error bars are within the size of the data points.

As found for the PVA/propylene glycol system, there is a substantial increase in the size of the free volume holes with increasing glycerol concentration, confirming the plasticisation effect. However, in contrast to propylene glycol, two regions are apparent for the glycerol system: the first at low concentrations, ($<$ 15 wt.%), where increasing the plasticiser concentration results in a negligible increase on R, and the second at higher concentrations ($>$ 15 wt.%), where R increases significantly when additional plasticiser is incorporated.

As observed for propylene glycol, a slight decrease in I_3 with increasing plasticiser concentration can be observed, which as discussed in relation to the previous system, is unlikely to reflect a decrease in free volume void concentration upon increasing glycerol loading.

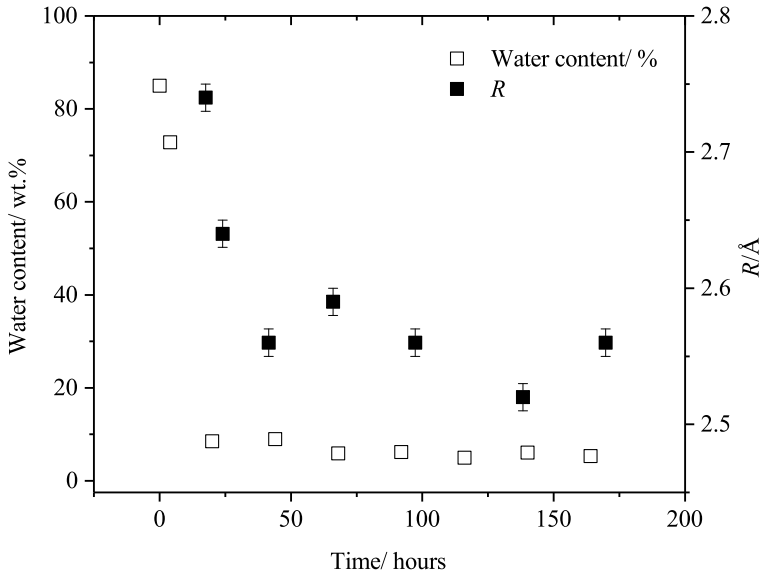

Figure 9.3: Decrease in film water content of non-plasticised PVA during solution-casting in air (hollow symbols) and decrease in cavity radius during the solution-casting of films in air (filled symbols).

Comparison of the PALS parameters in the vacuum-dried and air-dried films reveals that PVA/glycerol system follows the same trends in the presence and absence of water, with the cavity radius systematically shifted to higher values when water is present. This clearly demonstrates the additional plasticisation effect of water. The presence of water can also be seen to cause a small decrease in I_3.

Figure 9.3 shows the change in water content and cavity radius over an 8 day air-drying period in the absence of additional plasticisers. Water content in the film decreases from 8.5 % after 24 h, to an equilibrium value of 5-6 % after 3 days. This is accompanied by a decrease in the cavity radius, corresponding to the decreasing void size as water is lost from the film. The presence of low amounts of water can be seen to have a significant impact on the cavity radius; the 3.2 % decrease in water content leads to a 4 % reduction in R.

9.2.1.2 Relating Glass Transition Temperature to the Free Volume

As plasticisers are used to lower the glass transition temperatures (T_g) of polymers including PVA,[11,18,19] it would be expected that an increase in free volume cavity radius would lead to a decrease in the T_g. Although not easily calorimetrically detectable, the glass transition temperatures of the solution cast PVA resins can be determined using dynamic mechanical analysis (DMA) (Section 3.11), allowing the effect of plasticiser inclusion on the macroscopic polymer properties to be compared with the microscopic free volume properties. The glass transition

temperature and cavity radius of partially-hydrolysed PVA, both non-plasticised and in the presence of 20 wt.% glycerol and 20 wt.% propylene glycol, are compared in Table 9.1 and Figure **??**. Propylene glycol causes a greater depression in T_g than glycerol at the equivalent wt.% loading, (47.4 °C vs. 29.6 °C), correlating well with the greater percentage increase in cavity radius upon propylene glycol compared to glycerol incorporation (11% vs. 2%).

Table 9.1: Comparison of the effect of plasticisation and residual water on the glass transition temperature and cavity radius of solution cast PVA films.

Plasticiser	Drying method	R/Å	T_g/°C
None	Air	2.64	53.3
None	Vacuum	2.45	65.1
Glycerol	Air	2.74	26.8
Glycerol	Vacuum	2.50	35.5
Propylene glycol	Vacuum	2.72	17.7

9.2.1.3 Influence of Plasticisation on Crystallinity

From the PALS results, it is apparent that there are clear differences in the microscopic plasticisation behaviour of propylene glycol and glycerol in PVA film, which is manifested in differences in macroscopic properties of the polymer. X-ray diffraction (XRD) was used to gain further insight into the effect of these additives on the resin properties, by assessing sample crystallinity. Although PALS measures the free volume void size solely in the amorphous regions of the polymer, insight into these different plasticising behaviours and effects on the polymer can be gained from the polymer crystal structure. The XRD patterns obtained from the non-plasticised film, and films plasticised with 20 wt.% glycerol and 20 wt.% propylene glycol are shown in Fig. 9.4. The characteristic peak at approximately 20 ° confirms the semi-crystalline nature of the polymer.[271] The apparent crystallite size in the PVA samples, t_{crys}, can be estimated from the inverse peak width using Scherrer equation,

$$t_{crys} = \frac{k\lambda}{\beta \cos\theta} \tag{9.1}$$

where k is a shape factor for the crystallite, here assumed to be unity, λ is the X-ray wavelength, β is the peak full width-half maximum (FWHM) determined by fitting the peaks to a Lorentzian function after a linear background subtraction, and θ is the scattering angle of the peak. The crystallite sizes estimated using this equation are tabulated below (Table 9.2). It can be seen that incorporating 20 wt.% plasticizer significantly reduces the degree of crystallinity of the PVA

resin since the Bragg peak is less distinct from the background than for pure PVA. It is also apparent that this reduction is substantially greater for propylene glycol than for glycerol. Comparing the values of t_{crys} reveals that there is only a small decrease in crystallite size upon glycerol incorporation, but propylene glycol causes a substantial increase in crystallite size. This significant difference in the behaviours of the two systems is interesting, particularly as the lack of change of crystallite size in the PVA containing 10 wt.% glycerol correlates well with the lack of cavity radius increase compared to pure PVA. In addition, the 30 % increase in crystallite size of PVA containing 10 wt.% propylene glycol correlates with the substantial increase in cavity radius observed. This suggests that the incorporation of propylene glycol allows PVA crystals to grow when they are better able to move in the plasticised state.

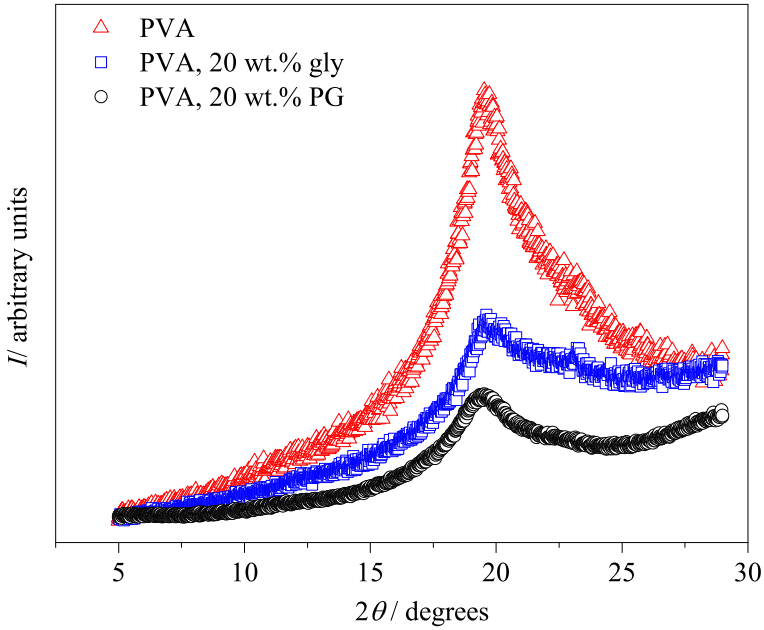

Figure 9.4: XRD patterns obtained for vacuum dried, solution cast films of pure PVA (red), with 20 wt.% glycerol incorporated (black) and with 20 wt.% propylene glycol incorporated (blue).

Table 9.2: Comparison of the effect of plasticisation on integrals and FWHM of XRD peaks for vacuum-dried films containing non-plasticised PVA, PVA plasticised with glycerol and PVA plasticised with propylene glycol.

Sample	FWHM /°	t_{crys}/nm
PVA	4.19 ± 0.04	2.18 ± 0.02
PVA/glycerol	4.24 ± 0.04	2.08 ± 0.02
PVA/propylene glycol	3.25 ± 0.04	2.77 ± 0.03

9.2.1.4 Effect of Temperature on Glycerol-Plasticised PVA

Cavity radii in vacuum-dried PVA samples heated incrementally to 110 °C were determined in order to assess the effect of temperature on the free volume properties of the unplasticised and plasticised polymer. Fig. 9.5 shows the temperature dependence of R for the pure PVA and for PVA containing 3 different loadings of glycerol. For each sample, it is clear that increasing T increases the cavity radius. A change in gradient is apparent at 45 °C for the PVA samples containing 0, 5 and 10 wt.% glycerol. This is likely to be due to the T_g,[259] and the temperature of this transition in R is consistent with the T_g of the unplasticised resin determined by DMA. The absence of this transition in the sample containing 24 wt.% glycerol is likely to be due to the much lower T_g of this sample, consistent with the measured T_g of a highly plasticised resin (27 °C, Table 9.1). The data in Figure 9.5 confirms the negligible change in cavity radius upon inclusion of up to 10 wt.% glycerol, relative to the pure PVA. Up to 65 °C, this level of glycerol incorporation has no effect on R, although some divergence is apparent at higher temperatures. Throughout the entire temperature range studied, the PVA films containing 5 wt.% and 10 wt.% glycerol contain voids of equal size.

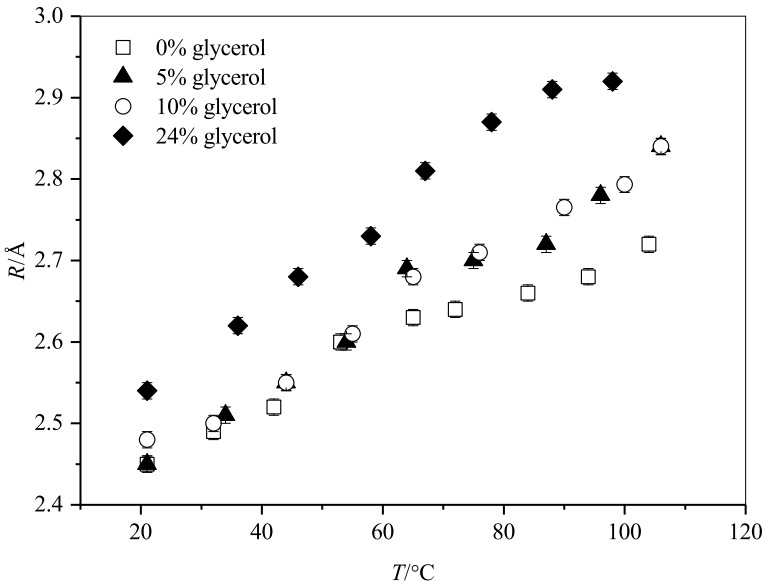

Figure 9.5: Effect of temperature on the cavity radii in non-plasticised and glycerol-plasticised PVA films.

9.2.1.5 Effect of Surfactant Inclusion on Film Free Volume

PALS has revealed the huge impact of commonly used plasticisers on the microscopic free volume properties of PVA. Complex industrial formulations can contain a wide range of molecules besides traditional plasticisers as additives,

and migration of encapsulated components into the film is also likely to affect the free volume properties of the film, which itself is then likely to affect matrix permeability. To extend this study and explore the use of PALS as a tool to understand the free volume properties upon incorporation of a wider range of additives, the effect of a model surfactant on the free volume properties of PVA was explored. CTAB was selected as a model surfactant due to its high compatibility with PVA, demonstrated by its phase behaviour (Chapter 5) and its lack of segregation in binary films.[168] The change in cavity radius with CTAB concentration is shown in Fig. 9.6. It can be seen that there is an almost linear increase in R when CTAB concentration is increased from 0 wt.% to 10 wt.%, above which void size remains approximately constant. Comparison with Figures 9.1 and 9.2 shows that over the concentration range of 0-10 wt.%, CTAB causes a greater increase in cavity radius than either of the two conventional plasticisers studied.

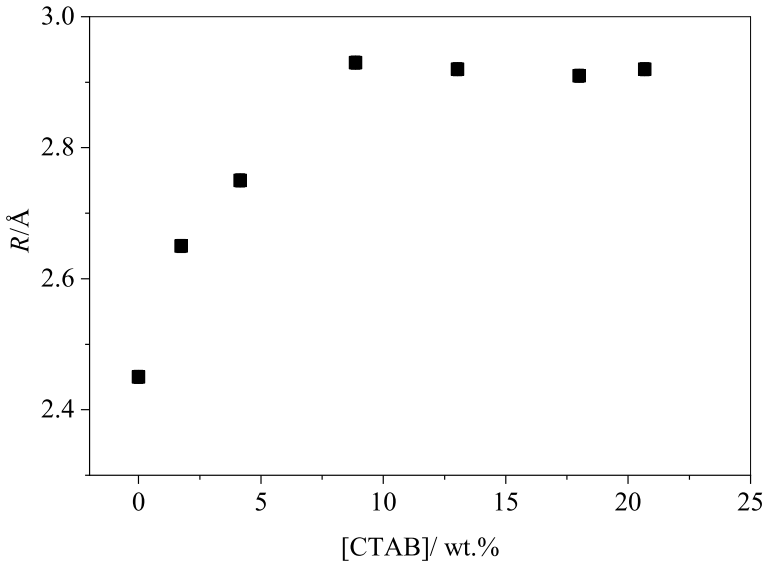

Figure 9.6: Change in cavity radius of solution-cast PVA/CTAB films with CTAB loading.

9.2.2 Influence of Degree of Hydrolysis on PVA Properties

9.2.2.1 Influence of Degree of Hydrolysis on Free Volume

The degree of hydrolysis (DH) is a key property of PVA, capable of influencing its physical and mechanical properties. DH also affects the nature of the interactions in the matrix, both between polymer chains and between the polymer and small additive molecules such as plasticisers. By blending relevant proportions of solutions of PVA with degrees of hydrolysis of 88 % and 98 %, series of polymer films with a range of overall DH were produced for three molecular weights of PVA (13-23 kg mol^{-1}, 31-50 kg mol^{-1} and 125 kg mol^{-1}). The miscibility of the 88 % and 98 % DH polymers for each molecular weight was confirmed from the DSC curves of each of the pure polymers and a blend, which revealed a single melting point (T_m) of the blend at an intermediate value of the melting points of the pure polymers. Values for T_m are tabulated below (Table 9.3), with the DSC curves included in Appendix E. Were these blends to phase separate, two distinct melting points would be observed, corresponding to each of the pure polymers. The compatibility of the two resins should also be discerned from the glass transition of the blends as an approximation of the glass transition of miscible blends is given by the Fox equation, Equation 9.2, where x_1 and x_2 are the weight fractions of components 1 and 2 respectively. However, as previously mentioned, the T_g of these resins is not always calorimetrically detectable.

$$\frac{1}{T_g} = \frac{x_1}{T_{g1}} + \frac{x_2}{T_{g2}} \tag{9.2}$$

Table 9.3: Melting points of pure PVA resins and their 50:50 (w/w) blend.

M_w/ kg mol^{-1}	T_m/°C		
	88% DH	98% DH	Blend
13-23	198	229	215
31-50	201	222	217
125	196	226	218

Fig. 9.7 shows that the cavity radii are similar for each molecular weight, confirming that the chain ends do not significantly contribute to plasticising the polymer in this molecular weight range. For each molecular weight, as DH of the blend increases from 88 % to 98 % there is a modest decrease in R. This suggests that the replacement of a greater fraction of acetate groups with hydroxyl groups causes a slight contraction of the void size in the resins.

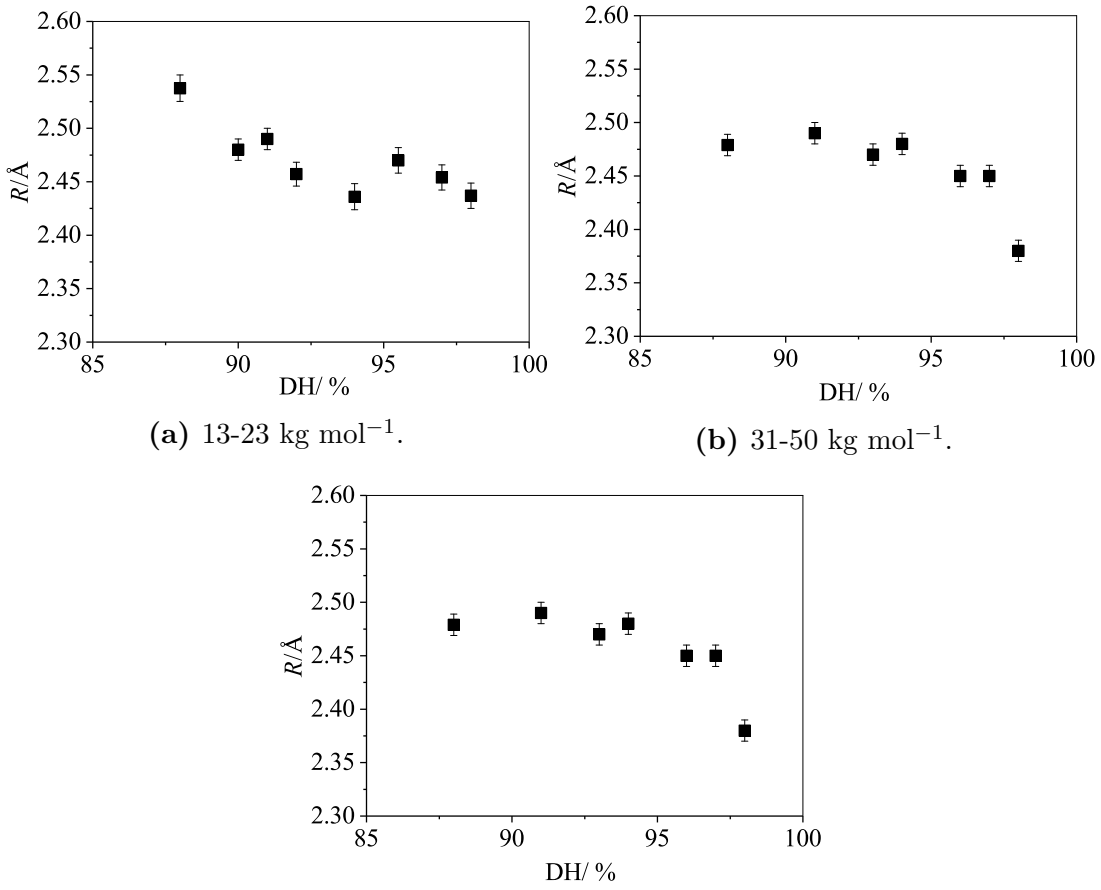

(a) 13-23 kg mol^{-1}.

(b) 31-50 kg mol^{-1}.

(c) 31-50 kg mol^{-1}.

Figure 9.7: Effect of degree of hydrolysis on the cavity radius in non-plasticised, vacuum-dried PVA resins of different molecular weights.

As discussed in Section 9.2.1.2, the link between the macroscopic properties of the polymer and its microscopic free volume properties can be assessed by considering how the glass transition temperatures relate to the cavity radii. Table 9.4 shows the effect of degree of hydrolysis on both cavity radius and glass transition temperature of air-dried films of PVA with a molecular weight 31-50 kg mol^{-1}. This is also illustrated in Fig. **??**. As observed upon plasticiser incorporation, the decrease in cavity radius upon increasing the degree of hydrolysis is also reflected in the increase in glass transition temperature.

Table 9.4: Comparison of the cavity radius and T_g in vacuum-dried films with degrees of hydrolysis.

DH/%	R/Å	T_g
88	2.64	53.3
98	2.45	65.1

9.2.2.2 Influence of Degree of Hydrolysis on Crystallinity

XRD was subsequently used to gain insight into the nature of the effect of the number of acetate groups on the properties of the resin by assessing sample crystallinity. Fig. 9.8 shows the superimposed XRD pattern of PVA resins with DH of 88 % and 98 %. The consistent peak position confirms that altering the degree of hydrolysis does not significantly alter the inter-chain spacing of the crystal structure, with only a very slight shift of the peak to higher angle for 98 % DH, consistent with its tighter packing. However, it can be seen that the XRD pattern for the PVA with a DH of 98 % has a Bragg peak of higher intensity and greater peak integral, revealing a higher degree of crystallinity. Values for FWHM and t_{crys} calculated using Equation 9.1 are included in Table 9.5. It can be seen that the films with the greater DH have a substantially greater crystallite size. In agreement to the observations for the plasticised films, the polymer with the smaller free volume cavities exhibits the larger crystallites, and it is plausible that the greater mobility as a result of larger free volume cavities facilitates a greater extent of crystallisation in these domains, despite the lower overall crystallinity of the sample.

Table 9.5: Comparison of the effect of DH on FWHM of XRD peaks and crystallite size in solution-cast PVA films.

Sample	FWHM /°	t_{crys}/nm
88% DH	4.09 ± 0.04	2.20 ± 0.02
98% DH	2.90 ± 0.03	3.10 ± 0.03

As previously mentioned, PALS measures only the size of cavities present in the amorphous regions of the polymer. This means that the crystallinity of the polymer should not directly affect the measured cavity radius. The simultaneous increase in cavity radius and decrease in crystallinity upon increasing the degree of hydrolysis from 88 % to 98 % therefore demonstrates the profound effect of this relatively subtle change in the chemistry of the polymer. This could have significant implications for additive interactions with the polymer.

9.2.2.3 Influence of Degree of Hydrolysis on Interaction of PVA with Glycerol

As PALS and XRD revealed that the slight change in DH from 88 % to 98 % has a substantial effect on the free volume properties and crystallinity of the polymer, the effect of DH on the interaction of the resin with other additives was subsequently assessed. PALS was used to compare the behaviour of the *o*-Ps

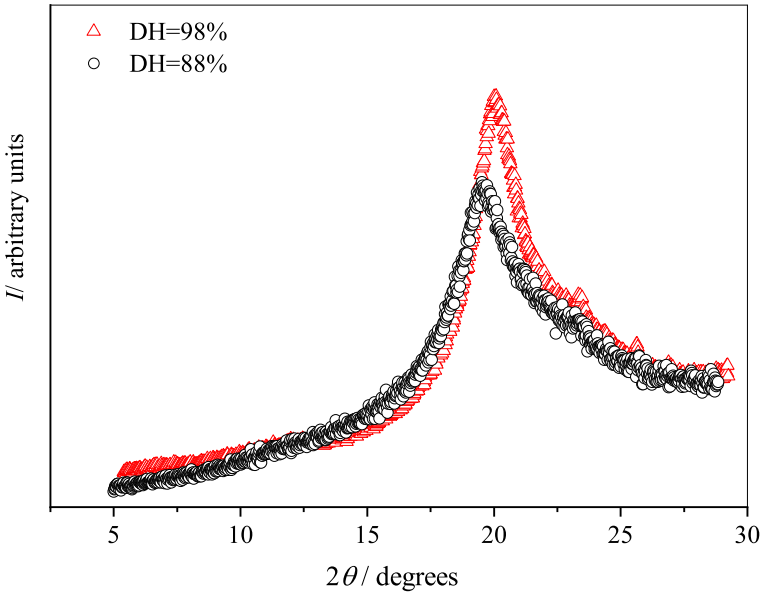

Figure 9.8: XRD patterns obtained for vacuum dried, solution-cast film of PVA (molecular weight 31-50 kg mol^{-1}) with DH of 88 % and 98 %.

lifetime in glycerol-plasticised PVA films with degrees of hydrolysis of 88 % and 98 % (M_w=31-50 kg mol^{-1}). Figure 9.9 shows that the behaviour of the resin with 88 % DH is consistent with the results presented in Section 9.2.1.1, where up to a critical concentration glycerol incorporation causes a negligible change in R, but as glycerol loading is increased further a substantial increase in this parameter is observed. However, this behaviour is not observed for the resin with 98 % DH. Here, an almost linear increase in cavity radius was found with glycerol loading throughout the whole plasticiser concentration range (as previously observed for PVA of lower DH plasticised with propylene glycol).

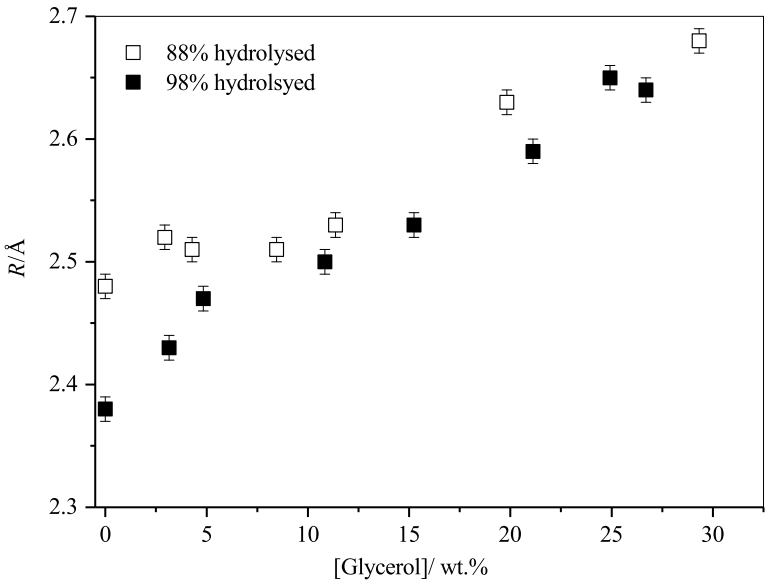

Figure 9.9: Comparison of the effect of glycerol loading on the cavity radius in solution-cast, vacuum-dried PVA resins with DH of 88 % and 98 %.

9.3 Discussion

9.3.1 Effect of Plasticisation on the Free Volume Properties of PVA

From Figures 9.1b and 9.2b, a modest decrease in I_3 is apparent upon increasing the concentration of both propylene glycol and glycerol. Although this parameter is typically inversely related to the concentration of free volume voids in the matrix, in this case an increase in plasticiser concentration is unlikely to reduce the number of cavities present. However, an alternative explanation for the decrease in this parameter upon plasticiser incorporation could be taken from Mohamed et al.,[265] who suggested that an unexpected decrease in the *o*-Ps intensity with increasing temperature is instead due to an increasing number of sites where the positronium precursors can be trapped, although little is known about the nature of these sites. The authors also suggested the possibility of the increase in molecular mobility above the T_g, causing the free volume holes to appear occupied due to segmental mobility at high frequencies. Forsyth et al.[272] highlighted the importance of considering the concept of dynamic free volume, as well as static free volume, both of which are probed by PALS. The static, or interstitial, free volume sites are the pre-existing free volume cavities which are required for the flow of polymer chains, whereas dynamic free volume is the time-dependent fraction of the total free volume. The detection of dynamic free volume by PALS is dependent on the frequency of molecular motion. However, Yoshinori et al.[273]

showed that the *o*-Ps pickoff lifetime is correlated with the free volume for both glassy and rubbery polymers, indicating its sensitivity to changes in free volume, whether it is dominated by changes in the static or dynamic free volume. In the systems studied here, the decrease in I_3 could therefore feasibly be attributed to the increase in molecular mobility in the presence of plasticiser.

However, another explanation to consider is the possible inhibition of the *o*-Ps formation by plasticiser molecules. It has been previously observed that changing polarity can affect *o*-Ps intensity through inhibition of positronium formation, leading to misleading values of I_3.[274] As a result, the effect of plasticiser inclusion on the I_3 parameter will not be used quantitatively as it cannot be reliably interpreted. It should perhaps be noted that polarity has also been observed to be capable of affecting *o*-Ps lifetime,[274] and thus R, by quenching. However, given that quenching would reduce R upon plasticiser incorporation, rather than causing any increase in apparent cavity radius, it can be assumed that the trends discussed here are valid, although exact values extracted from the τ_3 should be treated with caution.

A fair comparison of the microscopic effects of the plasticisation of the two additives can be made by plotting the change in cavity radius against additive concentration in units of mol g^{-1}. This is shown in Figure 9.10. It can be seen that incorporation of propylene glycol results in the greater increase in cavity radius of the two plasticisers. Although there remains the possibility that there may be some difference in any quenching effects of the two plasticisers, and thus it cannot be unequivocally concluded that propylene glycol has a greater effect of microscopic free volume, the corroboration of the microscopic plasticisation behaviour with the macroscopic properties of the resins, as evidenced by the greater reduction in T_g by propylene glycol, strongly suggests that this is the case. Figure 9.10 also shows that the behaviour of the *o*-Ps parameter in partially hydrolysed PVA is different for the two plasticisers studied. Although a linear increase in cavity radius is observed throughout the entire concentration range of propylene glycol, up to 20 wt.% glycerol can be incorporated into the same resin whilst having a negligible impact on the measured void size. One interpretation for this substantial increase in void size with plasticiser concentration is the phase separation of glycerol from the polymer matrix, and formation of pure plasticiser domains at concentrations higher than a critical loading. This possibility is discounted, however, as phase separation would provide another location for *o*-Ps annihilation, and result in a poor fit of the PALS data to a three-component model. At glycerol loadings higher than 20 wt.% the PALS data can still be fitted well with three components, with negligible improvement in variance attained by

introducing a fourth, making this explanation unlikely. Additionally, it has been shown elsewhere that glycerol and partially hydrolysed PVA are compatible to 39 wt.%, determined by the plasticiser loading at which the heat of fusion drastically reduces.[257] The high compatibility of PVA and glycerol was also demonstrated by the even distribution throughout spin cast films, as shown by neutron reflectivity,[147] and the lack of any visible bloomed droplets on the surface of solution cast samples containing glycerol up to 40 wt.%.

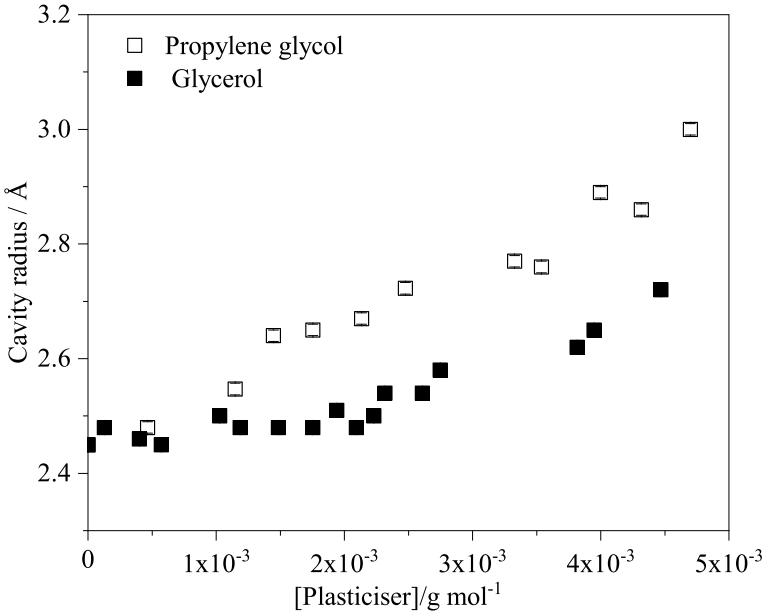

Figure 9.10: Comparison of the effect of glycerol and propylene glycol on cavity radius in PVA.

An alternative explanation for the observed behaviour can be proposed by considering the nature of the interactions of the plasticisers with the polymer, and how these may differ for glycerol and propylene glycol. It is widely accepted that the plasticisation of PVA can be attributed to the formation of hydrogen bonds between plasticiser and polymer chains.[11,19] The molecular structures of the two plasticisers are shown in Fig. 9.11. Glycerol, with three hydroxyl groups, has higher -OH group functionality than propylene glycol (two hydroxyl groups). It is therefore plausible that glycerol more readily forms hydrogen bonds with the hydroxyl groups present on the PVA chains, and can be accommodated into the matrix whilst causing minimal impact on chain separation up to a threshold. On the other hand, propylene glycol contains a methyl group which, although may interact more favourably with residual acetate groups on the polymer backbone, is much more likely to disrupt hydrogen bonding between adjacent polymer chains, and may also inhibit plasticiser-polymer hydrogen bonding. This could then lead to an immediate increase in free volume cavity radius upon incorporation into the

matrix. This effect can also be considered in terms of the observed macroscopic properties of the polymer, notably the greater reduction in the crystallinity of the PVA when plasticised with propylene glycol compared to when it is plasticised with glycerol. Furthermore, from the glass transition temperatures in Table 9.1, it is apparent that both the non-plasticised PVA and PVA containing 20 wt.% glycerol were below their glass transition temperatures when the PALS measurements were taken (20 °C), whereas the film containing 20 wt.% propylene glycol was above its glass transition temperature. As it can be seen in Fig. 9.5 that the glass transition causes only subtle changes in the free volume cavity radii, it is sensible to suggest that the substantial increase in void size, due to the nature of the PVA-propylene glycol interactions, results in the significant depression of the observed T_g. A lesser depression in the T_g of the glycerol-plasticised films can be identified. As the glass transition of this system occurs above the temperature at which PALS measurements were conducted, this corresponds well to the relatively slight increase in cavity radius detected.

(a) Propylene glycol **(b)** Glycerol

Figure 9.11: Plasticiser molecular structures.

9.3.2 Effect of Plasticisation by Water on the Free Volume Properties

Water is ubiquitous in nearly all industrial applications of PVA. It is therefore important to assess the significant plasticising behaviour of water in these systems. Comparing Figures 9.1, 9.2 and 9.3, reveals that the inclusion of 8 wt.% water in the PVA resin has a greater impact on the free volume void size than both glycerol and propylene glycol at this loading. The plasticisation of PVA by water has previously been reported and discussed, with a two-fold mechanism suggested based on studies into the changing properties of PVA as water is absorbed.[20] As well as increasing the size of the free volume cavities, water molecules bring about a lubrication effect. This promotes the mobility of the polymer chains and disrupts direct interchain hydrogen bonding. For the properties of solution-cast films used in this study, where water is gradually lost from films, the reverse process is more relevant and so the change in PALS parameters during the drying of the film was therefore studied. In contrast to the broad range of water con-

tents investigated by Hodge et al.,[20] the focus here is on a narrow range of low water contents. Nevertheless, comparable findings were identified. In the range between 8 % and 30 % water, Hodge et al. reported an increase in R and large decrease in I_3 (from 27 % to 20.5 %) with water content, which is consistent with that observed in the present study of the reverse (drying) system. This contrasts the behaviour observed for glycerol and propylene glycol, where only a modest decrease in I_3 is apparent as plasticiser loading increases. One important factor that should be considered it the high polarity of water. Polar molecules are capable of decreasing the probability of o-Ps formation and thus can affect I_3. However, Trotzig observed very little change in I_3 of poly(ethylene oxide) from 10-23 wt.% water content.[275] Although similar arguments to that used to address the modest decrease in I_3 upon plasticiser incorporation could be applied, it could alternatively be postulated that as well as increasing the size of the holes, water also occupies a fraction of the free volume cavities, decreasing their relative concentration. It is also possible that this substantial decrease in o-Ps intensity could be attributed to dynamic reordering of the PVA chains upon water loss. Thimmegowda et al.[276] observed an increase in I_3 of poly(2-hydroxyethyl methacrylate) upon water sorption, and attributed this to the reordering of the polymer chains as a result of the swelling by water. It is therefore feasible that the reverse argument can be applied here. In this case, a rearrangement of the PVA chains upon water loss could result in the division of comparatively large free volume holes into smaller ones, (causing a decrease in void size greater than can be accounted for by water loss from the cavities alone), thus increasing the number of free volume holes. Despite the apparent decrease in I_3 with increasing water content, indicating the decrease in concentration of free volume cavities, the high frequency of the plasticiser motion means that the water occupying the cavities can still contribute to polymer chain mobility, and thus the macroscopic plasticisation behaviour.

From the comparison of the change in R with glycerol concentration for air-dried and vacuum-dried films (Figure 9.2a), it is apparent that water has a greater effect on the void volume than glycerol. This can be attributed to the greater ability of water to disrupt the hydrogen bonding network within the PVA resin compared to glycerol. The observation of the significant plasticisation effect by water in films containing additional plasticising species highlights the industrial significance of humidity and its impact on PVA matrix properties.

9.3.3 Influence of CTAB Inclusion on PVA Free Volume Properties

The effect of CTAB on the free volume of PVA is interesting, demonstrating that a wide range of film additives are likely to be important in determining the free volume properties of the polymer matrix, even if there is little effect on the macroscopic plasticisation behaviour. Despite being a solid in its pure state, and by no means a traditional plasticiser, PALS reveals that CTAB causes a substantial increase in the cavity radius of free volume voids in PVA. Although only $\sim$ 10 wt.% CTAB can be incorporated without phase separation occurring, which is much lower than the amount of the traditional plasticisers that can be incorporated, the increase in free volume over this concentration is much higher than any other studied additive. This is likely to be a result of the large hydrophobic chain causing a large disruption in the packing of the polymer chains in the amorphous regions. The CTAB concentration at which no further increase in free volume is observed correlates very well with the compatibility limit with PVA as observed by the phase diagram (Chapter 5). This strongly suggests that at higher concentrations ($\sim$ 10 wt.%), CTAB is incorporated within the polymer matrix as a single phase, with the extra surfactant separated into a phase of pure surfactant, with no free volume voids where *o*-Ps can localise. As free volume is likely to have significant implications for the mobility of both additive molecules in the film and the encapsulated detergents in industrial systems, this finding demonstrates the importance of understanding the properties of all additives present, and proves the utility of PALS in delivering insights on their microscopic behaviour.

9.3.4 Influence of the Degree of Hydrolysis on PVA Free Volume Properties

The change in cavity radius can also provide insights into the influence of the polymer composition on the free volume properties of the matrix, probing the effect of increasing the degree of hydrolysis from 88% to 98%. Despite the narrow DH range studied, the observed decrease in R with DH shows that the replacement of residual acetate groups by hydroxyl groups causes a decrease in void size in the matrix. This qualitatively similar behaviour was found for each molecular weight of PVA. This is likely to be a result of an increased number density of hydrogen bonding sites and the formation of a tighter structure. Cowie et al.[258] previously reported the effect of varying the degree of hydrolysis of PVAc from 20 % to 85 %. They found that at low DH, where there is little hydrogen bonding,

increasing the vinyl alcohol content led to an increase in free volume cavity radius (increase in τ_3 from $\approx$ 1.9 ns to $\approx$ 1.95 ns), suggesting the formation of a more open structure. However, after a critical value of 35 % vinyl alcohol groups they observed a sudden decrease in R over a very narrow DH range (decrease of τ_3 to $\approx$ 1.7 ns). The authors suggested this was the result of both an increased number of hydrogen bonding sites and the replacement of the carbonyl group hydrogen bond acceptors, which favour a more open structure than hydroxyl groups.

In the work contained in this chapter, the effect of smaller changes in the PVA degree of hydrolysis on the matrix free volume properties are considered, where DH is higher and the polymer is well into the post-network collapse region identified by Cowie et al.[258] The length of the hydrogen bond lies within a narrow range of 2.6-3.1 Å, meaning that with a high proportion of alcohol groups there are stringent steric restrictions in the network. It was previously suggested that a critical concentration of hydrogen bond donors and hydroxyl group acceptors is needed to establish a tighter network, and so it could therefore be expected that following this network collapse, any further increase in hydroxyl groups would have little influence on the structure. However, the slight decrease in cavity radius in the range between 88 % and 98 % DH suggests that the removal of nearly all acetate groups permits the formation of an even tighter network. The microscopic free volume is reflected by the macroscopic polymer properties, as the glass transition temperature is shown to increase as void size decreases upon formation of a tighter network.

This result could have significant implications for the interactions of other additives in the PVA matrix. This is particularly important as it has been previously demonstrated that some surfactants have considerable affinity for glycerol, but very little affinity for PVA.[168,174] Comparison of the plasticisation effect of glycerol in resins of 88 % and 98 % reveals that although a limited content of glycerol can be incorporated into the 88 % DH resin without affecting the sizes of voids present, the inclusion of any amount of glycerol into an almost fully-hydrolysed resin increases the cavity radius. From this, it can be inferred that the glycerol molecules interact with the vinyl alcohol groups, occupying the larger cavities formed when these groups are sterically hindered from interacting with other vinyl alcohol groups due to the presence of acetate groups. However, in the absence of the more hydrophobic acetate groups, which are capable of disrupting the inter-chain hydrogen bonding, the introduction of plasticiser (such as glycerol) will disrupt the tighter hydrogen bonded network, even at very low loadings.

9.4 Chapter Conclusions

In this chapter, PALS has been used to study the effect of plasticiser incorporation and resin DH on the free volume properties of poly(vinyl alcohol) films, and efforts have been taken to link these microscopic properties to the macroscopic behaviour observed in these films.

PALS has revealed interesting differences in the plasticisation behaviours of propylene glycol, glycerol, and water, which have been attributed to their different functionality, and thus the different extent of interactions between the matrix and additive. Water was shown to have a more significant effect on free volume cavity size than either glycerol or propylene glycol. As well as studying the effect of glycerol and propylene glycol, by touching upon the effect of other additives on free volume properties, the huge effect of CTAB on cavity radius observed highlights the importance of considering the plasticising effect of all film additives, not only the conventional plasticisers. Increasing the DH of the PVA resin causes a decrease in free volume cavity radius, indicating that the absence of acetate groups permits the formation of a tighter network. When considering both the DH of the resin and the incorporation of plasticisers, the size of the microscopic free volume is shown to be qualitatively reflected in the glass transition temperature, although the relationship between these parameters is complex. From the variation in the plasticisation behaviour of glycerol with resin DH, it is likely that glycerol preferentially interacts with PVA in the vicinity of residual acetate groups as these cavities permit a limited concentration of the plasticiser to be accommodated in PVA without increasing the size of existing voids present in the matrix.

The findings from this chapter show that PALS can be a useful tool in understanding trends in the properties of PVA films. The aim of this work was to assess the utility of PALS in delivering insight into the properties of the polymer matrix that can influence the migration of film components. PALS has proven to be a valuable technique in gaining understanding of the free volume properties of PVA resins and exploring the polymer-plasticiser interactions, shedding light on the relationship between molecular structure and bulk material properties.

Chapter 10

Conclusions and Future Directions

10.1 Conclusion

Throughout this thesis, the surface and interfacial segregation of a number of surfactant additives in PVA films has been explored, with the aim of better understanding factors affecting the distribution of these additives. To this end, studies of the surfactants in solution were used to accompany the extensive depth profiling of a range of model films in order to assess the roles of surface energy and compatibility in segregation. By obtaining a fundamental understanding of the segregation of small molecules in simple model film systems, this should ultimately aid in predicting and controlling segregation in industrial films.

Surface tension can provide insight in understanding the role of surface energy. Although all surfactants studied throughout this thesis are more surface active than PVA, the polymer-surfactant interactions in solution are important in determining the surface activity of the surfactant in mixed solution. Surface tension was also used to understand interactions in more complex, mixed surfactant systems, in order to identify favourable interactions between each surfactant, which can ultimately impact surfactant distribution in films.

Compatibility has also been identified as an important factor in the distribution of film components and has been found to be strongly related to the extent of surfactant segregation in spin-cast films. By determining the PVA/surfactant/water phase diagrams during the solution casting of films, the compatibility of the surfactant and polymer can be easily assessed in the model systems. This experimental approach to determine phase behaviour could be valuable in guiding predictions of surfactant segregation in other systems.

The anionic surfactant SDS was found to segregate extensively from PVA, with its segregation usually enhanced in the presence of glycerol, a model plasticiser. Furthermore, in thicker films, stacked structures comprising surfactant bilayers separated by interstitial glycerol regions were identified on the film surface. It was confirmed that the glycerol-surfactant interactions provide a thermodynamic driving force for this segregation enhancement.

In contrast, zwitterionic amine oxide surfactants were found to exhibit very different segregation behaviour; at most a single surfactant monolayer is present on the surface of spin-cast films, with the remaining surfactant evenly distributed through the bulk. By determining the surfactant molecular area, it appears that the surface of the film resembles the surface of an aqueous surfactant solution. These surfactants are extremely compatible with PVA and in the bulk film, surfactant is localised in the amorphous regions of the polymer.

In mixed surfactant systems, the presence of multiple surfactants in PVA films was found to significantly affect the distribution of film components compared to in the single-surfactant model systems. With the exception of SDS promoting the segregation of DDAO, segregation of each surfactant studied was found to be suppressed in the presence of a second surfactant. Although this behaviour could largely be rationalised using surface energy and compatibility arguments, it is clear that the interaction between surfactants, notably the strong synergy between SDS and DDAO, has a significant role to play in determining the distribution of additives.

Although the majority of work comprising this thesis focuses on the vertical depth distribution of surfactants established during spin-casting, exploring the change in surfactant distribution upon heating the films has provided insight into the further migration of additives, as well as their loss from the films. Although difficult to separate the effect of temperature and time on the properties of the film, it is clear that film ageing can have significant implications for the surface properties of PVA films. This includes the hydrophilicity of the film, which is likely to be related to its sealing ability in industrial systems.

Finally, the free volume properties of PVA and the effect of plasticisation and resin degree of hydrolysis have been explored. It was found that the microscopic free volume properties correlate well to macroscopic plasticisation of the polymer. The different plasticisation behaviours of propylene glycol and glycerol, as well as the decrease in free volume upon increasing DH could be related to the extent of hydrogen bonding in the matrix. This greater fundamental understanding of the matrix properties will be essential in understanding migration of additives through the film. This is important for a number of reasons: first, as film perme-

ability is closely related to free volume and additive migration has been identified upon heating the film, understanding how each incorporated additive affects free volume is imperative in predicting and controlling additive distribution; second, a better understanding of free volume, and ultimately permeability, is essential in tackling the closely related problem of migration of encapsulated detergent components.

10.2 Future Directions

Throughout this thesis, the characterisation of a broad range of PVA/surfactant systems has yielded insights into the roles of surface energy and compatibility in the segregation of surfactants in PVA. In particular, the extension of the model systems to comprise multiple surfactants is valuable in bridging the gap between the simplest models and the complex industrial formulations. Although significant synergistic effects have been identified in the adsorption of these additives, which is related to their behaviour in solution, a better understanding of this effect could be obtained through the use of NR (to study the surface) and SANS (to study the bulk) of these mixed surfactant solutions.

For future studied on these model systems, steps should be taken to improve the robustness of fits through the use of constraints. This is particularly important given that in some systems lateral variation in the film surface make perfect fits impossible to achieve.

Focus should now be turned to better understanding the kinetics of migration over time. Whilst further migration and development of the surface excess has been identified in some systems upon heating the films, it is clear that loss of glycerol and other volatile additives creates difficulty in completely understanding this behaviour. Although additive loss has not yet been distinguished from water loss, this should be attempted using TGA-mass spectrometry, in order to understand the volatility of different film components.

A better understanding of the kinetics of migration and segregation could also be beneficially applied to address an accompanying problem in unit dose detergents: the migration of encapsulated detergent components, including fragrance molecules, through the PVA film. An interesting avenue to explore would therefore be to measure the ingress of small molecules into PVA films over time using NR. This would also help to understand the likely migration of $C_{12}E_5$ into the bulk PVA film upon heating.

Ion beam analysis is likely a valuable collection of techniques in characterising additive migration. As samples can be quenched after the desired time period

and subsequently measured, the effect of time on the depth profiles of films can be determined.

Additionally, monitoring of the change in depth profiles should be accompanied by characterisation of film topography both over time, and upon heating of the films. This would be important given that segregated SDS seems to rearrange upon heating of the film, leading to an increase in surface roughness.

PALS has proven useful in providing insights into the free volume properties of the polymer upon incorporation of a number of additives. From this initial exploration, it is clear that there is scope for this technique to be further exploited and extensively utilised in the context of molecular migration in order to obtain a more rigorous understanding of the role played by free volume. In particular, free volume effects of a wider range of additives should be explored. However, in order to relate the free volume properties of the matrix to molecular migration, film permeability studies should also be undertaken.

Furthermore, as PALS has revealed the importance of hydrogen bonding in the matrix in the free volume properties of the systems studied, accompanying Fourier transform infra-red (FTIR) spectroscopy could be used to assess the extent of hydrogen bonding between PVA and different additives, as well as in resins of different DH. This would help identify a relationship between the intermolecular forces in the matrix and the resulting free volume properties, providing a more comprehensive understanding of the film system as a whole.

Although the majority of this thesis focussed on a specific PVA resin, most closely related to industrial formulations, efforts to broaden the classes of polymers studies should be continued in order to better understand the influence of polarity, crystallinity and ultimately compatibility on segregation. PALS has revealed significant differences in the microscopic free volume properties of PVA upon plasticisation with glycerol and propylene glycol. Plasticisation by glycerol has also been shown to have a substantial effect on the distribution of surfactants. Ultimately it would be valuable for these observations to be considered together, by exploring the effect of plasticiser functionality and polymer degree of hydrolysis on surfactant segregation and migration.

It is clear that compatibility plays a huge role in determining the segregation behaviour of additives. Whilst phase diagram determination of the surfactant/polymer water systems has been useful in rationalising the observed segregation behaviours of different additives, this could be extended to determine compatibility in mixed surfactant systems and investigate the effect of temperature on compatibility. In order to employ this in the thorough prediction of segregation, a more quantitative measure for compatibility is required. One promising

approach would be to consider solubility parameters of film components.

Some of the greatest value from this project will ultimately come from its links with theory and simulation. Experimentally determined phase diagrams have proven to be a valuable and accessible tool that can be used to make sensible predictions about segregation behaviour based on the compatibility of components. However, they will also be useful in corroborating theoretical phase diagrams. Ultimately, this should enable the prediction of segregation in complex systems.

Finally, it is worth reiterating that the work undertaken throughout this thesis is in the context of small molecule segregation affecting the sealing ability of PVA films. Therefore, it would be useful to better understand the surface properties in the context of this application. Specifically, contact angle analysis would provide information on the effect of segregated surfactant on surface hydrophilicity, which is important for film sealing. An extension to this would be undertaking normal force measurements to determine the adhesion between two model films, and monitoring the interdiffusion of PVA using a deuterium-labelled polymer. Through this, the role of segregated surfactant on seal formation in simple model systems could be better understood. The use of deuterated PVA could also help to better resolve the distribution of film components in model systems.

Bibliography

[1] N. Ben Halima, *RSC Advances*, 2016, **6**, 39823–39832.

[2] M. Lim, D. Kim and J. Seo, *Polymer International*, 2016, **65**, 400–406.

[3] S. Jiang, S. Liu and W. Feng, *Journal of the Mechanical Behavior of Biomedical Materials*, 2011, **4**, 1228–1233.

[4] S. M. Pawde and K. Deshmukh, *Journal of Applied Polymer Science*, 2008, **109**, 3431–3437.

[5] A. Rafique, K. M. Zia, M. Zuber, S. Tabasum and S. Rehman, *International Journal of Biological Macromolecules*, 2016, **87**, 141–154.

[6] N. E. Vrana, Y. Liu, G. B. McGuinness and P. A. Cahill, *Macromolecular Symposia*, 2008, **269**, 106–110.

[7] C. M. Hassan and N. A. Peppas, in *Biopolymers · PVA Hydrogels, Anionic Polymerisation Nanocomposites*, Springer Berlin Heidelberg, Berlin, Heidelberg, 2000, pp. 37–65.

[8] C. H. Lee and W. H. Hong, *Journal of Membrane Science*, 1997, **135**, 187–193.

[9] T. Congdon, P. Shaw and M. I. Gibson, *Polymer Chemistry*, 2015, **6**, 4749.

[10] F. L. Marten, in *Kirk-Othmer Encyclopedia of Chemical Technology*, John Wiley & Sons, Inc., Hoboken, NJ, USA, 2000.

[11] M. Mohsin, A. Hossin and Y. Haik, *Journal of Applied Polymer Science*, 2011, **122**, 3102–3109.

[12] T. G. Fox and P. J. Flory, *Journal of Applied Physics*, 1950, **21**, 581–591.

[13] L. H. Cheng, A. A. Karim and C. C. Seow, *Journal of Food Science*, 2006, **71**, E62–E67.

[14] B. Cuq, N. Gontard, J.-L. Cuq and S. Guilbert, *J. Agric. Food. Chem.*, 1997, **45**, 622–626.

[15] I. G. Donhowe and O. Fennema, *Journal of Food Processing and Preservation*, 1993, **17**, 247–257.

[16] J. Gueguen, G. Viroben, P. Noireaux and M. Subirade, *Industrial Crops and Products*, 1998, **7**, 149–157.

[17] R. Sothornvit and J. M. Krochta, *Journal of Food Engineering*, 2001, **50**, 149–155.

[18] M. Mohsin, A. Hossin and Y. Haik, *Materials Science & Engineering A*, 2010, **528**, 925–930.

[19] Y. Han Cho, B. Chul Kim and K. Sik Dan, *Macromolecular Research*, 2009, **17**, 591–596.

[20] R. M. Hodge, G. H. Edward and G. P. Simon, *Polymer*, 1996, **37**, 1371–1376.

[21] B. Wang, S. Mukataka, M. Kodama and E. Kokufuta, *Langmuir*, 1997, **13**, 6108–6114.

[22] L. I. Atanase and G. Riess, *Colloids and Surfaces a-Physicochemical and Engineering Aspects*, 2010, **355**, 29–36.

[23] B. M. Budhlall, K. Landfester, E. D. Sudol, V. L. Dimonie, A. Klein and M. S. El-Aasser, *Macromolecules*, 2003, **36**, 9477–9484.

[24] F. F. Nord, M. Bier and S. N. Timasheff, *Journal of the American Chemical Society*, 1951, **73**, 289–293.

[25] S. N. Timasheff, M. Bier and F. F. Nord, *Proceedings of the National Academy of Sciences of the United States of America*, 1949, **35**, 364–368.

[26] T. Shiomi, K. Imai, C. Watanabe and M. Miya, *Journal of Polymer Science Part B-Polymer Physics*, 1984, **22**, 1305–1312.

[27] K. Furusawa and T. Tagawa, *Colloid and Polymer Science*, 1985, **263**, 353–360.

[28] N. J. Crowther, D. Eagland, F. F. Vercauteren and W. A. B. Donners, *European Polymer Journal*, 1993, **29**, 1553–1561.

[29] A. Bhattacharya and P. Ray, *Journal of Applied Polymer Science*, 2004, **93**, 122–130.

[30] S. Matsuzawa, K. Yamaura, N. Yoshimoto, I. Horikawa and M. Kuroiwa, *Colloid & Polymer Sci*, 1980, **258**, 131–135.

[31] J. De Feijter and J. Benjamins, *Journal of Colloid and Interface Science*, 1981, **81**, 91–107.

[32] C. J. Moll, K. Meister, J. Kirschner and H. J. Bakker, *The Journal of Physical Chemistry B*, 2018, **122**, 10722–10727.

[33] R. Rošic, J. Pelipenko, J. Kristl, P. Kocbek, M. Bešter-Rogač and S. Baumgartner, *European Polymer Journal*, 2013, **49**, 290–298.

[34] I. W. Hamley, *Introduction to Soft Matter*, John Wiley & Sons, Ltd, Chichester, UK, 2007.

[35] W. Griffin, *Journal of Cosmetic Science*, 1949, **1**, 311–326.

[36] W. Griffin, *Journal of the Society of Cosmetic Chemists*, 1954, **5**, 249–256.

[37] J. T. Davies, Gas/Liquid and Liquid/Liquid Interface (Proceedings of the International Congress of Surface Activity), 1957, pp. 426–438.

[38] R. L. Baldwin, *FEBS Letters*, 2013, **587**, 1062–1066.

[39] N. Khan, B. Brettmann, N. Khan and B. Brettmann, *Polymers*, 2019, **11**, 51.

[40] I. Quijada-Garrido, M. F. de Velasco-Ruiz and J. M. Barrales-Rienda, *Macromolecular Chemistry and Physics*, 2000, **201**, 375–381.

[41] K. J. Edler, M. J. Wasbrough, J. A. Holdaway and B. M. D. O'Driscoll, *Langmuir*, 2009, **25**, 4047–4055.

[42] R. A. Campbell and K. J. Edler, *Soft Matter*, 2011, **7**, 11125.

[43] M. Wakabayashi, T. Kohno, T. Kimura, S. Tamura, M. Endoh, S. Ohnishi, T. Nishioka, Y. Tanaka and T. Kanai, *Journal of Applied Polymer Science*, 2007, **104**, 3751–3757.

[44] M. Wakabayashi, T. Kohno, T. Kimura, S. Tamura, M. Endoh, S. Ohnishi, T. Nishioka, Y. Tanaka and T. Kanai, *Journal of Applied Polymer Science*, 2007, **106**, 1398–1404.

[45] E. Goddard, *Colloids and Surfaces*, 1986, **19**, 255–300.

[46] C. D. Bain, P. M. Claesson, D. Langevin, R. Meszaros, T. Nylander, C. Stubenrauch, S. Titmuss and R. von Klitzing, *Advances in Colloid and Interface Science*, 2010, **155**, 32–49.

[47] D. J. F. Taylor, R. K. Thomas and J. Penfold, *Advances in Colloid and Interface Science*, 2007, **132**, 69–110.

[48] E. Guzmán, S. Llamas, A. Maestro, L. Fernández-Peña, A. Akanno, R. Miller, F. Ortega and R. G. Rubio, *Advances in Colloid and Interface Science*, 2016, **233**, 38–64.

[49] R. Nagarajan, New Horizons: Detergents for the New Millennium Conference Invited Papers, Fort Myers, Florida, 2001.

[50] K. Shirahama and N. Ide, *Journal of Colloid and Interface Science*, 1976, **54**, 450–452.

[51] M. N. Jones, *Journal of Colloid and Interface Science*, 1967, **23**, 36–42.

[52] H. Lange, *Kolloid-Zeitschrift and Zeitschrift Fur Polymere*, 1971, **243**, 101–109.

[53] H. Lange and K. H. Beck, *Kolloid-Zeitschrift und Zeitschrift für Polymere*, 1973, **251**, 424–431.

[54] A. Dan, S. Ghosh and S. P. Moulik, *Journal of Physical Chemistry B*, 2008, **112**, 3617–3624.

[55] S. Saito and M. Yukawa, *Journal of Colloid and Interface Science*, 1969, **30**, 211–218.

[56] J. Penfold, I. Tucker, R. K. Thomas and J. Zhang, *Langmuir*, 2005, **21**, 10061–10073.

[57] M. Moglianetti, P. Li, F. L. G. Malet, S. P. Armes, R. K. Thomas and S. Titmuss, *Langmuir*, 2008, **24**, 12892–12898.

[58] R. Meszaros, I. Varga and T. Gilanyi, *Journal of Physical Chemistry B*, 2005, **109**, 13538–13544.

[59] K. Lewis and C. Robinson, *Journal of Colloid and Interface Science*, 1970, **32**, 539–546.

[60] Y. Liu, Z. Wu and Y. Zhao, *Thermochimica Acta*, 2015, **602**, 78–86.

[61] H. Arai and S. Horin, *Journal of Colloid and Interface Science*, 1969, **30**, 372–377.

[62] K. Shirahama, M. Ohishi and N. Takisawa, *Colloids and Surfaces*, 1989, **40**, 261–266.

[63] K. Shirahama and S. Nagao, *Colloids and Surfaces*, 1992, **66**, 275–279.

[64] C. Damas, T. Leprince, T. H. V. Ngo and R. Coudert, *Colloid and Polymer Science*, 2008, **286**, 999–1007.

[65] T. F. Tadros, *Journal of Colloid and Interface Science*, 1974, **46**, 528–540.

[66] X. Fang and O. Vitrac, *Critical Reviews in Food Science and Nutrition*, 2017, **57**, 275–312.

[67] I. S. Arvanitoyannis and L. Bosnea, *Critical Reviews in Food Science and Nutrition*, 2004, **44**, 63–76.

[68] N. Dulal, R. Shanks, D. Chalmers, B. Adhikari and H. Gill, *Journal of Applied Polymer Science*, 2018, **135**, 46822.

[69] T. F. Schaub, G. J. Kellogg, A. M. Mayes, Kulasekere. R/, J. F. Ankner and H. Kaiser, *Macromolecules*, 1996, **29**, 3982–3990.

[70] A. Rezaei Kolahchi, A. Ajji and P. J. Carreau, *The Journal of Physical Chemistry B*, 2014, **118**, 6316–6323.

[71] M. Torstensson, B. Ranby and A. Hult, *Macromolecules*, 1990, **23**, 126–132.

[72] V. M. Datla, E. Shim and B. Pourdeyhimi, *Journal of Applied Polymer Science*, 2011, **121**, 1335–1347.

[73] S. Zhu and D. E. Hirt, *J. Vinyl. Addit. Technol.*, 2007, **13**, 57–64.

[74] V. R. Gundabala, W. B. Zimmerman and A. F. Routh, *Langmuir*, 2004, **20**, 8721–8727.

[75] X. Chen, S. Fischer, Z. Yi, V. Boyko, A. Terrenoire, F. Reinhold, J. Rieger, X. Li and Y. Men, *Langmuir*, 2011, **27**, 8458–8463.

[76] H. Wagner and G. Fischer, *Kolloid-Zeitschrift*, 1936, **77**, 12–20.

[77] A. Tzitzinou, P. M. Jenneson, A. S. Clough, J. L. Keddie, J. R. Lu, P. Zhdan, K. E. Treacher and R. Satguru, *Progress in Organic Coatings*, 1999, **35**, 89–99.

[78] W. P. Lee, V. R. Gundabala, B. S. Akpa, M. L. Johns, C. Jeynes and A. F. Routh, *Langmuir*, 2006, **22**, 5414–5320.

[79] F. Belaroui, M. Hirn, Y. Grohens, P. Marie and Y. Holl, *Journal of Colloid and Interface Science*, 2003, **261**, 336–348.

[80] D. Juhué, Y. Wang, J. Lang, O.-M. Leung, M. C. Goh and M. A. Winnik, *Journal of Polymer Science Part B: Polymer Physics*, 1995, **33**, 1123–1133.

[81] C. L. Zhao, Y. Holl, T. Pith and M. Lambla, *Colloid & Polymer Science*, 1987, **265**, 823–829.

[82] E. Kientz and Y. Holl, *Colloids and Surfaces a-Physicochemical and Engineering Aspects*, 1993, **78**, 255–270.

[83] S. Hu, J. Rieger, Y. Lai, S. V. Roth, R. Gehrke and Y. Men, *Macromolecules*, 2008, **41**, 5073–5076.

[84] S. Hu, J. Rieger, Z. Yi, J. Zhang, X. Chen, S. V. Roth, R. Gehrke and Y. Men, *Langmuir*, 2010, **26**, 13216–13220.

[85] M. Joanicot, K. Wong and B. Cabane, *Macromolecules*, 1996, **29**, 4976–4984.

[86] F. Belaroui, B. Cabane, M. Dorget, Y. Grohens, P. Marie and Y. Holl, *Journal of Colloid and Interface Science*, 2003, **262**, 409–417.

[87] C. L. Zhao, Y. Holl, T. Pith and M. Lambla, *British Polymer Journal*, 1989, **21**, 155–160.

[88] C. L. Zhao, F. Dobler, T. Pith, Y. Holl and M. Lambla, *Journal of Colloid and Interface Science*, 1989, **128**, 437–469.

[89] K. W. Evanson and M. W. Urban, *Journal of Applied Polymer Science*, 1991, **42**, 2309–2320.

[90] K. W. Evanson, T. A. Thorstenson and M. W. Urban, *Journal of Applied Polymer Science*, 1991, **42**, 2297–2307.

[91] Y. Zhao and M. W. Urban, *Langmuir*, 2000, **16**, 9439–9447.

[92] Y. Zhao and M. W. Urban, *Macromolecules*, 2000, **33**, 2184–2191.

[93] M. Geoghegan, T. Nicolai, J. Penfold and R. A. L. Jones, *Macromolecules*, 1997, **30**, 4220–4227.

[94] H. Lee and L. A. Archer, *Macromolecules*, 2001, **34**, 4572–4579.

[95] S. Affrossman, M. Hartshorne, T. Kiff, R. A. Pethrick and R. W. Richards, *Macromolecules*, 1994, **27**, 1588–1591.

[96] M. O. Hunt, A. M. Belu, R. W. Linton and J. M. DeSimone, *Macromolecules*, 1993, **26**, 4854–4859.

[97] J. F. Elman, B. D. Johs, T. E. Long and J. T. Koberstein, *Macromolecules*, 1994, **27**, 5341–5349.

[98] D. R. Iyengar, S. M. Perutz, C.-A. Dai, C. K. Ober and E. J. Kramer, *Macromolecules*, 1996, **29**, 1229–1234.

[99] W. Chen and T. J. McCarthy, *Macromolecules*, 1999, **32**, 2342–2347.

[100] J. Reignier and B. D. Favis, *Macromolecules*, 2000, **33**, 6998–7008.

[101] J. Reignier, B. D. Favis and M.-C. Heuzey, *Polymer*, 2003, **44**, 49–59.

[102] A. R. Zanjanijam, S. Hakim and H. Azizi, *Polymer Bulletin*, 2018, **75**, 4671–4689.

[103] D. van Krevelen and K. te Nijenhuis, *Properties of Polymers*, 2009, pp. 1–1031.

[104] W. D. Harkins and A. Feldman, *Journal of the American Chemical Society*, 1922, **44**, 2665–2685.

[105] A. Taguet, M. A. Huneault and B. D. Favis, *Polymer*, 2009, **50**, 5733–5743.

[106] S. Hobbs, M. Dekkers and V. Watkins, *Polymer*, 1988, **29**, 1598–1602.

[107] H. F. Guo, S. Packirisamy, N. V. Gvozdic and D. J. Meieri, *Polymer*, 1997, **38**, 785–794.

[108] M. Hemmati, H. Nazokdast and H. Shariat Panahi, *Journal of Applied Polymer Science*, 2001, **82**, 1129–1137.

[109] C. A. de Freitas, T. S. Valera, A. M. Catelli de Souza and N. R. Demarquette, *Macromolecular Symposia*, 2007, **247**, 260–270.

[110] R. A. L. Jones and R. W. Richards, *Polymers at Surfaces and Interfaces*, Cambridge University Press, New York, 1999.

[111] S. K. Kumar and T. P. Russell, *Macromolecules*, 1991, **24**, 3816–3820.

[112] H. Lee and L. A. Archer, *Polymer*, 2002, **43**, 2721–2728.

[113] A. Hariharan, S. K. Kumar and T. P. Russell, *The Journal of Chemical Physics*, 1993, **99**, 4041–4050.

[114] A. Hariharan, S. K. Kumar and T. P. Russell, *J. Chem. Phys*, 1993, **98**, 4163.

[115] A. Hariharan, S. K. Kumar and T. P. Russell, *Surface Segregation in Binary Polymer Mixtures: A Lattice Model*, 1991.

[116] K. Tanaka, A. Takahara and T. Kajiyama, *Macromolecules*, 1998, **31**, 863–869.

[117] M. L. Huggins, *The Journal of Chemical Physics*, 1941, **9**, 440–440.

[118] P. J. Flory, *The Journal of Chemical Physics*, 1941, **9**, 660–660.

[119] H. B. Eitouni and N. P. Balsara, in *Physical Properties of Polymers Handbook*, ed. J. E. Mark, Springer, 2nd edn., 2007, pp. 93–339.

[120] C. C. Hsu and J. M. Prausnitz, *Macromolecules*, 1974, **7**, 320–324.

[121] V. Y. Senichev and V. V. Tereshatov, in *Handbook of Plasticizers*, ChemTec Publishing, 2017, pp. 135–164.

[122] M. Foroutan and M. Zarrabi, *The Journal of Chemical Thermodynamics*, 2008, **40**, 935–941.

[123] J. H. Hildebrand, *The Solubility of Nonelectrolytes*, Reinhold Pub. Corp., New York, 3rd edn., 1950.

[124] W. Zeng, D. Y., Y. Xue and H. L. Frisch, in *Physical Properties of Polymers Handbook*, 2007, pp. 289–303.

[125] D. G. Bucknall, J. S. Higgins and S. A. Butler, *Chemical Engineering Science*, 2001, **56**, 5473–5483.

[126] Z.-W. Wang, B. Li, Q.-B. Lin and C.-Y. Hu, *Packaging Technology and Science*, 2018, **31**, 277–295.

[127] D. G. Bucknall, J. S. Higgins and S. A. Butler, *Journal of Polymer Science Part B: Polymer Physics*, 2004, **42**, 3267–3281.

[128] N. Haider and S. Karlsson, *Biomacromolecules*, 2000, **1**, 481–487.

[129] S. C. Hsu, D. Linvien and R. N. French, *Applied Spectroscopy*, 1992, **46**, 225–228.

[130] S. Y. Sankhe and D. E. Hirt, *Using Synchrotron-Based FT-IR Microspectroscopy to Study Erucamide Migration in 50-mm-thick Bilayer Linear Low-Density Polyethylene and Polyole n Plastomer Films*, 1, 2003.

[131] G. S. Smith, C. B. Skidmore, P. M. Howe and J. Majewski, *Journal of Polymer Science Part B-Polymer Physics*, 2004, **42**, 3258–3266.

[132] S. R. Lustig and N. A. Peppas, *Journal of Applied Polymer Science*, 1987, **33**, 533–549.

[133] I. Quijada-Garrido, J. M. Barrales-Rienda and G. Frutos, *Macromolecules*, 1996, **29**, 7164–7176.

[134] I. Quijada-Garrido, J. M. Barrales-Rienda, L. Alejo Espinoza and J. L. G. Fierro, *Macromolecules*, 1996, **29**, 8791–8797.

[135] J. A. Taraszka and R. G. Weiss, *Macromolecules*, 1997, **30**, 2467–2473.

[136] M. Wakabayashi, T. Kohno, Y. Tanaka and T. Kanai, *International Polymer Processing*, 2009, **24**, year.

[137] O. Vitrac, J. Lézervant and A. Feigenbaum, *Journal of Applied Polymer Science*, 2006, **101**, 2167–2186.

[138] X. Fang, S. Domenek, V. Ducruet, M. Réfrégiers and O. Vitrac, *Macromolecules*, 2013, **46**, 874–888.

[139] A. Reynier, P. Dole, S. Humbel and A. Feigenbaum, *Journal of Applied Polymer Science*, 2001, **82**, 2422–2433.

[140] M. Hakkarainen, in *Chromatography for Sustainable Polymeric Materials*, Springer Berlin Heidelberg, Berlin, Heidelberg, 2008, pp. 159–185.

[141] P. D. Calvert and N. C. Billingham, *Journal of Applied Polymer Science*, 1979, **24**, 357–370.

[142] X.-F. Wei, E. Linde and M. S. Hedenqvist, *npj Materials Degradation*, 2019, **3**, 18.

[143] I. R. Bellobono, B. Marcandalli, E. Selli, A. Polissi and G. Leidi, *Journal of Applied Polymer Science*, 1984, **29**, 3185–3195.

[144] G. S. Smith, C. B. Skidmore, P. M. Howe and J. Majewski, *Journal of Polymer Science Part B: Polymer Physics*, 2004, **42**, 3258–3266.

[145] G. Wypych, *Handbook of plasticizers*, Elsevier Science, 2017.

[146] A. Sinha and B. Sharma, *Materials Research Bulletin*, 2002, **37**, 407–416.

[147] A. Briddick, *Ph.D. thesis*, 2017.

[148] J. Higgins and H. Benoit, *Polymers and neutron scattering*, Oxford University Press, Oxford, 1st edn., 1996.

[149] B. J. Gabrys, *Applications of neutron scattering to soft condensed matter*, Gordon & Breach, 2000, p. 362.

[150] A. J. Jackson, *Introduction to Small-Angle Neutron Scattering and Neutron Reflectometry*, 2008.

[151] M. Doucet, J. H. Cho, G. Alina, J. Bakker, W. Bouwman, P. Butler, K. Campbell, M. Gonzales, R. Heenan, A. Jackson, P. Juhas, S. King, P. Kienzle, J. Krzywon, A. Markvardsen, T. Nielsen, L. O'Driscoll, W. Potrzebowski, R. Ferraz Leal, T. Richter, P. Rozycko, T. Snow and A. Washington, *SasView version 4.2*, 2018, `http://www.sasview.org/contact.html`.

[152] J. Penfold and R. K. Thomas, *Journal of Physics: Condensed Matter*, 1990, **2**, 1369–1412.

[153] M. L. Goldberger and F. Seitz, *Physical Review*, 1947, **71**, 294–310.

[154] M. Born and E. Wolf, *Principles of optics : electromagnetic theory of propagation, interference and diffraction of light*, Pergammon, Oxford, 6th edn., 1980.

[155] F. Abelès, *Annales de Physique*, 1950, **12**, 596–640.

[156] O. S. Heavens, *Optical properties of solid thin films*, 1955.

[157] A. Nelson, *Journal of Applied Crystallography*, 2006, **39**, 273–276.

[158] C. A. Schneider, W. S. Rasband and K. W. Eliceiri, *Nature Methods*, 2012, **9**, 671–675.

[159] R. J. Composto, R. M. Walters and J. Genzer, *Materials Science & Engineering R-Reports*, 2002, **38**, 107–180.

[160] R. L. Thompson, in *Polymer Science: A Comprehensive Reference*, ed. K. Matyjaszwewski M. and Moller, Elsevier BV, Amsterdam, 2012, vol. 2, pp. 661–681.

[161] C. Jeynes, N. P. Barradas, P. K. Marriott, G. Boudreault, M. Jenkin, E. Wendler and R. P. Webb, *Journal of Physics D: Applied Physics*, 2003, **36**, R97–R126.

[162] G. Lomboy, S. Sundararajan, K. Wang and S. Subramaniam, *Cement and Concrete Research*, 2011, **41**, 1157–1166.

[163] J. Lyklema, H. P. van Leeuwen, T. van Vliet, A. M. Cazabat, A. de Keizer, B. H. Bijsterbosch, G. J. Fleer and M. A. Cohen Stuart, *Fundamentals of interface and colloid science*, 2000.

[164] Y. C. Jean, J. D. Van Horn, W.-S. Hung and K.-R. Lee, *Macromolecules*, 2013, **46**, 7133–7145.

[165] D. M. Bigg, *Polymer Engineering and Science*, 1996, **36**, 737–743.

[166] P. Kirkegaard, N. Pedersen and M. M. Eldrup, *PATFIT-88: A Data-Processing System for Positron Annihilation Spectra on Mainframe and Personal Computers*, 1989, `http://orbit.dtu.dk/files/104132675/ris{_}m{_}2740.pdf`.

[167] M. Eldrup, D. Lightbody and J. N. Sherwood, *Chemical Physics*, 1981, **63**, 51–58.

[168] A. Briddick, P. X. Li, A. Hughes, F. Courchay, A. Martinez and R. L. Thompson, *Langmuir*, 2016, **32**, 864–872.

[169] C. A. Bondi, J. L. Marks, L. B. Wroblewski, H. S. Raatikainen, S. R. Lenox and K. E. Gebhardt, *Environmental Health Insights*, 2015, **9**, 27–32.

[170] Laemmli U. K, *Nature*, 1970, **227**, 680–685.

[171] J. W. Rhim, A. Gennadios, C. Weller, M. Hanna, C. L. Weller and M. A. Hanna, *Industrial Crops and Products*, 2002, **15**, 199–205.

[172] A. P. Romani, M. H. Gehlen and R. Itri, *Langmuir*, 2005, **21**, 127–133.

[173] H. Arai, M. Murata and K. Shinoda, *Journal of Colloid and Interface Science*, 1971, **31**, 223–227.

[174] A. Briddick, R. J. Fong, E. F. D. Sabattié, P. Li, M. W. A. Skoda, F. Courchay and R. L. Thompson, *Langmuir*, 2018, **34**, 1410–1418.

[175] Y. Hendrikx, J. Charvolin, P. Kekicheff and M. Roth, *Liquid Crystals*, 1987, **2**, 677–687.

[176] P. Kekicheff, B. Cabane and M. Rawiso, *Journal de Physique Lettres*, 1984, **45**, 813–821.

[177] K. L. Browning, L. R. Griffin, P. Gutfreund, R. David Barker, L. A. Clifton, A. Hughes and S. M. Clarke, *J. Appl. Cryst*, 2014, **47**, 1638–1646.

[178] E. F. D. Sabattié, J. Tasche, M. R. Wilson, M. W. A. Skoda, A. Hughes, T. Lindner and R. L. Thompson, *Soft Matter*, 2017, **13**, 3580–3591.

[179] M. Sammalkorpi, M. Karttunen and M. Haataja, *The Journal of Physical Chemistry B*, 2009, **113**, 5863–5870.

[180] S. Wu, *The Journal of Physical Chemistry*, 1968, **72**, 3332–3334.

[181] L.-H. Lee, *Journal of Applied Polymer Science*, 1968, **12**, 719–730.

[182] K. E. Polmanteer, *Rubber Chemistry and Technology*, 1981, **54**, 1051–1080.

[183] P. J. Hoftyzer and D. W. van Krevelen, *Angewandte Makromolekulare Chemie*, 1976, **56**, 1–14.

[184] K. J. Mysels, *Langmuir*, 1986, **2**, 423–428.

[185] V. M. Coiro, M. Manigrasso, F. Mazza and G. Pochetti, *Acta Crystallogr.*, 1987, **C43**, 850–854.

[186] C. K. Bagdassarian, D. Roux, A. Ben-Shaul and W. M. Gelbart, *J. Chem. Phys*, 1991, **94**, 3030.

[187] X. Auvray, T. Perche, R. Anthore, C. Petipas, I. Rico and A. Lattes, *Langmuir*, 1991, **7**, 2385–2393.

[188] H. Sun, M. Resmini and A. Zarbakhsh, *Journal of Colloid and Interface Science*, 2018, **519**, 97–106.

[189] H. Sun, K. Zielinska, M. Resmini and A. Zarbakhsh, *Journal of Colloid and Interface Science*, 2019, **536**, 598–608.

[190] J. C. Brackman, N. M. Van Os and J. B. F. N. Engberts, *Langmuir*, 1988, **4**, 1266–1269.

[191] F. M. Winnik, *Langmuir*, 1990, **6**, 522–524.

[192] S. Bae, K. Haage, K. Wantke and H. Motschmann, *The Journal of Physical Chemistry B*, 1999, **103**, 1045–1050.

[193] K. Tajima, M. Muramatsu and T. Sasaki, *Bulletin of the Chemical Society of Japan*, 1970, **43**, 1991–1998.

[194] F. Hernáinz and A. Caro, *Variation of surface tension in aqueous solutions of sodium dodecyl sulfate in the flotation bath*, 2002.

[195] G. D. Miles and L. Shedlovsky, *The Journal of Physical Chemistry*, 1944, **48**, 57–62.

[196] J. D. Hines, R. K. Thomas, G. R., G. K. Rennie and J. Penfold, *J. Phys. Chem. B*, 1997, **101**, 9215–9223.

[197] A. Bernheim-Groswasser, E. Wachtel and Y. Talmon, *Langmuir*, 2000, **16**, 4131–4140.

[198] K. Shinzawa-ltoh, H. Ueda, S. Yoshikawa, H. Aoyama, E. Yamashita and T. Tsukihara, *Journal of Molecular Biology*, 1995, **246**, 572–575.

[199] J. Brinck and F. Tiberg, *Langmuir*, 1996, **12**, 5042–5047.

[200] J. M. Neugebauer, in *Methods in Enzymology*, Academic Press, 1990, vol. 182, pp. 239–253.

[201] S. P. Moulik, M. E. H. Haque, P. K. Jana and A. R. Das, *J, Phys. Chem*, 1996, **100**, 701–708.

[202] A. Cifuentes, J. L. Bernal and J. C. Diez-Masa, *Anal. Chem.*, 1997, **69**, 4271–4274.

[203] K. Takamura, H. Fischer and N. R. Morrow, *Journal of Petroleum Science and Engineering*, 2012, **98-99**, 50–60.

[204] A. Hamel, M. Sacco, N. Mnasri, F. Lamaty, J. Martinez, F. De Angelis, E. Colacino and C. Charnay, *ACS Sustainable Chemistry & Engineering*, 2014, **2**, 1353–1358.

[205] G. D'Errico, D. Ciccarelli and O. Ortona, *Journal of Colloid and Interface Science*, 2005, **286**, 747–754.

[206] T. Wärnheim and A. Jönsson, *Journal of Colloid and Interface Science*, 1988, **125**, 627–633.

[207] P. Kékicheff, C. Grabielle-Madelmont and M. Ollivon, *Journal of Colloid and Interface Science*, 1989, **131**, 112–132.

[208] W. N. Maclay, *Journal of Colloid Science*, 1956, **11**, 272–285.

[209] K. Sharma, S. R. Patil and A. K. Rakshit, *Colloids and Surfaces A: Physicochemical and Engineering Aspects*, 2003, **219**, 67–74.

[210] *FAIRY Safety Data Sheet*.

[211] *Final Report on the Safety Assessment of Lauramine Oxide and Stearamine Oxide*, 1994.

[212] C. R. Birnie, D. Malamud and R. L. Schnaare, 2000, **44**, 2514–2517.

[213] S. Ikeda, M.-A. Tsunoda and H. Maeda, *Journal of Colloid and Interface Science*, 1978, **67**, 336–348.

[214] D. J. Barlow, M. J. Lawrence, T. Zuberi, S. Zuberi and R. K. Heenan, *Langmuir*, 2000, **16**, 10398–10403.

[215] W. Warisnoicharoen, A. B. Lansley and M. J. Lawrence, *International Journal of Pharmaceutics*, 2000, **198**, 7–27.

[216] C. D. Lorenz, C.-M. Hsieh, C. A. Dreiss and M. J. Lawrence, *Langmuir*, 2011, **27**, 546–553.

[217] M. Baglioni, Y. J. Benavides, D. Berti, R. Giorgi, U. Keiderling and P. Baglioni, *Journal of Colloid and Interface Science*, 2015, **440**, 204–210.

[218] H. Maeda and R. Kakehashi, *Advances in Colloid and Interface Science*, 2000, **88**, 275–293.

[219] E. Ruckenstein, G. Huber and H. Hoffmann, *Langmuir*, 1987, **3**, 382–387.

[220] J. C. Brackman and J. B. F. N. Engberts, *Langmuir*, 1992, **8**, 424–428.

[221] E. Poptoshev and P. M. Claesson, *Colloids and Surfaces A: Physicochemical and Engineering Aspects*, 2006, **291**, 45–50.

[222] D. Ngo and S. Baldelli, *The Journal of Physical Chemistry B*, 2016, **120**, 12346–12357.

[223] F. Tiberg and M. Landgren, *Langmuir*, 1993, **9**, 927–932.

[224] J. C. Schulz, G. G. Warr, W. A. Hamilton and P. D. Butler, *J. Phys. Chem. B*, 1999, **103**, 11057–11063.

[225] H. Kawasaki, M. Syuto and H. Maeda, *Langmuir*, 2001, **17**, 8210–8216.

[226] C. van Oss, M. Chaudhury and R. Good, *Advances in Colloid and Interface Science*, 1987, **28**, 35–64.

[227] F. Tokiwa and K. Ohki, *The Journal of Physical Chemistry*, 1966, **70**, 3437–3441.

[228] H. Maeda, M. Tsunoda and S. Ikeda, *The Journal of Physical Chemistry*, 1974, **78**, 1086–1090.

[229] H. Maeda, *Colloids and Surfaces A: Physicochemical and Engineering Aspects*, 1996, **109**, 263–271.

[230] H. Maeda, S. Muroi and R. Kakehashi, *J. Phys. Chem. B*, 1997, **101**, 7378–7382.

[231] E. P. Serjeant and B. Dempsey, *Ionisation Constants of Organic Acids in Aqueous Solution. International Union of Pure and Applied Chemistry (IUPAC). IUPAC Chemical Data Series No. 23.*, Permagon, Oxford, 1979, p. 384.

[232] B. Sarkar, S. Lam and P. Alexandridis, *Langmuir*, 2010, **26**, 10532–10540.

[233] *N,N-Dimethyldodecylamine N-oxide Safety Data Sheet*, `https://www.sigmaaldrich.com/MSDS/MSDS/DisplayMSDSPage.do?country=GB{&}language=en{&}productNumber=40234{&}brand=SIGMA{&}PageToGoToURL=https{%}3A{%}2F{%}2Fwww.sigmaaldrich.com{%}2Fcatalog{%}2Fproduct{%}2Fsigma{%}2F40234{%}3Flang{%}3Den`.

[234] *United States Environmental Protection Agency*, `https://comptox.epa.gov/dashboard/DTXSID1026906`.

[235] E. F. D. Sabattié, *Ph.D. thesis*, 2017.

[236] *Sodium Dodecyl Sulfate Safety Data Sheet*, https://www.sigmaaldrich.com/MSDS/MSDS/DisplayMSDSPage.do?country=GB{&}language=en{&}productNumber=L3771{&}brand=SIGMA{&}PageToGoToURL=https{%}3A{%}2F{%}2Fwww.sigmaaldrich.com{%}2Fcatalog{%}2Fproduct{%}2Fsigma{%}2Fl3771{%}3Flang{%}3Den.

[237] M. Hedenqvist and U. W. Gedde, *Progress in Polymer Science*, 1996, **21**, 299–333.

[238] C. A. Shuler, A. V. Janorkar and D. E. Hirt, *Polymer Engineering and Science*, 2004, **44**, 2247–2253.

[239] A. Hariharan, S. K. Kumar and T. P. Russell, *Macromolecules*, 1990, **23**, 3584–3592.

[240] P. M. Holland and D. N. Rubingh, in *Mixed Surfactant Systems*, Am. Chem. Soc, 1992.

[241] K. Tsujii, N. Saito and T. Takeuchi, *The Journal of Physical Chemistry*, 1980, **84**, 2287–2291.

[242] S. Soontravanich and J. F. Scamehorn, *Journal of Surfactants and Detergents*, 2010, **13**, 13–18.

[243] E. Summerton, M. J. Hollamby, G. Zimbitas, T. Snow, A. J. Smith, J. Sommertune, J. Bettiol, C. Jones, M. M. Britton and S. Bakalis, *Journal of Colloid and Interface Science*, 2018, **527**, 260–266.

[244] H. Nakayama and K. Shinoda, *Bulletin of the Chemical Society of Japan*, 1967, **40**, 1797–1799.

[245] H. V. Tartar and R. D. Cadle, *The Journal of Physical Chemistry*, 1939, **43**, 1173–1179.

[246] H. Hoffmann and G. Poessnecker, *Langmuir*, 1994, **10**, 381–389.

[247] X. Y. Hua and M. J. Rosen, *Journal of Colloid and Interface Science*, 1988, **125**, 730–732.

[248] T. Goloub, R. Pugh and B. Zhmud, *Journal of Colloid and Interface Science*, 2000, **229**, 72–81.

[249] M. J. Rosen, *Langmuir*, 1991, **7**, 885–888.

[250] R. Fong, A. Robertson, P. Mallon and R. Thompson, *Polymers*, 2018, **10**, 1036.

[251] S. L. Anderson, E. A. Grulke, P. T. DeLassus, P. B. Smith, C. W. Kocher and B. G. Landes, *Macromolecules*, 1995, **28**, 2944–2954.

[252] R. J. Elwell and R. A. Pethrick, *European Polymer Journal*, 1990, **26**, 853–856.

[253] A. O. Porto, G. G. Silva and W. F. Magalhaes, *Journal of Polymer Science Part B: Polymer Physics*, 1999, **37**, 219–226.

[254] S. Queiroz, J. Machado, A. Porto and G. Silva, *Polymer*, 2001, **42**, 3095–3101.

[255] J. Borek and W. Osoba, *Journal of Polymer Science Part B: Polymer Physics*, 1996, **34**, 1903–1906.

[256] J. Borek and W. Osoba, *Journal of Polymer Science Part B: Polymer Physics*, 1998, **36**, 1839–1845.

[257] J. Jang and D. K. Lee, *Polymer*, 2003, **44**, 8139–8146.

[258] J. M. G. Cowie, I. McEwan, I. J. McEwen and R. A. Pethrick, *Macromolecules*, 2001, **34**, 7071–7075.

[259] H. Cao, R. Zhang, J.-p. Yuan, E. E. Abdel-Hady, M. O. Abdel-Hamed, A. M. Hammam, H. F. M Mohamed and A. M. A El-Sayed, *J. Phys.: Condens. Matter*, 1999, **11**, 4461–4467.

[260] H. F. M. Mohamed, A. M. A. El-Sayed and E. E. Abdel-Hady, *Journal of Physics: Condensed Matter*, 1999, **11**, 4461–4467.

[261] S. J. Lue, D.-T. Lee, J.-Y. Chen, C.-H. Chiu, C.-C. Hu, Y. C. Jean and J.-Y. Lai, *Journal of Membrane Science*, 2008, **325**, 831–839.

[262] S. K. Sharma, J. Prakash and P. K. Pujari, *Physical Chemistry Chemical Physics*, 2015, **17**, 29201–29209.

[263] J. Fan, W. Zhou, Q. Wang, Z. Chu, L. Yang, L. Yang, J. Sun, L. Zhao, J. Xu, Y. Liang and Z. Chen, *Journal of Membrane Science*, 2018, **549**, 581–587.

[264] M. S. Peresin, Y. Habibi, A.-H. Vesterinen, O. J. Rojas, J. J. Pawlak and J. V. Sepp{\"a}l{\"a}, *Biomacromolecules*, 2010, **11**, 2471–2477.

[265] H. F. Mohamed, Y. Ito, A. M. El-Sayed and E. E. Abdel-Hady, *Polymer*, 1996, **37**, 1529–1533.

[266] A. E. El-Samahy, N. Abdel-Rehim and A. M. A. El-Sayed, *Polymer*, 1996, **37**, 4413–4415.

[267] A. El-Sayed, E. Abdel-Hady, M. Mohsen and A. Sawaby, *Polymer Degradation and Stability*, 1995, **47**, 339–341.

[268] T. Okada, S. Nishijima, Y. Honda and Y. Kobayashi, *Journal de Physique IV Colloque*, 1993, **3**, C4291–C4294.

[269] Y. C. Jean, P. E. Mallon and D. M. Schrader, in *Principles and applications of positron and positronium chemistry*, World Scientific, Singapore, 2003, pp. 253–307.

[270] M. V. Konidari, K. G. Papadokostaki and M. Sanopoulou, *Journal of Applied Polymer Science*, 2011, **120**, 3381–3386.

[271] H. Tian, D. Liu, Y. Yao, S. Ma, X. Zhang and A. Xiang, *Journal of Food Science*, 2017, **82**, 2926–2932.

[272] M. Forsyth, P. Meakin, D. R. MacFarlane and A. J. Hill, *Journal of Physics: Condensed Matter*, 1995, **7**, 7601–7617.

[273] K. Yoshinori, H. Kenji, K. Yoshinori and H. Shigeru, *Bulletin of the Chemical Society of Japan*, 1992, **65**, 160.

[274] C. Qi, S. Zhang, Y. Wu, Y. Zhong, D. Song and T. Wang, *Journal of Polymer Science Part B: Polymer Physics*, 1999, **37**, 465–472.

[275] C. Trotzig, S. Abrahmsén-Alami and F. H. J. Maurer, *Polymer*, 2007, **48**, 3294–3305.

[276] M. C. Thimmegowda, H. B. Ravi Kumar and C. Ranganathaiah, *Journal of Applied Polymer Science*, 2004, **92**, 1355–1366.

Appendix A

Additional dSDS and $dC_{12}E_5$ Depth Profiles

Calculation of z^* and f from depth profiles of dSDS and $dC_{12}E_5$ was used to quantitatively demonstrate the effect of the inclusion of a second surfactant (Chapter 8). The obtained neutron reflecitivty, fits, and corresponding volume fraction-depth profiles are included in this appendix.

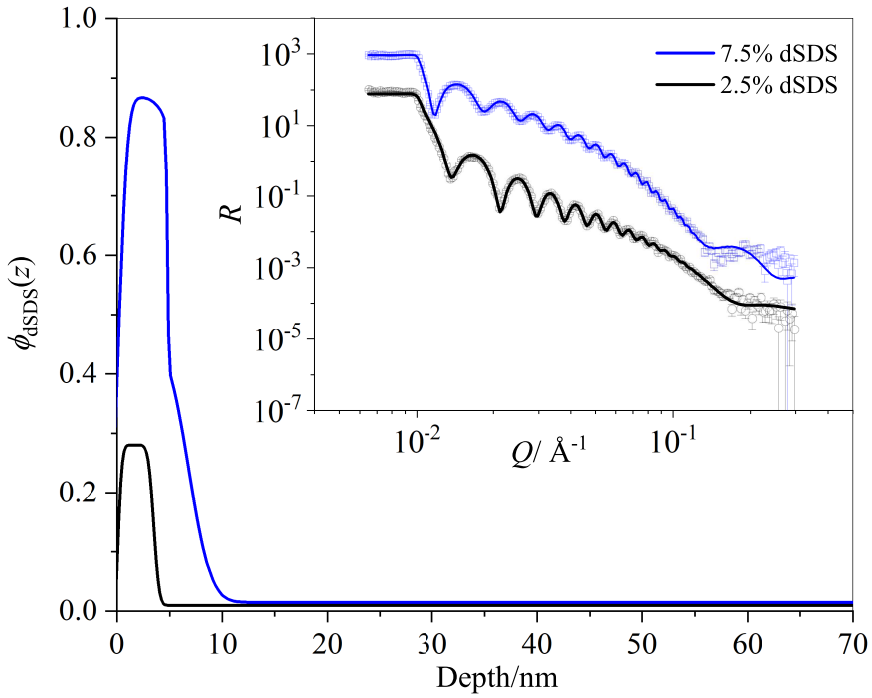

Figure A.1: Concentration-depth profiles of dSDS in PVA films. Neutron reflectivity data and fits (offset for clarity) are shown in the inset.

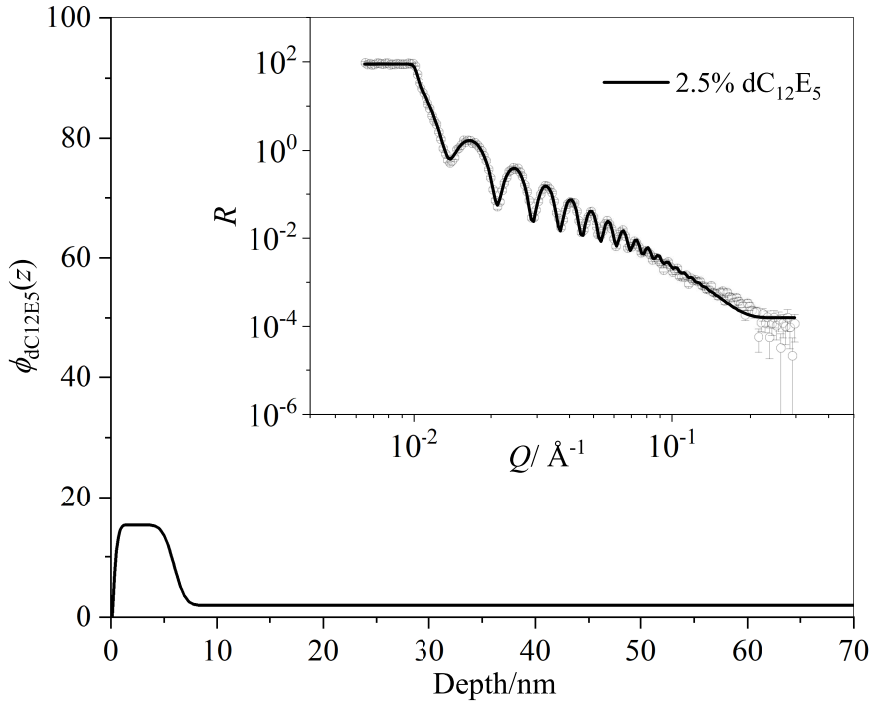

Figure A.2: Concentration-depth profiles of $dC_{12}E_5$ in PVA films. Neutron reflectivity data and fits (offset for clarity) are shown in the inset.

Appendix B

Neutron Reflectivity Fitted Parameters

PVA/SDS system

Binary Films

5 % dSDS $\chi^2 = 13.8$	Layer	Thickness/ Å	SLD/ 10^{-6} Å^{-2}	Roughness/ Å
	Fronting	∞	0	
	1	37.22	3.52	6.18
	2	872.96	0.92	4.31
	3	8.66	3.47	12.51
	Backing	∞	2.07	4.0

10 % dSDS $\chi^2 = 19.4$	Layer	Thickness/ Å	SLD/ 10^{-6} Å^{-2}	Roughness/ Å
	Fronting	∞	0	
	1	45.57	6.14	4.91
	2	954.06	0.87	3.50
	3	11.60	3.42	10.75
	Backing	∞	2.07	4.0

Plasticised Films

2 % dSDS 20 % hGly 4 % tot. solute $\chi^2 = 2.76$	Layer	Thickness/ Å	SLD/ 10^{-6} Å^{-2}	Roughness/ Å
	Fronting	∞	0	
	1	4.98	4.98	15.64
	2	537.42	0.71	18.86
	3	16.89	3.47	4.35
	Backing	∞	2.07	4.0

2 % dSDS 20 % hGly 6 % tot. solute $\chi^2 = 12.13$	Layer	Thickness/ Å	SLD/ 10^{-6} Å^{-2}	Roughness/ Å
	Fronting	∞	0	
	1	26.73	2.84	18.13
	2	1525.20	0.70	4.82
	3	46.62	3.47	3.11
	Backing	∞	2.07	4.0

2 % dSDS 20 % hGly 8 % tot. solute $\chi^2 = 13.71$	Layer	Thickness/ Å	SLD/ 10^{-6} Å^{-2}	Roughness/ Å
	Fronting	∞	0	
	1	21.87	6.22	12.16
	2	2127.70	0.74	12.89
	3	27.26	3.42	25.80
	Backing	∞	2.07	4.0

5 % dSDS 20 % hGly 4 % tot. solute $\chi^2 = 28.56$	Layer	Thickness/ Å	SLD/ 10^{-6} Å^{-2}	Roughness/ Å
	Fronting	∞	0	
	1	40.19	5.01	9.16
	2	825.67	0.88	2.52
	3	12.06	3.41	15.97
	Backing	∞	2.07	4.0

5 % dSDS 20 % hGly 6 % tot. solute $\chi^2 = 35.94$	Layer	Thickness/ Å	SLD/ 10^{-6} Å^{-2}	Roughness/ Å
	Fronting	∞	0	
	1	44.46	6.26	6.14
	2	975.07	0.81	7.05
	3	8.05	3.49	12.67
	Backing	∞	2.07	4.0

5 % dSDS 20 % hGly 8 % tot. solute $\chi^2 = 33.05$	Layer	Thickness/ Å	SLD/ 10^{-6} Å^{-2}	Roughness/ Å
	Fronting	∞	0	
	1	23.54	4.41	3.74
	2(3 repeats)	3.29	3.92	3.74
		30.68	6.79	4.81
	3	2951.50	0.83	5.21
	4	26.41	3.47	12.79
	Backing	∞	2.07	4.0

5 % dSDS 20 % hGly 10 % tot. solute $\chi^2 = 48.56$	Layer	Thickness/ Å	SLD/ 10^{-6} Å^{-2}	Roughness/ Å
	Fronting	∞	0	
	1	21.58	4.65	2.69
	2(3 repeats)	3.35	3.87	0.95
		32.71	6.75	3.88
	3	7013.60	0.98	1.44
	4	39.96	3.45	11.09
	Backing	∞	2.07	4.0

5 % dSDS 20 % hGly 12 % tot. solute $\chi^2 = 11.92$	Layer	Thickness/ Å	SLD/ 10^{-6} Å^{-2}	Roughness/ Å
	Fronting	∞	0	
	1	242.60	6.26	29.78
	2	29217	0.80	35.62
	3	25.62	3.45	8.68
	Backing	∞	2.07	4.0

10 % dSDS 20 % hGly 4 % tot. solute $\chi^2 = 6.17$	Layer	Thickness/ Å	SLD/ 10^{-6} Å^{-2}	Roughness/ Å
	Fronting	∞	0	
	1	40.49	6.33	8.64
	2	30.87	3.28	3.16
	3	633.66	0.82	3.89
	4	9.78	3.42	9.54
	Backing	∞	2.07	4.0

10 % dSDS 20 % hGly 8 % tot. solute $\chi^2 = 62.31$	Layer	Thickness/ Å	SLD/ 10^{-6} Å^{-2}	Roughness/ Å
	Fronting	∞	0	
	1	145.76	6.28	23.52
	2	3124.4	0.89	12.29
	3	37.03	3.45	5.85
	Backing	∞	2.07	4.0

10 % dSDS 20 % hGly 12 % tot. solute $\chi^2 = 18.9$	Layer	Thickness/ Å	SLD/ 10^{-6} Å^{-2}	Roughness/ Å
	Fronting	∞	0	
	1	599.51	6.55	72.11
	2	23164	0.73	14.78
	3	31.12	3.43	9.82
	Backing	∞	2.07	4.0

2 % hSDS 20 % dGly 4 % tot. solute $\chi^2 = 6.39$	Layer	Thickness/ Å	SLD/ 10^{-6} Å^{-2}	Roughness/ Å
	Fronting	∞	0	
	1	16.59	1.96	3.13
	2	544.40	1.49	15.67
	3	10.03	3.42	10.03
	Backing	∞	2.07	4.0

2 % hSDS 20 % dGly 6 % tot. solute $\chi^2 = 5.37$	Layer	Thickness/ Å	SLD/ 10^{-6} Å^{-2}	Roughness/ Å
	Fronting	∞	0	
	1	32.31	1.90	4.64
	2	985.32	1.48	11.92
	3	10.00	3.42	10.80
	Backing	∞	2.07	4.0

2 % hSDS 20 % dGly 8 % tot. solute $\chi^2 = 9.16$	Layer	Thickness/ Å	SLD/ 10^{-6} Å^{-2}	Roughness/ Å
	Fronting	∞	0	
	1	1.52	4.88	0.57
	2	32.96	0.35	9.89
	3	3296.60	1.41	0.97
	4	14.30	3.42	9.58
	Backing	∞	2.07	4.0

2 % hSDS 20 % dGly 12 % tot. solute $\chi^2 = 7.30$	Layer	Thickness/ Å	SLD/ 10^{-6} Å^{-2}	Roughness/ Å
	Fronting	∞	0	
	1	46.77	0.51	1.10
	2	11.33	2.98	4.34
	3	20.82	0.39	4.38
	4	7.52	3.24	3.59
	5	8077.20	1.60	3.99
	6	23.91	3.47	7.73
	Backing	∞	2.07	4.0

5 % hSDS 20 % dGly 6 % tot. solute $\chi^2 = 2.12$	Layer	Thickness/ Å	SLD/ 10^{-6} Å^{-2}	Roughness/ Å
	Fronting	∞	0	
	1	15.68	0.69	0.70
	2	5.35	4.48	14.04
	3	20.81	0.35	5.79
	4	6.26	4.50	7.71
	5	895.12	1.43	3.93
	6	7.80	3.47	10.24
	Backing	∞	2.07	4.0

5 % hSDS 20 % dGly 8 % tot. solute $\chi^2 = 8.81$	Layer	Thickness/ Å	SLD/ 10^{-6} Å^{-2}	Roughness/ Å
	Fronting	∞	0	
	1(3 repeats)	3.64	2.55	3.19
		34.82	0.35	3.69
	2	11.95	0.69	13.50
	3	3036.3	1.33	28.07
	4	8.79	3.47	6.18
	Backing	∞	2.07	4.0

5 % hSDS 20 % dGly 10 % tot. solute $\chi^2 = 11.11$	Layer	Thickness/ Å	SLD/ 10^{-6} Å^{-2}	Roughness/ Å
	Fronting	∞	0	
	1(5 repeats)	3.29	3.31	1.29
		35.89	0.91	1.06
	2	6316.60	1.40	38.83
	3	8.31	3.50	6.10
	Backing	∞	2.07	4.0

5 % hSDS 20 % dGly 12 % tot. solute $\chi^2 = 12.08$	Layer	Thickness/ Å	SLD/ 10^{-6} Å^{-2}	Roughness/ Å
	Fronting	∞	0	
	1(7 repeats)	4.82	3.05	1.95
		34.34	0.89	2.90
	2	6467.80	1.41	8.62
	3	12.06	3.42	7.57
	Backing	∞	2.07	4.0

10 % hSDS 20 % dGly 6 % tot. solute $\chi^2 = 6.58$	Layer	Thickness/ Å	SLD/ 10^{-6} Å^{-2}	Roughness/ Å
	Fronting	∞	0	
	1(3 repeats)	4.36	3.61	1.01
		34.46	0.94	10.57
	2	1022.20	1.46	2.30
	3	5.23	3.45	7.48
	Backing	∞	2.07	4.0

10 % hSDS 20 % dGly 12 % tot. solute $\chi^2 = 10.20$	Layer	Thickness/ Å	SLD/ 10^{-6} Å^{-2}	Roughness/ Å
	Fronting	∞	0	
	1(3 repeats)	5.49	3.27	0.10
		34.48	0.79	2.50
	2	11340	1.52	14.70
	3	13.83	3.48	1.30
	Backing	∞	2.07	4.0

PVA/*N*,*N*-dimethyldodecylamine *N*-oxide (DDAO)

Binary Films

2 % dDDAO $\chi^2 = 28.2$	Layer	Thickness/ Å	SLD/ 10^{-6} Å^{-2}	Roughness/ Å
	Fronting	∞	0	
	1	9.98	3.83	2.44
	2	979.3	0.81	5.57
	3	28.80	3.47	4.00
	Backing	∞	2.07	4.0

5 % dDDAO 3-layer model $\chi^2 = 7.34$	Layer	Thickness/ Å	SLD/ 10^{-6} Å^{-2}	Roughness/ Å
	Fronting	∞	0	
	1	11.31	4.60	5.26
	2	822.2	0.97	3.59
	3	34.5	3.47	2.59
	Backing	∞	2.07	4.0

5 % dDDAO 4-layer model $\chi^2 = 7.08$	Layer	Thickness/ Å	SLD/ 10^{-6} Å^{-2}	Roughness/ Å
	Fronting	∞	0	
	1	12.35	3.70	1.35
	2	826.15	0.95	4.47
	3	13.20	4.00	1.49
	4	19.79	3.47	5.38
	Backing	∞	2.07	4.0

10 % dDDAO $\chi^2 = 14.27$	Layer	Thickness/ Å	SLD/ 10^{-6} Å^{-2}	Roughness/ Å
	Fronting	∞	0	
	1	14.52	4.16	3.82
	2	827.27	1.38	3.26
	3	72.88	3.48	3.19
	Backing	∞	2.07	4.0

20 % dDDAO $\chi^2 = 7.56$	Layer	Thickness/ Å	SLD/ 10^{-6} Å^{-2}	Roughness/ Å
	Fronting	∞	0	
	1	12.09	4.18	2.79
	2	831.60	1.96	2.16
	3	20.06	3.47	3.41
	Backing	∞	2.07	4.0

40 % dDDAO $\chi^2 = 2.41$	Layer	Thickness/ Å	SLD/ 10^{-6} Å^{-2}	Roughness/ Å
	Fronting	∞	0	
	1	13.17	4.09	1.62
	2	758.80	2.92	2.63
	3	15.03	3.47	4.00
	Backing	∞	2.07	4.0

Plasticised Films

2 % dDDAO 20 % h-glycerol $\chi^2 = 5.14$	Layer	Thickness/ Å	SLD/ 10^{-6} Å^{-2}	Roughness/ Å
	Fronting	∞	0	
	1	8.50	3.77	3.76
	2	795.50	0.80	5.73
	3	29.44	3.47	4.00
	Backing	∞	2.07	4.0

5 % dDDAO 20 % h-glycerol $\chi^2 = 26.61$	Layer	Thickness/ Å	SLD/ 10^{-6} Å^{-2}	Roughness/ Å
	Fronting	∞	0	
	1	26.53	3.21	2.61
	2	475.64	1.15	3.75
	3	20.42	3.47	9.75
	Backing	∞	2.07	4.0

10 % dDDAO 20 % h-glycerol $\chi^2 = 7.94$	Layer	Thickness/ Å	SLD/ 10^{-6} Å^{-2}	Roughness/ Å
	Fronting	∞	0	
	1	21.10	3.62	7.63
	2	754.0	1.41	1.40
	3	25.72	3.47	3.88
	Backing	∞	2.07	4.0

20 % dDDAO 20 % h-glycerol $\chi^2 = 5.95$	Layer	Thickness/ Å	SLD/ 10^{-6} Å^{-2}	Roughness/ Å
	Fronting	∞	0	
	1	20.12	3.71	7.29
	2	443.50	1.84	5.20
	3	21.70	3.47	7.96
	Backing	∞	2.07	4.0

2 % dDDAO 20 % d-glycerol $\chi^2 = 38.61$	Layer	Thickness/ Å	SLD/ 10^{-6} Å^{-2}	Roughness/ Å
	Fronting	∞	0	
	1	14.89	3.46	3.73
	2	518.56	1.49	1.81
	3	9.06	3.41	6.78
	Backing	∞	2.07	4.0

5 % dDDAO 20 % d-glycerol $\chi^2 = 22.04$	Layer	Thickness/ Å	SLD/ 10^{-6} Å^{-2}	Roughness/ Å
	Fronting	∞	0	
	1	14.28	3.34	4.24
	2	521.99	1.40	2.56
	3	15.18	3.47	8.78
	Backing	∞	2.07	4.0

10 % dDDAO 20 % d-glycerol $\chi^2 = 22.04$	Layer	Thickness/ Å	SLD/ 10^{-6} Å^{-2}	Roughness/ Å
	Fronting	∞	0	
	1	13.64	3.20	2.29
	2	599.70	1.37	4.73
	3	47.92	3.47	2.32
	Backing	∞	2.07	4.0

20 % dDDAO 20 % d-glycerol $\chi^2 = 22.04$	Layer	Thickness/ Å	SLD/ 10^{-6} Å^{-2}	Roughness/ Å
	Fronting	∞	0	
	1	13.47	3.11	1.36
	2	522.18	1.35	1.65
	3	10.05	3.47	8.27
	Backing	∞	2.07	4.0

PVA/*N*,*N*-dimethyltetradecylamine *N*-oxide (DTAO)

Binary

20 % dDTAO $\chi^2 = 12.47$	Layer	Thickness/ Å	SLD/ 10^{-6} Å^{-2}	Roughness/ Å
	Fronting	∞	0	
	1	15.32	5.31	3.25
	2	562.12	1.78	2.18
	3	34.54	3.47	5.06
	Backing	∞	2.07	4.0

Plasticised

20 % dDTAO 20 % h-glycerol $\chi^2 = 9.58$	Layer	Thickness/ Å	SLD/ 10^{-6} Å^{-2}	Roughness/ Å
	Fronting	∞	0	
	1	16.65	4.39	4.12
	2	325.86	1.82	3.19
	3	57.37	3.47	8.85
	Backing	∞	2.07	4.0

Film Ageing

SDS

Binary

10 % dSDS 25 °C $\chi^2 = 14.92$	Layer	Thickness/ Å	SLD/ 10^{-6} Å^{-2}	Roughness/ Å
	Fronting	∞	0	
	1	60.78	6.71	9.91
	2	26.43	4.82	4.14
	3	485.91	1.20	1.37
	4	11.40	3.47	11.28
	Backing	∞	2.07	4.0

10 % dSDS 45 °C $\chi^2 = 16.00$	Layer	Thickness/ Å	SLD/ 10^{-6} Å^{-2}	Roughness/ Å
	Fronting	∞	0	
	1	59.34	6.79	10.97
	2	26.46	5.15	1.83
	3	473.70	1.24	2.17
	4	18.64	3.50	11.85
	Backing	∞	2.07	4.0

10 % dSDS 65 °C $\chi^2 = 16.66$	Layer	Thickness/ Å	SLD/ 10^{-6} Å^{-2}	Roughness/ Å
	Fronting	∞	0	
	1	62.82	6.88	18.83
	2	24.91	5.15	0.48
	3	452.93	1.25	4.65
	4	11.56	3.42	7.11
	Backing	∞	2.07	4.0

10 % dSDS 85 °C $\chi^2 = 12.80$	Layer	Thickness/ Å	SLD/ 10^{-6} Å^{-2}	Roughness/ Å
	Fronting	∞	0	
	1	74.48	6.32	24.00
	2	24.78	3.33	4.08
	3	427.83	1.19	3.36
	4	8.21	3.42	7.11
	Backing	∞	2.07	4.0

10 % dSDS 25 °C cooled $\chi^2 = 13.32$	Layer	Thickness/ Å	SLD/ 10^{-6} Å^{-2}	Roughness/ Å
	Fronting	∞	0	
	1	75.18	6.23	21.99
	2	24.83	3.44	4.22
	3	419.06	1.18	4.43
	4	8.31	3.41	7.21
	Backing	∞	2.07	4.0

Plasticised

10 % dSDS 20 % h-glycerol 25 °C $\chi^2 = 4.22$	Layer	Thickness/ Å	SLD/ 10^{-6} Å^{-2}	Roughness/ Å
	Fronting	∞	0	
	1	46.09	5.25	5.99
	2	32.86	2.12	1.16
	3	490.55	1.02	2.69
	4	14.34	3.42	11.58
	Backing	∞	2.07	4.0

10 % dSDS 20 % h-glycerol 45 °C $\chi^2 = 4.45$	Layer	Thickness/ Å	SLD/ 10^{-6} Å^{-2}	Roughness/ Å
	Fronting	∞	0	
	1	45.78	5.42	6.62
	2	36.02	2.26	4.83
	3	365.85	1.01	3.57
	4	11.10	3.43	12.49
	Backing	∞	2.07	4.0

10 % dSDS 20 % h-glycerol 65 °C $\chi^2 = 4.76$	Layer	Thickness/ Å	SLD/ 10^{-6} Å^{-2}	Roughness/ Å
	Fronting	∞	0	
	1	45.44	5.15	6.99
	2	34.50	2.43	1.94
	3	359.27	1.03	7.82
	4	11.15	3.42	11.88
	Backing	∞	2.07	4.0

10 % dSDS 20 % h-glycerol 85 °C $\chi^2 = 3.82$	Layer	Thickness/ Å	SLD/ 10^{-6} Å^{-2}	Roughness/ Å
	Fronting	∞	0	
	1	44.82	5.18	8.92
	2	33.56	2.58	4.93
	3	356.82	1.00	7.97
	4	9.19	3.42	11.80
	Backing	∞	2.07	4.0

10 % dSDS 20 % h-glycerol 25 °C cooled $\chi^2 = 3.82$	Layer	Thickness/ Å	SLD/ 10^{-6} Å^{-2}	Roughness/ Å
	Fronting	∞	0	
	1	45.67	5.43	8.76
	2	33.87	2.49	3.23
	3	362.51	0.97	5.41
	4	9.23	3.43	11.95
	Backing	∞	2.07	4.0

10 % hSDS 20 % d-glycerol 25 °C $\chi^2 = 13.84$	Layer	Thickness/ Å	SLD/ 10^{-6} Å^{-2}	Roughness/ Å
	Fronting	∞	0	
	1	54.49	2.43	4.03
	2	824.18	1.60	0.76
	3	8.16	3.47	9.34
	Backing	∞	2.07	4.0

10 % hSDS 20 % d-glycerol 85 °C $\chi^2 = 4.62$	Layer	Thickness/ Å	SLD/ 10^{-6} Å^{-2}	Roughness/ Å
	Fronting	∞	0	
	1	46.58	2.82	2.85
	2	773.21	1.55	4.31
	3	9.04	3.47	9.90
	Backing	∞	2.07	4.0

$C_{12}E_5$

Binary

10 % $dC_{12}E_5$ 25 °C $\chi^2 = 1.55$	Layer	Thickness/ Å	SLD/ 10^{-6} Å^{-2}	Roughness/ Å
	Fronting	∞	0	
	1	12.33	3.17	2.36
	2	35.25	1.28	0.97
	3	1000.30	0.71	2.76
	4	69.06	3.82	14.83
	5	26.76	3.40	8.58
	Backing	∞	2.07	4.0

10 % $dC_{12}E_5$ 45 °C $\chi^2 = 1.87$	Layer	Thickness/ Å	SLD/ 10^{-6} Å^{-2}	Roughness/ Å
	Fronting	∞	0	
	1	12.41	3.21	1.30
	2	31.36	1.32	3.96
	3	975.24	0.75	1.91
	4	68.84	3.85	17.94
	5	23.34	3.40	7.70
	Backing	∞	2.07	4.0

10 % $dC_{12}E_5$ 65 °C $\chi^2 = 1.32$	Layer	Thickness/ Å	SLD/ 10^{-6} Å^{-2}	Roughness/ Å
	Fronting	∞	0	
	1	11.69	3.25	4.33
	2	27.16	1.28	4.67
	3	963.65	0.76	1.13
	4	63.84	3.97	19.09
	5	25.88	3.44	4.84
	Backing	∞	2.07	4.0

10 % $dC_{12}E_5$ 85 °C $\chi^2 = 1.69$	Layer	Thickness/ Å	SLD/ 10^{-6} Å^{-2}	Roughness/ Å
	Fronting	∞	0	
	1	10.89	3.05	4.17
	2	29.43	1.33	6.67
	3	958.87	0.77	1.47
	4	57.19	3.92	19.54
	5	20.95	3.45	2.29
	Backing	∞	2.07	4.0

10 % $dC_{12}E_5$ 25 °C cooled $\chi^2 = 1.40$	Layer	Thickness/ Å	SLD/ 10^{-6} Å^{-2}	Roughness/ Å
	Fronting	∞	0	
	1	21.81	2.25	6.99
	2	967.64	0.90	6.76
	3	28.67	2.89	7.05
	4	22.69	3.45	5.90
	Backing	∞	2.07	4.0

Plasticised

10 % $dC_{12}E_5$ 20 % h-glycerol 25 °C $\chi^2 = 5.31$	Layer	Thickness/ Å	SLD/ 10^{-6} Å^{-2}	Roughness/ Å
	Fronting	∞	0	
	1	23.91	3.19.2.65	
	2	53.52	1.85	8.49
	3	552.42	1.16	8.84
	4	31.04	3.14	1.09
	5	19.17	3.47	3.33
	Backing	∞	2.07	4.0

10 % $dC_{12}E_5$ 20 % h-glycerol 45 °C $\chi^2 = 3.29$	Layer	Thickness/ Å	SLD/ 10^{-6} Å^{-2}	Roughness/ Å
	Fronting	∞	0	
	1	45.52	2.40	5.40
	2	539.00	1.20	5.17
	3	29.73	2.50	6.94
	4	29.97	3.47	2.55
	Backing	∞	2.07	4.0

10 % $dC_{12}E_5$ 20 % h-glycerol 65 °C $\chi^2 = 3.29$	Layer	Thickness/ Å	SLD/ 10^{-6} Å^{-2}	Roughness/ Å
	Fronting	∞	0	
	1	48.34	2.47	7.66
	2	522.73	1.26	6.93
	3	29.63	2.09	4.84
	4	29.19	3.47	4.67
	Backing	∞	2.07	4.0

10 % $dC_{12}E_5$ 20 % h-glycerol 85 °C $\chi^2 = 3.29$	Layer	Thickness/ Å	SLD/ 10^{-6} Å^{-2}	Roughness/ Å
	Fronting	∞	0	
	1	34.77	2.28	7.87
	2	500.12	1.10	7.51
	3	29.43	2.02	4.71
	4	25.57	3.47	5.69
	Backing	∞	2.07	4.0

10 % $dC_{12}E_5$ 20 % h-glycerol 25 °C cooled $\chi^2 = 4.52$	Layer	Thickness/ Å	SLD/ 10^{-6} Å^{-2}	Roughness/ Å
	Fronting	∞	0	
	1	30.70	1.90	7.17
	2	492.87	1.15	7.36
	3	29.88	1.90	3.71
	4	14.16	3.47	6.81
	Backing	∞	2.07	4.0

10 % $hC_{12}E_5$ 20 % d-glycerol 25 °C $\chi^2 = 7.66$	Layer	Thickness/ Å	SLD/ 10^{-6} Å^{-2}	Roughness/ Å
	Fronting	∞	0	
	1	27.55	3.24	5.73
	2	300.08	1.53	3.20
	3	12.24	3.41	7.97
	Backing	∞	2.07	4.0

10 % $hC_{12}E_5$ 20 % d-glycerol 85 °C $\chi^2 = 4.31$	Layer	Thickness/ Å	SLD/ 10^{-6} Å^{-2}	Roughness/ Å
	Fronting	∞	0	
	1	28.69	3.45	3.99
	2	279.44	1.63	1.07
	3	12.15	3.41	7.32
	Backing	∞	2.07	4.0

DDAO

Binary

10 % dDDAO 25 °C $\chi^2 = 5.15$	Layer	Thickness/ Å	SLD/ 10^{-6} Å^{-2}	Roughness/ Å
	Fronting	∞	0	
	1	13.39	3.29	1.10
	2	417.57	1.53	2.99
	3	24.32	3.49	2.93
	Backing	∞	2.07	4.0

10 % dDDAO 45 °C $\chi^2 = 3.04$	Layer	Thickness/ Å	SLD/ 10^{-6} Å^{-2}	Roughness/ Å
	Fronting	∞	0	
	1	11.56	3.46	3.70
	2	413.86	1.50	3.61
	3	24.82	3.49	2.24
	Backing	∞	2.07	4.0

10 % dDDAO 65 °C $\chi^2 = 3.41$	Layer	Thickness/ Å	SLD/ 10^{-6} Å^{-2}	Roughness/ Å
	Fronting	∞	0	
	1	14.87	3.45	4.42
	2	399.19	1.53	5.00
	3	21.51	3.42	4.17
	Backing	∞	2.07	4.0

10 % dDDAO 85 °C $\chi^2 = 3.41$	Layer	Thickness/ Å	SLD/ 10^{-6} Å^{-2}	Roughness/ Å
	Fronting	∞	0	
	1	12.18	2.51	8.11
	2	380.30	1.16	0.64
	3	26.67	3.50	2.07
	Backing	∞	2.07	4.0

10 % dDDAO 25 °C cooled $\chi^2 = 3.41$	Layer	Thickness/ Å	SLD/ 10^{-6} Å^{-2}	Roughness/ Å
	Fronting	∞	0	
	1	9.73	2.51	2.93
	2	387.52	1.15	1.89
	3	26.70	3.51	2.10
	Backing	∞	2.07	4.0

Plasticised

10 % dDDAO 20 % h-glycerol 25 °C $\chi^2 = 2.84$	Layer	Thickness/ Å	SLD/ 10^{-6} Å^{-2}	Roughness/ Å
	Fronting	∞	0	
	1	18.37	3.42	6.77
	2	935.18	1.36	1.94
	3	28.28	3.47	6.69
	Backing	∞	2.07	4.0

10 % dDDAO 20 % h-glycerol 45 °C $\chi^2 = 2.55$	Layer	Thickness/ Å	SLD/ 10^{-6} Å^{-2}	Roughness/ Å
	Fronting	∞	0	
	2	833.33	1.44	0.26
	3	29.10	3.41	1.88
	Backing	∞	2.07	4.0

10 % dDDAO 20 % h-glycerol 65 °C $\chi^2 = 1.21$	Layer	Thickness/ Å	SLD/ 10^{-6} Å^{-2}	Roughness/ Å
	Fronting	∞	0	
	1	833.33	1.41	1.93
	2	29.94	3.50	2.15
	Backing	∞	2.07	4.0

10 % dDDAO 20 % h-glycerol 85 °C $\chi^2 = 1.99$	Layer	Thickness/ Å	SLD/ 10^{-6} Å^{-2}	Roughness/ Å
	Fronting	∞	0	
	1	808.56	1.30	10.12
	2	30.02	3.51	2.95
	Backing	∞	2.07	4.0

10 % dDDAO 20 % h-glycerol 25 °C cooled $\chi^2 = 1.17$	Layer	Thickness/ Å	SLD/ 10^{-6} Å^{-2}	Roughness/ Å
	Fronting	∞	0	
	1	795.39	1.20	0.91
	2	31.41	3.51	2.17
	Backing	∞	2.07	4.0

10 % DDAO 20 % d-glycerol 25 °C $\chi^2 = 5.05$	Layer	Thickness/ Å	SLD/ 10^{-6} Å^{-2}	Roughness/ Å
	Fronting	∞	0	
	1	474.43	1.21	3.36
	2	9.18	3.46	2.45
	Backing	∞	2.07	4.0

10 % DDAO 20 % d-glycerol 85 °C $\chi^2 = 1.80$	Layer	Thickness/ Å	SLD/ 10^{-6} Å^{-2}	Roughness/ Å
	Fronting	∞	0	
	1	401.74	0.64	3.48
	2	14.53	3.41	7.71
	Backing	∞	2.07	4.0

Synergy of surfactant segregation

DDAO/SDS system

Non-plasticised films

2.5 % dDDAO, 7.5 % hSDS $\chi^2 = 3.57$	Layer	Thickness/ Å	SLD/ 10^{-6} Å^{-2}	Roughness/ Å
	Fronting	∞	0	
	1	43.92	2.04	29.35
	2	533.24	0.77	18.02
	3	41.85	3.41	5.72
	Backing	∞	2.07	4.0

7.5 % dDDAO, 2.5 % hSDS $\chi^2 = 12.80$	Layer	Thickness/ Å	SLD/ 10^{-6} Å^{-2}	Roughness/ Å
	Fronting	∞	0	
	1	78.91	2.08	1.06
	2	645.14	1.06	29.04
	3	82.85	2.66	5.68
	4	29.23	3.44	3.98
	Backing	∞	2.07	4.0

7.5 % hDDAO, 2.5 % dSDS $\chi^2 = 13.53$	Layer	Thickness/ Å	SLD/ 10^{-6} Å^{-2}	Roughness/ Å
	Fronting	∞	0	
	1	44.44	1.65	11.34
	2	11.29	1.49	37.87
	3	744.66	1.00	6.98
	4	10.78	3.47	7.86
	Backing	∞	2.07	4.0

2.5 % dSDS $\chi^2 = 8.87$	Layer	Thickness/ Å	SLD/ 10^{-6} Å^{-2}	Roughness/ Å
	Fronting	∞	0	
	1	34.83	2.44	3.52
	2	719.23	0.81	4.14
	3	10.80	3.46	8.84
	Backing	∞	2.07	4.0

7.5 % dSDS $\chi^2 = 4.03$	Layer	Thickness/ Å	SLD/ 10^{-6} Å^{-2}	Roughness/ Å
	Fronting	∞	0	
	1	47.60	5.91	7.32
	2	20.62	3.45	1.05
	3	821.20	0.76	16.54
	4	18.37	3.47	8.63
	Backing	∞	2.07	4.0

Plasticised films

2.5 % dDDAO, 7.5 % hSDS 20 % h-glycerol $\chi^2 = 3.57$	Layer	Thickness/ Å	SLD/ 10^{-6} Å^{-2}	Roughness/ Å
	Fronting	∞	0	
	1	43.92	2.04	29.35
	2	533.24	0.77	18.02
	3	41.85	3.41	5.72
	Backing	∞	2.07	4.0

7.5 % dDDAO, 2.5 % hSDS 20 % h-glycerol $\chi^2 = 5.81$	Layer	Thickness/ Å	SLD/ 10^{-6} Å^{-2}	Roughness/ Å
	Fronting	∞	0	
	1	24.17	2.83	3.52
	2	474.86	0.94	8.16
	3	21.38	1.72	8.01
	4	24.90	3.50	7.10
	Backing	∞	2.07	4.0

2.5 % hDDAO, 7.5 % dSDS 20 % h-glycerol $\chi^2 = 15.29$	Layer	Thickness/ Å	SLD/ 10^{-6} Å^{-2}	Roughness/ Å
	Fronting	∞	0	
	1	76.37	3.24	19.72
	2	479.70	0.98	13.29
	3	22.68	3.45	5.66
	Backing	∞	2.07	4.0

7.5 % hDDAO, 2.5 % dSDS 20 % h-glycerol $\chi^2 = 4.50$	Layer	Thickness/ Å	SLD/ 10^{-6} Å^{-2}	Roughness/ Å
	Fronting	∞	0	
	1	539.19	0.77	19.96
	2	20.56	3.47	9.81
	Backing	∞	2.07	4.0

7.5 % hDDAO, 2.5 % hSDS 20 % d-glycerol $\chi^2 = 3.99$	Layer	Thickness/ Å	SLD/ 10^{-6} Å^{-2}	Roughness/ Å
	Fronting	∞	0	
	1	43.05	0.72	18.91
	2	458.83	1.10	5.25
	3	11.50	3.47	2.95
	Backing	∞	2.07	4.0

DDAO/$C_{12}E_5$ system

Non-plasticised films

2.5 % dDDAO, 7.5 % h$C_{12}E_5$ $\chi^2 = 3.20$	Layer	Thickness/ Å	SLD/ 10^{-6} Å^{-2}	Roughness/ Å
	Fronting	∞	0	
	1	556.92	0.96	16.62
	2	36.41	3.49	12.26
	Backing	∞	2.07	4.0

7.5 % dDDAO, 2.5 % h$C_{12}E_5$ $\chi^2 = 10.30$	Layer	Thickness/ Å	SLD/ 10^{-6} Å^{-2}	Roughness/ Å
	Fronting	∞	0	
	1	14.22	2.41	1.98
	2	785.56	1.21	0.29
	3	39.18	3.42	11.58
	Backing	∞	2.07	4.0

2.5 % hDDAO, 7.5 % $dC_{12}E_5$ $\chi^2 = 2.16$	Layer	Thickness/ Å	SLD/ 10^{-6} Å^{-2}	Roughness/ Å
	Fronting	∞	0	
	1	11.43	3.33	2.63
	2	748.42	0.94	1.17
	3	31.38	2.25	3.08
	4	17.18	3.48	4.05
	Backing	∞	2.07	4.0

7.5 % hDDAO, 2.5 % $dC_{12}E_5$ $\chi^2 = 5.19$	Layer	Thickness/ Å	SLD/ 10^{-6} Å^{-2}	Roughness/ Å
	Fronting	∞	0	
	1	6.29	2.57	1.80
	2	1089.30	0.82	4.93
	3	39.10	4.36	25.64
	4	10.26	3.46	4.45
	Backing	∞	2.07	4.0

Plasticised films

2.5 % dDDAO, 7.5 % $hC_{12}E_5$ 20 % h-glycerol $\chi^2 = 3.10$	Layer	Thickness/ Å	SLD/ 10^{-6} Å^{-2}	Roughness/ Å
	Fronting	∞	0	
	1	20.12	2.08	22.39
	2	910.37	0.85	6.38
	3	16.48	4.96	15.99
	4	33.79	3.46	4.20
	Backing	∞	2.07	4.0

7.5 % dDDAO, 2.5 % $hC_{12}E_5$ 20 % h-glycerol $\chi^2 = 3.53$	Layer	Thickness/ Å	SLD/ 10^{-6} Å^{-2}	Roughness/ Å
	Fronting	∞	0	
	1	11.36	2.74	4.00
	2	645.39	1.12	1.75
	3	40.18	3.43	5.82
	Backing	∞	2.07	4.0

2.5 % hDDAO, 7.5 % $dC_{12}E_5$ 20 % h-glycerol $\chi^2 = 3.42$	Layer	Thickness/ Å	SLD/ 10^{-6} Å^{-2}	Roughness/ Å
	Fronting	∞	0	
	1	11.51	3.48	5.12
	2	612.70	0.86	3.10
	3	33.21	1.50	3.92
	4	15.24	3.47	8.57
	Backing	∞	2.07	4.0

7.5 % hDDAO, 2.5 % $dC_{12}E_5$ 20 % h-glycerol $\chi^2 = 5.82$	Layer	Thickness/ Å	SLD/ 10^{-6} Å^{-2}	Roughness/ Å
	Fronting	∞	0	
	1	381.19	0.84	16.78
	2	27.77	1.42	4.72
	3	15.98	3.41	6.13
	Backing	∞	2.07	4.0

2.5 % hDDAO, 7.5 % $hC_{12}E_5$ 20 % d-glycerol $\chi^2 = 6.21$	Layer	Thickness/ Å	SLD/ 10^{-6} Å^{-2}	Roughness/ Å
	Fronting	∞	0	
	1	362.26	1.14	20.93
	2	12.23	3.42	6.24
	Backing	∞	2.07	4.0

7.5 % hDDAO, 2.5 % $hC_{12}E_5$ 20 % d-glycerol $\chi^2 = 3.88$	Layer	Thickness/ Å	SLD/ 10^{-6} Å^{-2}	Roughness/ Å
	Fronting	∞	0	
	1	398.52	1.05	13.49
	2	11.28	3.47	6.87
	Backing	∞	2.07	4.0

SDS/$C_{12}E_5$ system

Non-plasticised films

2.5 % dSDS, 7.5 % h$C_{12}E_5$ $\chi^2 = 9.82$	Layer	Thickness/ Å	SLD/ 10^{-6} Å^{-2}	Roughness/ Å
	Fronting	∞	0	
	1	28.19	2.98	1.58
	2	13.25	3.84	2.18
	3	614.54	1.17	7.51
	4	10.04	3.49	9.81
	Backing	∞	2.07	4.0

7.5 % dSDS, 2.5 % h$C_{12}E_5$ $\chi^2 = 14.77$	Layer	Thickness/ Å	SLD/ 10^{-6} Å^{-2}	Roughness/ Å
	Fronting	∞	0	
	1	48.51	4.21	5.35
	2	34.07	1.44	2.01
	3	621.18	0.87	4.20
	4	9.32	3.45	10.82
	Backing	∞	2.07	4.0

2.5 % hSDS, 7.5 % d$C_{12}E_5$ $\chi^2 = 12.59$	Layer	Thickness/ Å	SLD/ 10^{-6} Å^{-2}	Roughness/ Å
	Fronting	∞	0	
	1	54.92	2.73	4.28
	2	39.33	1.29	2.47
	3	621.73	0.94	1.03
	4	37.49	1.89	2.22
	5	13.79	3.43	6.43
	Backing	∞	2.07	4.0

7.5 % hSDS, 2.5 % $dC_{12}E_5$ $\chi^2 = 3.88$	Layer	Thickness/ Å	SLD/ 10^{-6} Å^{-2}	Roughness/ Å
	Fronting	∞	0	
	1	45.87	1.52	5.67
	2	720.03	0.80	15.09
	3	29.49	1.56	2.90
	4	10.23	3.47	4.47
	Backing	∞	2.07	4.0

2.5 % $dC_{12}E_5$ $\chi^2 = 2.63$	Layer	Thickness/ Å	SLD/ 10^{-6} Å^{-2}	Roughness/ Å
	Fronting	∞	0	
	1	59.36	1.24	4.34
	2	729.44	0.81	8.38
	3	27.89	3.44	2.17
	Backing	∞	2.07	4.0

Plasticised films

2.5 % dSDS, 7.5 % $hC_{12}E_5$ 20 % h-glycerol $\chi^2 = 6.72$	Layer	Thickness/ Å	SLD/ 10^{-6} Å^{-2}	Roughness/ Å
	Fronting	∞	0	
	1	65.4	1.28	9.49
	2	346.89	0.80	0.13
	3	11.58	3.47	10.91
	Backing	∞	2.07	4.0

7.5 % dSDS, 2.5 % $hC_{12}E_5$ 20 % h-glycerol $\chi^2 = 3.12$	Layer	Thickness/ Å	SLD/ 10^{-6} Å^{-2}	Roughness/ Å
	Fronting	∞	0	
	1	45.46	5.06	2.52
	2	22.91	1.42	0.46
	3	390.19	0.85	1.66
	4	25.78	3.47	15.96
	Backing	∞	2.07	4.0

2.5 % hSDS, 7.5 % $dC_{12}E_5$ 20 % h-glycerol $\chi^2 = 4.20$	Layer	Thickness/ Å	SLD/ 10^{-6} Å^{-2}	Roughness/ Å
	Fronting	∞	0	
	1	45.62	1.10	6.95
	2	7.66	4.12	2.10
	3	382.09	0.96	1.88
	4	25.86	3.01	6.40
	5	25.79	3.48	9.21
	Backing	∞	2.07	4.0

7.5 % hSDS, 2.5 % $dC_{12}E_5$ 20 % h-glycerol $\chi^2 = 4.89$	Layer	Thickness/ Å	SLD/ 10^{-6} Å^{-2}	Roughness/ Å
	Fronting	∞	0	
	1	43.18	1.13	6.18
	2	8.38	4.00	2.02
	3	380.70	0.77	1.22
	4	28.40	2.88	8.13
	5	25.23	3.47	3.51
	Backing	∞	2.07	4.0

2.5 % hSDS, 7.5 % $hC_{12}E_5$ 20 % d-glycerol $\chi^2 = 7.90$	Layer	Thickness/ Å	SLD/ 10^{-6} Å^{-2}	Roughness/ Å
	Fronting	∞	0	
	1	564.35	1.23	25.61
	2	19.29	3.43	6.33
	Backing	∞	2.07	4.0

2.5 % hSDS, 7.5 % $hC_{12}E_5$ 20 % d-glycerol $\chi^2 = 7.52$	Layer	Thickness/ Å	SLD/ 10^{-6} Å^{-2}	Roughness/ Å
	Fronting	∞	0	
	1	564.35	1.23	25.61
	2	19.29	3.43	6.33
	Backing	∞	2.07	4.0

7.5 % hSDS, 2.5 % $hC_{12}E_5$ 20 % h-glycerol $\chi^2 = 7.52$	Layer	Thickness/ Å	SLD/ 10^{-6} Å^{-2}	Roughness/ Å
	Fronting	∞	0	
	1(2 repeats)	33.29	0.44	5.39
		4.63	4.26	2.40
	2	26.87	0.64	7.76
	3	901.31	1.20	2.60
	4	14.68	3.49	6.78
	Backing	∞	2.07	4.0

Appendix C

SANS Fitted Parameters

Sample	B/cm^{-1}	A	n	C	q_0/Å^{-1}	m	ξ/Å	χ^2_R
PVA	4.57	1.85E-5	2.50	0.14	0.054	1.86	31.61	1.04
2% dDDAO	4.06	2.14E-3	1.96	4.51	0.056	1.79	4.38	0.72
5% dDDAO	3.95	1.02E-2	1.47	10.58	0.057	1.64	1.91	0.72
10% dDDAO	2.71	1.00E0	0.26	14.35	0.058	1.58	35.82	1.24
20% dDDAO	8.06	1.07E-3	2.24	30.10	0.056	2.93	42.11	0.84
40% dDDAO	6.08	1.00E-2	1.68	89.65	0.038	2.45	35.93	1.01
2% dDTAO	4.21	5.10E-2	1.88	6.35	0.056	1.75	41.43	0.87
5% dDTAO	3.51	1.30E-2	1.56	16.17	0.056	1.38	31.38	0.62
10% dDTAO	3.99	2.45E-2	1.34	30.10	0.059	1.47	29.55	0.85
20% dDTAO	14.13	1.62E-3	2.32	55.49	0.056	2.00	40.92	0.92
20% gly	4.27	5.02E-10	1.43	1.31	0.050	1.56	37.77	0.69
2% dDDAO, 20% gly	2.77	5.12E-2	1.56	3.02	0.054	1.90	36.34	0.55
5% dDDAO, 20% gly	2.78	2.02E-1	0.86	8.05	0.047	1.50	31.72	0.54
10% dDDAO, 20% gly	4.97	3.90E-2	1.27	15.66	0.040	2.70	45.99	0.75
20% dDDAO, 20% gly	4.06	1.02E-2	1.69	47.05	0.035	2.90	43.77	1.08
5% dDTAO, 20% gly	3.09	2.00E-2	1.34	9.35	0.045	1.48	27.29	0.58
10% dDTAO, 20% gly	11.84	2.00E-1	1.06	33.91	0.039	2.95	43.28	0.65
20% dDTAO, 20% gly	6.47	7.00E-1	0.95	95.59	0.037	3.07	43.57	0.91
20% d-gly, 20% gly	3.09	7.92E-4	0.80	6.33	0.057	2.63	36.77	1.09
20% DDAO Contrast matched (d-gly)	5.07	1.00E-6	3.12	17.01	0.054	2.51	42.17	1.11

Appendix D

DMA

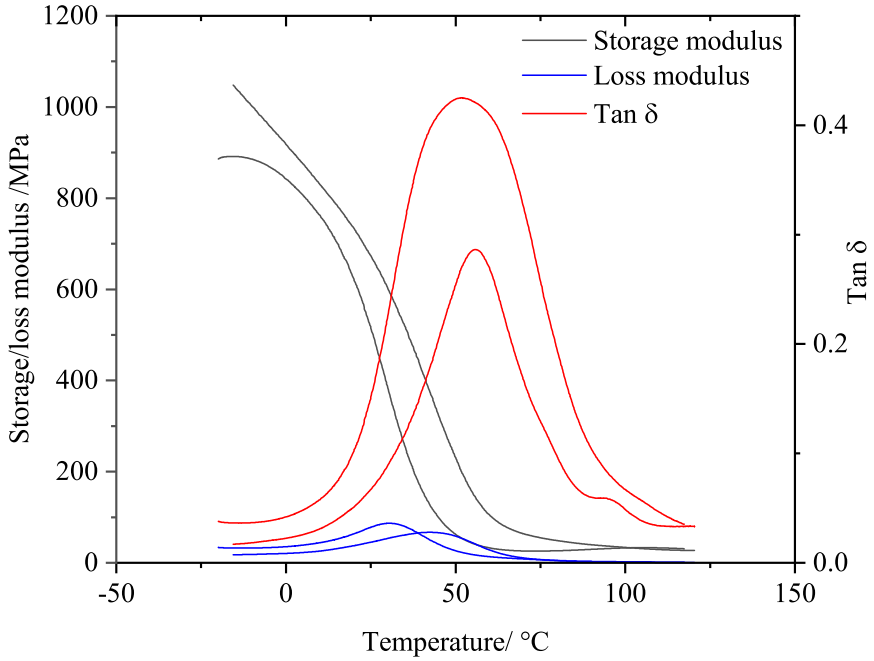

Figure D.1: DMA data used to determine T_g for a solution-cast PVA film containing 5 wt.% DDAO. The two sets of data are obtained from heating and cooling the sample, and the position of tan delta is averaged to determine T_g.

Appendix E

DSC for PVA blends

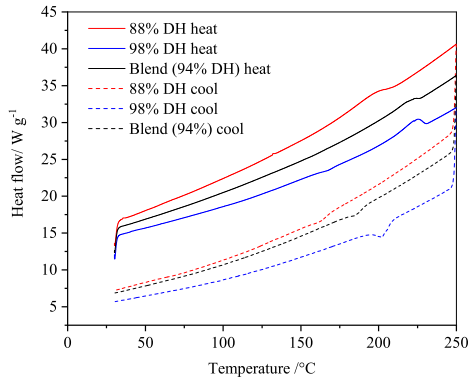

(a) 13-23 kg mol^{-1}

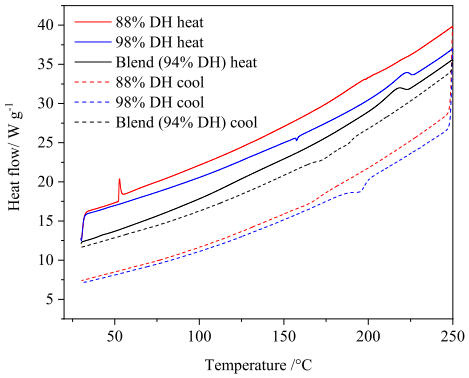

(b) 31-50 kg mol^{-1}

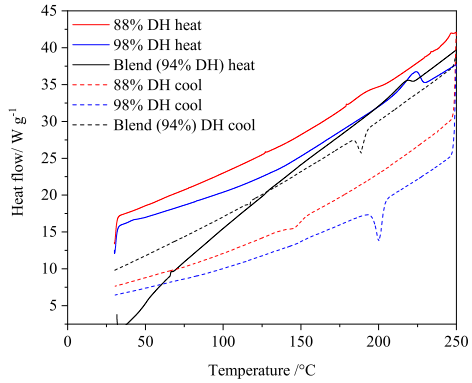

(c) 125 kg mol^{-1}

Figure E.1: DSC data for PVA of 88% DH, 98% DH and a blend of the two grades, showing an averaging of the melting points.

Appendix F

TGA for PVA/Additive films

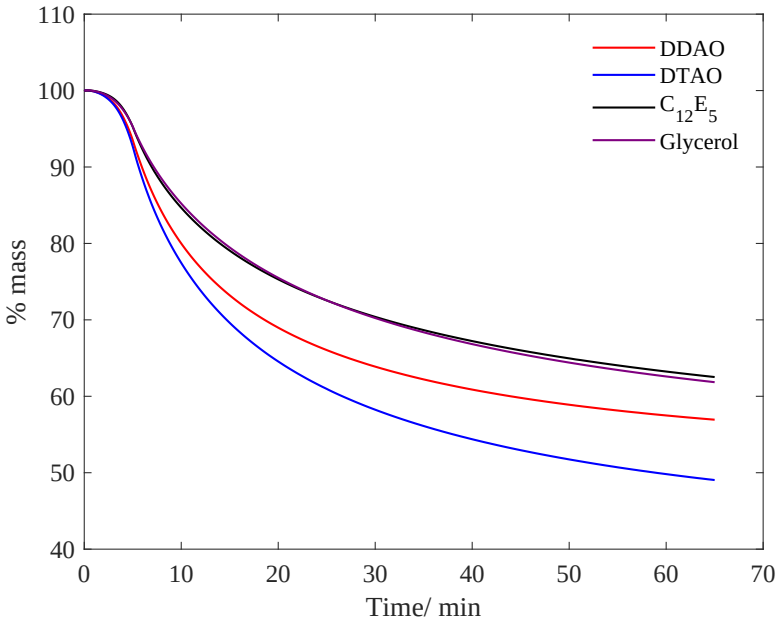

Figure F.1: TGA curves of PVA/additive films produced by solution casting at 40 °C. After heating at 10 °C min^{-1} from 25 to 80 °C, the samples were isothermed at 80 °C for 1 hour. Each film contains 10 wt.% additive.